Understanding the genetic and molecular mechanisms of neurological diseases associated with cortical spreading depression: REST and P2X7 receptor

Thesis submitted in accordance with the requirements of the University of Liverpool for the degree of Doctor in Philosophy by Dongqing Ma

Primary supervisor: Dr. Minyan Wang

Co-supervisor: Prof. John Paul Quinn

Molecular and Clinical Pharmacology

Institute of Translational Medicine

Faculty of Health and Life Science

University of Liverpool

UK

March 2018

Acknowledgements

First of all, I would like to express my utmost gratitude to my primary and secondary supervisors Dr. Minyan Wang and Prof. John Quinn for their continuous support, critical guidance and endless encouragement throughout my PhD I will never forget. Their guidance helped not only in academic affairs, but also on a personal level. Their helps are essential to my success.

A massive thanks to Alix Warburton for her generous help in molecular technical training and idea development especially in the initial of my project; Fan Bu for his guidance and training on the *in vivo* work; Liwen Jiang for her support on experiments using mouse cortical slice; Yan Wang for her training and technical support on intrinsic optical imaging recording in the chick retina; Mingming Yang for his technical support in a preliminary experiment during my three month visit to UoL. I would be also grateful for developing the script of Labview software from Dr. Shanbin Chen at Wuhan Laboratory for Optoelectronics, Huazhong University of Science and Technology.

I would also like to extend my thanks to all other PhD students and staffs in the Department of Biological Science for making me a happy time in the lab; Prof John Quinn's group and also all other members of White Block for their help and hospitality during my three month visit to Liverpool University.

The financial support from XJTLU research development fund, XJTLU PhD studentship and Wangwenli Charitable Foundation.

Finally, I also am extremely grateful to my Daddy Mingzhen Ma, Mum Xinchun Xing, lovely sisters Donghe Ma and Dongxiao Ma and brother Shubo Ma for supporting me throughout my life and being the most happiness family, making me smile every single day! And a huge thanks for all other family members and friends, who keep encouraging and supporting me over the years.

Contents

Publications and Presentations

Publications

MA, D.,WARBURTON, A., ZHAO, J., BUBB, V., QUINN, J. P. & WANG, M. 2018. Temporal changes in transcriptional activity of REST and MIR137HG gene after multiple cortical spreading depression correlate with the reduction of both REST binding to the MIR137 internal promoter and GRIN2A mRNA level. Cephalalgia Reports (Under preparation)

JIANG, L., WANG, Y., XU, Y., **MA, D.,** WANG, M. 2018. The transient receptor potential ankyrin type 1 plays a critical role in cortical spreading depression. Neuroscience, 382, 23-34.

BU, F., WANG, Y., JIANG, L., **MA, D**., QUINN, J. P. & WANG, M. 2017. Sarcoma family kinase activity is required for cortical spreading depression. Cephalalgia,

WANG, Y., TYE, A. E., ZHAO, J., **MA, D.**, RADDANT, A. C., BU, F., SPECTOR, B. L., WINSLOW, N. K., WANG, M. & RUSSO, A. F. 2016. Induction of calcitonin gene-related peptide expression in rats by cortical spreading depression. Cephalalgia.

Poster presentations

MA, D., BU, F., JIANG, L., QUINN, J. P. &WANG, M. 09/2017. The anti-P2X7R antibody suppressed CSD. Poster number: EP-02-046. The 18th Congress of the International Headache Society, Vancouver, Canada

MA, D., ZHAO, J., QUINN, J. P. & WANG, M. 09/2015. Contribution of NR2A, GABAα2 and P2X7R in the Early Stage of Migraine. The 6th FAONS Congress and 11th Biennial Conference of CNS. Tongxiang, China.

Abbreviations

5-HT	Serotonin
ACh	Acetycholine
ACSF	Artificial cerebral spinal fluid
AMPA	α-amino-3-hydroxy-5-methyl-4-isoxazoleproppionic acid
AOI	Area of interest
ATP	Adenosine 5'-triphosphate
ATPase	Adenosine triphosphase
AUC	Area under the curve
BCA	Bicinchoninic acid
BDNF	Brain-derived neurotrophic factor
BSA	Bovine serum albumin
CBF	Cerebral blood flow
CGRP	Calcitonin gene-related peptide
ChIP	Chromatin immunoprecipitation
CNS	Central nervous system
CSD	Cortical spreading depression
DC	Direct current
DMSO	Dimethylsulfoxide
EEG	Electroencephalograph
FHM	Familial hemiplegic migraine
GABA	gamma-aminobutyric acid
GAD1	Glutamate decarboxylase 1
i.c.v.	Intracerebroventricular
IL-1β	Interleukin-1β
JUN	Jun oncogene
MIR137HG	MIR137 host gene
NKB	Neurokinin B
NMDA	N-methyl-D-aspartate
NO	Nitric oxide
NRSE	Neuron restrictive silencing elemen
NRSF	Neuron restrictive silencing factor
Pannexin	Panx
RE1	Repressor element 1
RELN	Reelin
REST	Repressor element-1 silencing factor
RSD	Retinal spreading depression
SFK	Src family kinase
SH3	Src homology 3
TBI	Traumatic brain injury
TNF-α	Tumor necrosis factor-α
VIP	Vasoactive intestinal peptide

Abstract

Cortical spreading depression (CSD) is a transient propagating wave of neuronal and glial excitation, followed by depression, which is implicated in migraine, traumatic brain injury (TBI) and stroke. Yet mechanisms of these diseases associated with CSD are not fully understood. The transcription factor, repressor element-1 silencing factor (REST), plays a critical role in the processes of central nervous system (CNS) and REST binding to MIR137 internal promoter can be reduced by multiple CSD events. The first objective of this project was to explore if REST signalling is involved in CSD. CSD was induced by KCl and *in vivo* electrophysiology was used for recording CSD. Polymerase chain reaction (PCR) was applied for measuring gene expression levels. The results showed that multiple CSD events did not alter gene expression of REST and its truncated isoform REST4 in cortices of rats, although a slight but insignificant up-regulation of REST4 was observed. Interestingly, there was a significant reduction in NR2A coding gene Grin2a in the ipsilateral cortices of rats at 24 hours after multiple CSD. Using qPCR and western blot methods, this project further examined whether multiple CSD events would induce the expression of α2, the major subunit of gamma-aminobutyric acid A ($GABA_A$) receptor and its coding gene. The results showed that both the mRNA and protein level of $GABA_A$ α2 was not altered at 3 and 24 hours post multiple CSD, although an elevation trend of $GABA_A$ α2 protein level was observed. Collectively, due to small sample size, these data did not support the role of REST in CSD however, it would worth further investigation by increasing sample number to four for statistical significance.

Given that N-methyl-D-aspartate (NMDA) receptor plays a key role in CSD genesis and propagation and NMDA-receptor mediated currents and glutamate release can be reduced by blockade of P2X7 receptor (P2X7R); whilst inhibition of P2X7R channel and pore formation reduces CSD susceptibility in rats; the 2nd part of my project aims to study the role of C-terminal domain of P2X7R in CSD using an anti-P2X7R antibody. CSD was induced by KCl and was recorded using intrinsic optical imaging *in vitro* and electrophysiology method *in vivo*. The results showed that A740003, which antagonizes the P2X7R channel and pore complex, suppressed CSD with a marked prolongation of CSD latency and a reduced magnitude in the mouse brain slice. Consistently, the anti-P2X7R antibody also suppressed the occurrence of CSD in the mouse brain slice and in rats. Further q-PCR analysis showed that the CSD-induced gene expression of key neuroinflammatory factors, tumor necrosis factor-α (TNF-α) and interleukin-1β (IL-1β) was not altered by the antibody. These data demonstrate that this anti-P2X7R antibody is capable of suppressing CSD and does not alter gene expression of TNF-α and IL-1β immediately post CSD. It is necessary to clarify the role of C-terminal domain of P2X7R in CSD by expressing a C-terminal truncated variant of P2X7R in the *P2rx7* gene deficient rats/mice in future.

In summary, this study demonstrated that multiple CSD events does not alter REST gene expression but can induce a slight but insignificant up-regulation of REST4 in ipsilateral cerebral cortices of rats. Further work by increasing sample number is necessary to confirm REST4 implications to TBI and stroke. The fact that the anti-P2X7R antibody suppresses CSD suggests a possible role of P2X7R in CSD involving the C-terminal domain, however, further studies using C-terminal domain knockout animals will help to elucidate the contribution of this domain to CSD.

Brief process of my PhD project

The original aim of this thesis was to explore the role of miR-137 in migraine aura pathogenesis. The effect of silencing miR-137 was first examined on CSD using miR-137 antagomir. I had spent ~6 months to optimise the concentration and incubation time of miR-137 antagomir for silencing miR-137, however, the experiments were not successful because this antagomir and other relevant reagents/kits may lost their efficiency due to inappropriate storage and delivery resulting from the long-term custom issues encountered. Nevertheless, through this process, I have gained relevant background in MIR137 and laboratory techniques such as cell culture, transfection and PCR techniques. As a result, part of experimental data was included in this thesis that greatly helped my PhD training. Due to above reasons, the first part of my thesis shifted to REST signaling pathways in CSD that is relevant to MIR137 from the start of my year 2 PhD training. As the P2X7R project was developed at the same time whilst formulating the REST project, this thesis has two main topics on REST and P2X7R that are associated with CSD.

Chapter 1

General Introduction

1.1 Cortical spreading depression

Cortical spreading depression (CSD) is a slowly propagating wave of neuronal and glial depolarization across the brain surface at a slow speed of approximate 3 mm/minute. It was firstly described as a new propagating and reversible electrophysiological phenomenon in the brain surface of rabbits by Leao in the 1940s (Leao, 1944a, Leao, 1944b). CSD is accompanied by a transient negative direct current (DC) potential change of the electroencephalograph (EEG) depressed cortical surface (Leao, 1947). CSD can occur in nearly all cortical regions and is associated with shrinkage of the extracellular space, redistribution of ions (Hansen and Zeuthen, 1981), increased brain energy metabolism (Lauritzen et al., 2011), dilation and constriction of pial vessels (Leao, 1944a, Leao, 1947).

1.1.1 Clinical relevance of CSD

A large number of studies support the involvement of CSD in a range of neurological disorders. A single CSD is believed to be the putative cause of migraine aura and multiple CSD can cause secondary neuronal damage post traumatic brain injury (TBI) and stroke (Lauritzen, 1994, Somjen et al., 1990, Sunami et al., 1989, Gorji, 2001, Dreier and Reiffurth, 2015, Rogatsky et al., 1996, Strong et al., 2002). On the other hand, the preconditioning of CSD may also have neuroprotective role to subsequent ischemic insult (Shen et al., 2016, Shen et al., 2017).

1.1.1.1 CSD is putative cause of migraine aura

Migraine is a disabling neurovascular disorder characterized by recurrent unilateral headache that is moderate to severe pain intensity with duration from hours to 2-3

days. Some migraine patients experience an aura, which is usually visual, but can also be a sensory, motor or verbal disturbance that occurs before the headache begins. Despite the fact that migraine affects approximately 10% of the population worldwide and causes marked disability, it remains under diagnosed and under treated.

A variety of experimental and clinical studies have demonstrated that a single CSD is the electrophysiological substrate of migraine aura and a trigger for headache (Lauritzen, 1994, Lauritzen, 2001, Hadjikhani et al., 2001, Ayata, 2010, Smith et al., 2006). A number of messengers are released post CSD to sensitize or activate pain-signalling pathways. These messengers mainly include adenosine 5'-triphosphate (ATP) (Schock et al., 2007), nitric oxide (NO) (Colonna et al., 1997, Obrenovitch et al., 2002), calcitonin gene-related peptide (CGRP) (Tozzi et al., 2012, Wang et al., 2016b), high mobility group protein B1 (Karatas et al., 2013), and gamma-aminobutyric acid (GABA) (Rodrigues et al., 1988), which are known to play important roles in CSD. CSD is also capable of activating trigeminal nociceptive neurons, as evidenced by electrophysiological recording of neurons in the brainstem and trigeminal ganglion (Zhang et al., 2010, Zhang et al., 2011), as well as promoting the pain marker, c-Fos levels by immunohistological labeling in the brainstem (Bolay et al., 2002). However, how CSD causes migraine headache still remains obscure and the contribution of some key receptors, such as ATP-gated P2X7 receptors, need to be further investigated.

Another supporting evidence that CSD is the underlying cause of migraine aura is the discovery of similar changes in cerebral blood flow (CBF) between the two neurological abnormalities. There is a long lasting reduction in CBF of brain post

CSD (Lauritzen, 1984), and a similar change was observed in the visual area in the cortex of migraine patient suffering visual aura, with perfusion-weighted imaging (Cutrer et al., 2000). Moreover, CSD-like neuro-electric events are observed in the occipital cortex of patients during both spontaneous or visual stimuli triggered migraine aura (Bowyer et al., 2001). Additionally, CO_2/O_2 induced hypercapnia shows suppressive effects on both CSD propagation and migraine attacks (Gardner-Medwin, 1981).

Causative genes for migraine were discovered to be involved in defects in calcium or sodium channels, or in the Na/K-ATPase (Barrett et al., 2008). The genetic form of migraine, identified as familial hemiplegic migraine (FHM), is a rare autosomal-dominant subtype of migraine with aura with strong penetrance. Mouse models with mutations of migraine-related genes show facilitation in the induction and propagation of CSD waves, supporting CSD as the underlying mechanism involved in the functional consequences of these mutations associated with migraine aura (van den Maagdenberg et al., 2004, Leo et al., 2011, Hansen, 2010, Unekawa et al., 2017).

A range of studies show that many known and putative therapies for migraine prevention reduce the tissue susceptibility to CSD. One study found that the frequency of multiple CSD triggered by continuous stimulation can be reduced by chronic treatment with migraine preventive medications, such as valproate, topiramate, propranolol, methysergide and amitriptyline (Ayata et al., 2006). Additionally, acute treatment of topiramate was reported to block CSD (Akerman and Goadsby, 2005, Unekawa et al., 2012). Similar inhibition on CSD was also observed by the acute treatment of an acid-sensing ion channel blocker amiloride, a

potential migraine preventive therapy (Holland et al., 2012). These studies demonstrate the capacity to suppress CSD as a common, but not necessarily universal feature of migraine preventive therapies.

Consistent with significant higher prevalence of migraine in women than men, CSD in rodents shows an increased propensity in female than male sex. Female mice have been reported to have a reduced threshold for CSD induction (Brennan et al., 2007b). Also, an increased susceptibility to CSD was observed in female transgenic mice expressing migraine-associated genes compared with male counterparts (Brennan et al., 2013, Eikermann-Haerter et al., 2009b). These may be caused by sex hormone: exposure to oestrogen shows higher CSD susceptibility, whereas exposure to testosterone shows opposite effects (Eikermann-Haerter et al., 2009b, Eikermann-Haerter et al., 2009a).

Collectively, CSD has become a useful tool for studying migraine aura mechanism and anti-CSD drugs may have potential use for migraine aura prevention. However, in spite of the above, there are still some arguments against the role of CSD in migraine aura (Borgdorff, 2018). For example, water diffusion caused cell swelling in CSD was not observed during or after migraine aura (Gorji, 2001, Hansen and Olsen, 1980, Cutrer et al., 1998); cerebral metabolism in experimental rat CSD is enhanced (Piilgaard and Lauritzen, 2009), while it remains unchanged in some migraineurs with aura (Jafarian et al., 2010).

1.1.1.2 CSD and stroke, traumatic brain injury

Whilst single CSD is a putative cause of migraine aura, multiple CSD events are associated with stroke and TBI (Somjen et al., 1990, Sunami et al., 1989). Stroke

occurs when the blood supply to the brain is suddenly either blocked or ruptured, leading to insufficient supply of oxygen and nutrients to the brain and causing brain cell death. Studies show that spontaneous CSD-like depolarization was observed in the surrounding of focal ischemic lesions (Hossmann, 1996, Dreier, 2011). Moreover, the spontaneous CSD surrounding the ischemic core promotes the progression of lesion and worsens the outcome in models of stroke (Hossmann, 1996). The extent of ischemic damage is closely correlated with CSD number in focal ischemia in rats (Tatlisumak et al., 2000). The N-methyl-D-aspartate (NMDA) antagonists, which suppress CSD initiation and propagation, reduce the volume of the ischemic lesion (Tatlisumak et al., 2000, Gill et al., 1992, Iijima et al., 1992).

In addition to ischemic stroke, multiple CSD is also implicated in TBI (Strong et al., 2002, Rogatsky et al., 1996). TBI happens when an external force, such as bump, jolt and blow, injures the brain. The spontaneous occurrence of CSD in 50% to 60% of patients has been observed by different monitoring techniques (Mayevsky et al., 1996, Strong et al., 2002, Fabricius et al., 2006, Hartings et al., 2009). CSD-like DC shifts are detected after cortical cold injury, fluid percussion injury and penetrating ballistic brain injury (Williams et al., 2005, Hermann et al., 1999, Rogatsky et al., 2003). Severe physical injuries on the cortical tissue could become initiation regions for CSD and seizures (Fabricius et al., 2008). The neuronal excitability in and around the injury area post TBI is affected with a marked increase of local glutamate signalling (Goodrich et al., 2013, Hosseini-Zare et al., 2017). The elevated glutamate level post TBI may contribute to the initiation of CSD.

1.1.2 CSD models and experimental approaches

Both whole-system and reductionist models are required for the comprehensive investigation of CSD. These *in vitro* and *in vivo* models can provide complementary approaches to study underlying ionic, neurochemical and cellular mechanisms.

In vitro models, such as chick retina (RSD) (Maranhao-Filho et al., 1997, Skelton et al., 1983, Dahlem et al., 2003) and brain slice (Dietz et al., 2008, Tang et al., 2014), can provide high throughput and have been widely applied to address the effects of pharmacological agents on CSD. Unlike conventional slices, the isolated retina is a complete biological circuit. Its characteristics are similar with those of the brain slice. The size and thickness of chick retina are comparable to brain slices. One key advantage of *in vitro* model is that it could complete control the oxygenation, temperature, pH and pharmacological environment. *In vitro* studies bypass the blood-brain barrier (BBB) and eliminate pharmacokinetic, hemodynamic, systemic physiological and anesthesia-related factors. But due to exposure to hypoxia, lack of vasculature and trauma during tissue preparation, the metabolism and tissue oxygenation differ from these in *in vivo* models (Galeffi et al., 2011, Turner et al., 2007).

Most *in vivo* studies are carried out on rodents and limited on cerebral cortex due to ease of access. A range of species are also applied *in vivo* from monkeys to pigeons and cats (Shima et al., 1963, Van Harreveld et al., 1956). There is a fair degree of interspecies variability in CSD susceptibility. Although it has not been systematically studied the species difference in CSD susceptibility, usually, gyrencephalic species are less susceptible to CSD than lissencephalic species. The

determinants for the species differences in CSD susceptibility have not been fully studied. The increasing ratio of astrocyte/neuron in higher species is usually cited as a potential cause (Tower and Young, 1973, Gardner-Medwin, 1981), but it seems not the only determinant. *In vivo* CSD models are able to provide important physiological information on the dynamic implications of metabolism and neurovascular coupling.

CSD can be evoked by a variety of chemical (e.g. high extracellular K^+, Ca^{2+} channel openers, Na^+ channel activators or agonist of glutamate receptor), direct electrical (e.g. cathodal stimulation), and mechanical depolarizing stimulation (e.g. puncture of cortex) on one point of cortical surface. KCl is usually the first choice for concentration threshold and frequency, and is more consistent than electrical threshold, which usually shows large variability due to irregularities at the contact between electrode and tissue, such as drying and bleeding. Mechanical stimulation, such as needle prick, is usually less reproducible and more injurious. The CSD threshold is hard to be determined under mechanical stimulation. Thus the CSD susceptibility is an "all or none" response after being triggered by a single mechanical stimulus (Akerman and Goadsby, 2005). There are also some other ways to evoke CSD, such as focal cerebral ischemia and high-frequency afferent pathway (Nozari et al., 2010), but they are not suitable for experimental high throughput.

1.1.3 Key features of CSD

1.1.3.1 Changes in cellular ionic homeostasis

The initial depolarization of CSD wave is associated with a massive translocation of ions, such as a reduction in extracellular Na^+ and Ca^{2+}, a large increase in extracellular K^+, and a significant redistribution of other ions including Cl^-, Mg^{2+} and Zn^{2+} (Hansen and Zeuthen, 1981, Dietz et al., 2008). The changes in cellular ionic homeostasis usually last one to two minutes and can be spontaneously reversed (Kraig and Nicholson, 1978, Martins-Ferreira et al., 2000). They are accompanied with water entry into cells, resulting in cell swelling and therefore a reduction of the volume of the extracellular compartment (Martins-Ferreira et al., 2000). The DC potential changes of CSD waves show greater correlation with astrocyte membrane potential than neuronal membrane potential (Sugaya et al., 1975), demonstrating the critical role of astrocytes in the physiological process of CSD. Astrocytes act as a sink for extracellular K^+ and a buffer for the ionic changes for initiating and propagating CSD. Ca^{2+} waves of astrocytes are associated with the active release of glutamate, ATP and K^+ (Haydon and Carmignoto, 2006).

1.1.3.2 Changes in brain energy metabolism

CSD imposes a large energy demand on brain tissue both under physiological condition and after brain injury (Dreier, 2011, Lauritzen et al., 2011), evidenced by increased oxygen consumption (Mayevsky and Weiss, 1991), glucose utilization (Hashemi et al., 2009) and lactate production (Kraig et al., 1985, Feuerstein et al., 2010) during CSD. The restoration of ion homeostasis is achieved by activation of transmembrane adenosine triphosphase (ATPase) ion pumps, which utilizes ATP to

transport K^+ into, Na^+ out of the cells. The increased ATP hydrolysis can in turn stimulate glycolysis and oxidative phosphorylation with high consumption of cellular oxygen. The early breakdown of glycogen is the first process to contribute to ATP formation during increased energy demand. Neuronal ATP production depends on increased glycolysis, followed by increased oxidation of glucose (Feuerstein et al., 2016).

1.1.3.3 Release of neurotransmitters and regulation of their receptors

CSD is associated with an efflux of a range of neurotransmitters, which mainly include glutamate, acetylcholine, dopamine, serotonin (5-HT), CGRP, NO, GABA (Rodrigues et al., 1988, Fabricius et al., 1993, Read et al., 1997, Storer and Goadsby, 1997, Yavich and Ylinen, 2005, Shi et al., 2010). Release of these transmitters and activation of their receptors play vital roles in the remarkable brain alterations. The synchronous release of neurotransmitters is related with dramatic changes in intracellular and extracellular ions during CSD, therefore it is proposed to have a vital role in CSD initiation. For example, extracellular glutamate is increased during CSD (Zilkha et al., 1995, Basarsky et al., 1999) and the activation of the glutamate-NMDA-receptor is required for CSD genesis (Marrannes et al., 1988). Not only excitatory NMDA receptor, but also inhibitory neurotransmitter receptors mediate CSD genesis and propagation. Topiramate, a GABA-receptor agonist, functions to elevate CSD threshold (Green et al., 2013) and reduce CSD frequency and propagation (Unekawa et al., 2012). In addition, blockade of CGRP receptor by antagonist suppresses CSD propagation in chick retina (Wang et al., 2016a). The genetic deletion of ATP-gated P2X7 receptor reduces the cerebral cortex susceptibility to CSD and suppresses subsequent activation of the

trigeminovascular system (Chen et al., 2017b). All above evidences indicate that neurotransmitters and their receptors may play crucial roles in modulating the transduction events of intracellular signalling, as well as the formation and alteration of neural circuit during CSD processes.

1.1.3.4 Changes in cerebral blood flow

CSD is also characterized by a complex pattern of alterations in regional cerebral blood flow (CBF). The changes of regional CBF related with CSD show a marked hyperemia under normal condition (Fabricius et al., 1995, Read et al., 1997, Gold et al., 1998, Hashimoto et al., 2000), followed by a sustained hypoperfusion in cortical region (Shimazawa and Hara, 1996, Lauritzen, 1984). In some studies, an initial brief hypoperfusion is observed prior to the hyperemia associated with CSD waves (Fabricius et al., 1995, Ayata and Lauritzen, 2015). While no changes of regional CBF are observed in subcortical region by either multiple or single CSD at any time (Kuge et al., 2000).

The underlying mechanism of CSD associated hyperemia is unclear, but one possible mechanism may be associated with the release of vasoactive compounds, such as CGRP, glutamate, nitric oxide (NO), acetycholine (ACh) and cyclic GMP (Read et al., 1997, Read et al., 2001, Rodrigues and Martins-Ferreira, 1980, Basarsky et al., 1999, Wang et al., 2016a). Both topical and systemic administration of CGRP, a potent dilator of vessels, significantly elevates dural blood flow (Levy et al., 2005). Brian's study also shows that CGRP may limit constriction of cerebral vessels induced by noradrenaline and contribute to dilatation during hypotension and CSD (Brian et al., 1996). Moreover, the inhibitor of CGRP receptor attenuates CSD-induced pial dilation (Colonna et al., 1994) and

CSD-associated hyperperfusion in rats (Reuter et al., 1998). Different with CGRP, endothelium-regulated dilation does not contribute to CSD-induced hyperemia in rats (Shimizu et al., 2002).

Notably, the vascular response induced by CSD may proceed independently through its vascular conduction. This is evidenced by the following findings: (i) the propagation of arteriole dilation is at a faster speed than the CSD wave on the cortical surface and spread into the region not reached by CSD wave (Brennan et al., 2007a); (ii) spontaneous CBF changes can be observed in the contralateral cerebral cortex post multiple CSD waves (Hosseinzadeh-Nik et al., 2016). Moreover, the vascular response seems not essential for the process of spreading depression waves, as the spreading depression can proceed in the absence of the vascular response in isolated chick retina (Dahlem and Muller, 2000) and brain slice (Dietz et al., 2008).

1.1.3.5 Gene changes

CSD regulates a large range of genes expression clustered in following functional groups: (i) vasodilation, e.g. the gene expression of vasodilator atrial natriuretic peptide and CGRP are up-regulated post CSD, while the vasoconstrictor neuropeptide Y is reduced (Choudhuri et al., 2002, Wiggins et al., 2003, Wang et al., 2016a); (ii) inflammation, e.g. both tumor necrosis factor-α (TNF-α) and interleukin-1β (IL-1β) mRNA level are induced by CSD (Jander et al., 2001); (iii) pain, e.g. the neural maker of pain, c-fos mRNA level is significantly up-regulated post CSD (Tepe et al., 2015, Herrera and Robertson, 1990), (iv) oxidative stress, e.g. glutathione-S-transferase-5 gene expression is down-regulated by CSD, while major prion protein is up- regulated (Choudhuri et al., 2002) (v) neuroprotection,

e.g. mRNA level of brain-derived neurotrophic factor (BDNF) and heat shock protein 70 are both up-regulated after CSD (Kokaia et al., 1993, Medhurst et al., 2000, Rangel et al., 2001, Faraguna et al., 2010). Some of these gene changes underlie the pathological process of CSD-related disease, while some are associated with increased adaptive tolerance induced by CSD preconditioning to further brain injury.

1.2 The REST signalling pathway

A range of gene expression is altered in response to CSD stimuli as mentioned above. This is modified by the changes in transcriptional repressors or enhancers, subsequently influencing neuronal phenotype and behavior. Repressor element-1 silencing factor (REST), also named neuron restrictive silencing factor (NRSF), is one of such transcriptional regulator, which is widely known due to its function in modulating the expression of neuron-specific genes. REST is identified in 1995 as a zinc finger protein that binds to a conserved 21 bp consensus sequence termed neuron restrictive silencing element (NRSE) or repressor element 1 (RE1) (Schoenherr and Anderson, 1995, Chong et al., 1995).

1.2.1 Regulation of REST expression

High level of REST is expressed in non-neuronal cells in mature tissue, while much lower level of its expression is found in specific neuronal tissue types, demonstrating that the expression of REST is highly dependent on cellular types and physiological conditions. Moreover, increased expression of REST is observed in different regions of adult brains, such as cerebral cortex and hippocampus, in response to neuronal activation by treatment with cocaine or the glutamate

analogue kainic acid (Palm et al., 1998, Spencer et al., 2006, Chandrasekar and Dreyer, 2009).

REST binds to its target sequences via its zinc-finger DNA binding domain, whereas its repressor activity is mediated by recruitment of co-repressor complexes to its either N-terminal or C-terminal repressor domains (Tapia-Ramirez et al., 1997, Naruse et al., 1999). Its N-terminal can interact with mammalian homologue of yeast Sin3A (mSin3A) (Naruse et al., 1999, Huang et al., 1999, Grimes et al., 2000), a transcriptional co-repressor, mediating active gene repression via its recruitment of histone deacetylases 1/2 (HDAC1/2) (Ballas and Mandel, 2005), while its C-terminal interacts with co-factor for REST, potentiating long-term gene silencing (Lunyak et al., 2002, Andres et al., 1999). Other chromatin modifying complex involved in gene repression are also recruited by cofactor for REST, such as HDACs, the histone methyltransferase C9a and methyl-CpG binding protein MeCP2 (Lunyak et al., 2002, Battaglioli et al., 2002, Roopra et al., 2004, Lee et al., 2005), enabling REST to orchestrate a set of epigenetic signatures which change the chromatin structure to a condensed heterochromatin state. The co-repressor complex varies depending on promoter sequences and cell types, suggesting that REST can mediate both long-term silencing and transient repression.

REST is more complex than its initial role of transcriptional repression within CNS. It may also act as a transcriptional activator or enhancer depending on isoform usage, genomic location, cellular types and associated co-factor binding assembly at the target sequence (Kallunki et al., 1998, Coulson et al., 1999, Coulson et al., 2000, Yoo et al., 2001, Kim et al., 2008). REST has several isoforms generated via alternative splicing. One of the most well studied is REST4, which is a truncated

protein lacking C-terminal domain. This isoform arises via coding of an alternative N exon and produces a premature stop codon (Figure 1.1 A) (Palm et al., 1998). REST4 is especially expressed in neurons or certain cancer cells (Coulson et al., 2000, Palm et al., 1998, Wagoner et al., 2010) and antagonise the effects of the full length REST (Figure 1.1 B) (Coulson et al., 2000, Shimojo et al., 1999).

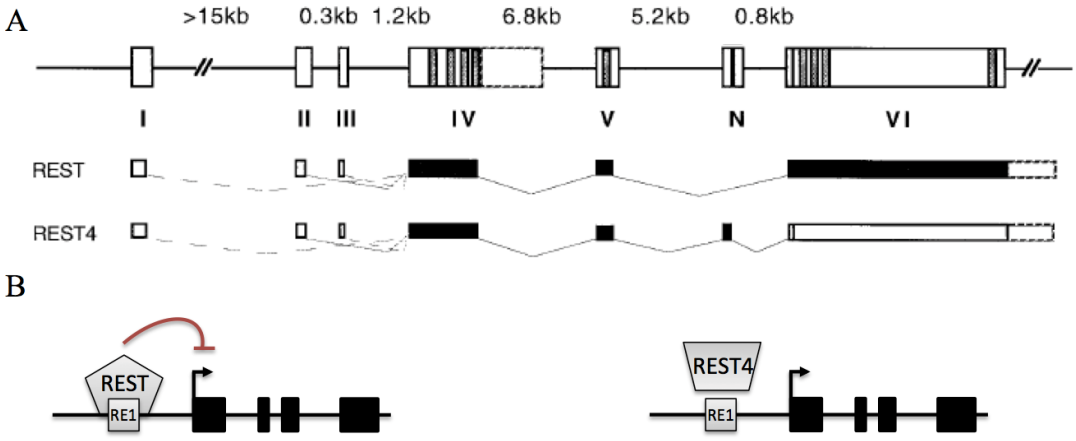

Figure 1.1 Structure and function of REST and REST4. (A) The structural organisation and alternative transcripts for REST and REST4 (Palm et al., 1998). Exons are shown as boxes and introns as lines. The respective sizes of introns are shown as above numbers. Vertical bars within exons indicate zinc finger motifs. Exon numbers in roman characters (I-VI) are shown below the respective exons. An alternative exon N introduces a premature stop codon, giving rise to the truncated protein variant REST4, which lacks four of the mine zinc fingers. (B) Regulation of REST/REST4 on the expression of target genes.

1.2.2 The REST signalling in disease conditions

REST signalling is implicated in variety of neurological disorders, such as epilepsy, ischemic stroke, schizophrenia, Alzheimer (Spencer et al., 2006, Warburton et al., 2015, Loe-Mie et al., 2010, Noh et al., 2012, Calderone et al., 2003, Hu et al., 2011, Lu et al., 2014). Up-regulation of both REST and REST4 are observed in rat hippocampal neurons in both *in vitro* and *in vivo* epilepsy models (Spencer et al.,

2006). This increase correlated with increased of mRNA level for the proconvulsant gene TAC1 (Spencer et al., 2006). Additionally, conditional deletion of REST in mouse forebrain neurons exhibited dramatically accelerated seizure progression in a epilepsy model, suggesting that REST may function as a repressor of epileptogenesis (Hu et al., 2011). Ischemic insults promote REST binding to miR-132 promoter and silencing miR-132 expression, whilst overexpression of miR-132 afforded protection against ischemia-induced neuronal death, suggesting a role of REST in the neuronal death associated with global ischemia (Hwang et al., 2014). Also, distinct isoforms of REST mediate differential expression of miR137 parent transcript, which is identified as a candidate gene of schizophrenia (Warburton et al., 2015). Collectively, these findings highlight the importance of REST-mediated regulation in diverse neurological disorder diseases. Yet it is unknown if REST and its isoforms REST4 play important roles in the context of CSD-linked progression of TBI, stroke and migraine aura.

REST has an overlap role with microRNA as a negative regulator of target genes. In mammals, approximately 70% microRNAs are detected in primary neuronal cultures or in the brain (Cao et al., 2006) with a small set of brain specific and enriched microRNA (Landgraf et al., 2007). MicroRNAs are a large family of single-stranded non-coding RNAs of approximately 18-25 nucleotides in length, which are highly conserved through evolution (Bartel, 2004). Mature microRNA guides RNA-induced silencing complex (RISC) to the 3'-untranslated region of the target mRNAs for RNA-interference based gene regulation, which is thought to occur through several different mechanisms (Vimalraj and Selvamurugan, 2013): (A) blocking of cap recognition by inhibition of joining of the large ribosomal subunit and inhibition of initiation factor of translation by Ago

protein of RISC; (B) deadenylation and degradation of target mRNA; (C) RISC induce proteolysis to degrade the newly synthesized polypeptides; (D) premature termination of ribosomes.

Comparative sequence analysis shows that REST and its co-repressors coREST and MeCP2 could target several brain-enriched microRNAs, such as microRNA137 (miR137) (Soldati et al., 2013, Warburton et al., 2015). In a mouse cell line model of Huntington's disease, knock-down of REST up-regulates several microRNAs, including miR137, which is validated as a target of REST by chromatin immunoprecipitation (ChIP) (Soldati et al., 2013). Also in a human cell line SH-SY5Y, MIR137 gene is validated as a REST target (Warburton et al., 2015). Additionally, in a mouse model of Rett syndrome, miR137 expression is shown to be regulated by MeCP2, a core member of the REST-complex (Szulwach et al., 2010). Notably, the NR2A subunit of NMDA receptor coding gene, Grin2a, is one of miR137 target genes. Reduced miR137 level in the brain tissue correlated with increased Grin2a level in a rat stroke model (Zhao et al., 2013). Additionally, the NR2A subunit of NMDA receptor contributes to CSD genesis and propagation (Peeters et al., 2007, Bu et al., 2016a).

Collectively, it is likely that REST, MIR137 and their target genes may also have a role in CSD associated neurological disease. Yet whether REST plays an important role in the context of CSD-linked progression of migraine and TBI has not been elucidated.

1.3 Net-work of NMDA receptor and P2X7R in central nervous system

1.3.1 NMDA receptor signalling

Glutamate is one of the most important excitatory neurotransmitters that contribute to CSD by acting on its receptors, one of which is NMDA ionotropic receptors that are widely expressed in CNS.

NMDA receptors are tetramers, which consist of different subunits: 2 mandatory NR1 and 2 NR2 (NR2A, 2B, 2C and 2D) and/or one NR3 (two isoforms, A and B). The assembly of functional NMDA receptor is usually formed by a combination of two mandatory NR1 subunits, two NR2 subunits and/or one NR3 subunit (Sasaki et al., 2002, Flores-Soto et al., 2012). The NR1 subunits are essential for receptor functionality, and the NR2 subunits determine the biophysical property of this channel conductance (Rambhadran et al., 2010). The NR2A-containing receptors typically mediate synaptic transmission, whereas the receptors with NR2B subunit are mainly expressed extrasynaptically and in astrocytes (Sanz-Clemente et al., 2013, Dzamba et al., 2013). The activation of NMDA receptors requires membrane depolarization, which can remove Mg^{2+} present in the ion channel pore following the binding of ligands, such as glutamate and glycine (or D-serine).

NMDA receptors have vital roles in the CNS development and the processes underlying memory, learning and neuroplasticity. Consequently, altered NMDA receptor expression levels or abnormal function of NMDA receptors are implicated in a range of pathological conditions and neurological disorders. Therefore, NMDA receptor is a potential therapeutic target due to its wide involvement in many brain disorders, such as migraine, stroke, head trauma, ischemia, neuropathic pain,

epilepsy, Alzheimer's and Parkinson's disease. (Kemp and McKernan, 2002, Jansen and Dannhardt, 2003, Chazot, 2004, Farlow, 2004, Wood, 2005, Cai, 2006, Missale et al., 2006, Brown and Krupp, 2006). NMDA receptor plays a vital role in excitotoxicity. During this process, excessive release of glutamate leads to over-activation of NMDA receptors and accumulation of intracellular calcium, which usually occurs during cerebral ischemia following brain trauma or stroke and in neurodegenerative disorders, such as schizophrenia and Parkinson (Paoletti and Neyton, 2007). Numerous evidences demonstrate the critical role of NMDA receptors in CSD mechanisms. MK801, a non-competitive inhibitor of NMDA receptor, appears to be one of the most effective anti-CSD compounds in rats (Marrannes et al., 1988, Peeters et al., 2007). However, NMDA receptor antagonists developed to treat these brain disorders failed in clinical trials due to unacceptable side effects, such as hallucinations, anesthesia, ataxia and memory deficits (Kristensen et al., 1992, Rockstroh et al., 1996, Huang et al., 2014). In this case, disruption of specific NMDA involved interaction may trigger an intense interest to develop new therapeutic drug targets with fewer side effects. Notably, inhibition of specific NR2A or NR2B subunit of NMDA receptor can suppress CSD, demonstrating the significant contribution of these two subunits in CSD generation and propagation (Shatillo et al., 2015a, Bu et al., 2016a, Wang et al., 2012) and indicating such subtype selective drugs might have potential use for migraine prevention with a better safety profile.

1.3.2 P2X7 receptor signalling

It is well known that the activation of P2X7 receptors (P2X7R) results in increased release of glutamate from cerebrocortical nerve terminals and hippocampal slices

(Sperlagh et al., 2002, Alloisio et al., 2008, Csolle et al., 2013). The NMDA-receptor mediated currents and glutamate release are reduced by both pharmacological blockade and genetic deletion of P2X7R mice (Kovanyi et al., 2016). The P2X7R belongs to the purinergic P2X family of ATP-gated cation channels (Figure 1.2). Currently, seven different P2X subtypes have been identified, P2X1-7 (Burnstock, 2006). P2X7R is a distinct subtype among other subforms of P2X receptors because of its following characters: (i) its monomeric subunit is the largest one and is characterized by a relative long intracellular carboxyl (C) – terminal tail, which plays a critical role in regulation of channel activity and P2X7R signal transduction (Kim et al., 2001, North, 2002); (ii) much higher ATP concentration is required for the activation of P2X7R, than other P2X subtypes; (iii) it has an essential role in inflammatory cascades. P2X7R is widely expressed in both central and peripheral nervous systems throughout mammals (Sperlagh et al., 2006), involving in various of physiological and pathological processes (Baroja-Mazo et al., 2013).

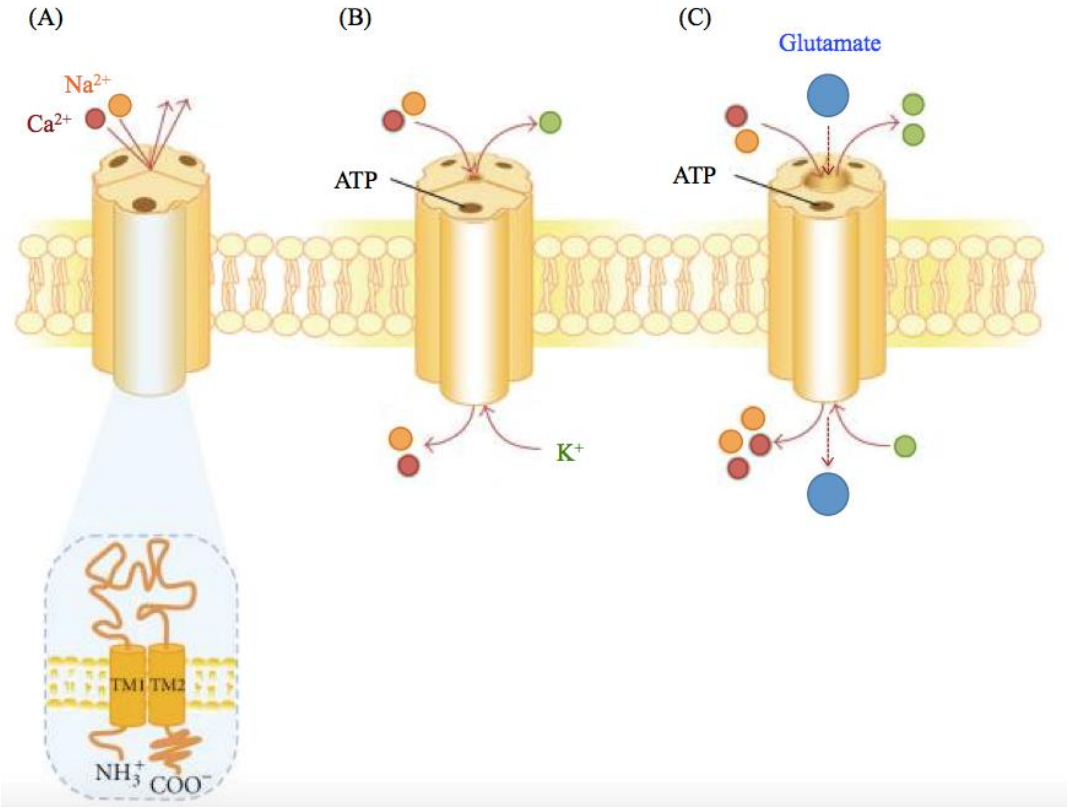

Figure 1.2 Structure and signaling function of P2X7R. (A) P2X7R is a trimer. Each subunit possesses two transmembrane domains (TM1 and TM2), intracellular amino and carboxyl termini and a large extracellular loop with ATP binding site. (B) Brief stimulation of P2X7R by ATP (< 10 s) lead to rapid and reversible channel opening, allowing the passage of K^+, Na^+ and Ca^{2+}, across the plasma membrane. (C) Continued stimulation by ATP results in the formation of a larger plasma membrane pore, which is permeable to molecules up to 900 Da, such as glutamate. Figure adapted from (Skaper et al., 2009).

Stimulation of P2X receptor by ATP opens the channel and allows the passage of small cations, such as K^+, Na^+ and Ca^{2+}, across the plasma membrane (Surprenant et al., 1996, Chessell et al., 1998, Kawate et al., 2011). P2X7R activation causes induction of cytosolic Ca^{2+} and reduction of intracellular K^+ induces the activation of caspases-1 (Perregaux and Gabel, 1994, Ferrari et al., 1997, Kahlenberg and Dubyak, 2004, Perregaux and Gabel, 1998), which can further cause the release of pro-inflammatory cytokine IL-1β by activating IL-1β from its inactive form, pro-

IL-1β (Kahlenberg and Dubyak, 2004). Accumulation of IL-1β can trigger inflammatory cascades and induce other inflammatory mediators, such as tumor necrosis factor-alpha (TNF-α) (Woolf et al., 1997), nitric oxide synthase (NOS) (Kahlenberg and Dubyak, 2004), nuclear factor kappa-B (NF-κB) (Aga et al., 2002), cyclooxygenase-2 (COX-2) (Samad et al., 2001). Notably, activation of NF-κB in astrocytes can be promoted by pannexin 1 (Panx1) channel opening and caspase-1 activation induced by CSD (Karatas et al., 2013). Additionally, a significant induction of pro-inflammatory factors, IL-1β and TNF-α, is observed post CSD (Jander et al., 2001). Collectively, above evidences demonstrate the potential contribution of P2X7R to CSD-induced inflammation cascades.

Among all purinergic receptors, P2X7R shows functional linkage with Panx1 in many studies. Panx1 is a membrane channel and abundantly expressed in CNS of mammals in all cell types (neurons, astrocytes, microglia and oligodendrocytes). The synergistic activation of P2X7R and Panx1 is demonstrated in inflammation, calcium waves and apoptosis (Pelegrin, 2008). When activated, the P2X7R are highly permeable to calcium and increase the intracellular concentration of calcium, therefore activating Panx1 channels (Ma et al., 2009). Panx1, in turn, promote the release of ATP to the extracellular space, which re-activates the P2X7R as a positive loop. The reversible opening of P2X7R channels and the subsequent calcium influx into cells are associated with release of neurotransmitters, such as glutamate (Duan et al., 2003), GABA (Wang et al., 2002) and acetylcholine (Patti et al., 2006). All of these neurotransmitters are known to be released post CSD, indicating the potential involvement of P2X7R activation in CSD-related disorders. P2X7Rs have been efficacious in experimental epilepsy models (Henshall et al., 2013, Jimenez-Pacheco et al., 2013), which may mechanistically share with

migraine (Davies and Panayiotopoulos, 2011, Rogawski, 2012). In fact, the critical role of P2X7R-Panx1 interaction in CSD is supported by a recent study that inhibition of P2X7R-Panx1 channel and pore formation reduces CSD susceptibility in rats (Chen et al., 2017b). Yet the underlying mechanism of P2X7R contribution to CSD is not fully known.

Chapter 2

Overall Aim

The overall aim of this study is to improve our understanding on the pathophysiological mechanisms of neurological diseases associated with CSD by focusing on two factors: **REST and P2X7R**.

The first part of this thesis was to explore the role of REST and MIR137 signalling in CSD. The second part of this thesis was to further understand the role of P2X7R in CSD.

Specific objectives will be introduced in each specific chapter following further introduction.

Chapter 3

Materials and Methods

Multiple disciplinary methods were used for this study. CSD was induced by KCl both *in vitro* (chick retina and mouse brain slice) and *in vivo* (rat). Intrinsic optical signal (IOS) was applied *in vitro* (chapter 6) and electrophysiology method was applied *in vivo* for CSD recording (chapter 4, 5 & 6), PCR was applied for gene expression analysis (chapter 4, 5 & 6), western blot was applied for protein expression analysis (chapter 5). Cell culture was applied to optimise the concentration and incubation time of miR-137 antagomir, which functions to silencing miR-137 and was used to investigate the effects of silencing miR-137 on CSD (chapter 4). The overall technical route and work flow were shown as below:

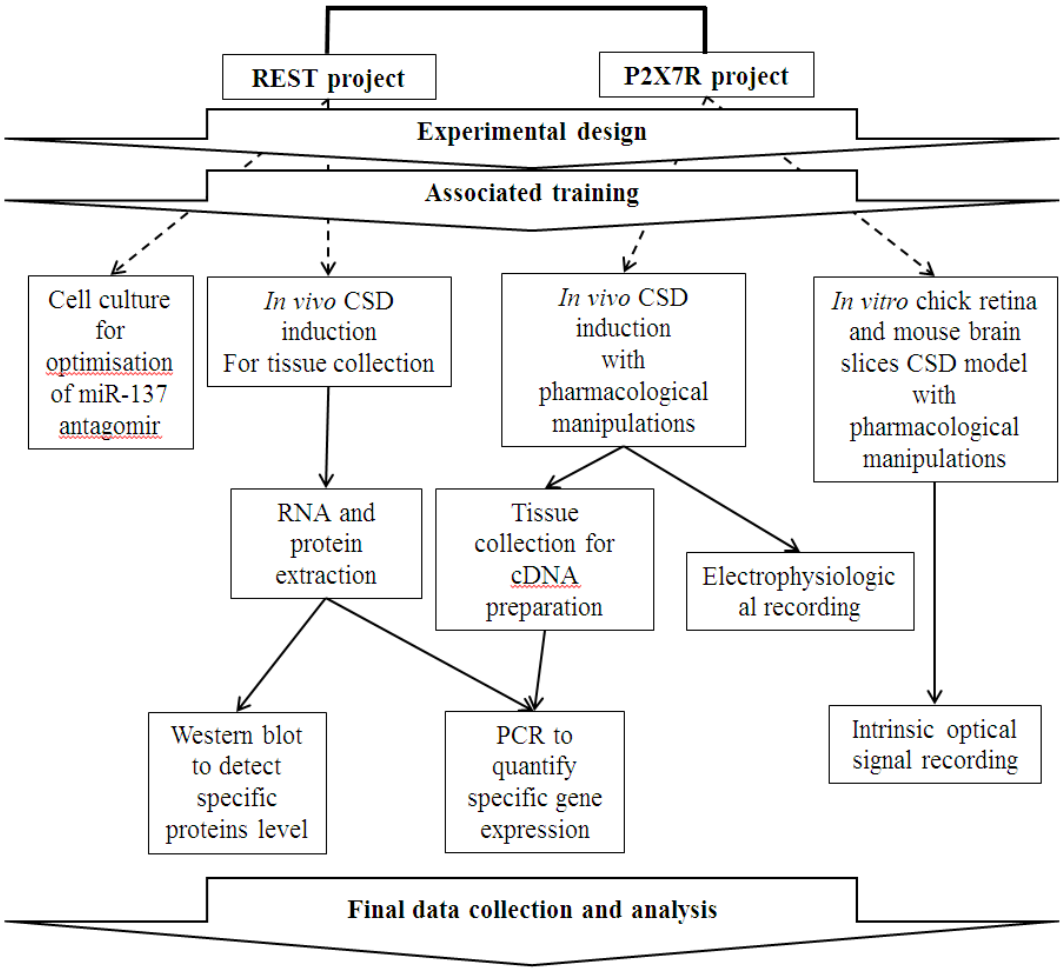

3.1 Animal work

All animals were purchased from Shanghai SLAC Laboratory Animal Corporation Ltd and were housed in an animal unit of Soochow University for at least one-week before use. All animal procedures were approved by the Ethic Review Panels of Xi'an Jiaotong-Liverpool University and Soochow University and performed in accordance with the relevant national guideline.

3.1.1 In vivo CSD induction and recording in rats

In vivo work in rats was carried out for tissue collection to analyse how CSD would affect gene or protein expression (chapter 4, 5 & 6) and to investigate effects of specific antibodies on CSD propagation (chapter 6).

3.1.1.1 Surgical preparation, CSD induction and recording

Adult, male Sprague Dawley rats (280 -370 g, Shanghai SLAC Laboratory Animal Corporation Ltd) with food and water available ad libitum were used. Surgical procedures were described previously (Wang et al., 2003). Briefly, one recoding electrode was implanted into the rat under anaesthesia with isoflurane in O2:N2O (1:2, maintained at 37°C) at 3 mm anterior and 2 mm lateral to bregma 0.8-0.9 mm deep into the right cerebral cortex. A burr hole was also drilled with intact aura at 4 mm posterior, 2 mm lateral to bregma at the same hemisphere for eliciting CSD with 3 M KCl (Figure 3.1 A). Throughout the experiment, the depth of anaesthesia was monitored and adjusted according to the EEG and through observation of the reflexes of the animal.

Both EEG signal and DC potential were derived from the Ag/AgCl electrode (Applied Neuroscience, London, UK) and the reference electrode (Applied Neuroscience, London, UK) placed under the scalp. EEG and DC signals were amplified using an AC/DC pre-amplifier (NL834, Neurolog System, Digitimer Ltd., Welwyn Garden City, UK) and recorded as reported previously (Wang et al., 2003). The alternating current component in the 1-30 Hz window provided the EEG (overall ×5000 amplification) and the 0-30 Hz window provided the extracellular DC potential (overall ×250 amplification). All the recorded variables were continuously digitised, displayed and recorded with Labview software (National Instruments, NI) via an analogue/digital-converter (USB6009, NI Instruments). CSD was recognized as a transient, negative shift on the extracellular DC potential (Figure 3.1 C).

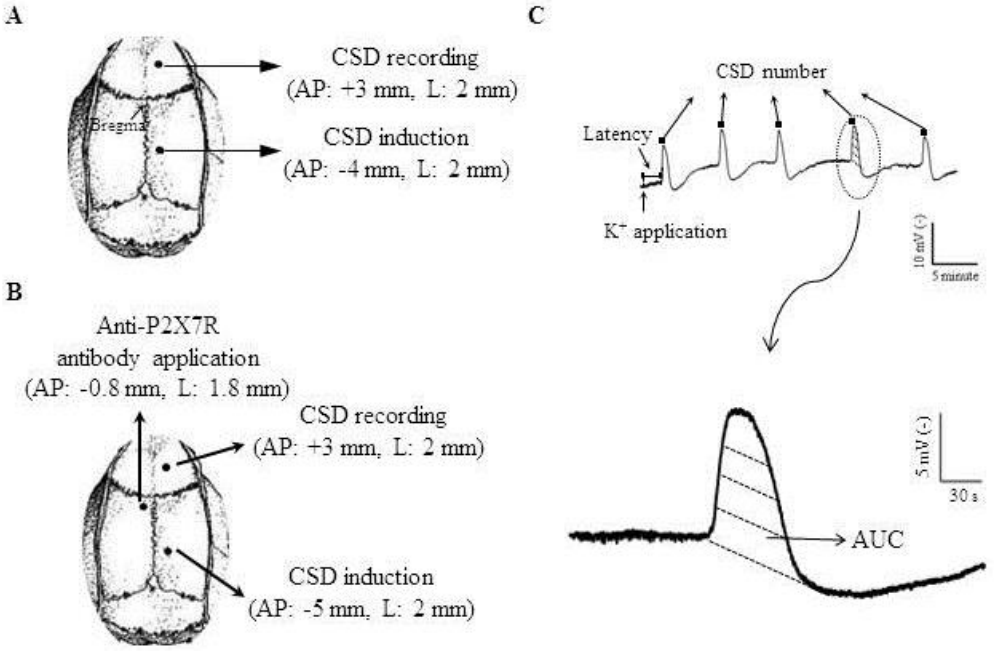

Figure 3.1 Induction of unilateral CSD in the rat ipsilateral cerebral cortex and representative traces in DC potential indicating CSD. A. Two bur holes were drilled on the right hemisphere of rat brain. KCl was applied onto the posterior hole with intact dura mater for CSD induction. An Ag/AgCl electrode was implanted into the anterior hole for CSD recording and a reference electrode placed under the scalp. Artificial cerebral spinal fluid (ACSF, 125 mM NaCl, 2.5 mM KCl, 1.18 mM MgCl2, 1.26 mM CaCl2; pH 7.3), instead of KCl was used in sham group. **B.** In the intracerebroventricular (*i.c.v.)* based experiments, one bur hole drilled on the left hemisphere for ACSF or antibody *i.c.v.*; Two bur holes were drilled on the right: one bur hole with dura mater intact was used for CSD induction; the other bur hole was used for CSD recording through the Ag/AgCl electrode implanted into cerebral cortex. **C.** representative changes in the DC potential recorded indicating multiple CSD: area under the curve (AUC) was measured to determine CSD magnitude. CSD number and CSD latency were used to indicate the tissue susceptibility to CSD.

3.1.1.2 *In vivo* protocol and tissue collection

In order to analyse CSD effects on specific gene and protein expression, tissue was collected at different time points post multiple CSD. Five episodes of CSD with 40 minute interval were induced at time points 24 hours and 72 hours post CSD. As some gene changes were transient, to explore the immediately effects of multiple CSD, tissue was collected at closer time points 15 minutes and 3 hours post 20-minute continuous 3 M KCl treatment.

As single CSD has different clinical implication with multiple CSD, single CSD was also induced to compare with changes in some gene expression after multiple CSD. Cortical tissue was collection 24 hours post the single CSD.

Both left (contralateral) and right (ipsilateral) cerebral cortex were rapidly dissected and snap frozen in liquid nitrogen and stored at -80°C. The frozen tissue was then ground into powder, which was aliquot into two parts for both RNA and protein extraction.

3.1.1.3 Intracerebroventricular perfusion experiment and protocol

In order to examine the role of P2X7R C-terminus in regulating CSD in rats (chapter 6) and investigate whether inhibition of P2X7R alters whether CSD-induced gene expression of TNF-α, IL-1β and CGRP (chapter 6), we carried out the following experiments. Three burr holes were drilled: (i) one with dura mater intact in the right parietal bone (coordinates: 5 mm posterior and 2 mm lateral to bregma) for CSD induction by 2 M KCl application for 30 minutes; (ii) one was drilled on the ipsilateral side (coordinates: 3 mm anterior and 2 mm lateral

to bregma) for CSD recording by Ag/AgCl electrodes; (iii) one was drilled on the contralateral skull (coordinates: 0.8-0.84 mm posterior and 1.7-1.9 mm lateral to bregma, 3.5-3.6 mm deep from the cortical surface) for artificial cerebral spinal fluid (ACSF, 125 mM NaCl, 2.5 mM KCl, 1.18 mM $MgCl_2$, 1.26 mM $CaCl_2$; pH 7.3)/antibody perfusion into the ventricle through a stainless steel cannula (inner diameter: 0.38 mm, RWD Life Science, Shenzhen, China), which is held in place by acrylic dental cement.

Three groups were designed (Figure 3.2): (i and ii) 0.6 μg monoclonal rabbit anti-P2X7R antibody (ab109246, Abcam, targeting the P2X7R C-terminus PKSEGQYSGFKSPY, corresponding to amino acids 582 to 595 of human P2X7R, n = 8) or 0.8 μg rabbit anti-IgG antibody (D110502, Sangon, n = 9) was intracerebroventricular *(i.c.v.)* perfused four days prior to the CSD induction by 30 minute continual KCl application; (iii) ACSF was *i.c.v.* perfused in sham group (n=8). After 40 minute recording of CSD, tissue was dissected immediately and snaps frozen in liquid nitrogen and stored at -80°C.

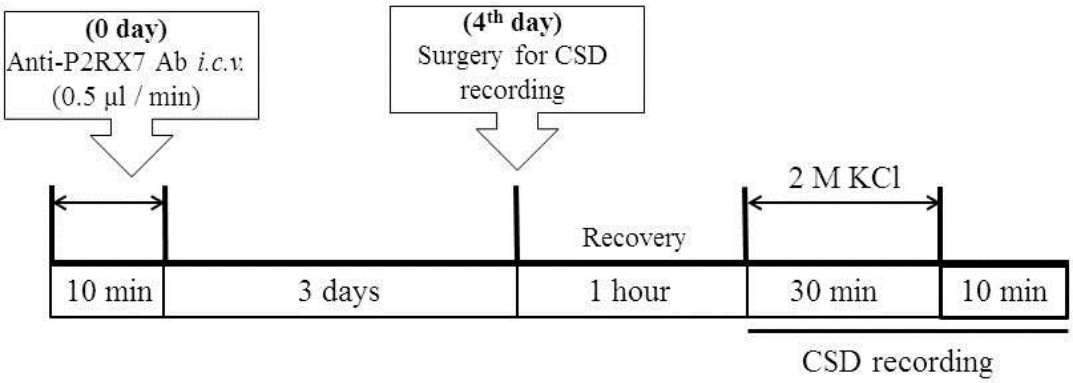

Figure 3.2 Experimental protocol for tissue collection to investigate the effect of pretreatment of the anti-P2X7R antibody on the CSD occurrence and CSD-induced expression of inflammatory factors, TNF-α, IL-1β and CGRP. In each experiment, 0.6 µg anti-P2X7R antibody or 0.8 µg anti-IgG antibody was *i.c.v.* perfused four days KCl application for 30 minutes. ACSF was *i.c.v.* perfused in sham group. After 40 minute recording of CSD, tissue was collected immediately for subsequent analysis.

3.1.1.4 Data presentation

For the *in vivo* electrophysiological data, the following parameters were analysed: the area under the curve (AUC, mV × minute) of each CSD wave was calculated and the averaged AUC was used for indicate the CSD magnitude for data comparison; CSD latency was calculated by the time used to elicit the first CSD wave in the recording site after the KCl application; CSD number induced by each KCl application was also counted; CSD propagation rate (mm/minute) was calculated by the distance between the CSD elicitation site and recording site dividing by the time difference.

3.1.2 In vitro CSD model in chick retina

In order to explore if the role of P2X7R in CSD is of non-vascular origin, *in vitro* tissue using both chick retina and mouse brain slice were applied using a P2X7R

antagonist, which blocks both P2X7R channel and pore formation (chapter 6). These models were validated previously in our laboratory using drugs targeting the NR2A subunit of NMDA receptor, which showed inhibitory effects on propagation rate and magnitude of RSD and CSD (Bu et al., 2016a, Bu et al., 2017).

3.1.2.1 Chick retina preparation

Male Hyline Brown Chicks (Wuxi poultry Ltd, Jiangsu, China) were purchased at one-day old. As previously described (Wang et al., 2012), chicks were killed by decapitation. The right eye was immediately taken off and sectioned close to the equator. The posterior eyecup with retina attached was placed in a tissue chamber and submerged in perfused Ringer's solution (100 mM NaCl, 6 mM KCl, 1 mM $MgSO_4$, 30 mM NaH_2PO_3, 1 mM CaCl and 20 mM glucose; adjust pH to 7.35-7.45; 32°C) bubbled with 5% CO_2 and 95% O_2, at perfusion rate of 0.5 ml/min. The volume of perfused media was kept constant in the chamber by a suction pump (BT100-1L, Longer Pump Led, China) to ensure the placidity of the liquid surface. The tissue was initially incubated in Ringer's solution for 30 minutes to guarantee recovery from preparation.

3.1.2.2 RSD induction and intrinsic optical imaging

Repeated CSD was elicited at the eyecup edge by 1 μl of 0.1 M KCl with 20 minute interval for recovery. The tissue was illuminated for 5 ms per second with 2 Hz frequency by applying a high-power LED spotlight (625 nm peak wavelength, SLS-0307-A, Mightex, Pleasanton, CA, USA) and the reflected light was recorded with a monochrome camera (QIC-F-M-12, Media Cybernetics, Marlow, UK). Image sequences were taken at one frame per second for 3 min. The illumination

and camera capture were synchronized using the same external trigger (Figure 3.3). Image Pro Plus software (IPP7; Media Cybernetics, UK) was applied for image acquisition, storage and analysis.

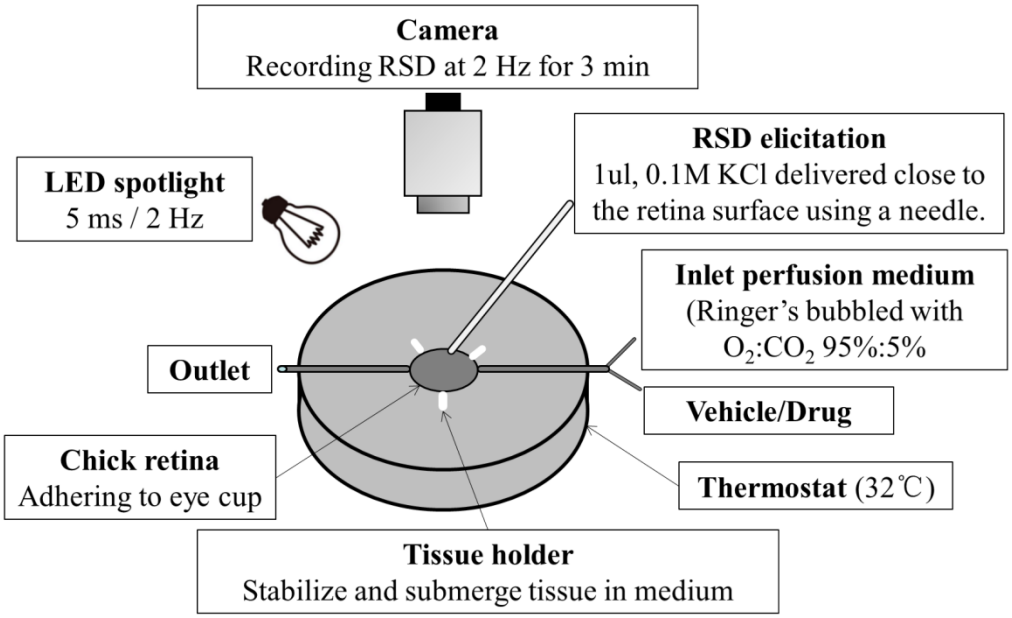

Figure 3.3 Diagram showing RSD model based on intrinsic optical imaging in chick retina.

3.1.2.3 Experimental design

In order to examine whether the inhibitory action of P2X7R inhibition could be also observed *in vitro*, RSD model was induced in the chick retina and the receptor antagonist, A740003 (Tocris), which inhibit both P2X7R ion channel and pore formation (Honore et al., 2006) was applied. Ten repeated RSD were induced by KCl, with the first two recorded RSD for initial Ringer's control (Figure 3.4). The perfusion medium was switched to 10 μM A740003 dissolved in 0.01% DMSO or DMSO vehicle group (diluted in Ringer's solution, 0.01%, n = 3) and six RSD were recorded undergoing drug/vehicle conditions. Finally, after drug removal, two more post-treatment RSD were recorded.

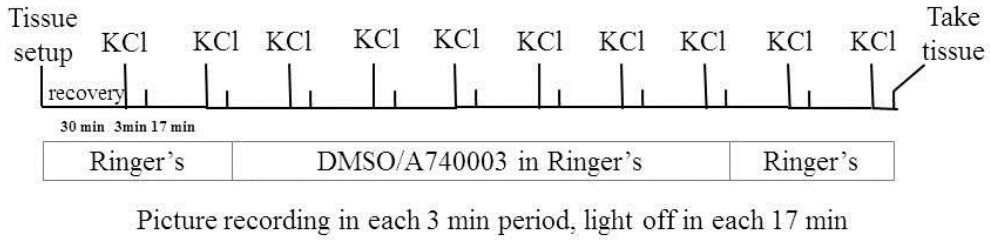

Figure 3.4 Experimental protocol to investigate effect of P2X7R antagonist A740003 on RSD in chick retina. Two groups were designed with DMSO control and A740003 drug group. In each experiment, ten repeated RSD was induced by KCl with 20 minute interval for tissue recovery. The first two RSD were initial Ringer's control. Six RSD undergoes DMSO vehicle or drug test, with the last two for post-treatment recording with Ringer's control (drug removal).

3.1.2.4 Image analysis

The signal of intrinsic optical imaging affects the intensity of diffusely reflected light and derives from characteristic physiological changes in the tissue surface. Changes in light scattering attributed to interstitial volume changes resulting from cellular swelling due to water and ion movement and neurotransmitter release.

For all image sequences, the same area of interest (AOI) parallel to the RSD wave was selected and delineated manually (Figure 3.5). The recorded signal is synchronous with cellular depolarization, which characterizes RSD (Farkas et al., 2008). The same AOI was selected among all sequence pictures under one experiment. The averaged grey level of the pixels constituting the AOI was plotted against time to obtain a RSD wave plot, from which the AUC was measured by image analysis as an index of RSD magnitude to quantify drug effects. In addition, the propagation rate was also determined to reflect the excitability of retinal tissue.

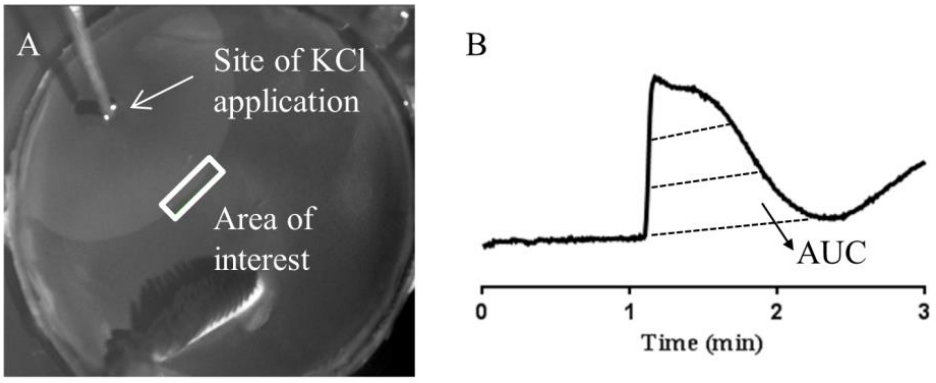

Figure 3.5 Representative image (A) and plot of RSD (B) wave induced by K^+ in the chick retina. The changes in gray level intensity within the selected area of interest (AOI) against time. The same AOI (rectangle within left picture) along RSD wave front was selected and used for all images of the sequence under study. From these plots, the AUC (gray level x minute) of RSD wave and propagation rate (mm/minute) were determined by image analysis to quantify drug effects.

3.1.3 In vitro CSD model in mouse brain slices

Mouse brain slice CSD model was further applied to examine if P2X7R inhibition suppresses CSD can be observed *in vitro* as mice are mammals and more close to human than chick; secondly, P2X7R are also expressed in mouse cerebral cortex (Jimenez-Pacheco et al., 2013).

3.1.3.1 Mouse brain slice preparation

C57BL6 male mice (15-25 g, Shanghai SLAC Laboratory Animal Corporation Ltd) were killed by rapid cervical dislocation. The brain was dissected and transferred quickly into pre-freeze NMDG-HEPES cutting solution (93 mM NMDG, 2.5 mM KCl, 1.2 mM NaH_2PO_4, 30 mM $NaHCO_3$, 20 mM HEPES, 25 mM glucose, 5 mM L-ascorbic acid, 2 mM thiourea, 3 mM sodium pyruvate, 10 mM $MgSO_4$, 0.5 mM $CaCl_2{\cdot}2H_2O$; bubbled with 95% O_2 and 5% CO_2; pH 7.4). The cerebrum was sectioned along the midline. A vibratome (7000 smz-2, Campden, Leicestershire, UK) was applied to prepare right coronal slices at 400 μm thickness in the cortical visual and somatosensory regions, where are considered to be highly associated with migraine pain (Lauritzen and Fabricius, 1995, Hadjikhani et al., 2001). Slices were maintained in the NMDG-HEPES cutting solution bubbled with 5% CO_2 and 95% O_2 at room temperature for 15 minutes and then transferred to Kreb's solution.

3.1.3.2 CSD induction in the mouse brain slice

A cortical slice (from bregma -1 to -3 mm) was placed in a chamber and submerged in Kreb's solution (25°C) at perfusion rate of 3 ml/minutes using a peristaltic pump (Reglo ICC, Ismatec; Wertheim, Germany) for at least 80 minutes to guarantee recovery from tissue dissection. CSD was induced in the IV-V layer of

somatosensory region of the slice by 80 second ejection of 33 µl of 260 mM KCl through a 200 µm diameter glass needle linked to a high-precision syringe pump (CMA/100, CMA/ Microdialysis; Solna, Sweden).

3.1.3.3 Experimental design

Series 1: To examine if blockade of the P2X7R channel and pore complex suppressing CSD could also be observed in the mouse brain slice, the following four groups were considered: (i and ii) A740003 at 0.1 and 0.3 µM (n = 6 in each group), at which concentration, the drug was selective for P2X7R (Honore et al., 2006); (iii and iv) Kreb's and 0.03% DMSO were used as the control and vehicle control, respectively (n = 6 in each group).

For this series, two CSD episodes were induced with 45 minutes interval for tissue recovery. Corresponding drugs or vehicles were perfused 45 minutes prior to the 2nd CSD induction for 1 hour (Figure 3.6 A).

Series 2: To examine if blockade of the P2X7R C-terminal domain could prevent the occurrence of CSD, a monoclonal rabbit anti-P2X7R antibody was examined in the mouse brain slice. Three groups were designed by incubation of brain slices with (i) the anti-P2X7R antibody at 3 µg/ml (n = 6) or (ii) the anti-IgG antibody at 3 µg/ml (n = 7) as a negative control or (iii) Kreb's as the blank control (n = 6).

For this series, two CSD episodes in each experiment were induced by KCl with 2-hour interval for tissue recovery. The brain slice was incubated in the chamber with the Kreb's solution or antibody for 1 hour starting from the end of the first CSD recording (Figure 3.6 B).

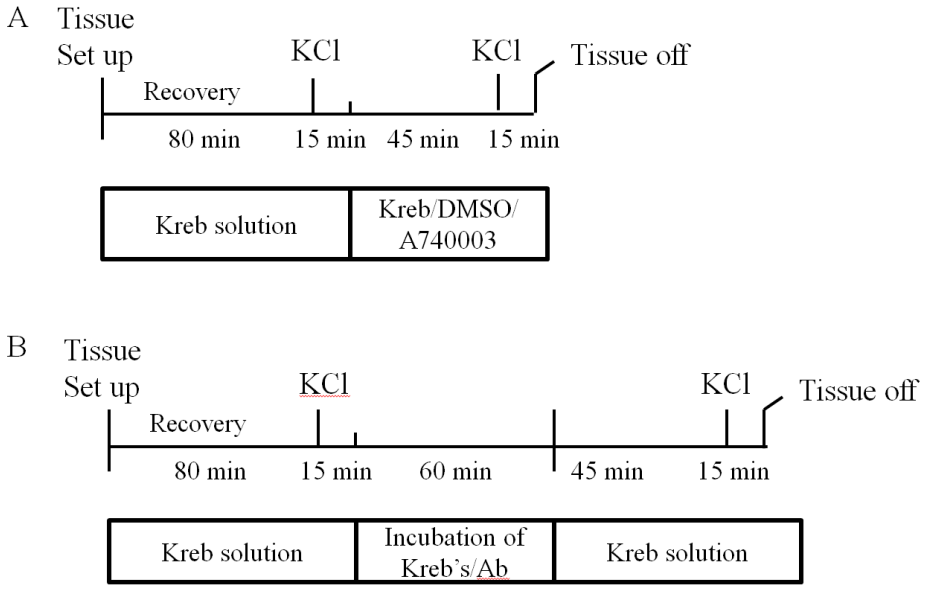

Figure 3.6 Experimental protocol to investigate the role of P2X7R in CSD in the mouse cortical slices. **A**. drug protocol: four groups were designed with Kreb's control group, DMSO vehicle group and P2X7R antagonist A740003 at 0.1 and 0.3 μM. **B**. The antibody protocol: three groups were designed with Kreb's control group, anti-IgG antibody negative group and anti-P2X7R antibody group.

3.1.3.4 Intrinsic optical imaging

The cortical slice preparation was illuminated for 50 ms at 2 Hz for 15 min, started as CSD was elicited, using a high-power LED spotlight (625 nm peak wavelength, SLS-0307-A, Mightex, Pleasanton, USA) driven by a computer controlled power supply (LED controller, SLC-SA04-US; Mightex, Pleasanton, USA). The reflected IOS changes in cortical slices were recorded with a charge-coupled device monochrome camera (Rolera-XR, ROL-XR-F-M-12, Qimaging, Surrey, Canada) at the maximum spatial resolution using Image Pro Plus software (IPP7; Media Cybernetics, UK). Camera exposure and illumination were synchronized by using an external trigger (TG1006, TTI, Cambridgeshire, UK).

3.1.3.5 Image analysis

Image analysis was as that was described in section 3.1.2.4 except the following: the AOI was selected in layers 4-6 of the somatosensory cortex that were distant from the site of KCl application (Figure 3.7). Additionally, CSD latency was also calculated and shown as the percentage relative to that of the first CSD wave to reflect cerebral cortex susceptibility to CSD. While CSD propagation rate was presented as the real value.

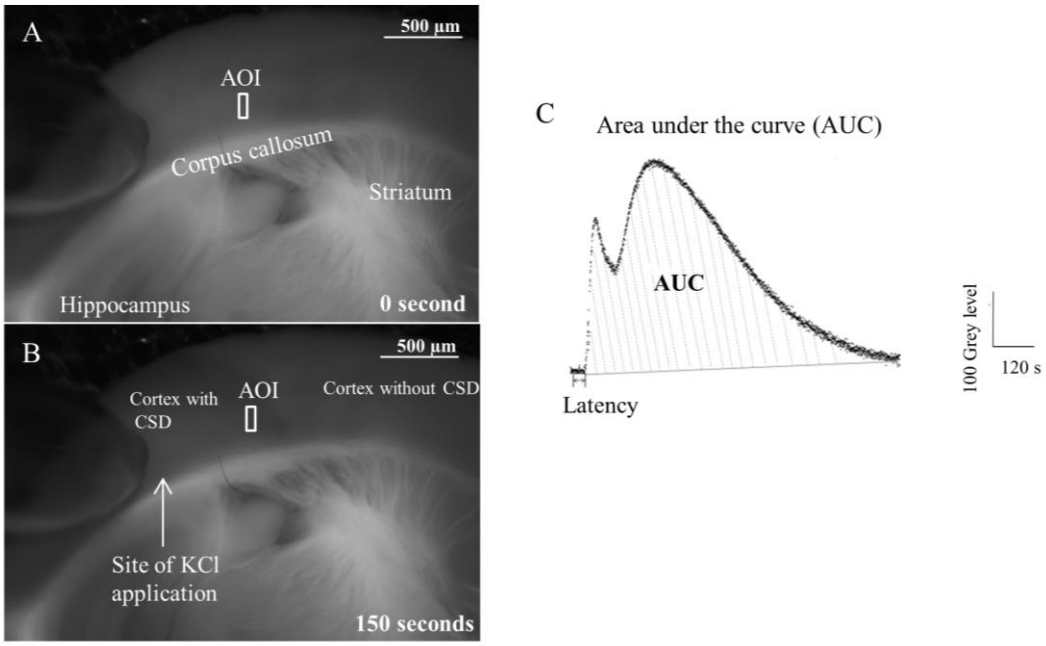

Figure 3.7 representative images before (A) and after (B) CSD, and plot of CSD wave (C) in the mouse cortical slice: the changes in gray level intensity within the selected area of interest (AOI) against time. The same AOI (rectangle within left picture) along CSD wave front was selected and used for all images of the sequence under study. From these plots, the area under the curve (AUC, gray level x minute) of CSD wave and propagation rate (mm/minute) and CSD latency (second. time interval required for eliciting depolarization from the start point of KCl application) were determined by image analysis to quantify drug effects.

3.2 Cell culture

Cell culture was applied to optimise the concentration and incubation time of miR-137 antagomir, which is chemically engineered oligonucleotide and functions to silence endogenous miR-137, before exploring the effects of silencing miR-137 on CSD and subsequent miR-137 target gene expression post CSD (chapter 4).

3.2.1 Culture SH-SY5Y cells

Human-derived neuroblastoma cell line SH-SY5Y was maintained in culture media [HAM's F12 (Sigma) and Minimum Essential Medium Eagle (Sigma) at a ratio of 1:1, supplemented with 10% foetal bovine serum (Sigma), 1% 100 mM sodium pyruvate (Sigma), 1% 200 mM L-glutamine (Sigma) and 100 U/ml penicillin/100 μg/ml streptomycin (Sigma)] at 37°C in a humidified atmosphere 5% CO_2 in T175 flask. To passage cells, cells were cultured to 70%-80% confluent, media was removed and cells were washed down with pre-warmed sterile PBS. Following removal of PBS, cells were washed over by 5 ml of pre-warmed 1x trypsin (Sigma) and then removed trypsin. The cells were incubated at 37°C for 3 minutes to be detached from flask bottom. Cells were then washed with 10 ml of pre-warmed culture media to neutralize the trypsin and pipetted into single cell suspension. Finally, 1 ~ 2 ml of cell suspension (approximately 1-2.5 million cells) was transferred into a new T175 tissue culture flask with 35~40 ml of culture media.

3.2.2 Cell counting

A heamocytometer was applied to count cell number per ml of media. First of all, both the coverslip and the counting surface of the haemocytometer were washed with 70% ethanol. There are 5 x 5 squares each containing 5 x 5 smaller squares on

the centre of the counting surface of the haemocytometer. To perform the cell count, single cell suspension was generated as described above, 20 µl of the cell suspension was dropped on the centre counting surface and covered by the coverslip. The counting surface was visualized under a microscope with 10 x objective. The cells within the 25 larger squares were counted including those in contact with right or top borders of the 25 squares and excluding those touching left or bottom borders. This area corresponds to 0.1 mm^3, so the number multiplied by 1 x 10^4 give the cell number in 1 ml (1 cm^3). Knowing the cell number per ml of media, the density could be calculated to seed cells as required in following experiments.

3.2.3 Freezing cell for storage and defrost frozen cells

For long time storage, cells were frozen in freezing media in liquid nitrogen. Cells were cultured to 70~80% confluent in T175 flask and passaged as described above, but instead of 10 ml culture media, 10 ml of freezing media (90% FBS and 10% DMSO) was used to wash cells from the flask bottom. Then the cell suspension split across cryovials with approximate 1.7 - 1.9 ml in each cryovial. The cryovials were then placed in a Mr Frosty with isopropanol at -80°C for at least 24 hours before transferring into liquid nitrogen for long term storage.

To defrost frozen cells, one cryovial was taken out from liquid nitrogen, defrosted in 37°C water bath until only a few ice crystals present and transferred into 10 ml pre-warmed 37°C culture media in T25 flask. Usually after three days, cells were grown to 70~80% confluent and passaged into T75 flask. Similarly, when cell were grown to70~80% confluent in T75 flask, they were passaged into T175 flask and ready for further experimental use.

3.2.4 Optimisation transfection in SH-SY5Y cell line

A concentration gradient of miR137 antagomir (1 nM, 10 nM, 15 nM, 50 nM and 100 nM)) and incubation time were carried out to optimise the most efficiency of transfection.

SH-SY5Y cells were seeded at 1 x 10^5 cells per well of a 24-well plate in 0.5 ml antibiotic-free media 24 hours before transfection. The transfection condition was listed as below:

Cell density (cells/well)	100,000	100,000	100,000	100,000	100,000
Antagomir/scramble	0.5 pmol	5 pmol	7.5 pmol	25 pmol	50 pmol
Lipofectamine 2000	2.5 µl	2.5 µl	2.5 µl	2.5 µl	2.5 µl
Final volume per well	500 µl	500 µl	500 µl	500 µl	500 µl
Antagomir/scramble conc.	1 nM	10 nM	15 nM	50 nM	100 nM
Ratio of oligo and lipofect	0.2 pmol/µl	2 pmol/µl	3 pmol/µl	10 pmol/µl	20 pmol/µl

The lipofectamine 2000 (Invitrogen) was mixed with oligonucleotides (miR137 antagomir or its negative scramble control) and incubated for 5 minutes at room temperature. The master mix added as list above and RNA was processed following 24 or 72 hours incubation to analyse subsequent gene expression of miR137 targets.

3.3 Gene expression analysis

3.3.1 RNA extraction

TRIzol reagent (Sigma-Aldrich) was applied to extract RNA following the manufacturer's instruction. Briefly, cortical tissue or cells was homogenized in TRIzol (1 ml per 50-100 mg) by tissue ruptor. 200 µl chloroform per 1 ml of TRIzol was added to each sample, shaken by hand vigorously for 15 seconds. After

5 minutes incubation at room temperature, samples were centrifuged at 12,000 xg for 15 minutes at 4°C, separating phase into three layers: RNA-containing colourless aqueous upper layer, a thin middle interphase layer and a bottom DNA-and-protein-containing red organic layer. The upper layer was carefully transferred into a new microfuge tube. 500 µl of isopropanol per 1 ml of Trizol was added to each sample and incubated for 10 minutes at room temperature, followed by centrifugation at 12,000 xg for 10 minutes at 4°C. After discarding the supernatant, RNA pellet was purified by adding 1 ml 75% molecular grade ethanol (per 1 ml TRIzol used in the initial step). Samples were shake and centrifuged at 7,500 xg for 5 minutes at 4°C. The supernatant was discarded and the RNA pellet was air dried for 20 to 30 minutes at room temperature. Finally, the RNA pellet was re-suspended in 30-50 µl nuclease free water and incubated on a heat block at 55°C for 15 minutes. RNA samples were placed on ice for later quantification and cDNA synthesis or stored at -80°C.

3.3.2 RNA quantification

RNA concentration was measured by Nanodrop 2000c (Thermo Scientific). The sample reader was washed with nuclease free water and dried with KimWipe. Following the instruction of the software, the Nanodrop was set to RNA. 1 µl of elution nuclease free water was loaded and set as blank. Then 1 µl of sample was loaded and the absorbance measured. The absorbance of UV light by nucleic acid at 260 nm depends on their concentration. After reading completion, the RNA concentration in ng/µl was obtained. The quality of the RNA was also assessed by the Nanodrop through measuring the ratios of A260/A280 and A260/A230;

expected values for high RNA purity are approximately 2.0 and 2.0-2.2, respectively.

3.3.3 First strand cDNA synthesis

The GoScript Reverse Transcription System (Promega) was used for first strand cDNA synthesis from total RNA following the manufacturer's protocol. Briefly, 1 µg of RNA was used for each sample in the reverse transcriptase reaction, mixed in a PCR tube with the following components:

Component	Volume
RNA (up to 1 µg)	x µl
Random primers (0.5 µg/reaction)	1 µl
Oligo(dT)$_{15}$ Primers (0.5 µg/reaction)	1 µl
Nuclease free water	x µl
Final volume	5 µl

The mixture was incubated at 70°C for 5 minutes, immediately cooled down on ice, and added the following reverse transcription mix to a final 20 µl reaction volume.

Component	Volume	Final concentration
GoScript 5X reaction buffer	4 µl	1x
$MgCl_2$ (25 mM)	4 µl	5 mM
PCR nucleotide mix (10 mM of each dNTP)	1 µl	0.5 mM
Recombinant RNasin Rinonuclease inhibitor (40 U/µl)	0.5 µl	1 U/µl
GoScript Reverse Transcriptase	1 µl	-
Nuclease free water	4.5 µl	-
Final volume	15 µl	

The final reaction mixture was incubated as following: at 25°C for 5 minutes for primer annealing; at 42°C for 60 minutes for extension; finally at 70°C for 15 minutes to inactivate the reverse transcriptase. The cDNA was stored at -20°C for later use.

3.3.4 PCR primer designing

The online primer-designing tool Primer 3 was used to design PCR primers. A list of recommended PCR primers for amplification of the sequence of interest was generated based on appropriate GC% content, melting temperature and potential self-complementarity. Generally, primers were picked with 18-25 nucleotides in length, 58-65°C melting temperature and 40-60% GC content. The primer specificity was further determined by *In-Silico PCR* tool available from the UCSC Genome browser (http://genome.ucsc.edu/cgi-bin/hgPcr). Primers were ordered from Sangon Biotech (Shanghai) Co., Ltd and listed as below:

Gene	Forward (5'-3')	Reverse (5'-3')
ACTB	CTGTCCACCTTCCAGCAGAT	CGCAGCTCAGTAACAGTCCG
CGRP	AACCTTGGAAAGCAGCCCAGGCATG	GTGGGCACAAAGTTGTCCTTCACCA
c-jun	AGCCAAGAACTCGGACCTTC	TCGGTGTAGTGGTGATGTGC
Gabra2	CCAGGATGACGGAACATTGC	GGAAAGTCCTCCAAGTGCATTG
GAD1	TCTCCTGGGGGAGCCATATC	TGAAGAGGACCAGTTTGGGC
Grin2a	CAGCAGGACTGGTCACAGAA	TTCCCTGTCCTTGAGGCTTA
IL-1β	GCTGTGGCAGCTACCTATGTCTTG	AGGTCGTCATCATCCCACGAG
MIR137HG	CAGAGGAAAGCACTGGGAGA	CACCCAAGAATACCCGTCAC
NKB	CCACCCCTGCTTCGGAGACT	GATATGGGGGTAGAGGCTGTTCA
PPIA	TTGCTGCAGACATGGTCAAC	TGTCTGCAAACAGCTCGAAG
RELN	CGTCCTAGTAAGCACTCGCA	TATCGCCTAAGCGACCTTCG
REST	AGCGAATACCACTGGCGGAAACA	AATTAAGAGGTTTAGGCCCGTTG
REST4	AGCGAATACCACTGGCGGAAACA	TCACCCAACTAGATCACACT
Tac 1	CGACCGCAAAATCCAACATG	AAAGAACTGCTGAGGCTTGG
VIP	CAGAAGCAAGCCTCAGTTCC	CATTCTCCGCTAAGGCATTC

3.3.5 Semi-quantitative PCR analysis

PCR analysis was performed using cDNA template on Veriti 96-well Thermal cycler (Applied Biosystems™) using DNA polymerase (TaKaRa). The DNA polymerase master mix is list below:

Component	Volume (n=1)	Final concentration
TaKaRa Taq (5 U/µl)	0.15 µl	0.025 U/µl
10x PCR buffer	3 µl	1x
dNTP mixture	2 µl	0.66 mM
cDNA template	X µl	-
Forward primer	0.5 µl	0.33 µM
Reverse primer	0.5 µl	0.33 µM
Nuclease free water	X µl	-
Final volume	30 µl	

The amount of cDNA template used varied for each primer set depending on the abundance of the target for amplification. The thermal cycling conditions were as follows:

	Cycling Program	Cycles
Initial denature	95°C for 30 s	1
Denature	95°C for 30 s	
Annealing	60°C for 30 s	30
Extension	72°C for 1 min	
Final extension	72°C for 10 min	1

The analysis of PCR product was performed on 1% agarose gels supplemented with 1:10000 dilution GelRed (Biotium). The voltage and time for gel running depended on the DNA fragment size to achieve adequate separation of the bands. The DNA was visualised using a UV transillumintor.

3.3.6 Quantitative PCR (qPCR)

qPCR was performed using GoTaq qPCR Master Mix (Promega) following the manufacturer's instruction. The reaction component is:

Component	Volume (n=1)	Final concentration
2X GoTaq qPCR Master Mix	5 µl	0.025 U/µl
cDNA template	X µl	-
Forward primer	0.1 µl	0.33 µM
Reverse primer	0.1 µl	0.33 µM
Nuclease free water	X µl	-
Final volume	20 µl	

Analysis was performed on 7500 fast Real-Time PCR system (Applied Biosystems™) with the following thermal cycling conditions:

	Cycling Program	Cycles
Hot-start Activation	95°C for 2 min	1
Denaturation Anealing/Extension	95°C for 15 s 60°C for 1 min	40
Dissociation	60-95°C	1

Relative gene expression was calculated using the Pfaffl method with reference genes, PPIA and β-actin (ACTB), which were most commonly used in CSD condition (Wang et al., 2016b).

$$ratio = \frac{(E_{target})^{\Delta Ct_{target}(control-sample)}}{(E_{ref})^{\Delta Ct_{ref}(control-sample)}}$$

3.4 Protein expression analysis

3.4.1 Protein extraction

Total protein was extracted from (i) sham and CSD ipsilateral cerebral cortices of rats to analyse how CSD affect specific protein expression 3 hour and 24 hour post CSD; (ii) chick retina to test the presence of P2X7R in chick retina. The tissue was homogenized in the presence of protease inhibitor (Roche). The homogenate was

centrifuged at 13,000 rpm for 10 minutes at 4°C. The supernatant was aliquot and stored at -80°C.

3.4.2 Bicinchoninic acid (BCA) assay

Protein concentration was determined by BCA kit (Beyotime) using bovine serum albumin (BSA) as standard curve. Briefly, a series of dilution BSA standard and protein extract with TBS were prepared to a total 20 μl/well in a 96-well plate with duplicates. BCA working solution was prepared with solution A and B at 50/1 ratio and 200 μl was added into each well. The plate was sealed and incubated in water bath at 37°C for 20 minutes. The absorbance was measured by a spectrophotometer with wavelength at 562 nm. The standard curve was prepared by plotting the mean blank-corrected 562 nm measurement for each BSA standard versus its concentration. The protein concentration of each sample was calculated according to this standard curve.

3.4.3 Western blot

Western blot was applied to (i) determine the protein level of NR2A and $GABA_A$ α2; (ii) determine the presence of P2X7R in chick retina with rat cortex as a positive control, as P2X7R was reported to be expressed in rat cortex (Franke et al., 2004). Protein samples are separated by 10% SDS-PAGE and transferred onto nitrocellulose membrane. 5% non-fat milk in TBST (20 mM Tris, 150 mM NaCl, 1‰ Tween 20; pH 7.6) was applied to block non-specific binding. The membrane was then incubated with rabbit anti-NR2A antibody (1 in 2000 dilution, ab124913, abcam) or anti-$GABA_A$ receptor α2 antibody (1 in 500 dilution, ab72445, abcam) or anti-P2X7R antibody (1 in 1000 dilution) overnight at 4°C with gentle rocking.

Excess primary antibody was washed three times by TBST and then incubated with IRDye 800CW Donkey anti-Rabbit IgG secondary antibody (1 in 5000 dilution, 926-32213, LI-COR) at room temperature for 1 hour with gentle rocking. The membrane was then washed three times by TBST for later detection. The membrane was then scanned by the Odyssey scanner with selection of channel 800.

The membrane was then stripped by 0.2 M NaOH for 15 minutes at room temperature to further detect β-actin, which was used as a reference. Then the membrane was washed out by TBST and the same process was carried out was described above starting from non-specific blocking with 5% non-fat milk in TBST. Finally, the membrane was scanned and saved as a tif format. The density and volume of signal each band was analysed quantified using Image J software.

3.5 Data presentation and statistical analysis

All data was shown as mean ± SEM. For the image data and the *in vivo* electrophysiological data relevant P2X7R project, abnormal distribution of the data was confirmed using Shapiro-Wilk test and one-tailed Mann-Whitney U test was applied to compare each parameter between two independent groups within each data set, as previous publication has showed suppressive effects of blockade of P2X7R on CSD (Chen et al., 2017b).

Correlation between CSD parameters was analysed. Abnormal/normal distribution of these data was checked using Shapiro-Wilk test. Abnormal distribution data was analysed by Spearman's correlation, while normal distribution data was analysed by Pearson's correlation, with an "r" value ranging from +1 to -1. A value of 0 indicates that there is no association between the two variables. A value greater

than 0 indicates a positive association. A value less than 0 indicates a negative association. *$p < 0.05$, **$p < 0.01$ ***$p < 0.001$, and ****$p < 0.0001$ indicate statistical significance.

All qPCR data were analysed using relative fold change (Pfaffl method). If data obeys normal distribution, two-tailed unpaired t-test was used for comparison between sham and CSD groups, and two-tailed paired t-test was used for comparison between ipsilateral and contralateral hemispheres within each group. While, if data doesn't obey normal distribution, unpaired two-tailed Mann-Whitney U-test and paired two-tailed Wilcoxon test were used respectively. Both PCR gel bands and western blot bands were quantified using Image J software and normalised to β-actin. Abnormal distribution of these data was confirmed using Shapiro-Wilk test. Unpaired two-tailed Mann-Whitney U-test and paired two-tailed Wilcoxon test were used as described above for different comparison. *$p < 0.05$, **$p < 0.01$ ***$p < 0.001$, and ****$p < 0.0001$ indicate statistical significance.

Power analysis was finally carried out using GPower 3.1.9.2 to estimate the minimum number of samples required to detect trends with a given degree of confidence. The input parameters were set as the following: the significance level α 0.05 and power (the likelihood of rejecting null hypothesis) 0.8; the effect size was determined by sample size and standard deviation.

Chapter 4

The REST pathway as a potential mechanism in CSD

4.1 Introduction

CSD is associated with alterations of gene expression (Shen and Gundlach, 1999, Shen et al., 2003, Faraguna et al., 2010), which can be modified by the changes in transcriptional repressors or enhancers, subsequently influencing neuronal phenotype and behavior. Altered REST expression is associated with physiological brain functions, but it is also highly responsive to brain injuries (Qureshi and Mehler, 2011, Warburton et al., 2016, Zhao et al., 2016). In such scenarios, differential spliced isoforms of REST are observed and distinct properties have often been attributed to the individual isoforms (Chen and Miller, 2013). Similarly, expression of REST truncated isoform REST4 is also reported to be associated with disease progression, such as epilepsy (Spencer et al., 2006, McClelland et al., 2014), which has moderate co-morbidity with migraine (Deprez et al., 2007, Sowell and Youssef, 2016).

In vitro, in human cells, REST has been demonstrated to regulate MIR137 expression, a microRNA involved in schizophrenia, in part via an internal promoter termed Imir137 (Warburton et al., 2014). A second promoter utilized by human MIR137 is upstream of MIR137 host gene (MIR137HG), which encodes for the full-length precursor mRNA. The mature miRNA-137 (miR-137) is implicated in several neurological disorders and regulates the dynamics between neuronal proliferation and differentiation during the different stages of neural development (Silber et al., 2008, Szulwach et al., 2010). Reduction in miR-137 expression leads to deregulation of genes involved in synaptogenesis and neuronal transmission (Strazisar et al., 2015). Variants within or upstream of genes regulated by miR-137,

in combination with MIR137HG risk variants, influence grey matter concentration in schizophrenia-related central nervous system regions (Wright et al., 2016).

REST and miR-137 target genes have been previously associated with epilepsy, schizophrenia, stroke and migraine (McClelland et al., 2014, Spencer et al., 2006, Wright et al., 2016, Zhao et al., 2016, Bu et al., 2016a). These include genes encoding for the P/Q type calcium channel (Antoniotti et al., 2016), N-methyl-D-aspartate (NMDA) receptor (Noh et al., 2012, Zhao et al., 2013) and neuropeptides, such as substance P (Quinn et al., 2002), which are implicated in migraine pathogenesis (Martins et al., 2017) and traumatic brain injury (TBI) (Vink et al., 2017); whilst inhibition of NMDA receptors and its major NR2 subtypes have been shown to suppress the genesis and propagation of CSD (Bu et al., 2016a, Peeters et al., 2007, Shatillo et al., 2015b). There are several putative REST target genes. RELN (Reelin), JUN (Jun oncogene) and GAD1 (glutamate decarboxylase 1) contained a predicted REST binding site and were regulated in response to sodium valproate (Warburton et al., 2015), which was an anticonvulsant drug applied in migraine treatment and reported to suppress the frequency of CSD *in vivo* (Ayata et al., 2006). Other putative REST target genes include VIP (vasoactive intestinal peptide), Tac 1 (substance P) and NKB (neurokinin B), which are clinically associated with migraine or epilepsy (Fusayasu et al., 2007, Nakano et al., 1993).

REST signalling pathway is important to modulate neuronal function and is implicated in neurological dysfunctions. Most importantly, my UoL supervisor Professor John Quinn's lab found that the binding of REST to the internal MIR137 (rImir137) promoter is markedly reduced 24 hours post multiple CSD in rats (see *Appendix 1,* Figure A) (Warburton, 2015 pp 277-281), suggesting REST/MIR137

signals may be involved in the process of multiple CSD. In this chapter, whether REST is involved in CSD was examined.

4.2 Objectives

(i) To address whether multiple CSD events alter the gene expression of REST and its truncated REST isoform REST4, as well as MIR137HG in rat cortex.

(ii) To investigate whether the reduced REST binding to rImir137 promoter affect subsequent miR137 target gene Grin2a expression.

(iii) To investigate whether silencing miR-137 by antagomir regulate CSD.

(iv) To address whether the change of REST variants in response to multiple CSD affect subsequence expression of its target genes.

4.3 Results

4.3.1 Successful induction of CSD by KCl

CSD was induced by KCl application in the rat cerebral cortex in order to explore if multiple CSD alters mRNA levels of REST, REST4, in rats. Changes in the DC potential were observed in ipsilateral motor cortices of all rats, indicating successful CSD induction at the somatosensory cortex (Figure 3.1 A & C). In the 3 hour series, 4 or 5 CSD waves were observed in all rats with 20 minutes KCl application. In the 24 and 72 hour series, typically one CSD wave was induced by each KCl application for all the 5 episodes, however two CSD waves were occasionally observed in 2/8 rats due to individual variation in cortical susceptibility to KCl stimuli. In the sham control groups, ACSF application did not induce CSD in any rats at any time point.

4.3.2 Multiple CSD effect on the mRNA levels of REST, REST4 and MIR137HG in ipsilateral cortices of rats at 3 hours

In order to address if multiple CSD alters gene expression of REST, REST4 and MIR137HG, I generated cDNA from both contralateral and ipsilateral cortices of sham and CSD rats and measured the respective mRNA levels at different time points post-CSD. Expression of REST, REST4 and MIR137HG were first identified by both RT-PCR and qPCR at 3 hour post CSD.

The RT-PCR gel data showed that there were no significant changes between the contralateral and ipsilateral cortices of sham group for all of the three genes (Figure 4.1A & B), indicating that surgery did not affect their mRNA levels. Also no changes were observed between sham contralateral and CSD contralateral group (Figure 4.1A & B), suggested that the CSD did not alter mRNA levels of REST, REST4 and MIR137HG on contralateral side. Compared to the sham ipsilateral group, CSD did not alter the gene expression of these three genes (Figure 4.1A & B), although there was a slight but insignificant increase of REST4 mRNA level in CSD ipsilateral group (Figure 4.1A & B).

Consistent with RT-PCR data, the increase trend of REST4 mRNA level by CSD were observed by qPCR (2.73 fold change when compared to the sham group) (Figure 4.1C). Also, no changes were observed by qPCR in the mRNA level of both REST and MIR137HG at 3 hour post CSD.

Based on the power analysis for REST4 gene expression at 3 hours, it could be able to reach significance with a sample size of four.

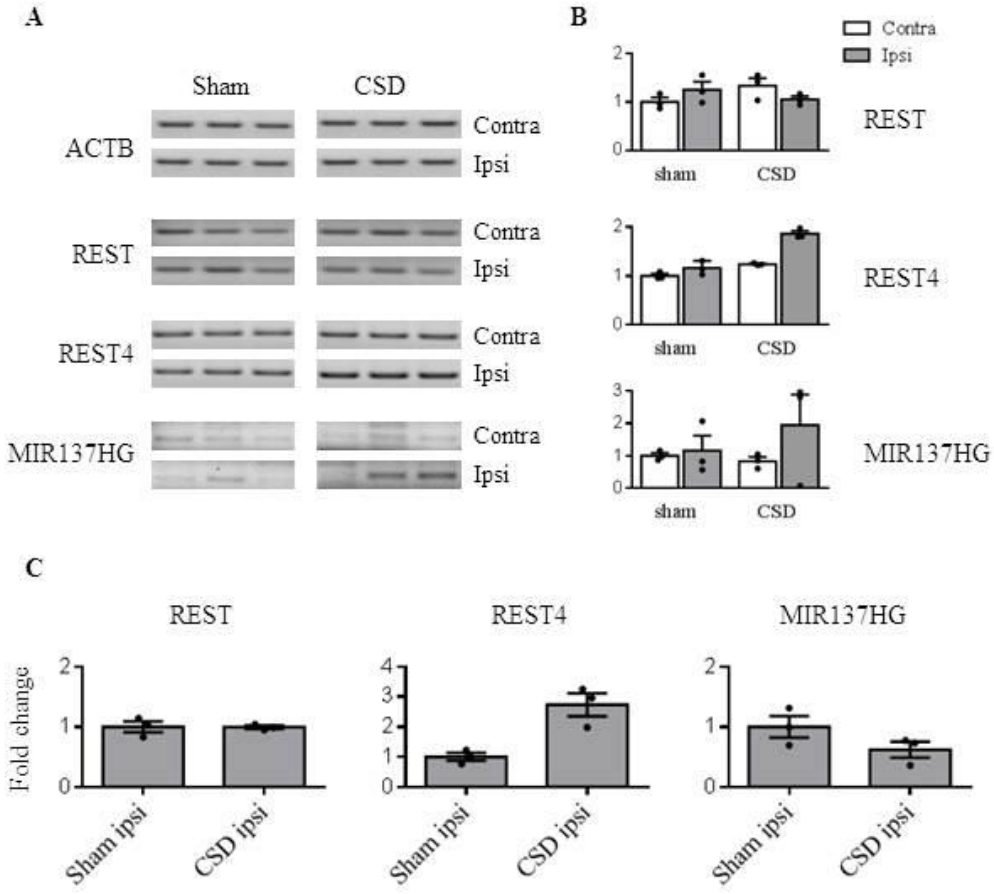

Figure 4.1 CSD increased mRNA level of REST4, but not REST and MIR137HG in ipsilateral cortices of rats at 3-hour post CSD. (A) RT-PCR analysis of REST, REST4 and MIR137HG in the rat from both contralateral and ipsilateral cerebral cortex of sham and CSD group; (B) Image J semi-quantitative analysis of RT-PCR data normalised to ACTB in CSD group compared with sham group. (C) qPCR analysis of REST, REST4 and MIR137HG in the rat ipsilateral cerebral cortex from sham and CSD group. Comparisons between sham and CSD groups were done using unpaired two-tailed Mann-Whitney U-test; Comparisons between ipsilateral and contralateral hemispheres within each group were done using paired two-tailed Wilcoxon test.

4.3.3 Multiple CSD effect on the mRNA levels of REST, REST4 and MIR137HG in ipsilateral cortices of rats at 24 and 72 hours

The mRNA level of REST, REST4 and MIR137HG were also identified by RT-PCR at 24 and 72 hour post CSD. Similar as 3 hour post CSD, the surgery also did not alter the gene expression of these three genes 24 and 72 hour post CSD, as no significant difference was observed between sham contralateral and ipsilateral group (Figure 4.2). The increase trend of REST4 mRNA was returned to basal level at 24 and 72 hour post CSD (Figure 4.2 A, B & C). Additionally, no significant changes in ipsilateral REST and MIR137HG mRNA levels were observed when compared to the sham group at both 24 hours and 72 hours post-CSD (Figure 4.2 A, B & C).

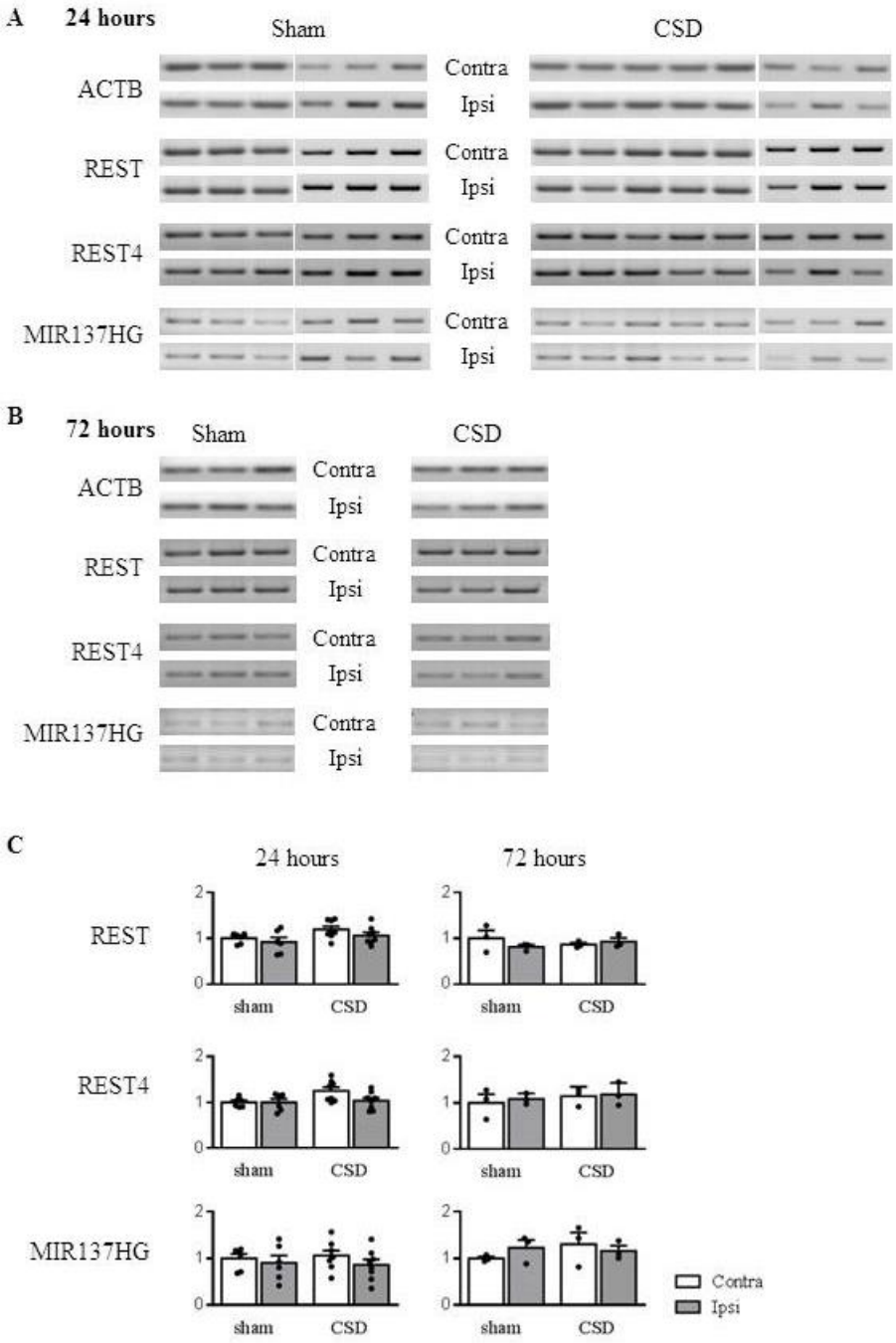

Figure 4.2 CSD did not alter the mRNA level of REST, REST4 and MIR137HG in ipsilateral cortices of rats at 24 and 72 hour post CSD in rats. RT-PCR analysis of REST, REST4 and MIR137HG in the rat both contralateral and ipsilateral cerebral cortex from sham and CSD group 24 (A) and 72 hours (B) post CSD in responsive order. (C) Image J semi-quantitative analysis of RT-PCR data normalised to ACTB in CSD group compared with sham group. Comparisons between sham and CSD groups were done using unpaired two-tailed Mann-Whitney U-test; Comparisons between ipsilateral and contralateral hemispheres within each group were done using paired two-tailed Wilcoxon test.

4.3.4 Reduction of Grin2a gene expression by multiple CSD

As REST binding over the rImir137 promoter was modulated in response to multiple CSD in rat cortical tissue (Figure A1), I further investigated if there is any change in the expression of miR-137 target gene, Grin2a. This was examined in both contralateral and ipsilateral cortices of sham and CSD treated rats (Figure 4.3). There was no significant change in Grin2a mRNA level between contralateral and ipsilateral cortices of sham rats at all time points analysed post ACSF application, indicating surgery did not alter Grin2a gene expression (Figure 4.3). Grin2a gene expression was not altered 3 hours post-CSD; However, a significant reduction of ipsilateral Grin2a mRNA levels was observed at 24 hours after CSD when compared to that of the sham ipsilateral cerebral cortex (p = 0.0357) and a reduction trend when compared with CSD contralateral cerebral cortex (p = 0.0625) (Figure 4.3). This reduction was no longer apparent at 72 hours post-CSD.

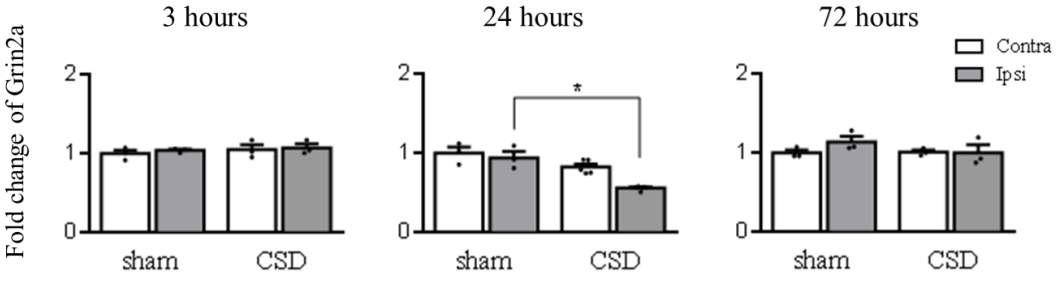

Figure 4.3 Gene expression of miR-137 target gene, Grin2a, at 3, 24 and 72 hour post-CSD in rat ipsilateral cerebral cortex of sham and CSD rats. CSD reduced Grin2a mRNA expression in ipsilateral cerebral cortex of rats 24 hours, but not 3 and 72 hours post-CSD (n = 3 in each group except n = 5 in 24 hours CSD group), Comparisons between sham and CSD groups were done using unpaired two-tailed Mann-Whitney U-test; Comparisons between ipsilateral and contralateral hemispheres within each group were done using paired two-tailed Wilcoxon test. *$p < 0.05$.

4.3.5 Optimisation of mir137 antagomir

Mir137 antagomir was applied to explore the effects of inhibition of miR-137 on CSD. Before application to our CSD model, the cell line SH-SY5Y was used to address the potential time points and concentration of the mir-137 antagomir as described in *section 3.2.4* that could be used to optimise the study in CSD. Unfortunately, this antagomir did not work at all concentration and incubation times in cell line. Also, the level of miR-137 failed to be examined. All the relevant reagents were delivered from Liverpool to Suzhou. Due to some custom issues on the import of biological samples and reagents, there was a 2-month delay. All of the dry ice, which was used for keep reagents cold, was used up and this is likely to have affected the loss of efficacy of the reagents. This experiment was not pursued further.

4.3.6. Multiple CSD effect on REST potential target genes

PCR was carried out to investigate how multiple CSD alter subsequent expression of a panel of REST putative target genes, Tac 1, NKB, VIP, GAD1, RELN and c-JUN.

To align our data with our collaborator Alix Warburton for paper publication purpose, RT-PCR was carried out to analyse Tac 1, NKB and VIP gene expression at time points post 15 min, 3 hour, 24 hour and 72 hour post CSD. For all of these genes, there was no difference between sham contralateral and ipsilateral group (Figure 4.4), indicating that the surgery did not affect their gene expression. Their gene expressions were also not altered in response to multiple CSD compared with sham ipsilateral cerebral cortex at all time points I tested (Figure 4.4).

To complement this data, qPCR was also used to analyse the effects of CSD on other REST putative targets, GAD1, RELN and c-JUN at time points 3 hour and 24 hours. Similar with above target genes, surgery did not affect their gene expression by comparing sham contralateral and ipsilateral cerebral cortex (Figure 4.5). The gene expression of both RELN and C-JUN were not altered at 3 hour and 24 hour post CSD (Figure 4.5 B & C). However, CSD slightly increased (1.5 fold) GAD1 gene expression in the ipsilateral group at 24 hours, compared with sham ipsilateral group (Figure 4.5 A).

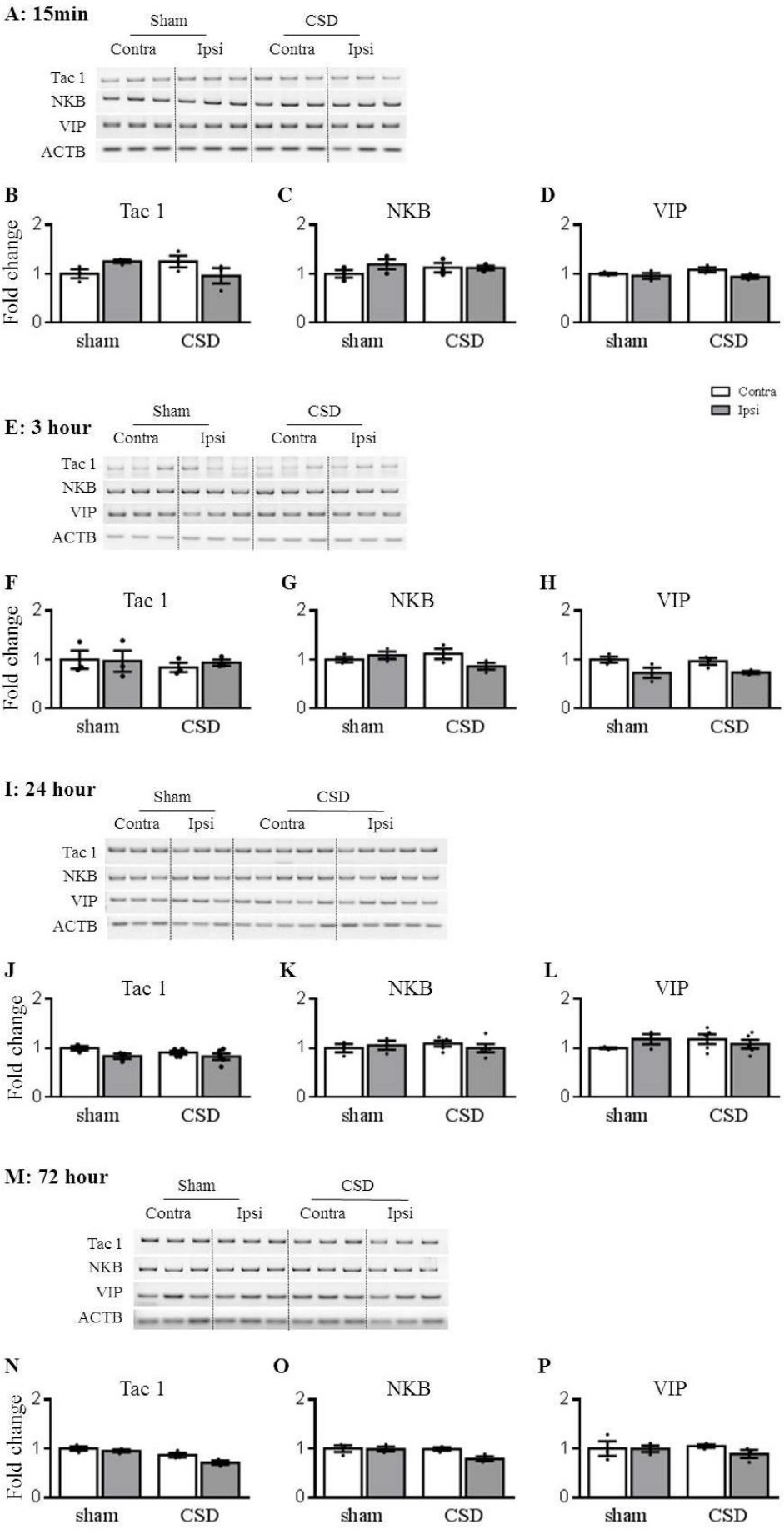
A: 15min
Sham
CSD
Contra
Ipsi
Contra
Ipsi
Tac 1
NKB
VIP
ACTB
B
Tac 1
C
NKB
D
VIP
Fold change
2
1
0
sham
CSD
Contra
Ipsi
E: 3 hour
F
G
H
I: 24 hour
J
K
L
M: 72 hour
N
O
P

Figure 4.4 Gene expression profiling of REST target genes at different time points post CSD. RT-PCR analysis of Tac1, NKB and VIP in the rat contralateral and ipsilateral cerebral cortex from sham and CSD group 15 minutes (A) 3 (E), 24 (I) and 72 hours (M) post CSD in responsive order. (B-D, F-H, J-L, N-P) showed the relative image J semi-quantitative analysis of RT-PCR data nomalised to ACTB in each group compared with sham contralateral group. (n = 3 in each group except n = 5 in 24 hours CSD group). Comparisons between sham and CSD groups were done using unpaired two-tailed Mann-Whitney U-test; Comparisons between ipsilateral and contralateral cortex within each group were done using paired two-tailed Wilcoxon test.

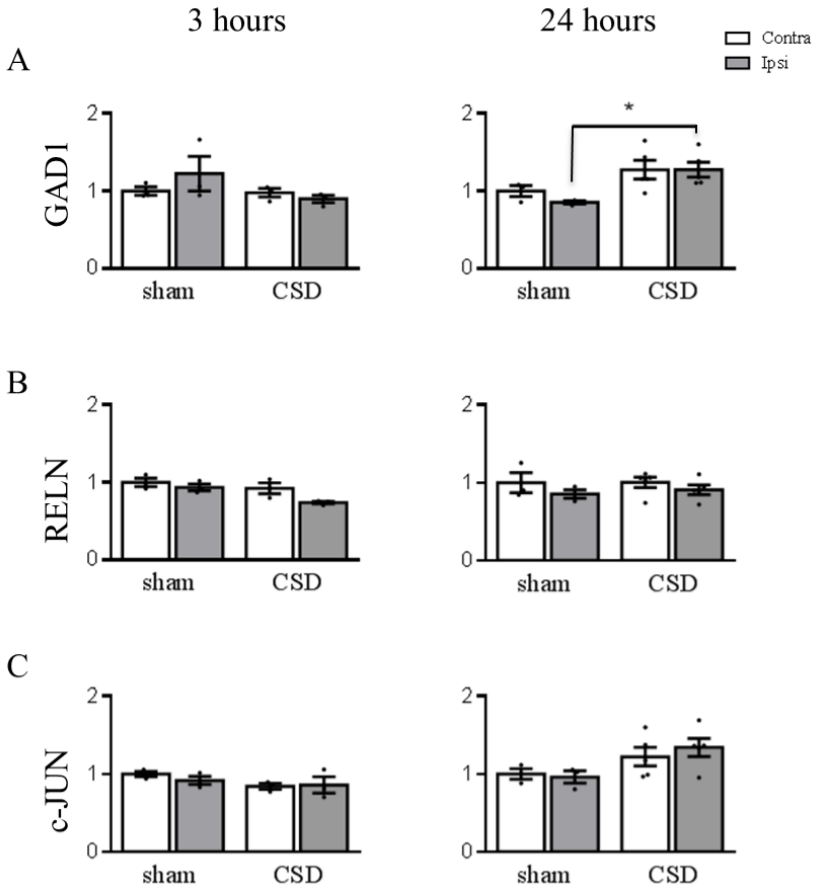

Figure 4.5 Gene expression profiling of REST target genes 3 & 24 hrs post CSD. Q-PCR analysis of putative NRSF target genes in rat cerebral cortex following CSD. Data were analysed by unpaired t-test between sham and CSD group (n = 3 in each group except n = 5 in 24 hours CSD group), Comparisons between sham and CSD groups were done using unpaired two-tailed Mann-Whitney U-test; Comparisons between ipsilateral and contralateral hemispheres within each group were done using paired two-tailed Wilcoxon test. *$p < 0.05$.

4.4 Discussion

Our results did not support the role of REST or REST4 in CSD, as multiple CSD events did not alter gene expression of REST and REST4 in cerebral cortices of rats, although a slight but insignificant up-regulation of REST4 was observed. Combining with the fact that CSD reduced REST binding to the rImir137 promoter in the ipsilateral cerebral cortex of rats (Figure A1) (Warburton, 2015 pp 277-281), further studies on increasing sample number are required for statistical significance to confirm the role of REST4 in multiple CSD-associated TBI and stroke.

Although did not reach significant, up-regulation trend of ipsilateral REST4 gene expression was observed in all the 3 rats at 3 hours after CSD, which was disappeared at 24 hours and 72 hours. This apparent elevation trend in ipsilateral cortices is unlikely to be related to the direct effect of KCl because using the same protocol, our lab previously showed that CGRP mRNA levels were similarly increased in multiple cortical regions (frontal, motor, somatosensory, and visual cortices) (Wang et al., 2016b), indicating that the elevated expression is attributed to CSD, rather than depolarization in the immediate area of KCl application. Monitoring changes in gene expression at the 3 specific time points may have missed some of the transient changes following CSD, which may at least partially account for that the transient elevation trend of REST4 at 3 hours post-CSD did not reach significance. It is clear from the literature that the time course of transient expression *in vivo* in the brain for many genes is quite distinct from that in tissue culture (Spencer et al., 2006). Another possibility account for this insignificance is due to small sample number (n = 3). Further power analysis of REST4 gene expression at 3 hours shows that it should be able to reach significance with a

sample size of four. Increasing sample number needs to be considered in the further work. Nevertheless, these data does allow us to follow the temporal expression *in vivo* after multiple CSD events.

Unlike REST4, REST mRNA levels did not show change trend in response to multiple CSD episodes. This is contrast to that reported previously that REST expression is highly responsive to epilepsy (Spencer et al., 2006). It is possible that REST gene expression is less dynamic than REST4 as previously observed in an epilepsy model (Spencer et al., 2006). The mechanism to account for the differential changes of these gene expression is unknown, however both transcriptional and post transcriptional mechanisms have been postulated.

As a potential consequence of reduced REST binding to rImir137 promoter (Figure 1A) (Warburton, 2015 pp 277-281), miR-137 target gene, Grin2a was significantly reduced 24 hours post-CSD. Grin2a encoded protein NR2A is an important subunit of NMDA receptor that is widely expressed in the brain, which functions in a variety of neurological diseases such as memory and post-stroke depression (Zhao et al., 2013, Allyson et al., 2010, Ali and Meier, 2009). Increasing evidence supports promising clinical use of drugs that selectively inhibit NR2A containing receptors with a lesser neurotoxicity than those fully block NMDA receptors and drugs antagonizing NR2A-containing NMDA receptors have been proven as effective CSD suppression compounds both *in vitro* and *in vivo* (Wang et al., 2012, Bu et al., 2016a). The fact that Grin2a mRNA expression was down-regulated at 24 hours post-CSD suggests multiple CSD suppresses Grin2a transcriptional activity. The Grin2a has been predicted as a miR-137 target gene (Wright et al., 2013, Strazisar et al., 2015) and the reduction of Grin2a corresponds with reduced REST

binding to rImir137 promoter, this finding suggests the potential involvement of REST/MIR137/Grin2a pathway in pathophysiology of CSD associated neurological diseases such as TBI and stoke (Figure 4.6). In a rodent model of stroke, reduced level of miR-137 in rat brain tissue correlated with increased Grin2a (Zhao et al., 2013). The depressive behavioural effects associated with increased levels of Grin2a in the post-stroke depression model were alleviated by injection of a miR-137 mimic, suggesting a neuroprotective role for this miRNA (Zhao et al., 2013).

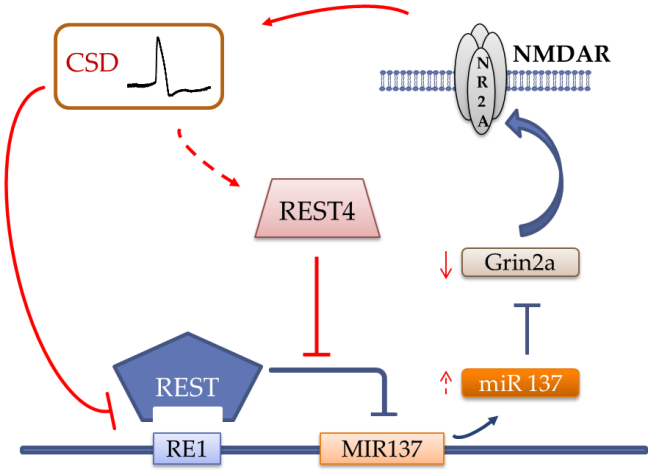

Figure 4.6 Schematic depiction of the potential involvement of REST/MIR137/Grin2a pathway in CSD processes. Blue lines indicate the pathway in normal condition. Red lines indicate the pathway in CSD condition. T-bars indicate the inhibitory effect. Arrow-bars indicate promote effect or increase/decrease expression. Dotted lines indicate a (predicted) change trend, which need to be further confirmed. Abbreviations: CSD, cortical spreading depression; REST, repressor element-1 silencing transcription factor; RE1, repressor element 1. NMDA, N-methyl-D-aspartic acid.

Gene expression analysis of cortical samples from sham ipsilateral and CSD ipsilateral groups showed that multiple CSD was able to induce GAD1 gene expression in our model (Figure 4.5). The mRNA level of Tac1, NKB, VIP, RELN and c-JUN were not changed at time points analysed. However we cannot rule out

the possibility that this may reflect the time-course used in our experiment not being appropriate to identify any transient changes in their expression at other time points. The induction of GAD1 may be related to the potential increase of REST4 mRNA level after multiple CSD, as REST4 can antagonise the function of full-length REST protein (Tabuchi et al., 2002, Coulson et al., 2000). GAD1 encodes one of several isoforms of GAD, which is a key enzyme during the synthesis of GABA. GABA is an inhibitory neurotransmitter and is known to be released post CSD (Clark and Collins, 1976). Topiramate, a GABA-receptor agonist, functions to elevate CSD threshold (Green et al., 2013) and reduce CSD frequency and propagation (Unekawa et al., 2012). It is necessary to further study whether these changes influence subsequent GABA protein synthesis.

In summary, although this study found that multiple CSD did not change the gene expression of REST and REST4, a slight but insignificant up-regulation of REST4 was observed. Considering the subsequent reduction of both REST binding to the rImir137 promoter and the downstream miR137 target of NR2A coding gene expression, and induction of REST target gene GAD1 post CSD, it cannot deny the potential involvement of REST or REST4 in CSD processes. Future study should be carried out to confirm the statistically significance of REST4 by increasing sample number and to examine if overexpression or knockout of REST would regulate CSD events in rats.

Chapter 5

Regulation of $GABA_A$ α2 and NR2A gene and protein expression by CSD

5.1 Introduction

NMDA receptor is known to be contribute to CSD genesis and propagation and the receptor antagonism have been proven as effective CSD suppression compounds (Gill et al., 1992). Of the NR2 subunits of the receptor, NR2A subunit has a dominant role relative to NR2B in CSD elicitation and propagation (Wang et al., 2012). Further, not only the excitatory, but also the inhibitory neurotransmitter receptor mediates CSD genesis and propagation. These were supported by that topiramate, a GABA-receptor agonist, can elevate CSD threshold (Green et al., 2013) and reduce CSD frequency and propagation (Unekawa et al., 2012). The suppressive effect on RSD is attributed to $GABA_A$ receptor α2 (Wang et al., 2015). The data in chapter 4 demonstrate that reduction of NR2A coding gene Grin2a in response to multiple CSD stimulation (Figure 4.3). How CSD would alter inhibitory neurotransmitter receptor subunits and whether CSD alter their protein expression remains unclear and these questions will be addressed in this chapter. It is generally considered that single CSD is more clinical relevant with migraine aura and is considered as the potential trigger for migraine headache (Ayata, 2010, Hadjikhani et al., 2001, Smith et al., 2006). Whether single CSD shows different effects on their gene expression is also explored in this chapter.

5.2 Objectives

(i) To address whether multiple CSD alters $GABA_A$α2 coding gene expression at 15 min, 3 hours, 24 hours and 72 hours post CSD.

(ii) To address whether multiple CSD alters NR2A and $GABA_A$α2 protein level at 3 hours and 24 hours post CSD.

(iii) To address whether single CSD alters NR2A and $GABA_A\alpha2$ coding gene expression.

5.3 Results

5.3.1 $GABA_A\alpha2$ gene expression is not altered post multiple CSD

The mRNA level of Gabra2, encoding for $GABA_A\alpha2$ subunit, there was no significant difference between contralateral and ipsilateral in the sham group at all time points (Figure 5.1), indicating that the surgery procedure did not affect Gabra2 gene expression. Different from Grin2a shown in chapter 4 (Figure 4.3), ipsilateral Gabra2 mRNA level is not altered between sham and CSD group at all time points I tested, indicating that multiple CSD did not influence the gene expression of Gabra2 (Figure 5.1).

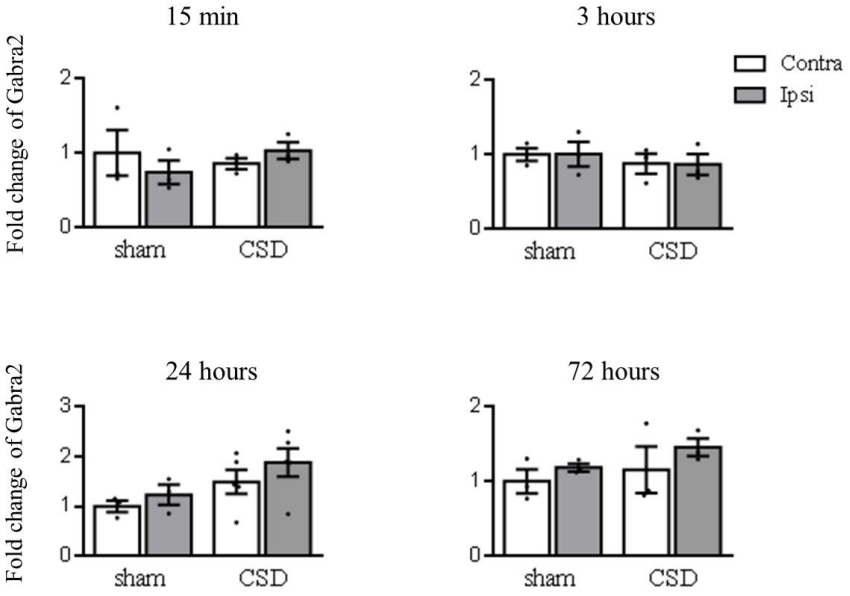

Figure 5.1 mRNA level of Gabra2 was not altered at 15 minutes, 3, 24 and 72 hours post-multiple CSD. The gene expression of Gabra2 at different time points post CSD was analysed by qPCR among both contralateral and ipsilateral groups of sham and CSD. There was no significant difference among all groups. (n=3 in each group, except n = 5 in CSD 24 hours group). Comparisons between sham and CSD groups were done using unpaired two-tailed Mann-Whitney U-test; Comparisons between ipsilateral and contralateral hemispheres within each group were done using paired two-tailed Wilcoxon test.

5.3.2 Multiple CSD effect on the protein levels of NR2A and GABA$_A$α2

How multiple CSD alters the protein level of NR2A and GABA$_A$α2 was explored by western blot analysis. Comparing with sham ipsilateral group, both NR2A and GABA$_A$α2 protein level were not altered at 3 and 24 hours post CSD (Figure 5.2). But there was a reduction trend of GABA$_A$α2 protein level in the ipsilateral cerebral cortex 3 hours post CSD and this reduction trend was returned to normal level 24 hours post CSD (Figure 5.2 D-F). Based on the power analysis for GABA$_A$α2 protein level at 3 hours, it should be able to reach significance with a sample size of four.

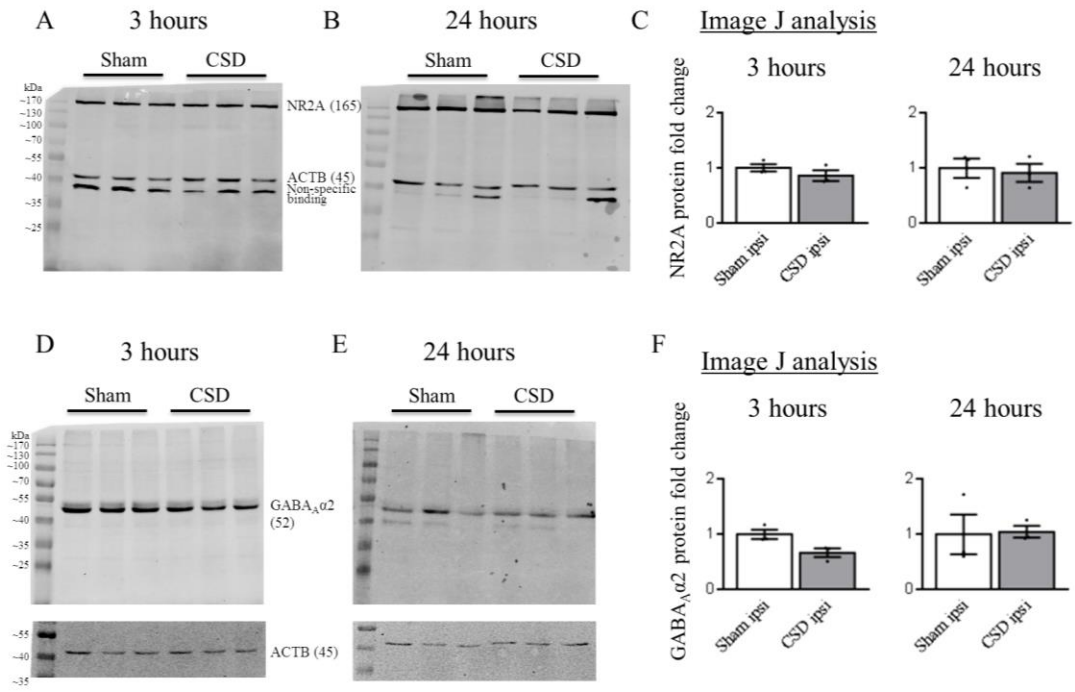

Figure 5.2. Multiple CSD reduced GABA$_A$ α 2, but not NR2A protein level. The translational changes of NR2A (A & B) and GABA$_A$ α 2 (D & E) were determined by western blot. Bands intensity was measured by Image J (C & F). Data was shown as mean ± SEM. Unpaired two-tailed Mann-Whitney U-test was used for comparison between sham ipsilateral and CSD ipsilateral groups.

5.3.3 Single CSD did not alter the gene expression of Grin2a and Gabra2

To explore whether single CSD shows different effect on their gene expression, the mRNA level of Grin2a and Gabra2 was detected by qPCR at 24 hours post single CSD. There were no significant changes in both Grin2a and Gabra2 mRNA levels between CSD contralateral and CSD ipsilateral (Figure 5.3). Sham samples were not included in this study, as it was shown in Figure 4.3 and Figure 5.1 that the mRNA levels of Grin2a and Gabra2 were not altered by surgery during the multiple CSD tests.

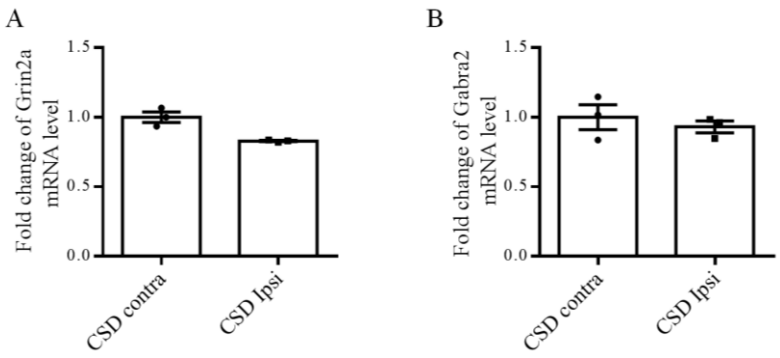

Figure 5.3 Ipsilateral Grin2a and Gabra2 gene expression was not altered 24 hours post single CSD. Comparison of Grin2a and Gabra2 mRNA between CSD contralateral (contra) cortices normalized to CSD ipsilateral (ipsi) cortices. There was no significant difference. (n = 3 in each group). Data was shown as mean ± SEM. Paired two-tailed Wilcoxon test was used for comparison between CSD contralateral and ipsilateral group.

5.4 Discussion

One main finding of this chapter is that the protein level of $GABA_A\alpha2$ showed a reduced trend, but insignificant, post multiple CSD in ipsilateral cortices in rats (Figure 5.2), suggesting that $GABA_A\alpha2$-containing inhibitory receptors may be involved in multiple CSD-associated TBI and stroke. This finding is in line with down-regulation of the $GABA_A\alpha2$ subunit observed in the lesioned cortex associated with a stroke (Sacco et al., 2009). This reduced trend of $GABA_A\,\alpha2$ adds new evidence supporting the vital role of $GABA_A$ receptors in the pathophysiology of stroke as there are increased expression of $GABA_A\,\alpha3$ subunit and a reduction in $GABA_A\,\alpha1$, $\alpha2$, $\alpha5$ and $\gamma2$ subunits in a range of animal studies (Redecker et al., 2002, Kharlamov et al., 2008, Schwartz-Bloom and Sah, 2001). In particular, $GABA_A\,\alpha2$ subtype activation suppresses retinal spreading depression (Wang et al., 2015). Collectively, it is proposed that $GABA_A\,\alpha2$-containing receptors play a key role of in CSD associated with diseases.

The reduction of $GABA_A\alpha2$ protein level 3 hours post CSD may not be associated with its reduced synthesis as mRNA levels of Gabra2 were not altered after multiple CSD at all the time points tested (Figure 5.1). The reduction of $GABA_A\,\alpha2$ after CSD may be associated with its internalization as a previous study showed that an internalization of $GABA_A$ receptors by endocytosis was observed in status epilepticus (Goodkin et al., 2005), which may share similar mechanisms with cortical spreading depolarisation (Kramer et al., 2017). It should be noted that given that activation of $GABA_A$ receptor in response to GABA leads to reduction of CGRP release (Bourgoin et al., 1992), a key target for migraine prevention,

suggesting that $GABA_A\alpha2$-containing receptor may contribute to multiple CSD-induced CGRP elevation.

Differently from Gabra2, NR2A expression was not altered post multiple CSD at all the points tested in ipsilateral cortices of rats (Figure 5.2). This data is consistent with a previous study that the immunoreactivity of NR2A was not changed on mouse cerebral cortex 24 hours post CSD (Chazot et al., 2002). However, a reduction of Grin2a expression at 24 hours, but not at 3 hours and 72 hours, post multiple CSD, was observed (Figure 4.3), suggesting multiple CSD led to a transient mRNA reduction of Grin2a. This transient reduction may not have affected NR2A levels post CSD as NR2A was not altered (Figure 5.2). Notably, inhibition of NR2A-containing NMDA receptors prevents the occurrence of CSD both in chick retina (Wang et al., 2012) and rats (Bu et al., 2016a). Taken together, it is possible that there is a negative feedback that NR2A activation contributes to CSD genesis and propagation, which may in return lead to down regulation of Grin2a expression. Further studies on a more extensive template changes of NR2A post multiple CSD will help to elucidate this notion. A relevant study is that in combined striatum-hippocampus-cortex slices, there is a local and remote increase of NMDA receptor binding sites was observed 1 hour post CSD induction (Haghir et al., 2009), which supports the important involvement of NR2A in CSD.

Unlike multiple CSD, Grin2a level was not altered by single CSD in rat ipsilateral cerebral cortices at 24 hour post CSD (Figure 5.3). This data are in line with the induction of CGRP gene expression was observed by multiple but not single CSD (Wang et al., 2016b). The single CSD event is associated with human migraine aura; whilst multiple CSD events are more commonly associated with TBI. This

data support that multiple CSD has more pronounced impacts on altering gene expression involved in pathogenesis of TBI or stroke associated with CSD. Taken together that antagonism of NR2A-containing NMDA receptors show protective effects against TBI (Katayama et al., 1990, LaPlaca and Thibault, 1998, Merchant et al., 1999). These results that the reduction of NR2A mRNA level post multiple, not single CSD, suggested the protective role of NR2A-containing NMDA receptors in the pathological processes of TBI.

In summary, multiple CSD events does not alter $GABA_A$ α2 gene expression but can cause a slight but insignificant down-regulation of its protein level in ipsilateral cerebral cortices of rats. Further work by increasing sample number is necessary to confirm $GABA_A$ α2 containing inhibitory receptors REST4 implications to TBI and stroke.

Chapter 6

P2X7R contributes to CSD

6.1 Introduction

The endogenous nucleotide, ATP, has been known to be involved in migraine (Burnstock and Ralevic, 2014) and can be released in response to both CSD (Schock et al., 2007) and CGRP in meninges (Yegutkin et al., 2016). The ATP-gated P2X7R is of particular interest as in a nitroglycerin (NTG)-induced mouse model of migraine, a selective P2X7R antagonist, brilliant blue G, completely prevented the effect of NTG in wild-type, but not in knockout mice (Goloncser and Sperlagh, 2014). Additionally, Panx1 is considered to either regulate P2X7R pore formation or form the pore itself by tightly coupling with the P2X7R after activation (Pelegrin and Surprenant, 2006). Indeed, inhibition of the P2X7R-Panx1 complex suppresses spreading depolarization (Chen et al., 2017b). Furthermore, P2X7R deficient mice were found to have reduced CSD (Chen et al., 2017b) and lack of hypersensitivity to mechanical and thermal stimuli (Chessell et al., 2005). Blockade of P2X7R attenuates post-ischemic damage (Cisneros-Mejorado et al., 2015) and shows seizure suppressive and neuroprotective effect in epilepsy models (Henshall et al., 2013, Jimenez-Pacheco et al., 2013, Engel et al., 2012), which shows moderate co-morbidity with migraine (Deprez et al., 2007, Farkas et al., 2008). Notably, the C-terminus of P2X7R is implicated in regulating receptor function, such as pathway activation and protein-protein interaction (Costa-Junior et al., 2011).

In light of this evidence, this part of the thesis studied whether the suppressive effects on CSD by inhibition of both P2X7R ion channel and the pore formation could be also observed in the mouse slice and the role of P2X7R in CSD is of non-vascular origin. Then this project further explored if an anti-P2X7R antibody

acting on the C-terminus of this receptor could inhibit the occurrence of CSD using both *in vitro* and *in vivo* models. Knowing that CSD can increase the mRNA levels of proinflammatory cytokines, such as IL-1β and TNF-α at 4 hours and CGRP at 24 hours post multiple CSD waves (Jander et al., 2001, Wang et al., 2016b), this study also examined whether C-terminus of P2X7R would lead to an induction of IL-1β, TNF-α and CGRP gene expression induced by CSD in the rat cerebral cortex.

6.2 Objectives

(i) To determine whether the action of P2X7R ion channel and P2X7R- Panx1 pore complex on CSD is of non-vascular origin using chick retina and mouse brain slice.

(ii) To examine whether blockade of P2X7R C-terminal domain by an antibody could prevent CSD occurrence.

(iii) To investigate whether an anti-P2X7R antibody would alter the gene expression of IL-1β, TNF-α and CGRP in cerebral cortex of rats immediately after CSD.

6.3 Results

6.3.1 P2X7R is expressed in chick retina

Before determining effects of P2X7R antagonism on RSD genesis and propagation, P2X7R protein expression was tested on chick retina by western blot. As P2X7R protein is expressed in the rat cerebral cortex (Franke et al., 2004), rat cortex was also tested as the positive control. Abundant protein expression was observed in chick retina, which shows similar levels as those of rat cerebral cortex (Figure 6.1),

indicating that chick retina is a suitable tissue for P2X7R pharmacological study and indicating an important functional role of P2X7R in chick retina.

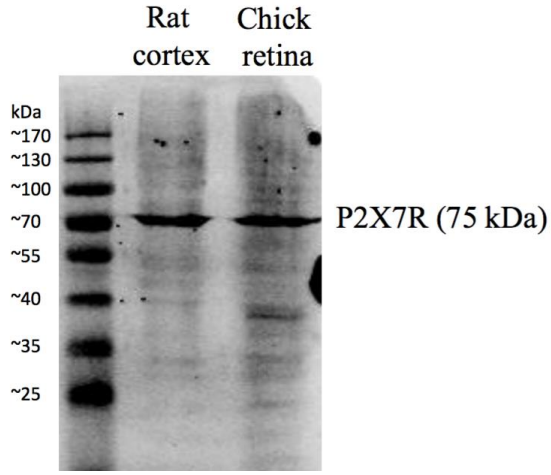

Figure 6.1 Expression of P2X7R in the chick retina. The P2X7R protein expression in chick retina was detected by western blot. The rat cerebral cortex was used as a positive control (left column).

6.3.2 P2X7R antagonist A740003 did not suppress RSD in chick retina

A740003, a competitive P2X7R antagonist inhibiting both P2X7R ion channel and pore formation (Honore et al., 2006), was used to investigate the role of P2X7R in RSD genesis and propagation. In the DMSO control group, RSD magnitude slightly reduced over 10 repeated RSD and the propagation rate was not altered throughout experiment (Figure 6.2). A740003 at concentration 10 μM showed no suppressive effects on both the RSD magnitude and propagation rate, when compared with the DMSO control group (Figure 6.2).

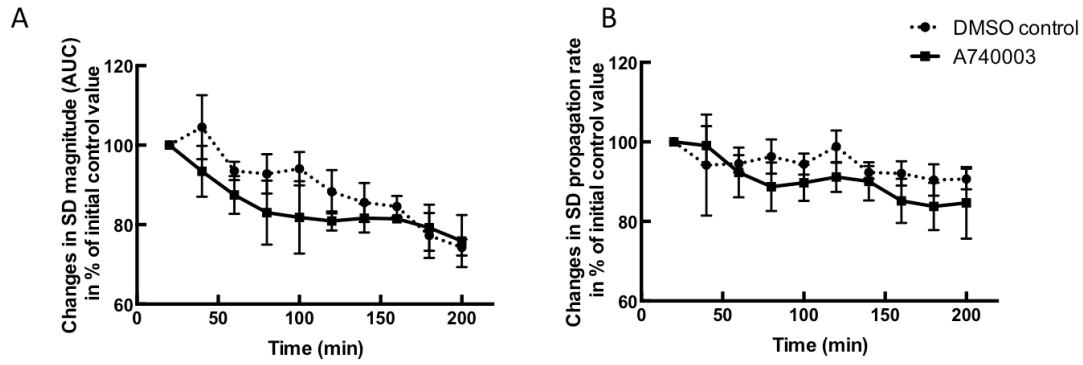

Figure 6.2 Effects of A740003 on the magnitude (AUC) (A) propagation rate (B) of RSD induced by 0.1 M KCl in the chick retina. P2X7R antagonist A740003 (dissolved in DMSO) treatment group and one vehicle DMSO group were tested (n=3 in each group). Ten RSD in total were induced with 20 minute interval and three perfusion media were tested in each experiment: initial two RSD in perfused ringer's solution, six RSD in 10 μM A740003 drug perfused solution and final two RSD in Ringer's solution. Data (mean ± SEM) were plotted as percentage of initial control value. Unpaired two-tailed Mann-Whitney U-test was used for comparison between DMSO and A740003 group at each time point.

6.3.3 P2X7R antagonist A740003 suppress CSD in the mouse brain slice

Whether blockade of the P2X7R channel and pore complex could suppress CSD was further examined in mouse brain slice. In the 2nd CSD of the Kreb's control group, CSD latency and magnitude were 128.7% ± 67.3% and 108.8% ± 13.4% and relative to their respective baselines (the 1st CSD) (Figure 6.3 A and C) and the propagation rate was 5.9 ± 2.4 mm/minute (Figure 6.3 B). Neither 0.03% DMSO nor A740003 at 1 μM changed these parameters when compared with respective Kreb's control group (Figure 6.3). Notably, A740003 at 3 μM increased the CSD latency to 3.3-fold relative to its initial control value and this prolongation was significant when compared with that of the Kreb's control and DMSO vehicle controls (p = 0.0011 and p =0.0043 respectively, Figure 6.3 A and D). Additionally, the drug at 3μM also markedly reduced the CSD magnitude to 55.8% relative to its

initial control value and this reduction was significant when compared with that of both Kreb's control and 0.03% DMSO vehicle group (p = 0.013 and p = 0.0076, respectively, Figure 6.3 C and D). Conversely, unlike the CSD magnitude and latency, A740003 at both concentrations applied did not alter CSD propagation rate (Figure 6.3 B).

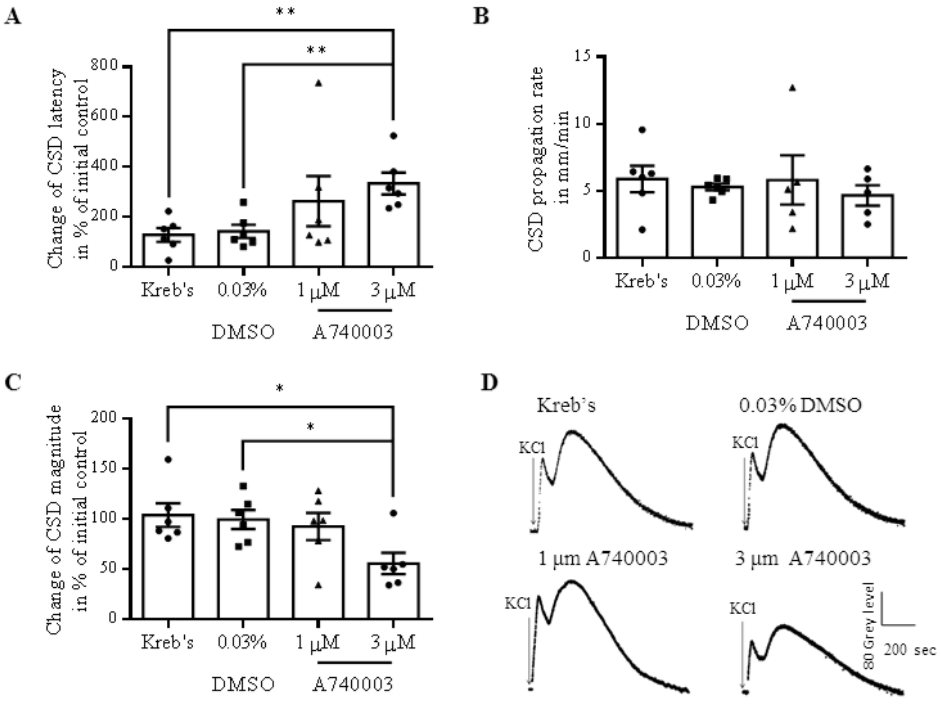

Figure 6.3 Inhibitory effects of the P2X7R antagonist, A740003, on the latency (A), propagation rate (B), magnitude (C) of CSD induced by 260 mM KCl ejection onto mouse brain slices and representative traces showing CSD waves in each group (D). Four groups were designed including Kreb's as the control, DMSO as the vehicle control, 1 µM and 3 µM of A740003 drug (n = 6 in each group). Data was shown as mean ± SEM. Unpaired one-tailed Mann-Whitney U-test was used for comparison between each group. *p < 0.05; **p < 0.01.

6.3.4 Suppression of CSD by an anti-P2X7R antibody in the mouse brain slice

Whether blockade of the C-terminus of P2X7R by an anti-P2X7R antibody suppress CSD was further examined in the mouse brain slice. In the Kreb's control group, the CSD latency and magnitude were 170.1% ± 38.9% and 72.1% ± 6.0% relative to their respective baseline (Figure 6.4 A and C) and the propagation rate was 5.0 ± 1.1 mm/minute (Figure 6.4 B). The anti-IgG antibody had no effects on CSD when compared to that of Kreb's control. The CSD latency, magnitude and propagation rate were 162.1% ± 33.4%, 72.4% ± 7.1% and 5.6 ± 1.6 mm/minute in respective order in the anti-IgG antibody group (Figure 6.4). Consistent with the P2X7R antagonist, pre-incubation of the brain slice with the anti-P2X7R antibody at 3 μg/ml markedly prolonged CSD latency to 451.0% ± 120.0% (Figure 6.4 A), which was significant when compared to that of the Kreb's group ($p = 0.0465$) and anti-IgG antibody control ($p = 0.0206$). CSD magnitude was also slightly reduced by the antibody, but this reduction did not reach significance (Figure 6.4 C) and it showed no effect on CSD propagation rate (Figure 6.4 B).

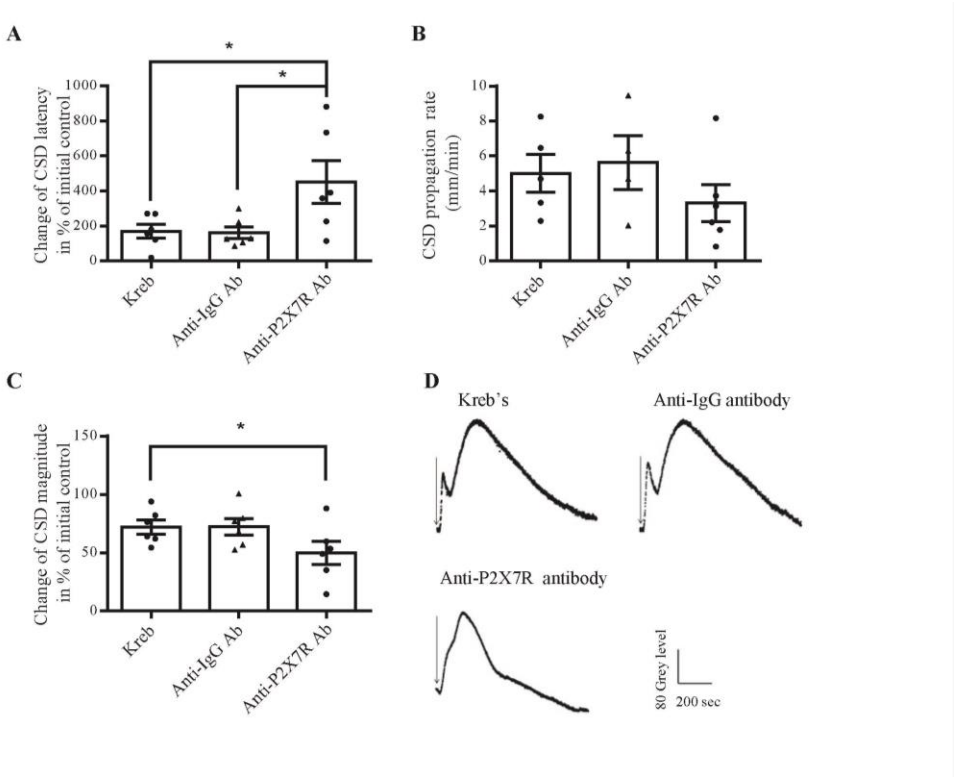

Figure 6.4 Effects of the anti-P2X7R antibody on the latency (A), propagation rate (B), magnitude (C) of CSD induced by 260 mM KCl onto the somatosensory cortex of mouse and representative traces of CSD wave in each group (D). Four groups were designed including Kreb's as control, glycerol (n = 6) as the vehicle control, anti-IgG antibody was negative control, 3 μg/ml of anti-P2X7R antibody (n = 6). Data was shown as mean ± SEM. Unpaired one-tailed Mann-Whitney U-test was used for comparison between each group. *$p < 0.05$.

6.3.5 Correlation analysis of CSD latency with magnitude in mouse brain slices

I further carried out correlation analysis of CSD latency with CSD magnitude in mouse brain slices. The results showed that after treatment of 0.3 μM A740003 and anti-P2X7R antibody, reduced CSD magnitude showed a negative correlation with the increased CSD latency (r = -0.507, $p = 0.0006$, Figure 6.5).

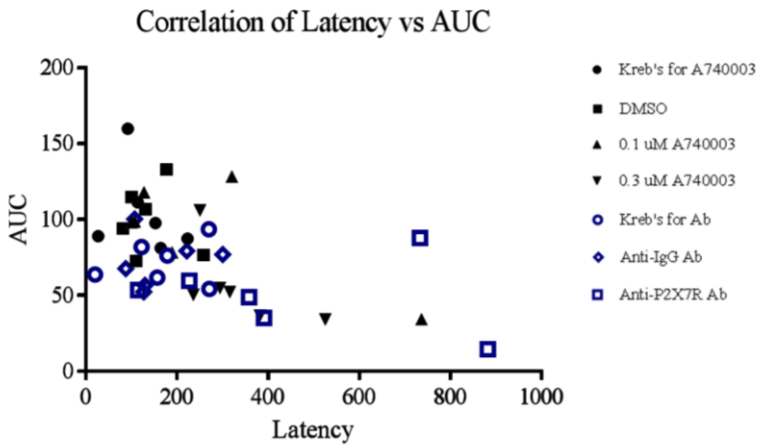

Figure 6.5 Correlation analysis of CSD latency with magnitude (AUC) in mouse brain slices. The reduced CSD magnitude negatively correlated with the increased of CSD latency after treatment of 0.3 μM A740003 and anti-P2X7R antibody. Two-tailed Spearman's correlation analysis.

6.3.6 Suppression of CSD by an anti-P2X7R antibody in vivo in rats

Whether the anti-P2X7R antibody could suppress the occurrence of CSD was further explored in rats. In the sham group, no CSD could be induced when glycerol was perfused into the *i.c.v.* in the absence of KCl application. Topical application of 2M KCl for 30 minutes induced multiple CSD waves in anti-IgG and anti-P2X7R antibody. In the anti-IgG group, the CSD latency, magnitude, propagation rate and number were 149.6 ± 9.0 seconds, 3.3 ± 0.2 mm/minute, 7.0 ± 0.9 mV× minute and 5.8 ± 0.4 in respective order (Figure 6.6 A-D). Similar as that in the mouse brain slice, perfusion of 0.6 μg of the anti-P2X7R antibody into the contralateral *i.c.v.* significantly prolonged the CSD latency to 272.9 ± 9.4 seconds (p = 0.0013 Figure 6.6 A). Corresponding to this, the anti-P2X7R antibody markedly reduced the propagation rate to 1.9 ± 0.2 mm/minute (p = 0.0013, Figure 6.6 B) and CSD number to 4.2 ± 0.2 (p = 0.0058, Figure 6.6 D) compared with the

anti-IgG antibody group. The anti-P2X7R antibody did not alter the CSD magnitude (p = 0.2317, Figure 6.6 C).

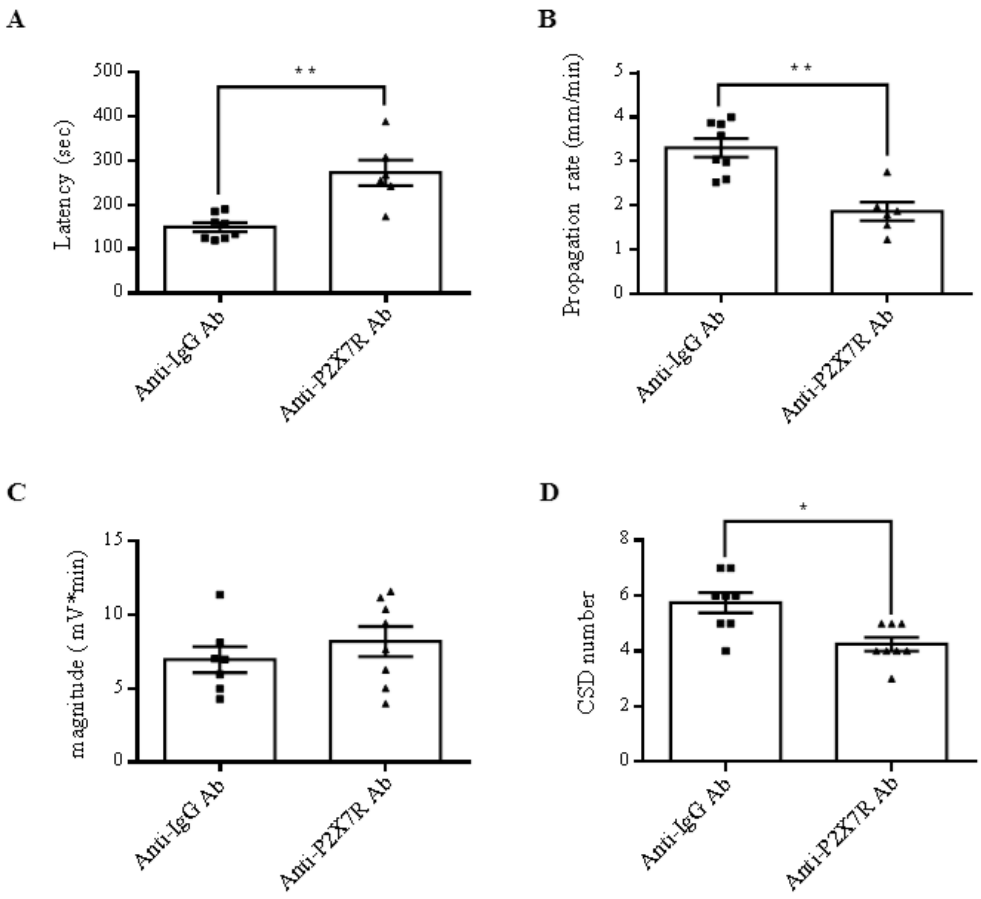

Figure 6.6 Inhibitory effects of the anti-P2X7R antibody on the CSD latency (A) propagation rate (B) magnitude (C), number (D) in rats. Two groups were designed including anti-IgG antibody (n = 8) as the negative control and anti-P2X7R antibody (n = 8). Data was shown as mean ± SEM. Unpaired one-tailed Mann-Whitney U-test was used for comparison between the two groups. *$p < 0.05$; **$p < 0.01$.

6.3.7 Correlation analysis of CSD latency with CSD number in vivo

Correlation of CSD parameters *in vivo* was also analysed in rats. As the CSD propagation rate was calculated by the distance (5 mm) between the two holes dividing the CSD latency, the negative correlation ship between CSD latency and

propagation rate was caused by calculation method. In this case, only correlation of CSD latency with CSD number was analysed. The reduced CSD number negatively correlated with the increased of CSD latency, but this correlation did not reach significant (r = -0.3536, p = 0.2148, Figure 6.7).

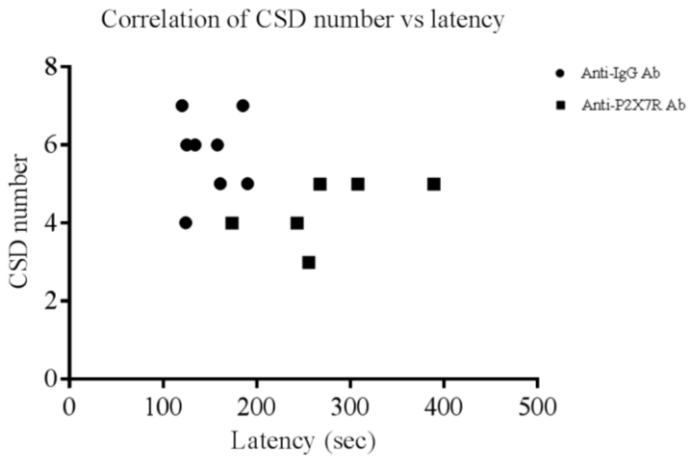

Figure 6.7 Correlation analysis of CSD latency with CSD number in rats. Two-tailed Pearson's correlation analysis.

6.3.8 The anti-P2X7R antibody did not alter the rapid induction of IL-1β and TNF-α mRNA level by CSD

Whether multiple CSD could immediately induce rapid induction of IL-1β, TNF-α and CGRP gene expression and whether P2X7R contributes to the CSD-induced induction of TNF-α, IL-1β and CGRP gene expression was examined. As described above, anti-P2X7R antibody or anti-IgG antibody was pre-perfused into contralateral *i.c.v* 4 days prior to CSD induction by KCl in rats. Compared with the sham group, the gene expression of IL-1β and TNF-α, but not CGRP, were significantly induced immediately after multiple CSD induction in the anti-IgG antibody group and the mRNA levels increased to 9.94 ± 1.63 (10-fold, $p < 0.001$) and 2.99 ± 0.21 (3-fold, $p < 0.0001$) respectively (Figure 6.8).

Pretreatment of the anti-P2X7R antibody into *i.c.v.* did not alter the CSD-induced rapid induction of ipsilateral IL-1β and TNF-α gene expression in rats compared with anti-IgG antibody group. The mRNA levels were maintained at the same levels as those of the anti-IgG antibody group (Figure 6.8 A &.B). The antibody also did not alter the basal level of CGRP gene expression maintained immediately post-CSD (Figure 6.8 C).

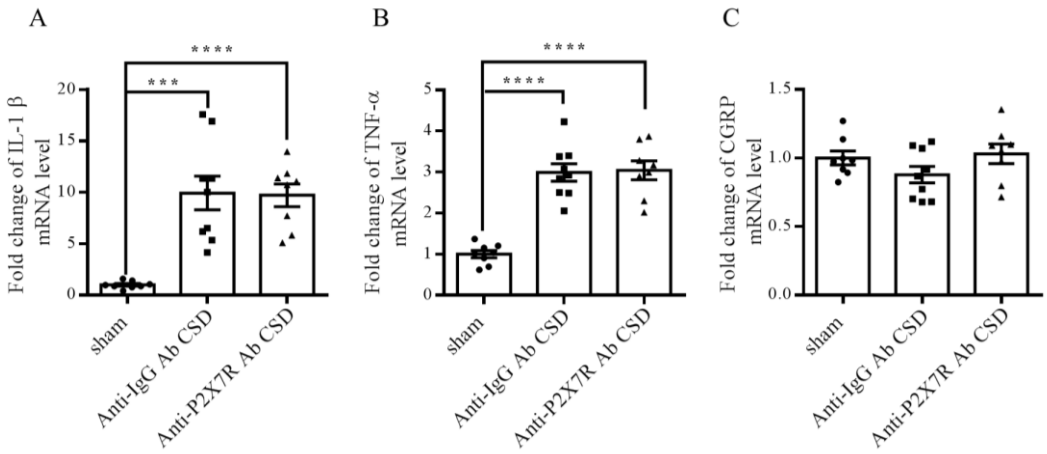

Figure 6.8 Effects of the multiple CSD and anti-P2X7R antibody on the gene expression of TNF-α, IL-1β and CGRP in rat cortices. CSD rapidly induced ipsilateral IL-1β and TNF-α gene expression, but not CGRP. Anti-P2X7R antibody did not alter the rapid induction of IL-1β and TNF-α gene expression by CSD (n = 8 in sham and anti-P2X7R antibody group, n = 9 in anti-IgG antibody group).. Data was shown as mean ± SEM. Two-tailed unpaired t-test was used for comparison between each group. ***$p < 0.001$; ****$p < 0.0001$. Abbreviation: *Ab, antibody.*

6.4 Discussion

This chapter showed that both P2X7R antagonist, A740003, and anti-P2X7R antibody are capable of suppressing CSD. First, pharmacological blockade of the P2X7R channel and pore complex by antagonist A740003 suppressed CSD with a significant prolongation of CSD latency and a reduced magnitude in the mouse

brain slice (Figure 6.3). These data suggest that mouse brain slice CSD is valid for the pharmacological study of P2X7R and P2X7R plays a key role in regulating CSD. Second, consistent with the mouse brain slice data, pretreatment of the anti-P2X7R antibody also suppressed CSD with a reduced cerebral cortex susceptibility to CSD in rats as evidenced by the extended CSD latency and reduced propagation rate and number of CSD waves (Figure 6.6). Finally, these data are consistent with a previous finding that inhibition of P2X7R-Panx1 channel and pore formation reduces CSD susceptibility in rats (Chen et al., 2017b). Collectively, these results support the critical role of P2X7R in the underlying mechanism of CSD-associated neurological diseases, such as migraine, TBI and stroke.

It was noted that unlike in the mouse brain slice (Figure 6.3), rat cortex *in vivo* (Figure 6.6) and a previous study in rats (Chen et al., 2017b), the suppressive effect of P2X7R antagonist was not observed in the RSD model (Figure 6.2). The reason to account for these differences is not known. It was demonstrated that the presence of P2X7R was detected in the tissue (Figure 6.1), which complements previous findings that P2X7R was expressed on chick embryo retina cells (Anccasi et al., 2013). Therefore, the negative results on suppressing RSD in the chick retina cannot be due to the lack of receptor. It is possible that there are marked species differences leading to functional difference in antagonist pharmacology for P2X7R. Isoquinolone derivatives such as KN-04 and KN-62 block human P2X7R with low nanomolar concentration, but little effects at rodent P2X7R, even at high micromolar concentration (Humphreys et al., 1998, Baraldi et al., 2004). Conversely, Brilliant Blue G is twenty times more potent at rat P2X7R than human (Jiang et al., 2000). Another possibility may be due to the small sample number (n

= 3 only) used in chick retina as preliminary data. As the drug concentration used in chick retina is quite high, to save the drug, I did not further increase sample number. Whether the negative data in the chick retina is associated with the lack of blood vessels in the chick retina is uncertain as the fact that inhibition of P2X7R by A740003 suppressed CSD was observed in the mouse brain slice argues this possibility. The finding that mouse brain slice lacks blood vessels and the suppressive effect on CSD was observed in this tissue suggest the neuronal/glial action and unlikely to involve the blood vessels.

The anti-P2X7R antibody is capable of suppressing CSD both *in vitro* and *in vivo*. This finding extends to the previous publication that blockade of the receptors ion channel and pore formation as well as genetic deletion of P2X7R suppressed CSD (Chen et al., 2017b). Notably, the CSD propagation rate and magnitude were distinct between *in vitro* and *in vivo* studies using anti-P2X7R antibody. Also, the negative correlation of CSD latency with magnitude *in vitro* was not observed *in vivo*. These may result from the lack of blood vessels in the mouse brain slice model compared that of the rat, in the former relevant signalling molecules released from these cells after CSD being removed by the continuous Kreb's perfusion. It's not clear how the antibody enters the cells, acting on the intracellular C-terminus of P2X7R. Perhaps there was a change of the membrane property in response to CSD allowing the antibody to cross the membrane. This is possible as increased permeability of neuronal membranes to large molecules is observed following experimental TBI *in vivo* (Pettus et al., 1994, Pettus and Povlishock, 1996). Nevertheless, it assumes that the mechanism of the anti-P2X7R antibody in suppressing CSD elicitation and propagation may be related to the function of the receptor C-terminus for several reasons. First, the pore formation of P2X7 receptor

is regulated by a distal C-terminal region (Smart et al., 2003), whilst blockade of the pore formation suppresses CSD. Second, the Src homology 3 (SH3) domain of the C-terminus of the P2X7R functions to interact with Src family kinase (SFK) (Iglesias et al., 2008, Suadicani et al., 2009); whilst SFK activation is required for CSD propagation as a single CSD can induce SFK activation and its inhibitor suppresses CSD in rats (Bu et al., 2017). Third, the arginine and lysine residues at positions R578 and K579 within the C-terminus of the P2X7R are essential to locate P2X7R on the cell surface (Denlinger et al., 2003); It is likely that blocking the vicinity region of the C-terminus would have an influence on the P2X7R cell surface expression thus controlling receptor trafficking and modulating the channel activity, which may subsequently alter CSD (Chen et al., 2017a). The suppressive effects on CSD by this antibody may due to function loss of C-terminus or the function changed of P2X7R channel and pore complex which is caused by complex conformation change due to combination of anti-P2X7R antibody. Another possibility is that this antibody did not work selectivity as the antibody also recognised an unspecific protein (70 kDa), which was close to P2X7R (75 kDa) in negative control HEK293 cells (Communications with Abcam), for which reason, the manufacture of anti-P2X7R antibody applied was discontinued by Abcam after completion of all the experiments. Therefore, the major limitation of this study is that there is no direct evidence showing the blockade of P2X7R C-terminus by the antibody. In the future, it is necessary to confirm the role of C-terminal domain of P2X7R in CSD by expressing a C-terminal truncated variant of P2X7R in the *P2rx7* gene deficient rats/mice.

The possibilities to account for the suppression of CSD by blockade of P2X7R may be associated with a range of signaling pathways (Figure 6.9). As CSD induces

ATP release (Schock et al., 2007), partially acting on P2X7R (Yegutkin et al., 2016), which activation in return mediates cerebral cortex susceptibility to CSD, we therefore propose a possible positive feedback loop of P2X7R during CSD associated neurological disease. Another possibility may link to glutamate receptor signalling. P2X7R activation leads to glutamate release from rat cortical nerve terminals (Marcoli et al., 2008, Di Cesare Mannelli et al., 2015); whereas the NMDA receptor of glutamate and its major NR2 subunits (NR2A and NR2B)-containing receptors are known to contribute to the initiation and propagation of CSD (Bu et al., 2016a, Obrenovitch et al., 1996, Peeters et al., 2007, Wang et al., 2012, Deuchars et al., 2001). Moreover, SH3 domain of the P2X7R C-terminus is involved in the initial step of the signal transduction events causing the activation of Panx1 channel, the latter of which is induced following multiple CSD (Karatas et al., 2013). In fact, blockade of the interaction between P2X7R and Panx1 was recently reported to suppress CSD depolarization in rodents (Chen et al., 2017b). Furthermore, Both P2X7R antagonists and Panx1 inhibitors can revert oxaliplatin-induced neuropathic pain (Di Cesare Mannelli et al., 2015). Moreover, P2X7R channels are highly permeable to Ca^{2+} and calcium influx accelerates CSD propagation in rats (Torrente et al., 2014). Collectively, the underlying mechanism underlying the role of P2X7R in CSD is therefore multifactorial.

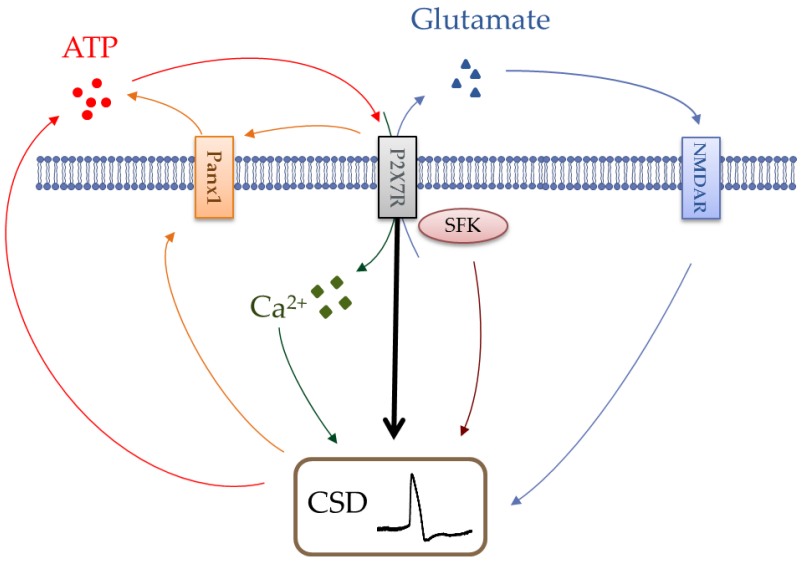

Figure 6.9 Schematic depiction of the potential underlying mechanisms of P2X7R contribution to CSD. First, the C-terminus of P2X7R can interact with SFK, while SFK activation is required for CSD induction. Second, The C-terminus of P2X7R is involved in Panx1 activation, which can be induced by multiple CSD. Third, CSD can induce ATP release, which activates P2X7R. Moreover, P2X7R activation leads to glutamate release whereas its NMDA receptors are known to contribute to the CSD initiation and propagation. Finally, P2X7R channels are highly permeable to Ca2+ and calcium influx accelerates CSD propagation in rats.

We explored if our antibody model not only modulated CSD but the associated differential gene expression observed. Gene expression of pro-inflammatory cytokines can be induced within 4 hours post CSD in the rat brain (Jander et al., 2001) and their protein levels can also be increased by CSD (Kunkler et al., 2004, Grinberg et al., 2013). The present study extends these findings demonstrating a rapid induction of TNF-α and IL-1β gene expression in the ipsilateral cerebral cortex of rat immediately after multiple CSD. The immediate induction of IL-1β and TNF-α mRNA level by CSD is unlikely to result from the action of the anti-IgG antibody, because our preliminary experiments examined that CSD glycerol *i.c.v* significantly induced IL-1β and TNF-α mRNA level compared with

sham glycerol *i.c.v.* group. The brain inflammatory response is likely to occur as a consequence of microglia activation, which is related to astrocytosis during CSD in rat brain tissues (Ghaemi et al., 2017). Given that IL-1β can exacerbate ischaemic brain damage in middle cerebral artery occlusion models in rats (Yamasaki et al., 1995), the CSD-induced IL-1β and TNF-α upregulation may become a therapeutic target for preventing stroke and TBI associated with multiple CSD.

Different from a marked elevation of CGRP mRNA level at 24 hours post multiple CSD (Wang et al., 2016b), the induction of CGRP gene expression was not observed immediately post CSD and anti-P2X7R antibody also did not alter its gene expression in our study. This may reflect the time course used in this experiment. Although qPCR analysis of CGRP gene did not show any significant changes, it does provide a negative control for gene expression changes in response to CSD and provides support that the observed induction of TNF-α and IL-1β was a specific response to CSD rather than an experimental artifact.

P2X7R activation is known to promote release of TNF-α (Suzuki et al., 2004) and IL-1β in hippocampus slice (Verhoef et al., 2003, Bernardino et al., 2008). Additionally, a significant down-regulation of IL-1β mRNA level after 30 minutes pretreatment of a P2X7/Panx1 pore inhibitor, A438079, was observed 4 hours post CSD (Chen et al., 2017b). On contrary, in this study, pretreatment of the anti-P2X7R antibody 4 days before the CSD induction did not influence CSD-induced rapid induction of ipsilateral cortical IL-1β and TNF-α gene expression. It is possible that changes of these gene expression have temporal profile. Such mRNA level change may have not been picked up at the time point

immediately post CSD. Extensive time points may help to address this result in future.

In conclusion, the data demonstrates that the anti-P2X7R antibody is capable of suppressing CSD, which may attribute to the C-terminal domain of P2X7R, or the non-specific binding of this antibody.. This data may offer a novel therapeutic strategy for CSD associated neurological disease, such as migraine, TBI and stoke, as antibodies have been increasingly used to prevent CSD associated diseases, which are clinically acceptable (Khan et al., 2017).

Chapter 7

Summary

The key findings of this thesis have two folds: (i) A slight but insignificant up-regulation of REST4 was observed post CSD. This statistically insignificance mainly attribute to the small sample number. The potential involvement of REST4 in CSD processes cannot be ruled out as power analysis suggests a significance can be reached when the sample size increases to four. (ii) Blockade of P2X7R by both the receptor antagonist and an antibody was capable of suppressing CSD, although studies on the latter using an alternative monoclonal antibody requires further clarification. These data suggest P2X7R as potential target for the therapy of CSD-associated neurological disease, such as TBI, stroke and migraine aura.

One key finding is that REST4 may be involved in the progression of CSD by influencing subsequent targets and the target-associated genes as the mRNA level of transcriptional regulator REST4 showed a transient up-regulation, although insignificant, in the ipsilateral cerebral cortex of rats post 3 hours of multiple CSD. The mechanism to account for this change has not been well explored. It is known that REST4 functions as antagonism of full-length REST (Tabuchi et al., 2002). Whilst CSD-induced transient elevation trend of REST4 (Figure 4.1) is associated with the reduced binding of full-length REST to rImir137 promoter after CSD in ipsilateral cerebral cortices of rats (Warburton, 2015 pp 277-281). Given that a significant reduction of Grin2a was observed in ipsilateral cerebral cortices of rats 24 hours post multiple CSD (Figure 4.3), it is possible that the reduced binding of REST to rImir137 promoter by CSD may cause increased miR-137 level, whilst miR-137 functions to suppress its target genes Grin2a.

It is proposed that the transient up-regulation trend of the REST4 transcript after multiple CSD may confer an adaptive neuroprotective effect, providing ischemic tolerance against subsequent insults after TBI. This notion was proposed based on the

following facts: Activation of Grin2a encoding NR2A-containing NMDA receptor is required for the CSD initiation (Bu et al., 2016a, Wang et al., 2012); whilst, the altered expression of Grin2a corresponds with the time frame in which increased tolerance to subsequent neuronal attacks induced by various preconditioning methods (Yanamoto et al., 2004). Additionally, the REST target GAD1 mRNA level was slightly increased by multiple CSD. GAD1 encodes a key enzyme during the synthesis of GABA, which is released post CSD (Clark and Collins, 1976). Whilst, activation of $GABA_A$ receptor is known to suppress the initiation and propagation of CSD (Akerman and Goadsby, 2005). Collectively, we propose that up-regulation of the REST4 transcript after multiple CSD may confer an adaptive neuroprotective effect, providing ischemic tolerance against subsequent insults after TBI.

There are several main limitations of REST study, which are as follows: (i) The data for REST4 gene expression lacks statistical significance, which may be caused by the small sample number, increasing sample number need to be considered in further work. (ii) These three specific time points may have missed some of the transient changes of REST and MIR137HG mRNA levels following CSD. Extensive time scale and other brain regions are necessary to explore their gene expression under both multiple and single CSD condition. (iii) Due to the lack of commercial specific anti-REST4 antibody, further studies are necessary to develop anti-REST4 specific antibody to explore specific REST4 binding over rImir137 promoter, as well as the effects of CSD on the protein expression of REST and REST4. (iv) Other MIR137 parent transcripts, as well as the mature miR-137 level are necessary to be explored to address the consequences of the increased REST4 mRNA levels. (v) Future study should be carried out to examine if overexpression or knockout of REST would influence the initiation of CSD, as well as its subsequent gene expression.

Another key finding of this thesis is that the C-terminal domain of P2X7R may play a pivotal role of CSD genesis and propagation. The anti-P2X7R antibody targeting its C-terminus suppresses CSD both *in vitro* mouse brain slices and *in vivo* rats. Its C-terminal domain functions to regulate the pore formation of this receptor (Smart et al., 2003). Pharmacological inhibition of the P2X7R channel and pore complex suppressed CSD in mouse brain slices, which are in line with previous findings in rats (Chen et al., 2017a). The molecular mechanism by which P2X7R modulate cortical susceptibility to CSD has not been studied previously, but P2X7R signal is divergent involving multiple pathways. One plausible explanation is that P2X7R C-terminus functions to interact with SFK, while, the activation of this receptor is required for CSD genesis and propagation (Bu et al., 2017). Secondly, P2X7R activation leads to glutamate release (Marcoli et al., 2008, Di Cesare Mannelli et al., 2015). The NMDA receptor of glutamate is known to contribute to the initiation and propagation of CSD (Bu et al., 2016b, Obrenovitch et al., 1996, Peeters et al., 2007, Wang et al., 2012, Deuchars et al., 2001). Moreover, the function of P2X7R on CSD may attribute to its highly permeable property to Ca^{2+} and calcium influx accelerates CSD propagation in rats (Torrente et al., 2014). These data offers a novel antibody therapeutic strategy for CSD-associated neurological disease to increase the efficacy to toxicity window for the therapy, as well as lower the dosage needed, as drugs usually need to be dosed at, or very near, their maximum tolerated dose in order to achieve the desired therapeutic efficacy.

The main limitation of P2X7R study is lack of direct evidence showing the blockade of P2X7R C-terminus by the antibody. Further *in vivo* experiments are necessary to expresses a C-terminal truncated variant of P2X7R in the P2rx7 gene deficient rats/mice to confirm the role of specific C-terminal region of P2X7R in CSD. Also,

the potential underlying mechanisms mentioned above are worth to be explored in future studies.

In conclusion, this project focused on two factors in CSD as follows: (i) This study does not support the truncated isoform of transcriptional regulator REST, REST4, is implicated in CSD progression. However, the transient but insignificant increase by CSD may be associated with changes of subsequent target gene expression, such as GAD1 and Grin2a; (ii) P2X7R plays a pivotal role in CSD. Whether C-terminal domain is involved in regulating CSD requires further clarification. These studies provide insight into the genetic and molecular mechanisms of CSD and offers novel therapeutic strategy for preventing CSD-associated neurological diseases, such as migraine with aura, TBI and stroke.

References

References

ADDAE, J. I., EVANS, S. M., ALI, N. & STONE, T. W. 2000. NMDA-induced changes in a cortical network in vivo are prevented by AMPA. *Brain Res,* 869**,** 211-5.

AGA, M., JOHNSON, C. J., HART, A. P., GUADARRAMA, A. G., SURESH, M., SVAREN, J., BERTICS, P. J. & DARIEN, B. J. 2002. Modulation of monocyte signaling and pore formation in response to agonists of the nucleotide receptor P2X(7). *J Leukoc Biol,* 72**,** 222-32.

AKERMAN, S. & GOADSBY, P. J. 2005. Topiramate inhibits cortical spreading depression in rat and cat: impact in migraine aura. *Neuroreport,* 16**,** 1383-7.

ALI, F. & MEIER, R. 2009. Primate home range and GRIN2A, a receptor gene involved in neuronal plasticity: implications for the evolution of spatial memory. *Genes Brain Behav,* 8**,** 435-41.

ALLOISIO, S., CERVETTO, C., PASSALACQUA, M., BARBIERI, R., MAURA, G., NOBILE, M. & MARCOLI, M. 2008. Functional evidence for presynaptic P2X7 receptors in adult rat cerebrocortical nerve terminals. *FEBS Lett,* 582**,** 3948-53.

ALLYSON, J., DONTIGNY, E., AUBERSON, Y., CYR, M. & MASSICOTTE, G. 2010. Blockade of NR2A-containing NMDA receptors induces Tau phosphorylation in rat hippocampal slices. *Neural Plast,* 2010**,** 340168.

AMIRI, S., EIDI, A. & GORJI, A. 2015. The Effect of Repetitive Cortical Spreading Depression on the Expression of GABA Aα Receptors in the Mesencephalic Trigeminal Nucleus in Male Adult Rats. *The Neuroscience Journal of Shefaye Khatam,* 3**,** 11-20.

ANCCASI, R. M., ORNELAS, I. M., COSSENZA, M., PERSECHINI, P. M. & VENTURA, A. L. 2013. ATP induces the death of developing avian retinal neurons in culture via activation of P2X7 and glutamate receptors. *Purinergic Signal,* 9**,** 15-29.

ANDRES, M. E., BURGER, C., PERAL-RUBIO, M. J., BATTAGLIOLI, E., ANDERSON, M. E., GRIMES, J., DALLMAN, J., BALLAS, N. & MANDEL, G. 1999. CoREST: a functional corepressor required for regulation of neural-specific gene expression. *Proc Natl Acad Sci U S A,* 96**,** 9873-8.

ANTONIOTTI, S., RUFFINATTI, F. A., TORRIANO, S., LUGANINI, A., D'ALESSANDRO, R. & LOVISOLO, D. 2016. REST levels affect the functional expression of voltage dependent calcium channels and the migratory activity in immortalized GnRH neurons. *Neurosci Lett,* 629**,** 19-25.

AYATA, C. 2010. Cortical spreading depression triggers migraine attack: pro. *Headache,* 50**,** 725-30.

AYATA, C., JIN, H., KUDO, C., DALKARA, T. & MOSKOWITZ, M. A. 2006. Suppression of cortical spreading depression in migraine prophylaxis. *Ann Neurol,* 59**,** 652-61.

AYATA, C. & LAURITZEN, M. 2015. Spreading Depression, Spreading Depolarizations, and the Cerebral Vasculature. *Physiol Rev,* 95**,** 953-93.

BALLAS, N. & MANDEL, G. 2005. The many faces of REST oversee epigenetic programming of neuronal genes. *Curr Opin Neurobiol,* 15**,** 500-6.

BARALDI, P. G., DI VIRGILIO, F. & ROMAGNOLI, R. 2004. Agonists and antagonists acting at P2X7 receptor. *Curr Top Med Chem,* 4**,** 1707-17.

BARGIOTAS, P., MONYER, H. & SCHWANINGER, M. 2009. Hemichannels in cerebral ischemia. *Curr Mol Med,* 9**,** 186-94.

BAROJA-MAZO, A., BARBERA-CREMADES, M. & PELEGRIN, P. 2013. The participation of plasma membrane hemichannels to purinergic signaling. *Biochim Biophys Acta,* 1828**,** 79-93.

BARRETT, C. F., VAN DEN MAAGDENBERG, A. M., FRANTS, R. R. & FERRARI, M. D. 2008. Familial hemiplegic migraine. *Adv Genet,* 63**,** 57-83.

BARTEL, D. P. 2004. MicroRNAs: genomics, biogenesis, mechanism, and function. *Cell,* 116**,** 281-97.

BARTEL, D. P. 2009. MicroRNAs: target recognition and regulatory functions. *Cell,* 136**,** 215-33.

BASARSKY, T. A., FEIGHAN, D. & MACVICAR, B. A. 1999. Glutamate release through volume-activated channels during spreading depression. *J Neurosci,* 19**,** 6439-45.

BATTAGLIOLI, E., ANDRES, M. E., ROSE, D. W., CHENOWETH, J. G., ROSENFELD, M. G., ANDERSON, M. E. & MANDEL, G. 2002. REST repression of neuronal genes requires components of the hSWI.SNF complex. *J Biol Chem,* 277**,** 41038-45.

BERNARDINO, L., BALOSSO, S., RAVIZZA, T., MARCHI, N., KU, G., RANDLE, J. C., MALVA, J. O. & VEZZANI, A. 2008. Inflammatory events in hippocampal slice cultures prime neuronal susceptibility to excitotoxic injury: a crucial role of P2X7 receptor-mediated IL-1beta release. *J Neurochem,* 106**,** 271-80.

BOLAY, H., REUTER, U., DUNN, A. K., HUANG, Z., BOAS, D. A. & MOSKOWITZ, M. A. 2002. Intrinsic brain activity triggers trigeminal meningeal afferents in a migraine model. *Nat Med,* 8**,** 136-42.

BORGDORFF, P. 2018. Arguments against the role of cortical spreading depression in migraine. *Neurol Res,* 40**,** 173-181.

BOURGOIN, S., POHL, M., BENOLIEL, J. J., MAUBORGNE, A., COLLIN, E., HAMON, M. & CESSELIN, F. 1992. gamma-Aminobutyric acid, through GABAA receptors, inhibits the potassium-stimulated release of calcitonin gene-related peptide- but not that of substance P-like material from rat spinal cord slices. *Brain Res,* 583**,** 344-8.

BOWYER, S. M., AURORA, K. S., MORAN, J. E., TEPLEY, N. & WELCH, K. M. 2001. Magnetoencephalographic fields from patients with spontaneous and induced migraine aura. *Ann Neurol,* 50**,** 582-7.

BRAVO, D., MATURANA, C. J., PELISSIER, T., HERNANDEZ, A. & CONSTANDIL, L. 2015. Interactions of pannexin 1 with NMDA and P2X7 receptors in central nervous system pathologies: Possible role on chronic pain. *Pharmacol Res,* 101**,** 86-93.

BRENNAN, K. C., BATES, E. A., SHAPIRO, R. E., ZYUZIN, J., HALLOWS, W. C., HUANG, Y., LEE, H. Y., JONES, C. R., FU, Y. H., CHARLES, A. C. & PTACEK, L. J. 2013. Casein kinase idelta mutations in familial migraine and advanced sleep phase. *Sci Transl Med,* 5**,** 183ra56, 1-11.

BRENNAN, K. C., BELTRAN-PARRAZAL, L., LOPEZ-VALDES, H. E., THERIOT, J., TOGA, A. W. & CHARLES, A. C. 2007a. Distinct vascular conduction with cortical spreading depression. *J Neurophysiol,* 97**,** 4143-51.

BRENNAN, K. C., ROMERO REYES, M., LOPEZ VALDES, H. E., ARNOLD, A. P. & CHARLES, A. C. 2007b. Reduced threshold for cortical spreading depression in female mice. *Ann Neurol,* 61**,** 603-6.

BRIAN, J. E., JR., FARACI, F. M. & HEISTAD, D. D. 1996. Recent insights into the regulation of cerebral circulation. *Clin Exp Pharmacol Physiol,* 23**,** 449-57.

BROWN, D. G. & KRUPP, J. J. 2006. N-methyl-D-aspartate receptor (NMDA) antagonists as potential pain therapeutics. *Curr Top Med Chem,* 6**,** 749-70.

BU, F., DU, R., LI, Y., QUINN, J. P. & WANG, M. 2016a. NR2A contributes to genesis and propagation of cortical spreading depression in rats. *Sci Rep,* 6**,** 23576.

BU, F., DU, R., LI, Y., QUINN, J. P. & WANG, M. 2016b. NR2A contributes to genesis and propagation of cortical spreading depression in rats. *Sci Rep,* 6**,** 1-9.

BU, F., WANG, Y., JIANG, L., MA, D., QUINN, J. P. & WANG, M. 2017. Sarcoma family kinase activity is required for cortical spreading depression. *Cephalalgia***,** 333102417748572.

BURNSTOCK, G. 2006. Pathophysiology and therapeutic potential of purinergic signaling. *Pharmacol Rev,* 58**,** 58-86.

BURNSTOCK, G. & RALEVIC, V. 2014. Purinergic signaling and blood vessels in health and disease. *Pharmacol Rev,* 66**,** 102-92.

CAI, S. X. 2006. Glycine/NMDA receptor antagonists as potential CNS therapeutic agents: ACEA-1021 and related compounds. *Curr Top Med Chem,* 6**,** 651-62.

CALDERONE, A., JOVER, T., NOH, K. M., TANAKA, H., YOKOTA, H., LIN, Y., GROOMS, S. Y., REGIS, R., BENNETT, M. V. & ZUKIN, R. S. 2003. Ischemic insults derepress the gene silencer REST in neurons destined to die. *J Neurosci,* 23**,** 2112-21.

CAO, X., YEO, G., MUOTRI, A. R., KUWABARA, T. & GAGE, F. H. 2006. Noncoding RNAs in the mammalian central nervous system. *Annu Rev Neurosci,* 29**,** 77-103.

CHANDRASEKAR, V. & DREYER, J. L. 2009. microRNAs miR-124, let-7d and miR-181a regulate cocaine-induced plasticity. *Mol Cell Neurosci,* 42**,** 350-62.

CHAZOT, P. L. 2004. The NMDA receptor NR2B subunit: a valid therapeutic target for multiple CNS pathologies. *Curr Med Chem,* 11**,** 389-96.

CHAZOT, P. L., GODUKHIN, O. V., MCDONALD, A. & OBRENOVITCH, T. P. 2002. Spreading depression-induced preconditioning in the mouse cortex: differential changes in the protein expression of ionotropic nicotinic acetylcholine and glutamate receptors. *J Neurochem,* 83**,** 1235-8.

CHEN, G. L. & MILLER, G. M. 2013. Extensive alternative splicing of the repressor element silencing transcription factor linked to cancer. *PLoS One,* 8**,** e62217.

CHEN, S. P., QIN, T., SEIDEL, J. L., ZHENG, Y., EIKERMANN, M., FERRARI, M. D., VAN DEN MAAGDENBERG, A., MOSKOWITZ, M. A., AYATA, C. & EIKERMANN-HAERTER, K. 2017a. Inhibition of the P2X7-PANX1 complex suppresses spreading depolarization and neuroinflammation. *Brain,* 140**,** 1643-1656.

CHEN, S. P., QIN, T., SEIDEL, J. L., ZHENG, Y., EIKERMANN, M., FERRARI, M. D., VAN DEN MAAGDENBERG, A., MOSKOWITZ, M. A., AYATA, C. & EIKERMANN-HAERTER, K. 2017b. Inhibition of the P2X7-PANX1 complex suppresses spreading depolarization and neuroinflammation. *Brain*.

CHESSELL, I. P., HATCHER, J. P., BOUNTRA, C., MICHEL, A. D., HUGHES, J. P., GREEN, P., EGERTON, J., MURFIN, M., RICHARDSON, J., PECK, W. L., GRAHAMES, C. B., CASULA, M. A., YIANGOU, Y., BIRCH, R., ANAND, P. & BUELL, G. N. 2005. Disruption of the P2X7 purinoceptor gene abolishes chronic inflammatory and neuropathic pain. *Pain,* 114**,** 386-96.

CHESSELL, I. P., SIMON, J., HIBELL, A. D., MICHEL, A. D., BARNARD, E. A. & HUMPHREY, P. P. 1998. Cloning and functional characterisation of the mouse P2X7 receptor. *FEBS Lett,* 439**,** 26-30.

CHONG, J. A., TAPIA-RAMIREZ, J., KIM, S., TOLEDO-ARAL, J. J., ZHENG, Y., BOUTROS, M. C., ALTSHULLER, Y. M., FROHMAN, M. A., KRANER, S. D. & MANDEL, G. 1995. REST: a mammalian silencer protein that restricts sodium channel gene expression to neurons. *Cell,* 80**,** 949-57.

CHOUDHURI, R., CUI, L., YONG, C., BOWYER, S., KLEIN, R. M., WELCH, K. M. & BERMAN, N. E. 2002. Cortical spreading depression and gene regulation: relevance to migraine. *Ann Neurol,* 51**,** 499-506.

CISNEROS-MEJORADO, A., GOTTLIEB, M., CAVALIERE, F., MAGNUS, T., KOCH-NOLTE, F., SCEMES, E., PEREZ-SAMARTIN, A. & MATUTE, C. 2015. Blockade of P2X7 receptors or pannexin-1 channels similarly attenuates postischemic damage. *J Cereb Blood Flow Metab,* 35**,** 843-50.

CLARK, R. M. & COLLINS, G. G. 1976. The release of endogenous amino acids from the rat visual cortex. *J Physiol,* 262**,** 383-400.

COLONNA, D. M., MENG, W., DEAL, D. D. & BUSIJA, D. W. 1994. Calcitonin gene-related peptide promotes cerebrovascular dilation during cortical spreading depression in rabbits. *Am J Physiol,* 266**,** H1095-102.

COLONNA, D. M., MENG, W., DEAL, D. D., GOWDA, M. & BUSIJA, D. W. 1997. Neuronal NO promotes cerebral cortical hyperemia during cortical spreading depression in rabbits. *Am J Physiol,* 272**,** H1315-22.

COSTA-JUNIOR, H. M., SARMENTO VIEIRA, F. & COUTINHO-SILVA, R. 2011. C terminus of the P2X7 receptor: treasure hunting. *Purinergic Signal,* 7**,** 7-19.

COULSON, J. M., EDGSON, J. L., WOLL, P. J. & QUINN, J. P. 2000. A splice variant of the neuron-restrictive silencer factor repressor is expressed in small cell lung cancer: a potential role in derepression of neuroendocrine genes and a useful clinical marker. *Cancer Res,* 60**,** 1840-4.

COULSON, J. M., FISKERSTRAND, C. E., WOLL, P. J. & QUINN, J. P. 1999. Arginine vasopressin promoter regulation is mediated by a neuron-restrictive silencer element in small cell lung cancer. *Cancer Res,* 59**,** 5123-7.

CSOLLE, C., BARANYI, M., ZSILLA, G., KITTEL, A., GOLONCSER, F., ILLES, P., PAPP, E., VIZI, E. S. & SPERLAGH, B. 2013. Neurochemical Changes in the Mouse Hippocampus Underlying the Antidepressant Effect of Genetic Deletion of P2X7 Receptors. *PLoS One,* 8**,** e66547.

CUTRER, F. M., O'DONNELL, A. & SANCHEZ DEL RIO, M. 2000. Functional neuroimaging: enhanced understanding of migraine pathophysiology. *Neurology,* 55**,** S36-45.

CUTRER, F. M., SORENSEN, A. G., WEISSKOFF, R. M., OSTERGAARD, L., SANCHEZ DEL RIO, M., LEE, E. J., ROSEN, B. R. & MOSKOWITZ, M. A. 1998. Perfusion-weighted imaging defects during spontaneous migrainous aura. *Ann Neurol,* 43**,** 25-31.

DAHLEM, M. A. & MULLER, S. C. 2000. Image processing techniques applied to excitation waves in the chicken retina. *Methods,* 21**,** 317-23.

DAHLEM, Y. A., DAHLEM, M. A., MAIR, T., BRAUN, K. & MULLER, S. C. 2003. Extracellular potassium alters frequency and profile of retinal spreading depression waves. *Exp Brain Res,* 152**,** 221-8.

DAVIES, P. T. & PANAYIOTOPOULOS, C. P. 2011. Migraine triggered seizures and epilepsy triggered headache and migraine attacks: a need for re-assessment. *J Headache Pain,* 12**,** 287-8.

DEPREZ, L., PEETERS, K., VAN PAESSCHEN, W., CLAEYS, K. G., CLAES, L. R., SULS, A., AUDENAERT, D., VAN DYCK, T., GOOSSENS, D., DEL-FAVERO, J. & DE JONGHE, P. 2007. Familial occipitotemporal lobe epilepsy and migraine with visual aura: linkage to chromosome 9q. *Neurology,* 68**,** 1995-2002.

DEUCHARS, S. A., ATKINSON, L., BROOKE, R. E., MUSA, H., MILLIGAN, C. J., BATTEN, T. F., BUCKLEY, N. J., PARSON, S. H. & DEUCHARS, J. 2001. Neuronal P2X7 receptors are targeted to presynaptic terminals in the central and peripheral nervous systems. *J Neurosci,* 21**,** 7143-52.

DI CESARE MANNELLI, L., MARCOLI, M., MICHELI, L., ZANARDELLI, M., MAURA, G., GHELARDINI, C. & CERVETTO, C. 2015. Oxaliplatin evokes P2X7-dependent glutamate release in the cerebral cortex: A pain mechanism mediated by Pannexin 1. *Neuropharmacology,* 97**,** 133-41.

DIETZ, R. M., WEISS, J. H. & SHUTTLEWORTH, C. W. 2008. Zn2+ influx is critical for some forms of spreading depression in brain slices. *J Neurosci,* 28**,** 8014-24.

DREIER, J. P. 2011. The role of spreading depression, spreading depolarization and spreading ischemia in neurological disease. *Nat Med,* 17**,** 439-47.

DREIER, J. P. & REIFFURTH, C. 2015. The stroke-migraine depolarization continuum. *Neuron,* 86**,** 902-922.

DUAN, S., ANDERSON, C. M., KEUNG, E. C., CHEN, Y., CHEN, Y. & SWANSON, R. A. 2003. P2X7 receptor-mediated release of excitatory amino acids from astrocytes. *J Neurosci,* 23**,** 1320-8.

DZAMBA, D., HONSA, P. & ANDEROVA, M. 2013. NMDA Receptors in Glial Cells: Pending Questions. *Curr Neuropharmacol,* 11**,** 250-62.

EIKERMANN-HAERTER, K., BAUM, M. J., FERRARI, M. D., VAN DEN MAAGDENBERG, A. M., MOSKOWITZ, M. A. & AYATA, C. 2009a. Androgenic suppression of spreading depression in familial hemiplegic migraine type 1 mutant mice. *Ann Neurol,* 66**,** 564-8.

EIKERMANN-HAERTER, K., DILEKOZ, E., KUDO, C., SAVITZ, S. I., WAEBER, C., BAUM, M. J., FERRARI, M. D., VAN DEN MAAGDENBERG, A. M., MOSKOWITZ, M. A. & AYATA, C. 2009b. Genetic and hormonal factors modulate spreading depression and transient hemiparesis in mouse models of familial hemiplegic migraine type 1. *J Clin Invest,* 119**,** 99-109.

ENGEL, T., GOMEZ-VILLAFUERTES, R., TANAKA, K., MESURET, G., SANZ-RODRIGUEZ, A., GARCIA-HUERTA, P., MIRAS-PORTUGAL, M. T., HENSHALL, D. C. & DIAZ-HERNANDEZ, M. 2012. Seizure suppression and neuroprotection by targeting the purinergic P2X7 receptor during status epilepticus in mice. *FASEB J,* 26**,** 1616-28.

FABRICIUS, M., AKGOREN, N. & LAURITZEN, M. 1995. Arginine-nitric oxide pathway and cerebrovascular regulation in cortical spreading depression. *Am J Physiol,* 269**,** H23-9.

FABRICIUS, M., FUHR, S., BHATIA, R., BOUTELLE, M., HASHEMI, P., STRONG, A. J. & LAURITZEN, M. 2006. Cortical spreading depression and peri-infarct depolarization in acutely injured human cerebral cortex. *Brain,* 129**,** 778-90.

FABRICIUS, M., FUHR, S., WILLUMSEN, L., DREIER, J. P., BHATIA, R., BOUTELLE, M. G., HARTINGS, J. A., BULLOCK, R., STRONG, A. J. & LAURITZEN, M. 2008. Association of seizures with cortical spreading depression and peri-infarct depolarisations in the acutely injured human brain. *Clin Neurophysiol,* 119**,** 1973-84.

FABRICIUS, M., JENSEN, L. H. & LAURITZEN, M. 1993. Microdialysis of interstitial amino acids during spreading depression and anoxic depolarization in rat neocortex. *Brain Res,* 612**,** 61-9.

FARAGUNA, U., NELSON, A., VYAZOVSKIY, V. V., CIRELLI, C. & TONONI, G. 2010. Unilateral cortical spreading depression affects sleep need and induces molecular and electrophysiological signs of synaptic potentiation in vivo. *Cereb Cortex,* 20**,** 2939-47.

FARKAS, E., PRATT, R., SENGPIEL, F. & OBRENOVITCH, T. P. 2008. Direct, live imaging of cortical spreading depression and anoxic depolarisation using a fluorescent, voltage-sensitive dye. *J Cereb Blood Flow Metab,* 28**,** 251-62.

FARLOW, M. R. 2004. NMDA receptor antagonists. A new therapeutic approach for Alzheimer's disease. *Geriatrics,* 59**,** 22-7.

FERRARI, D., CHIOZZI, P., FALZONI, S., DAL SUSINO, M., MELCHIORRI, L., BARICORDI, O. R. & DI VIRGILIO, F. 1997. Extracellular ATP triggers IL-1 beta release by activating the purinergic P2Z receptor of human macrophages. *J Immunol,* 159**,** 1451-8.

FEUERSTEIN, D., BACKES, H., GRAMER, M., TAKAGAKI, M., GABEL, P., KUMAGAI, T. & GRAF, R. 2016. Regulation of cerebral metabolism during cortical spreading depression. *J Cereb Blood Flow Metab,* 36**,** 1965-1977.

FEUERSTEIN, D., MANNING, A., HASHEMI, P., BHATIA, R., FABRICIUS, M., TOLIAS, C., PAHL, C., ERVINE, M., STRONG, A. J. & BOUTELLE, M. G. 2010. Dynamic metabolic response to multiple spreading depolarizations in patients with acute brain injury: an online microdialysis study. *J Cereb Blood Flow Metab,* 30**,** 1343-55.

FLORES-SOTO, M. E., CHAPARRO-HUERTA, V., ESCOTO-DELGADILLO, M., VAZQUEZ-VALLS, E., GONZALEZ-CASTANEDA, R. E. & BEAS-ZARATE, C. 2012. [Structure and function of NMDA-type glutamate receptor subunits]. *Neurologia,* 27**,** 301-10.

FRANKE, H., GUNTHER, A., GROSCHE, J., SCHMIDT, R., ROSSNER, S., REINHARDT, R., FABER-ZUSCHRATTER, H., SCHNEIDER, D. & ILLES, P. 2004. P2X7 receptor expression after ischemia in the cerebral cortex of rats. *J Neuropathol Exp Neurol,* 63**,** 686-99.

FUSAYASU, E., KOWA, H., TAKESHIMA, T., NAKASO, K. & NAKASHIMA, K. 2007. Increased plasma substance P and CGRP levels, and high ACE activity in migraineurs during headache-free periods. *Pain,* 128**,** 209-14.

GALEFFI, F., SOMJEN, G. G., FOSTER, K. A. & TURNER, D. A. 2011. Simultaneous monitoring of tissue PO2 and NADH fluorescence during synaptic stimulation and spreading depression reveals a transient dissociation between oxygen utilization and mitochondrial redox state in rat hippocampal slices. *J Cereb Blood Flow Metab,* 31**,** 626-39.

GARDNER-MEDWIN, A. R. 1981. Possible roles of vertebrate neuroglia in potassium dynamics, spreading depression and migraine. *J Exp Biol,* 95**,** 111-27.

GHAEMI, A., ALIZADEH, L., BABAEI, S., JAFARIAN, M., KHALEGHI GHADIRI, M., MEUTH, S. G., KOVAC, S. & GORJI, A. 2017. Astrocyte-mediated inflammation in cortical spreading depression. *Cephalalgia***,** 333102417702132.

GILL, R., ANDINE, P., HILLERED, L., PERSSON, L. & HAGBERG, H. 1992. The effect of MK-801 on cortical spreading depression in the penumbral zone following focal ischaemia in the rat. *J Cereb Blood Flow Metab,* 12**,** 371-9.

GOLD, L., BACK, T., ARNOLD, G., DREIER, J., EINHAUPL, K. M., REUTER, U. & DIRNAGL, U. 1998. Cortical spreading depression-associated hyperemia in rats: involvement of serotonin. *Brain Res,* 783**,** 188-93.

GOLONCSER, F. & SPERLAGH, B. 2014. Effect of genetic deletion and pharmacological antagonism of P2X7 receptors in a mouse animal model of migraine. *J Headache Pain,* 15**,** 24.

GOODKIN, H. P., YEH, J. L. & KAPUR, J. 2005. Status epilepticus increases the intracellular accumulation of GABAA receptors. *J Neurosci,* 25**,** 5511-20.

GOODRICH, G. S., KABAKOV, A. Y., HAMEED, M. Q., DHAMNE, S. C., ROSENBERG, P. A. & ROTENBERG, A. 2013. Ceftriaxone treatment after traumatic brain injury restores expression of the glutamate transporter, GLT-1, reduces regional gliosis, and reduces post-traumatic seizures in the rat. *J Neurotrauma,* 30**,** 1434-41.

GORJI, A. 2001. Spreading depression: a review of the clinical relevance. *Brain Res Brain Res Rev,* 38**,** 33-60.

GREEN, A. L., GU, P., DE FELICE, M., DODICK, D., OSSIPOV, M. H. & PORRECA, F. 2013. Increased susceptibility to cortical spreading depression in an animal model of medication-overuse headache. *Cephalalgia,* 34**,** 594-604.

GRIMES, J. A., NIELSEN, S. J., BATTAGLIOLI, E., MISKA, E. A., SPEH, J. C., BERRY, D. L., ATOUF, F., HOLDENER, B. C., MANDEL, G. & KOUZARIDES, T. 2000. The co-repressor mSin3A is a functional component of the REST-CoREST repressor complex. *J Biol Chem,* 275**,** 9461-7.

GRINBERG, Y. Y., DIBBERN, M. E., LEVASSEUR, V. A. & KRAIG, R. P. 2013. Insulin-like growth factor-1 abrogates microglial oxidative stress and TNF-alpha responses to spreading depression. *J Neurochem,* 126**,** 662-72.

HADJIKHANI, N., SANCHEZ DEL RIO, M., WU, O., SCHWARTZ, D., BAKKER, D., FISCHL, B., KWONG, K. K., CUTRER, F. M., ROSEN, B. R., TOOTELL, R. B., SORENSEN, A. G. & MOSKOWITZ, M. A. 2001. Mechanisms of migraine aura revealed by functional MRI in human visual cortex. *Proc Natl Acad Sci U S A,* 98**,** 4687-92.

HAGHIR, H., KOVAC, S., SPECKMANN, E. J., ZILLES, K. & GORJI, A. 2009. Patterns of neurotransmitter receptor distributions following cortical spreading depression. *Neuroscience,* 163**,** 1340-52.

HANSEN, A. J. & OLSEN, C. E. 1980. Brain extracellular space during spreading depression and ischemia. *Acta Physiol Scand,* 108**,** 355-65.

HANSEN, A. J. & ZEUTHEN, T. 1981. Extracellular ion concentrations during spreading depression and ischemia in the rat brain cortex. *Acta Physiol Scand,* 113**,** 437-45.

HANSEN, J. M. 2010. Familial hemiplegic migraine. *Dan Med Bull,* 57**,** B4183.

HARTINGS, J. A., STRONG, A. J., FABRICIUS, M., MANNING, A., BHATIA, R., DREIER, J. P., MAZZEO, A. T., TORTELLA, F. C., BULLOCK, M. R. & CO-OPERATIVE STUDY OF BRAIN INJURY, D. 2009. Spreading depolarizations and late secondary insults after traumatic brain injury. *J Neurotrauma,* 26**,** 1857-66.

HASHEMI, P., BHATIA, R., NAKAMURA, H., DREIER, J. P., GRAF, R., STRONG, A. J. & BOUTELLE, M. G. 2009. Persisting depletion of brain glucose following cortical spreading depression, despite apparent hyperaemia: evidence for risk of an adverse effect of Leao's spreading depression. *J Cereb Blood Flow Metab,* 29**,** 166-75.

HASHIMOTO, M., TAKEDA, Y., SATO, T., KAWAHARA, H., NAGANO, O. & HIRAKAWA, M. 2000. Dynamic changes of NADH fluorescence images and NADH content during spreading depression in the cerebral cortex of gerbils. *Brain Res,* 872**,** 294-300.

HAYDON, P. G. & CARMIGNOTO, G. 2006. Astrocyte control of synaptic transmission and neurovascular coupling. *Physiol Rev,* 86**,** 1009-31.

HENSHALL, D. C., DIAZ-HERNANDEZ, M., MIRAS-PORTUGAL, M. T. & ENGEL, T. 2013. P2X receptors as targets for the treatment of status epilepticus. *Front Cell Neurosci,* 7**,** 237.

HERMANN, D. M., MIES, G. & HOSSMANN, K. A. 1999. Biochemical changes and gene expression following traumatic brain injury: Role of spreading depression. *Restor Neurol Neurosci,* 14**,** 103-8.

HERRERA, D. G. & ROBERTSON, H. A. 1990. Application of potassium chloride to the brain surface induces the c-fos proto-oncogene: reversal by MK-801. *Brain Res,* 510**,** 166-70.

HOLLAND, P. R., AKERMAN, S., ANDREOU, A. P., KARSAN, N., WEMMIE, J. A. & GOADSBY, P. J. 2012. Acid-sensing ion channel 1: a novel therapeutic target for migraine with aura. *Ann Neurol,* 72**,** 559-63.

HONORE, P., DONNELLY-ROBERTS, D., NAMOVIC, M. T., HSIEH, G., ZHU, C. Z., MIKUSA, J. P., HERNANDEZ, G., ZHONG, C., GAUVIN, D. M., CHANDRAN, P., HARRIS, R., MEDRANO, A. P., CARROLL, W., MARSH, K., SULLIVAN, J. P., FALTYNEK, C. R. & JARVIS, M. F. 2006. A-740003 [N-(1-{[(cyanoimino)(5-quinolinylamino) methyl]amino}-2,2-dimethylpropyl)-2-(3,4-dimethoxyphenyl)acetamide], a novel and selective P2X7 receptor antagonist, dose-dependently reduces neuropathic pain in the rat. *J Pharmacol Exp Ther,* 319**,** 1376-85.

HOSSEINI-ZARE, M. S., GU, F., ABDULLA, A., POWELL, S. & ZIBURKUS, J. 2017. Effects of experimental traumatic brain injury and impaired glutamate transport on cortical spreading depression. *Exp Neurol,* 295**,** 155-161.

HOSSEINZADEH-NIK, T., EFTEKHARI, A., SHAHROUDI, A. S. & KHARRAZIFARD, M. J. 2016. Changes of the Mandible after Orthodontic Treatment with and without Extraction of Four Premolars. *J Dent (Tehran),* 13**,** 199-206.

HOSSMANN, K. A. 1996. Periinfarct depolarizations. *Cerebrovasc Brain Metab Rev,* 8**,** 195-208.

HOWARD, M. R., MILLWARD-SADLER, S. J., VASILLIOU, A. S., SALTER, D. M. & QUINN, J. P. 2008. Mechanical stimulation induces preprotachykinin gene expression in osteoarthritic chondrocytes which is correlated with modulation of the transcription factor neuron restrictive silence factor. *Neuropeptides,* 42**,** 681-6.

HU, X. L., CHENG, X., CAI, L., TAN, G. H., XU, L., FENG, X. Y., LU, T. J., XIONG, H., FEI, J. & XIONG, Z. Q. 2011. Conditional deletion of NRSF in forebrain neurons accelerates epileptogenesis in the kindling model. *Cereb Cortex,* 21**,** 2158-65.

HUANG, L., BOCEK, M., JORDAN, J. K. & SHEEHAN, A. H. 2014. Memantine for the prevention of primary headache disorders. *Ann Pharmacother,* 48**,** 1507-11.

HUANG, Y., MYERS, S. J. & DINGLEDINE, R. 1999. Transcriptional repression by REST: recruitment of Sin3A and histone deacetylase to neuronal genes. *Nat Neurosci,* 2**,** 867-72.

HUMPHREYS, B. D., VIRGINIO, C., SURPRENANT, A., RICE, J. & DUBYAK, G. R. 1998. Isoquinolines as antagonists of the P2X7 nucleotide receptor: high selectivity for the human versus rat receptor homologues. *Mol Pharmacol,* 54**,** 22-32.

HWANG, J. Y., KANEKO, N., NOH, K. M., PONTARELLI, F. & ZUKIN, R. S. 2014. The gene silencing transcription factor REST represses miR-132 expression in hippocampal neurons destined to die. *J Mol Biol,* 426**,** 3454-66.

IGLESIAS, R., LOCOVEI, S., ROQUE, A., ALBERTO, A. P., DAHL, G., SPRAY, D. C. & SCEMES, E. 2008. P2X7 receptor-Pannexin1 complex: pharmacology and signaling. *Am J Physiol Cell Physiol,* 295**,** C752-60.

IIJIMA, T., MIES, G. & HOSSMANN, K. A. 1992. Repeated negative DC deflections in rat cortex following middle cerebral artery occlusion are abolished by MK-801: effect on volume of ischemic injury. *J Cereb Blood Flow Metab,* 12**,** 727-33.

JAFARIAN, M., RAHIMI, S., BEHNAM, F., HOSSEINI, M., HAGHIR, H., SADEGHZADEH, B. & GORJI, A. 2010. The effect of repetitive spreading depression on neuronal damage in juvenile rat brain. *Neuroscience,* 169**,** 388-94.

JANDER, S., SCHROETER, M., PETERS, O., WITTE, O. W. & STOLL, G. 2001. Cortical spreading depression induces proinflammatory cytokine gene expression in the rat brain. *J Cereb Blood Flow Metab,* 21**,** 218-25.

JANSEN, M. & DANNHARDT, G. 2003. Antagonists and agonists at the glycine site of the NMDA receptor for therapeutic interventions. *Eur J Med Chem,* 38**,** 661-70.

JIANG, L. H., MACKENZIE, A. B., NORTH, R. A. & SURPRENANT, A. 2000. Brilliant blue G selectively blocks ATP-gated rat P2X(7) receptors. *Mol Pharmacol,* 58**,** 82-8.

JIMENEZ-PACHECO, A., MESURET, G., SANZ-RODRIGUEZ, A., TANAKA, K., MOONEY, C., CONROY, R., MIRAS-PORTUGAL, M. T., DIAZ-HERNANDEZ, M., HENSHALL, D. C. & ENGEL, T. 2013. Increased neocortical expression of the P2X7 receptor after status epilepticus and anticonvulsant effect of P2X7 receptor antagonist A-438079. *Epilepsia,* 54**,** 1551-61.

JOTHI, R., CUDDAPAH, S., BARSKI, A., CUI, K. & ZHAO, K. 2008. Genome-wide identification of in vivo protein-DNA binding sites from ChIP-Seq data. *Nucleic Acids Res,* 36**,** 5221-31.

KAHLENBERG, J. M. & DUBYAK, G. R. 2004. Mechanisms of caspase-1 activation by P2X7 receptor-mediated K+ release. *Am J Physiol Cell Physiol,* 286**,** C1100-8.

KALLUNKI, P., EDELMAN, G. M. & JONES, F. S. 1998. The neural restrictive silencer element can act as both a repressor and enhancer of L1 cell adhesion molecule gene expression during postnatal development. *Proc Natl Acad Sci U S A,* 95**,** 3233-8.

KARATAS, H., ERDENER, S. E., GURSOY-OZDEMIR, Y., LULE, S., EREN-KOCAK, E., SEN, Z. D. & DALKARA, T. 2013. Spreading depression triggers headache by activating neuronal Panx1 channels. *Science,* 339**,** 1092-5.

KATAYAMA, Y., BECKER, D. P., TAMURA, T. & HOVDA, D. A. 1990. Massive increases in extracellular potassium and the indiscriminate release of glutamate following concussive brain injury. *J Neurosurg,* 73**,** 889-900.

KAWATE, T., ROBERTSON, J. L., LI, M., SILBERBERG, S. D. & SWARTZ, K. J. 2011. Ion access pathway to the transmembrane pore in P2X receptor channels. *J Gen Physiol,* 137**,** 579-90.

KEMP, J. A. & MCKERNAN, R. M. 2002. NMDA receptor pathways as drug targets. *Nat Neurosci,* 5 Suppl**,** 1039-42.

KHAN, S., OLESEN, A. & ASHINA, M. 2017. CGRP, a target for preventive therapy in migraine and cluster headache: Systematic review of clinical data. *Cephalalgia***,** 333102417741297.

KHARLAMOV, E. A., DOWNEY, K. L., JUKKOLA, P. I., GRAYSON, D. R. & KELLY, K. M. 2008. Expression of GABA A receptor alpha1 subunit mRNA and protein in rat neocortex following photothrombotic infarction. *Brain Res,* 1210**,** 29-38.

KIM, C. S., HWANG, C. K., SONG, K. Y., CHOI, H. S., KIM, D. K., LAW, P. Y., WEI, L. N. & LOH, H. H. 2008. Novel function of neuron-restrictive silencer factor (NRSF) for posttranscriptional regulation. *Biochim Biophys Acta,* 1783**,** 1835-46.

KIM, M., JIANG, L. H., WILSON, H. L., NORTH, R. A. & SURPRENANT, A. 2001. Proteomic and functional evidence for a P2X7 receptor signalling complex. *EMBO J,* 20**,** 6347-58.

KOKAIA, Z., GIDO, G., RINGSTEDT, T., BENGZON, J., KOKAIA, M., SIESJO, B. K., PERSSON, H. & LINDVALL, O. 1993. Rapid increase of BDNF mRNA levels in cortical neurons following

spreading depression: regulation by glutamatergic mechanisms independent of seizure activity. *Brain Res Mol Brain Res,* 19**,** 277-86.

KOVANYI, B., CSOLLE, C., CALOVI, S., HANUSKA, A., KATO, E., KOLES, L., BHATTACHARYA, A., HALLER, J. & SPERLAGH, B. 2016. The role of P2X7 receptors in a rodent PCP-induced schizophrenia model. *Sci Rep,* 6**,** 36680.

KRAIG, R. P. & NICHOLSON, C. 1978. Extracellular ionic variations during spreading depression. *Neuroscience,* 3**,** 1045-59.

KRAIG, R. P., PULSINELLI, W. A. & PLUM, F. 1985. Heterogeneous distribution of hydrogen and bicarbonate ions during complete brain ischemia. *Prog Brain Res,* 63**,** 155-66.

KRAMER, D. R., FUJII, T., OHIORHENUAN, I. & LIU, C. Y. 2017. Interplay between Cortical Spreading Depolarization and Seizures. *Stereotact Funct Neurosurg,* 95**,** 1-5.

KRISTENSEN, J. D., SVENSSON, B. & GORDH, T., JR. 1992. The NMDA-receptor antagonist CPP abolishes neurogenic 'wind-up pain' after intrathecal administration in humans. *Pain,* 51**,** 249-53.

KUGE, Y., HASEGAWA, Y., YOKOTA, C., MINEMATSU, K., HASHIMOTO, N., MIYAKE, Y. & YAMAGUCHI, T. 2000. Effects of single and repetitive spreading depression on cerebral blood flow and glucose metabolism in cats: a PET study. *J Neurol Sci,* 176**,** 114-23.

KUNKLER, P. E., HULSE, R. E. & KRAIG, R. P. 2004. Multiplexed cytokine protein expression profiles from spreading depression in hippocampal organotypic cultures. *J Cereb Blood Flow Metab,* 24**,** 829-39.

LANDGRAF, P., RUSU, M., SHERIDAN, R., SEWER, A., IOVINO, N., ARAVIN, A., PFEFFER, S., RICE, A., KAMPHORST, A. O., LANDTHALER, M., LIN, C., SOCCI, N. D., HERMIDA, L., FULCI, V., CHIARETTI, S., FOA, R., SCHLIWKA, J., FUCHS, U., NOVOSEL, A., MULLER, R. U., SCHERMER, B., BISSELS, U., INMAN, J., PHAN, Q., CHIEN, M., WEIR, D. B., CHOKSI, R., DE VITA, G., FREZZETTI, D., TROMPETER, H. I., HORNUNG, V., TENG, G., HARTMANN, G., PALKOVITS, M., DI LAURO, R., WERNET, P., MACINO, G., ROGLER, C. E., NAGLE, J. W., JU, J., PAPAVASILIOU, F. N., BENZING, T., LICHTER, P., TAM, W., BROWNSTEIN, M. J., BOSIO, A., BORKHARDT, A., RUSSO, J. J., SANDER, C., ZAVOLAN, M. & TUSCHL, T. 2007. A mammalian microRNA expression atlas based on small RNA library sequencing. *Cell,* 129**,** 1401-14.

LAPLACA, M. C. & THIBAULT, L. E. 1998. Dynamic mechanical deformation of neurons triggers an acute calcium response and cell injury involving the N-methyl-D-aspartate glutamate receptor. *J Neurosci Res,* 52**,** 220-9.

LAURITZEN, M. 1984. Long-lasting reduction of cortical blood flow of the brain after spreading depression with preserved autoregulation and impaired CO2 response. *J Cereb Blood Flow Metab,* 4**,** 546-54.

LAURITZEN, M. 1994. Pathophysiology of the migraine aura. The spreading depression theory. *Brain,* 117 (Pt 1)**,** 199-210.

LAURITZEN, M. 2001. Cortical spreading depression in migraine. *Cephalalgia,* 21**,** 757-60.

LAURITZEN, M., DREIER, J. P., FABRICIUS, M., HARTINGS, J. A., GRAF, R. & STRONG, A. J. 2011. Clinical relevance of cortical spreading depression in neurological disorders: migraine, malignant stroke, subarachnoid and intracranial hemorrhage, and traumatic brain injury. *J Cereb Blood Flow Metab,* 31**,** 17-35.

LAURITZEN, M. & FABRICIUS, M. 1995. Real time laser-Doppler perfusion imaging of cortical spreading depression in rat neocortex. *Neuroreport,* 6**,** 1271-3.

LEAO, A. A. P. 1944a. Pial circulation and spreading depression of activity in the cerebral cortex *J. Neurophysiol. ,* 7**,** 391-396.

LEAO, A. A. P. 1944b. Spreading Depression of Activity in the Cerebral Cortex. *J. Neurophysiol.***,** 359-390.

LEAO, A. A. P. 1947. Further observations on the spreading depression of activity in the cerebral cortex. *J Neurophysiol,* 10**,** 409-14.

LEE, M. G., WYNDER, C., COOCH, N. & SHIEKHATTAR, R. 2005. An essential role for CoREST in nucleosomal histone 3 lysine 4 demethylation. *Nature,* 437**,** 432-5.

LEO, L., GHERARDINI, L., BARONE, V., DE FUSCO, M., PIETROBON, D., PIZZORUSSO, T. & CASARI, G. 2011. Increased susceptibility to cortical spreading depression in the mouse model of familial hemiplegic migraine type 2. *PLoS Genet,* 7**,** e1002129.

LEVY, D., BURSTEIN, R. & STRASSMAN, A. M. 2005. Calcitonin gene-related peptide does not excite or sensitize meningeal nociceptors: implications for the pathophysiology of migraine. *Ann Neurol,* 58**,** 698-705.

LOE-MIE, Y., LEPAGNOL-BESTEL, A. M., MAUSSION, G., DORON-FAIGENBOIM, A., IMBEAUD, S., DELACROIX, H., AGGERBECK, L., PUPKO, T., GORWOOD, P., SIMONNEAU, M. & MOALIC, J. M. 2010. SMARCA2 and other genome-wide supported schizophrenia-associated genes: regulation by REST/NRSF, network organization and primate-specific evolution. *Hum Mol Genet,* 19**,** 2841-57.

LU, T., ARON, L., ZULLO, J., PAN, Y., KIM, H., CHEN, Y., YANG, T. H., KIM, H. M., DRAKE, D., LIU, X. S., BENNETT, D. A., COLAIACOVO, M. P. & YANKNER, B. A. 2014. REST and stress resistance in ageing and Alzheimer's disease. *Nature,* 507**,** 448-54.

LUNYAK, V. V., BURGESS, R., PREFONTAINE, G. G., NELSON, C., SZE, S. H., CHENOWETH, J., SCHWARTZ, P., PEVZNER, P. A., GLASS, C., MANDEL, G. & ROSENFELD, M. G. 2002. Corepressor-dependent silencing of chromosomal regions encoding neuronal genes. *Science,* 298**,** 1747-52.

MA, W., HUI, H., PELEGRIN, P. & SURPRENANT, A. 2009. Pharmacological characterization of pannexin-1 currents expressed in mammalian cells. *J Pharmacol Exp Ther,* 328**,** 409-18.

MARANHAO-FILHO, P. A., MARTINS-FERREIRA, H., VINCENT, M. B., RIBEIRO, L. J. & NOVIS, S. A. 1997. Sumatriptan blocks spreading depression in isolated chick retina. *Cephalalgia,* 17**,** 822-5.

MARCOLI, M., CERVETTO, C., PALUZZI, P., GUARNIERI, S., ALLOISIO, S., THELLUNG, S., NOBILE, M. & MAURA, G. 2008. P2X7 pre-synaptic receptors in adult rat cerebrocortical nerve terminals: a role in ATP-induced glutamate release. *J Neurochem,* 105**,** 2330-42.

MARRANNES, R., WILLEMS, R., DE PRINS, E. & WAUQUIER, A. 1988. Evidence for a role of the N-methyl-D-aspartate (NMDA) receptor in cortical spreading depression in the rat. *Brain Res,* 457**,** 226-40.

MARTINS, L. B., TEIXEIRA, A. L. & DOMINGUES, R. B. 2017. Neurotrophins and Migraine. *Vitam Horm,* 104**,** 459-473.

MARTINS-FERREIRA, H., NEDERGAARD, M. & NICHOLSON, C. 2000. Perspectives on spreading depression. *Brain Res Brain Res Rev,* 32**,** 215-34.

MAYEVSKY, A., DORON, A., MANOR, T., MEILIN, S., ZARCHIN, N. & OUAKNINE, G. E. 1996. Cortical spreading depression recorded from the human brain using a multiparametric monitoring system. *Brain Res,* 740**,** 268-74.

MAYEVSKY, A. & WEISS, H. R. 1991. Cerebral blood flow and oxygen consumption in cortical spreading depression. *J Cereb Blood Flow Metab,* 11**,** 829-36.

MCCLELLAND, S., BRENNAN, G. P., DUBE, C., RAJPARA, S., IYER, S., RICHICHI, C., BERNARD, C. & BARAM, T. Z. 2014. The transcription factor NRSF contributes to epileptogenesis by selective repression of a subset of target genes. *Elife,* 3**,** e01267.

MEDHURST, A. D., HARRISON, D. C., READ, S. J., CAMPBELL, C. A., ROBBINS, M. J. & PANGALOS, M. N. 2000. The use of TaqMan RT-PCR assays for semiquantitative analysis of gene expression in CNS tissues and disease models. *J Neurosci Methods,* 98**,** 9-20.

MERCHANT, R. E., BULLOCK, M. R., CARMACK, C. A., SHAH, A. K., WILNER, K. D., KO, G. & WILLIAMS, S. A. 1999. A double-blind, placebo-controlled study of the safety, tolerability and pharmacokinetics of CP-101,606 in patients with a mild or moderate traumatic brain injury. *Ann N Y Acad Sci,* 890**,** 42-50.

MISSALE, C., FIORENTINI, C., BUSI, C., COLLO, G. & SPANO, P. F. 2006. The NMDA/D1 receptor complex as a new target in drug development. *Curr Top Med Chem,* 6**,** 801-8.

NAKANO, T., SHIMOMURA, T., TAKAHASHI, K. & IKAWA, S. 1993. Platelet substance P and 5-hydroxytryptamine in migraine and tension-type headache. *Headache,* 33**,** 528-32.

NARUSE, Y., AOKI, T., KOJIMA, T. & MORI, N. 1999. Neural restrictive silencer factor recruits mSin3 and histone deacetylase complex to repress neuron-specific target genes. *Proc Natl Acad Sci U S A,* 96**,** 13691-6.

NOH, K. M., HWANG, J. Y., FOLLENZI, A., ATHANASIADOU, R., MIYAWAKI, T., GREALLY, J. M., BENNETT, M. V. & ZUKIN, R. S. 2012. Repressor element-1 silencing transcription factor (REST)-dependent epigenetic remodeling is critical to ischemia-induced neuronal death. *Proc Natl Acad Sci U S A,* 109**,** E962-71.

NORTH, R. A. 2002. Molecular physiology of P2X receptors. *Physiol Rev,* 82**,** 1013-67.

NOZARI, A., DILEKOZ, E., SUKHOTINSKY, I., STEIN, T., EIKERMANN-HAERTER, K., LIU, C., WANG, Y., FROSCH, M. P., WAEBER, C., AYATA, C. & MOSKOWITZ, M. A. 2010. Microemboli may link spreading depression, migraine aura, and patent foramen ovale. *Ann Neurol,* 67**,** 221-9.

OBRENOVITCH, T. P., URENJAK, J. & WANG, M. 2002. Nitric oxide formation during cortical spreading depression is critical for rapid subsequent recovery of ionic homeostasis. *J Cereb Blood Flow Metab,* 22**,** 680-8.

OBRENOVITCH, T. P., ZILKHA, E. & URENJAK, J. 1996. Evidence against high extracellular glutamate promoting the elicitation of spreading depression by potassium. *J Cereb Blood Flow Metab,* 16**,** 923-31.

PALM, K., BELLUARDO, N., METSIS, M. & TIMMUSK, T. 1998. Neuronal expression of zinc finger transcription factor REST/NRSF/XBR gene. *J Neurosci,* 18**,** 1280-96.

PAOLETTI, P. & NEYTON, J. 2007. NMDA receptor subunits: function and pharmacology. *Curr Opin Pharmacol,* 7**,** 39-47.

PATTI, L., RAITERI, L., GRILLI, M., PARODI, M., RAITERI, M. & MARCHI, M. 2006. P2X(7) receptors exert a permissive role on the activation of release-enhancing presynaptic alpha7 nicotinic receptors co-existing on rat neocortex glutamatergic terminals. *Neuropharmacology,* 50**,** 705-13.

PEETERS, M., GUNTHORPE, M. J., STRIJBOS, P. J., GOLDSMITH, P., UPTON, N. & JAMES, M. F. 2007. Effects of pan- and subtype-selective N-methyl-D-aspartate receptor antagonists on

cortical spreading depression in the rat: therapeutic potential for migraine. *J Pharmacol Exp Ther,* 321**,** 564-72.

PELEGRIN, P. 2008. Targeting interleukin-1 signaling in chronic inflammation: focus on P2X(7) receptor and Pannexin-1. *Drug News Perspect,* 21**,** 424-33.

PELEGRIN, P. & SURPRENANT, A. 2006. Pannexin-1 mediates large pore formation and interleukin-1beta release by the ATP-gated P2X7 receptor. *EMBO J,* 25**,** 5071-82.

PERREGAUX, D. & GABEL, C. A. 1994. Interleukin-1 beta maturation and release in response to ATP and nigericin. Evidence that potassium depletion mediated by these agents is a necessary and common feature of their activity. *J Biol Chem,* 269**,** 15195-203.

PERREGAUX, D. G. & GABEL, C. A. 1998. Human monocyte stimulus-coupled IL-1beta posttranslational processing: modulation via monovalent cations. *Am J Physiol,* 275**,** C1538-47.

PETTUS, E. H., CHRISTMAN, C. W., GIEBEL, M. L. & POVLISHOCK, J. T. 1994. Traumatically induced altered membrane permeability: its relationship to traumatically induced reactive axonal change. *J Neurotrauma,* 11**,** 507-22.

PETTUS, E. H. & POVLISHOCK, J. T. 1996. Characterization of a distinct set of intra-axonal ultrastructural changes associated with traumatically induced alteration in axolemmal permeability. *Brain Res,* 722**,** 1-11.

PIILGAARD, H. & LAURITZEN, M. 2009. Persistent increase in oxygen consumption and impaired neurovascular coupling after spreading depression in rat neocortex. *J Cereb Blood Flow Metab,* 29**,** 1517-27.

QUINN, J. P., BUBB, V. J., MARSHALL-JONES, Z. V. & COULSON, J. M. 2002. Neuron restrictive silencer factor as a modulator of neuropeptide gene expression. *Regul Pept,* 108**,** 135-41.

QURESHI, I. A. & MEHLER, M. F. 2011. Chromatin-modifying agents for epigenetic reprogramming and endogenous neural stem cell-mediated repair in stroke. *Transl Stroke Res,* 2**,** 7-16.

RAMBHADRAN, A., GONZALEZ, J. & JAYARAMAN, V. 2010. Subunit arrangement in N-methyl-D-aspartate (NMDA) receptors. *J Biol Chem,* 285**,** 15296-301.

RANGEL, Y. M., KARIKO, K., HARRIS, V. A., DUVALL, M. E. & WELSH, F. A. 2001. Dose-dependent induction of mRNAs encoding brain-derived neurotrophic factor and heat-shock protein-72 after cortical spreading depression in the rat. *Brain Res Mol Brain Res,* 88**,** 103-12.

READ, S. J., HIRST, W. D., UPTON, N. & PARSONS, A. A. 2001. Cortical spreading depression produces increased cGMP levels in cortex and brain stem that is inhibited by tonabersat (SB-220453) but not sumatriptan. *Brain Res,* 891**,** 69-77.

READ, S. J., SMITH, M. I., HUNTER, A. J. & PARSONS, A. A. 1997. The dynamics of nitric oxide release measured directly and in real time following repeated waves of cortical spreading depression in the anaesthetised cat. *Neurosci Lett,* 232**,** 127-30.

REDECKER, C., WANG, W., FRITSCHY, J. M. & WITTE, O. W. 2002. Widespread and long-lasting alterations in GABA(A)-receptor subtypes after focal cortical infarcts in rats: mediation by NMDA-dependent processes. *J Cereb Blood Flow Metab,* 22**,** 1463-75.

REUTER, U., WEBER, J. R., GOLD, L., ARNOLD, G., WOLF, T., DREIER, J., LINDAUER, U. & DIRNAGL, U. 1998. Perivascular nerves contribute to cortical spreading depression-associated hyperemia in rats. *Am J Physiol,* 274**,** H1979-87.

ROCKSTROH, S., EMRE, M., TARRAL, A. & POKORNY, R. 1996. Effects of the novel NMDA-receptor antagonist SDZ EAA 494 on memory and attention in humans. *Psychopharmacology (Berl),* 124**,** 261-6.

RODRIGUES, P. S., GUIMARAES, A. P., DE AZEREDO, F. A. & MARTINS-FERREIRA, H. 1988. Involvement of GABA and ACh in retinal spreading depression: effects of "low calcium-high magnesium" solutions. *Exp Brain Res,* 73**,** 659-64.

RODRIGUES, P. S. & MARTINS-FERREIRA, H. 1980. Cholinergic neurotransmission in retinal spreading depression. *Exp Brain Res,* 38**,** 229-36.

ROGATSKY, G., MAYEVSKY, A., ZARCHIN, N. & DORON, A. 1996. Continuous multiparametric monitoring of brain activities following fluid-percussion injury in rats: preliminary results. *J Basic Clin Physiol Pharmacol,* 7**,** 23-43.

ROGATSKY, G. G., SONN, J., KAMENIR, Y., ZARCHIN, N. & MAYEVSKY, A. 2003. Relationship between intracranial pressure and cortical spreading depression following fluid percussion brain injury in rats. *J Neurotrauma,* 20**,** 1315-25.

ROGAWSKI, M. A. 2012. Migraine and Epilepsy-Shared Mechanisms within the Family of Episodic Disorders. *In:* TH, NOEBELS, J. L., AVOLI, M., ROGAWSKI, M. A., OLSEN, R. W. & DELGADO-ESCUETA, A. V. (eds.) *Jasper's Basic Mechanisms of the Epilepsies.* Bethesda (MD).

ROOPRA, A., QAZI, R., SCHOENIKE, B., DALEY, T. J. & MORRISON, J. F. 2004. Localized domains of G9a-mediated histone methylation are required for silencing of neuronal genes. *Mol Cell,* 14**,** 727-38.

SACCO, C. B., TARDIF, E., GENOUD, C., PROBST, A., TOLNAY, M., JANZER, R. C., VERNEY, C., KRAFTSIK, R. & CLARKE, S. 2009. GABA receptor subunits in human auditory cortex in normal and stroke cases. *Acta Neurobiol Exp (Wars),* 69**,** 469-93.

SAMAD, T. A., MOORE, K. A., SAPIRSTEIN, A., BILLET, S., ALLCHORNE, A., POOLE, S., BONVENTRE, J. V. & WOOLF, C. J. 2001. Interleukin-1beta-mediated induction of Cox-2 in the CNS contributes to inflammatory pain hypersensitivity. *Nature,* 410**,** 471-5.

SANZ-CLEMENTE, A., NICOLL, R. A. & ROCHE, K. W. 2013. Diversity in NMDA receptor composition: many regulators, many consequences. *Neuroscientist,* 19**,** 62-75.

SASAKI, Y. F., ROTHE, T., PREMKUMAR, L. S., DAS, S., CUI, J., TALANTOVA, M. V., WONG, H. K., GONG, X., CHAN, S. F., ZHANG, D., NAKANISHI, N., SUCHER, N. J. & LIPTON, S. A. 2002. Characterization and comparison of the NR3A subunit of the NMDA receptor in recombinant systems and primary cortical neurons. *J Neurophysiol,* 87**,** 2052-63.

SCHOCK, S. C., MUNYAO, N., YAKUBCHYK, Y., SABOURIN, L. A., HAKIM, A. M., VENTUREYRA, E. C. & THOMPSON, C. S. 2007. Cortical spreading depression releases ATP into the extracellular space and purinergic receptor activation contributes to the induction of ischemic tolerance. *Brain Res,* 1168**,** 129-38.

SCHOENHERR, C. J. & ANDERSON, D. J. 1995. The neuron-restrictive silencer factor (NRSF): a coordinate repressor of multiple neuron-specific genes. *Science,* 267**,** 1360-3.

SCHWARTZ-BLOOM, R. D. & SAH, R. 2001. gamma-Aminobutyric acid(A) neurotransmission and cerebral ischemia. *J Neurochem,* 77**,** 353-71.

SHATILLO, A., SALO, R. A., GINIATULLIN, R. & GROHN, O. H. 2015a. Involvement of NMDA receptor subtypes in cortical spreading depression in rats assessed by fMRI. *Neuropharmacology,* 93**,** 164-70.

SHATILLO, A., SALO, R. A., GINIATULLIN, R. & GROHN, O. H. 2015b. Involvement of NMDA receptor subtypes in cortical spreading depression in rats assessed by fMRI. *Neuropharmacology,* 93c**,** 164-170.

SHEN, P., HOU, S., ZHU, M., ZHAO, M., OUYANG, Y. & FENG, J. 2017. Cortical spreading depression preconditioning mediates neuroprotection against ischemic stroke by inducing AMP-activated protein kinase-dependent autophagy in a rat cerebral ischemic/reperfusion injury model. *J Neurochem,* 140**,** 799-813.

SHEN, P. J. & GUNDLACH, A. L. 1999. Prolonged induction of neuronal NOS expression and activity following cortical spreading depression (SD): implications for SD- and NO-mediated neuroprotection. *Exp Neurol,* 160**,** 317-32.

SHEN, P. J., LARM, J. A. & GUNDLACH, A. L. 2003. Expression and plasticity of galanin systems in cortical neurons, oligodendrocyte progenitors and proliferative zones in normal brain and after spreading depression. *Eur J Neurosci,* 18**,** 1362-76.

SHEN, P. P., HOU, S., MA, D., ZHAO, M. M., ZHU, M. Q., ZHANG, J. D., FENG, L. S., CUI, L. & FENG, J. C. 2016. Cortical spreading depression-induced preconditioning in the brain. *Neural Regen Res,* 11**,** 1857-1864.

SHI, H., LI, J. H., JI, C. F., SHANG, H. Y., QIU, E. C., WANG, J. J. & JING, X. H. 2010. [Effect of electroacupuncture on cortical spreading depression and plasma CGRP and substance P contents in migraine rats]. *Zhen Ci Yan Jiu,* 35**,** 17-21.

SHIMA, I., FIFKOVA, E. & BURES, J. 1963. Limits of Spreading Depression in Pigeon Striatum. *J Comp Neurol,* 121**,** 485-92.

SHIMAZAWA, M. & HARA, H. 1996. An experimental model of migraine with aura: cortical hypoperfusion following spreading depression in the awake and freely moving rat. *Clin Exp Pharmacol Physiol,* 23**,** 890-2.

SHIMIZU, K., MILLER, A. W., ERDOS, B., BARI, F. & BUSIJA, D. W. 2002. Role of endothelium in hyperemia during cortical spreading depression (CSD) in the rat. *Brain Res,* 928**,** 40-9.

SHIMOJO, M., PAQUETTE, A. J., ANDERSON, D. J. & HERSH, L. B. 1999. Protein kinase A regulates cholinergic gene expression in PC12 cells: REST4 silences the silencing activity of neuron-restrictive silencer factor/REST. *Mol Cell Biol,* 19**,** 6788-95.

SILBER, J., LIM, D. A., PETRITSCH, C., PERSSON, A. I., MAUNAKEA, A. K., YU, M., VANDENBERG, S. R., GINZINGER, D. G., JAMES, C. D., COSTELLO, J. F., BERGERS, G., WEISS, W. A., ALVAREZ-BUYLLA, A. & HODGSON, J. G. 2008. miR-124 and miR-137 inhibit proliferation of glioblastoma multiforme cells and induce differentiation of brain tumor stem cells. *BMC Med,* 6**,** 14.

SKAPER, S. D., DEBETTO, P. & GIUSTI, P. 2009. P2X(7) Receptors in Neurological and Cardiovascular Disorders. *Cardiovasc Psychiatry Neurol,* 2009**,** 861324.

SKELTON, J. L., GARDNER-MEDWIN, A. R. & GEORGE, S. A. 1983. The effects of carbon dioxide, oxygen and pH on spreading depression in the isolated chick retina. *Brain Res,* 288**,** 229-33.

SMART, M. L., GU, B., PANCHAL, R. G., WILEY, J., CROMER, B., WILLIAMS, D. A. & PETROU, S. 2003. P2X7 receptor cell surface expression and cytolytic pore formation are regulated by a distal C-terminal region. *J Biol Chem,* 278**,** 8853-60.

SMITH, J. M., BRADLEY, D. P., JAMES, M. F. & HUANG, C. L. 2006. Physiological studies of cortical spreading depression. *Biol Rev Camb Philos Soc,* 81**,** 457-81.

SOLDATI, C., BITHELL, A., JOHNSTON, C., WONG, K. Y., STANTON, L. W. & BUCKLEY, N. J. 2013. Dysregulation of REST-regulated coding and non-coding RNAs in a cellular model of Huntington's disease. *J Neurochem,* 124**,** 418-30.

SOMJEN, G. G., AITKEN, P. G., BALESTRINO, M., HERRERAS, O. & KAWASAKI, K. 1990. Spreading depression-like depolarization and selective vulnerability of neurons. A brief review. *Stroke,* 21**,** III179-83.

SONN, J. & MAYEVSKY, A. 2006. Effects of anesthesia on the responses to cortical spreading depression in the rat brain in vivo. *Neurol Res,* 28**,** 206-19.

SOWELL, M. K. & YOUSSEF, P. E. 2016. The Comorbidity of Migraine and Epilepsy in Children and Adolescents. *Semin Pediatr Neurol,* 23**,** 83-91.

SPENCER, E. M., CHANDLER, K. E., HADDLEY, K., HOWARD, M. R., HUGHES, D., BELYAEV, N. D., COULSON, J. M., STEWART, J. P., BUCKLEY, N. J., KIPAR, A., WALKER, M. C. & QUINN, J. P. 2006. Regulation and role of REST and REST4 variants in modulation of gene expression in in vivo and in vitro in epilepsy models. *Neurobiol Dis,* 24**,** 41-52.

SPERLAGH, B., KOFALVI, A., DEUCHARS, J., ATKINSON, L., MILLIGAN, C. J., BUCKLEY, N. J. & VIZI, E. S. 2002. Involvement of P2X7 receptors in the regulation of neurotransmitter release in the rat hippocampus. *J Neurochem,* 81**,** 1196-211.

SPERLAGH, B., VIZI, E. S., WIRKNER, K. & ILLES, P. 2006. P2X7 receptors in the nervous system. *Prog Neurobiol,* 78**,** 327-46.

STORER, R. J. & GOADSBY, P. J. 1997. Microiontophoretic application of serotonin (5HT)1B/1D agonists inhibits trigeminal cell firing in the cat. *Brain,* 120 (Pt 12)**,** 2171-7.

STRAZISAR, M., CAMMAERTS, S., VAN DER VEN, K., FORERO, D. A., LENAERTS, A. S., NORDIN, A., ALMEIDA-SOUZA, L., GENOVESE, G., TIMMERMAN, V., LIEKENS, A., DE RIJK, P., ADOLFSSON, R., CALLAERTS, P. & DEL-FAVERO, J. 2015. MIR137 variants identified in psychiatric patients affect synaptogenesis and neuronal transmission gene sets. *Mol Psychiatry,* 20**,** 472-81.

STRONG, A. J., FABRICIUS, M., BOUTELLE, M. G., HIBBINS, S. J., HOPWOOD, S. E., JONES, R., PARKIN, M. C. & LAURITZEN, M. 2002. Spreading and synchronous depressions of cortical activity in acutely injured human brain. *Stroke,* 33**,** 2738-43.

SUADICANI, S. O., IGLESIAS, R., SPRAY, D. C. & SCEMES, E. 2009. Point mutation in the mouse P2X7 receptor affects intercellular calcium waves in astrocytes. *ASN Neuro,* 1.

SUGAYA, E., TAKATO, M. & NODA, Y. 1975. Neuronal and glial activity during spreading depression in cerebral cortex of cat. *J Neurophysiol,* 38**,** 822-41.

SUNAMI, K., NAKAMURA, T., KUBOTA, M., OZAWA, Y., NAMBA, H., YAMAURA, A. & MAKINO, H. 1989. Spreading depression following experimental head injury in the rat. *Neurol Med Chir (Tokyo),* 29**,** 975-80.

SURPRENANT, A., RASSENDREN, F., KAWASHIMA, E., NORTH, R. A. & BUELL, G. 1996. The cytolytic P2Z receptor for extracellular ATP identified as a P2X receptor (P2X7). *Science,* 272**,** 735-8.

SUZUKI, T., HIDE, I., IDO, K., KOHSAKA, S., INOUE, K. & NAKATA, Y. 2004. Production and release of neuroprotective tumor necrosis factor by P2X7 receptor-activated microglia. *J Neurosci,* 24**,** 1-7.

SZULWACH, K. E., LI, X., SMRT, R. D., LI, Y., LUO, Y., LIN, L., SANTISTEVAN, N. J., LI, W., ZHAO, X. & JIN, P. 2010. Cross talk between microRNA and epigenetic regulation in adult neurogenesis. *J Cell Biol,* 189**,** 127-41.

TABUCHI, A., YAMADA, T., SASAGAWA, S., NARUSE, Y., MORI, N. & TSUDA, M. 2002. REST4-mediated modulation of REST/NRSF-silencing function during BDNF gene promoter activation. *Biochem Biophys Res Commun,* 290**,** 415-20.

TANG, Y. T., MENDEZ, J. M., THERIOT, J. J., SAWANT, P. M., LOPEZ-VALDES, H. E., JU, Y. S. & BRENNAN, K. C. 2014. Minimum conditions for the induction of cortical spreading depression in brain slices. *J Neurophysiol,* 112**,** 2572-9.

TAPIA-RAMIREZ, J., EGGEN, B. J., PERAL-RUBIO, M. J., TOLEDO-ARAL, J. J. & MANDEL, G. 1997. A single zinc finger motif in the silencing factor REST represses the neural-specific type II sodium channel promoter. *Proc Natl Acad Sci U S A,* 94**,** 1177-82.

TATLISUMAK, T., TAKANO, K., MEILER, M. R. & FISHER, M. 2000. A glycine site antagonist ZD9379 reduces number of spreading depressions and infarct size in rats with permanent middle cerebral artery occlusion. *Acta Neurochir Suppl,* 76**,** 331-3.

TEPE, N., FILIZ, A., DILEKOZ, E., AKCALI, D., SARA, Y., CHARLES, A. & BOLAY, H. 2015. The thalamic reticular nucleus is activated by cortical spreading depression in freely moving rats: prevention by acute valproate administration. *Eur J Neurosci,* 41**,** 120-8.

TORRENTE, D., MENDES-DA-SILVA, R. F., LOPES, A. A., GONZALEZ, J., BARRETO, G. E. & GUEDES, R. C. 2014. Increased calcium influx triggers and accelerates cortical spreading depression in vivo in male adult rats. *Neurosci Lett,* 558**,** 87-90.

TOWER, D. B. & YOUNG, O. M. 1973. The activities of butyrylcholinesterase and carbonic anhydrase, the rate of anaerobic glycolysis, and the question of a constant density of glial cells in cerebral cortices of various mammalian species from mouse to whale. *J Neurochem,* 20**,** 269-78.

TOZZI, A., DE IURE, A., DI FILIPPO, M., COSTA, C., CAPRONI, S., PISANI, A., BONSI, P., PICCONI, B., CUPINI, L. M., MATERAZZI, S., GEPPETTI, P., SARCHIELLI, P. & CALABRESI, P. 2012. Critical role of calcitonin gene-related peptide receptors in cortical spreading depression. *Proc Natl Acad Sci U S A,* 109**,** 18985-90.

TURNER, D. A., FOSTER, K. A., GALEFFI, F. & SOMJEN, G. G. 2007. Differences in O2 availability resolve the apparent discrepancies in metabolic intrinsic optical signals in vivo and in vitro. *Trends Neurosci,* 30**,** 390-8.

UNEKAWA, M., IKEDA, K., TOMITA, Y., KAWAKAMI, K. & SUZUKI, N. 2017. Enhanced susceptibility to cortical spreading depression in two types of Na+,K+-ATPase alpha2 subunit-deficient mice as a model of familial hemiplegic migraine 2. *Cephalalgia***,** 333102417738249.

UNEKAWA, M., TOMITA, Y., TORIUMI, H. & SUZUKI, N. 2012. Suppressive effect of chronic peroral topiramate on potassium-induced cortical spreading depression in rats. *Cephalalgia,* 32**,** 518-27.

VAN DEN MAAGDENBERG, A. M., PIETROBON, D., PIZZORUSSO, T., KAJA, S., BROOS, L. A., CESETTI, T., VAN DE VEN, R. C., TOTTENE, A., VAN DER KAA, J., PLOMP, J. J., FRANTS, R. R. & FERRARI, M. D. 2004. A Cacna1a knockin migraine mouse model with increased susceptibility to cortical spreading depression. *Neuron,* 41**,** 701-10.

VAN HARREVELD, A., STAMM, J. S. & CHRISTENSEN, E. 1956. Spreading depression in rabbit, cat and monkey. *Am J Physiol,* 184**,** 312-20.

VERHOEF, P. A., ESTACION, M., SCHILLING, W. & DUBYAK, G. R. 2003. P2X7 receptor-dependent blebbing and the activation of Rho-effector kinases, caspases, and IL-1 beta release. *J Immunol,* 170**,** 5728-38.

VIMALRAJ, S. & SELVAMURUGAN, N. 2013. MicroRNAs: Synthesis, Gene Regulation and Osteoblast Differentiation. *Curr Issues Mol Biol,* 15**,** 7-18.

VINK, R., GABRIELIAN, L. & THORNTON, E. 2017. The Role of Substance P in Secondary Pathophysiology after Traumatic Brain Injury. *Front Neurol,* 8**,** 304.

WAGONER, M. P., GUNSALUS, K. T., SCHOENIKE, B., RICHARDSON, A. L., FRIEDL, A. & ROOPRA, A. 2010. The transcription factor REST is lost in aggressive breast cancer. *PLoS Genet,* 6**,** e1000979.

WANG, C. M., CHANG, Y. Y., KUO, J. S. & SUN, S. H. 2002. Activation of P2X(7) receptors induced [(3)H]GABA release from the RBA-2 type-2 astrocyte cell line through a Cl(-)/HCO(3)(-)-dependent mechanism. *Glia,* 37**,** 8-18.

WANG, M., CHAZOT, P. L., ALI, S., DUCKETT, S. F. & OBRENOVITCH, T. P. 2012. Effects of NMDA receptor antagonists with different subtype selectivities on retinal spreading depression. *Br J Pharmacol,* 165**,** 235-44.

WANG, M., LI, Y. & LIN, Y. 2015. GABAA receptor alpha2 subtype activation suppresses retinal spreading depression. *Neuroscience,* 298**,** 137-44.

WANG, M., OBRENOVITCH, T. P. & URENJAK, J. 2003. Effects of the nitric oxide donor, DEA/NO on cortical spreading depression. *Neuropharmacology,* 44**,** 949-57.

WANG, Y., LI, Y. & WANG, M. 2016a. Involvement of CGRP receptors in retinal spreading depression. *Pharmacol Rep,* 68**,** 935-8.

WANG, Y., TYE, A. E., ZHAO, J., MA, D., RADDANT, A. C., BU, F., SPECTOR, B. L., WINSLOW, N. K., WANG, M. & RUSSO, A. F. 2016b. Induction of calcitonin gene-related peptide expression in rats by cortical spreading depression. *Cephalalgia*.

WARBURTON, A., BREEN, G., RUJESCU, D., BUBB, V. J. & QUINN, J. P. 2014. Characterization of a REST-Regulated Internal Promoter in the Schizophrenia Genome-Wide Associated Gene MIR137. *Schizophr Bull,* 41**,** 698-707.

WARBURTON, A., BREEN, G., RUJESCU, D., BUBB, V. J. & QUINN, J. P. 2015. Characterization of a REST-Regulated Internal Promoter in the Schizophrenia Genome-Wide Associated Gene MIR137. *Schizophr Bull,* 41**,** 698-707.

WARBURTON, A., MIYAJIMA, F., SHAZADI, K., CROSSLEY, J., JOHNSON, M. R., MARSON, A. G., BAKER, G. A., QUINN, J. P. & SILLS, G. J. 2016. NRSF and BDNF polymorphisms as biomarkers of cognitive dysfunction in adults with newly diagnosed epilepsy. *Epilepsy Behav,* 54**,** 117-27.

WIGGINS, A. K., SHEN, P. J. & GUNDLACH, A. L. 2003. Atrial natriuretic peptide expression is increased in rat cerebral cortex following spreading depression: possible contribution to sd-induced neuroprotection. *Neuroscience,* 118**,** 715-26.

WILLIAMS, A. J., HARTINGS, J. A., LU, X. C., ROLLI, M. L., DAVE, J. R. & TORTELLA, F. C. 2005. Characterization of a new rat model of penetrating ballistic brain injury. *J Neurotrauma,* 22**,** 313-31.

WOOD, P. L. 2005. The NMDA receptor complex: a long and winding road to therapeutics. *IDrugs,* 8**,** 229-35.

WOOLF, C. J., ALLCHORNE, A., SAFIEH-GARABEDIAN, B. & POOLE, S. 1997. Cytokines, nerve growth factor and inflammatory hyperalgesia: the contribution of tumour necrosis factor alpha. *Br J Pharmacol,* 121**,** 417-24.

WRIGHT, C., GUPTA, C. N., CHEN, J., PATEL, V., CALHOUN, V. D., EHRLICH, S., WANG, L., BUSTILLO, J. R., PERRONE-BIZZOZERO, N. I. & TURNER, J. A. 2016. Polymorphisms in MIR137HG and microRNA-137-regulated genes influence gray matter structure in schizophrenia. *Transl Psychiatry,* 6**,** e724.

WRIGHT, C., TURNER, J. A., CALHOUN, V. D. & PERRONE-BIZZOZERO, N. 2013. Potential Impact of miR-137 and Its Targets in Schizophrenia. *Front Genet,* 4**,** 58.

YAMASAKI, Y., MATSUURA, N., SHOZUHARA, H., ONODERA, H., ITOYAMA, Y. & KOGURE, K. 1995. Interleukin-1 as a pathogenetic mediator of ischemic brain damage in rats. *Stroke,* 26**,** 676-80; discussion 681.

YANAMOTO, H., XUE, J. H., MIYAMOTO, S., NAGATA, I., NAKANO, Y., MURAO, K. & KIKUCHI, H. 2004. Spreading depression induces long-lasting brain protection against infarcted lesion development via BDNF gene-dependent mechanism. *Brain Res,* 1019**,** 178-88.

YAVICH, L. & YLINEN, A. 2005. Spreading depression in the cortex differently modulates dopamine release in rat mesolimbic and nigrostriatal terminal fields. *Exp Neurol,* 196**,** 47-53.

YEGUTKIN, G. G., GUERRERO-TORO, C., KILINC, E., KOROLEVA, K., ISHCHENKO, Y., ABUSHIK, P., GINIATULLINA, R., FAYUK, D. & GINIATULLIN, R. 2016. Nucleotide homeostasis and purinergic nociceptive signaling in rat meninges in migraine-like conditions. *Purinergic Signal,* 12**,** 561-74.

YOO, J., JEONG, M. J., LEE, S. S., LEE, K. I., KWON, B. M., KIM, D. S., PARK, Y. M. & HAN, M. Y. 2001. The neuron restrictive silencer factor can act as an activator for dynamin I gene promoter activity in neuronal cells. *Biochem Biophys Res Commun,* 283**,** 928-32.

ZHANG, X., LEVY, D., KAINZ, V., NOSEDA, R., JAKUBOWSKI, M. & BURSTEIN, R. 2011. Activation of central trigeminovascular neurons by cortical spreading depression. *Ann Neurol,* 69**,** 855-65.

ZHANG, X., LEVY, D., NOSEDA, R., KAINZ, V., JAKUBOWSKI, M. & BURSTEIN, R. 2010. Activation of meningeal nociceptors by cortical spreading depression: implications for migraine with aura. *J Neurosci,* 30**,** 8807-14.

ZHAO, L., LI, H., GUO, R., MA, T., HOU, R., MA, X. & DU, Y. 2013. miR-137, a new target for post-stroke depression? *Neural Regen Res,* 8**,** 2441-8.

ZHAO, Y., ZHU, M., YU, Y., QIU, L., ZHANG, Y., HE, L. & ZHANG, J. 2016. Brain REST/NRSF Is Not Only a Silent Repressor but Also an Active Protector. *Mol Neurobiol*.

ZILKHA, E., OBRENOVITCH, T. P., KOSHY, A., KUSAKABE, H. & BENNETTO, H. P. 1995. Extracellular glutamate: on-line monitoring using microdialysis coupled to enzyme-amperometric analysis. *J Neurosci Methods,* 60**,** 1-9.

Appendix

Appendix 1: ChIP analysis of REST binding to the two MIR137 promoters

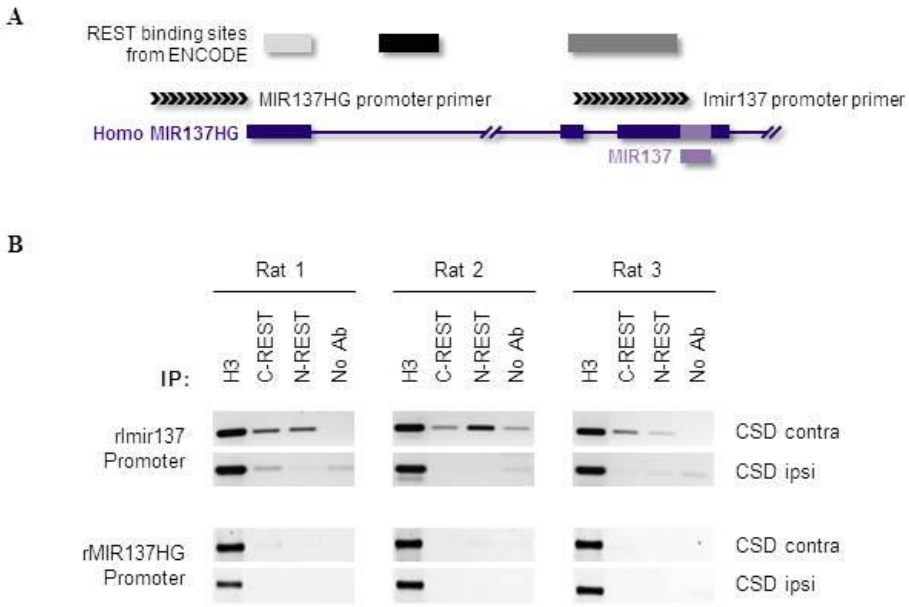

Figure A. Differential REST binding over the rImir137 and rMIR137HG promoter in rat cerebral cortex. **(A)** Illustrates predicted transcription factor binding for REST over the MIR137 locus from human ENCODE ChIP-seq data (March 2012 release), as well as primers spanning the MIR137HG and Imir137 promoters**. (B).** Multiple CSD reduced REST binding over the rImir137 promoter, but not rMIR137HG promoter, in ipsilateral cortex of rats at 24 hours post-CSD. ChIP analysis of chromatin extracted from both contralateral and ipsilateral cortices of rats 24-hour post-CSD (n = 3) was performed using antibodies against the C-REST and the N-REST, with histone H3 as a positive control. Abbreviation: *IP: immunoprecipitation*; *C-NRSF: the C-terminal of NRSF; N-NRSF the N-terminal of NRSF; No Ab: no antibody control.*

Original Article

Cephalalgia
An International Journal of Headache

International Headache Society

Cephalalgia
0(0) 1–9

DOI: 10.1177/0333102416678388
cep.sagepub.com

SAGE

Induction of calcitonin gene-related peptide expression in rats by cortical spreading depression

Yan Wang[1,*], Anne E Tye[2,*], Junli Zhao[1], Dongqing Ma[1,3], Ann C Raddant[4], Fan Bu[1,3], Benjamin L Spector[4], Nolan K Winslow[4], Minyan Wang[1,3,#] and Andrew F Russo[2,4,5,6,#]

Abstract

Objective: The neuropeptide calcitonin gene-related peptide (CGRP) has now been established as a key player in migraine. However, the mechanisms underlying the reported elevation of CGRP in the serum and cerebrospinal fluid of some migraineurs are not known. A candidate mechanism is cortical spreading depression (CSD), which is associated with migraine with aura and traumatic brain injury. The aim of this study was to investigate whether CGRP gene expression may be induced by experimental CSD in the rat cerebral cortex.

Methods: CSD was induced by topical application of KCl and monitored using electrophysiological methods. Quantitative PCR and ELISA were used to measure CGRP mRNA and peptide levels in discrete ipsilateral and contralateral cortical regions of the rat brain 24 hours following CSD events and compared with sham treatments.

Results: The data show that multiple, but not single, CSD events significantly increase CGRP mRNA levels at 24 hours post-CSD in the ipsilateral rat cerebral cortex. Increased CGRP was observed in the ipsilateral frontal, motor, somatosensory, and visual cortices, but not the cingulate cortex, or contralateral cortices. CSD also induced CGRP peptide expression in the ipsilateral, but not contralateral, cortex.

Conclusions: Repeated CSD provides a mechanism for prolonged elevation of CGRP in the cerebral cortex, which may contribute to migraine and post-traumatic headache.

Keywords

CGRP, migraine, traumatic brain injury, post-traumatic headache, gene expression

Date received: 2 May 2016; revised: 23 September 2016; accepted: 2 October 2016

Introduction

Migraine is a complex, multifactorial neurological disorder that is conservatively estimated to affect ~12% of Americans (1). The most prominent characteristic of migraine is the disabling headache, which manifests as a throbbing, unilateral pain made worse with routine activity, and coincident with nausea/vomiting and/or photophobia/phonophobia. Approximately one-third of migraineurs experience a premonitory aura, which typically manifests as a disruption in the ipsilateral visual hemifield (2). The pathophysiological substrate of the visual aura is cortical spreading depression (CSD), a transient wave of neuronal and glial depolarization, followed by a sustained depression of electrical activity (3,4). CSD is associated with a massive translocation of ions and release of nitric oxide, arachidonic acid, glutamate, and ATP (5,6). The sudden rise in extracellular K^+, arachidonic acid and nitric oxide is the likely trigger for CSD-induced activity in meningeal nociceptors (7) and central trigeminovascular neurons (8).

[1]Centre for Neuroscience and [3]Department of Biological Sciences, Xi'an Jiaotong-Liverpool University (XJTLU), SIP, Suzhou 215123, China; [2]Neuroscience Program, Departments of [4]Molecular Physiology and Biophysics, and [5]Neurology, University of Iowa, Iowa City, IA 52242, USA; [6]Veterans Affairs Medical Center, Iowa City, IA 52246, USA

*Yan Wang and Anne E Tye are equal contributors.

#Minyan Wang and Andrew F Russo are shared last authors.

Corresponding author:
Andrew Russo, Department of Molecular Physiology and Biophysics, University of Iowa, Iowa City, IA 52242, USA.
Email: andrew-russo@uiowa.edu

CSD may also lead to migraine by potentiation of an inflammatory response in the dura (9).

In addition to the connection between migraine and CSD, it is well accepted that CSD also occurs following acute brain injuries, such as traumatic brain injury (TBI) and strokes (10–12). Whereas the pattern of brain injury-triggered CSD is heterogeneous and influenced by many factors, a common feature is that there are multiple CSD events, often about every 30 minutes for many hours to days (11). For example, 72% of subarachnoid hemorrhage patients experience clusters of repetitive CSD events (13), and 56% of TBI patients experience repeated spreading depression events (mostly CSD), with a total of 1328 events observed in 58 patients over 67 hours (14). Hence, brain injury in humans can lead to tens to hundreds of CSD events over days. Repeated CSD events have also been observed for hours to days in some, but not all, animal TBI models (12).

It has been shown that multiple CSD events can modulate many genes at early (hours) and late (days to weeks) time points across a variety of gene ontologies (15,16). A potential candidate for regulation by CSD is calcitonin gene-related peptide (CGRP). CGRP is a vasoactive neuropeptide that is widely distributed in the central and peripheral nervous systems. Clinical and preclinical studies have established CGRP as a key player in migraine (17). Intravenous CGRP administration to migraineurs is sufficient to elicit a migraine-like headache (18,19), and CGRP levels have been reported to be elevated in both the serum and CSF of migraineurs (20). Importantly, CGRP receptor antagonists and CGRP-blocking antibodies can ameliorate migraine symptoms (21,22).

In this report, we have asked whether CSD is sufficient to alter CGRP expression. Such a link would fit in the context of interesting, but limited, evidence of CGRP involvement in CSD (17,23). In particular, a calcium-dependent release of CGRP was observed during CSD and inhibition of CGRP receptors reduced the magnitude of CSD in rat neocortical slices (24). Elevated CGRP may modulate neurotransmission and possibly contribute to sensory hypersensitivity (17,25). For this scenario, we reasoned that the elevated synthesis, if it occurred, would likely be maintained for a relatively long time (24 hours). Similar prolonged times were also required for activation of CGRP gene expression in trigeminal ganglia organ cultures (26), and by epigenetic reprogramming of glial cells (27). We therefore proposed that CSD might be a mechanism by which cortical levels of CGRP become elevated for a prolonged period in migraine and TBI patients.

Materials and methods

Animals

Adult male Sprague–Dawley rats ($n = 36$, 240–440 g; Shanghai SLAC Laboratory Animal Corporation, Ltd.) with food and water *ad libitum* were used. Experimental procedures were performed in the animal unit of Soochow University. All rats were healthy, with no drug treatments or previous tests carried out prior to experimentation. Animals were housed two per cage in specific pathogen-free conditions with standard bedding material and rat special synthetic feed. Animals were allowed to acclimate to the housing room for 7 days prior to the experiment, then matched by body weight into experimental groups of sham and CSD, which were performed randomly on different days using one rat per day at various times during the day. No animals were excluded from the analysis. During the experiment, rats were given isoflurane anesthesia, which was monitored by absence of whisker movements and lack of reaction to brief tail pinches. After surgeries, animals were given an antibiotic and anti-inflammatory, as described below, and outwardly appeared healthy. Euthanasia was by excess isoflurane exposure. All procedures were approved by the Ethic Review Panel of Soochow University under agreement with XJTLU, and performed in accordance with Chinese national guidelines and in adherence to ARRIVE guidelines.

CSD induction

Animals were anesthetized with isoflurane (5% induction, 2.5–3.5% during surgery, 1.0–1.5% maintenance) in O_2: N_2O (1:2). A small incision was made and two small burr holes were drilled carefully in the skull right frontoparietal region (1 mm i.d.; Figure 1). The posterior hole (4 mm posterior, 2 mm lateral to bregma) was prepared with extra care to minimize damage to the underlying dura. A silver chloride recording electrode was implanted through the anterior hole (3 mm anterior, 2 mm lateral to bregma) for recording of CSD waves. A reference electrode was placed under the scalp. Both holes were moisturized with artificial cerebrospinal fluid (ACSF; 125 mM NaCl, 2.5 mM KCl, 1.18 mM $MgCl_2$, 1.26 mM $CaCl_2$, pH 7.3). Rectal temperature was maintained at 37°C. Upon completion of surgery, rats were maintained under anesthesia for at least 1 hour to allow for stabilization and tissue recovery.

For the multiple CSD group ($n = 14$), 1 µl of 3 M KCl was carefully dropped into the posterior hole for single CSD wave elicitation. As soon as the first CSD wave was detected at the recording site, KCl was removed using a tissue, followed by washout with

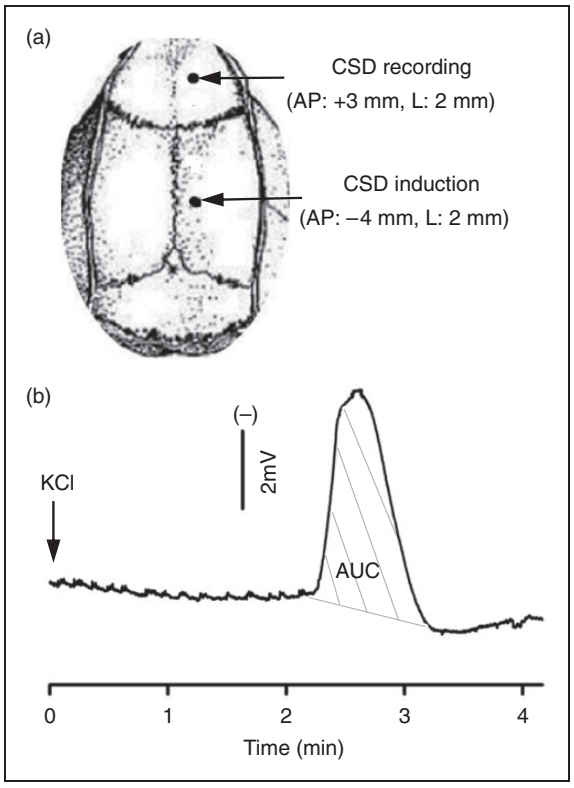

Figure 1. Cortical spreading depression (CSD) induction and propagation in the rat cortex. (A) CSD was induced with topical application of 1 μl 3 M KCl (or artificial cerebrospinal fluid for sham) onto the dura via a posterior burr hole. An anterior hole was used for CSD recording. A total of 36 rats were used. Of these, 26 rats were used for multiple CSD experiments including 14 for CSD induction and 12 for sham. To minimize the animal use, three of 14 rats in the CSD group and three of 12 in the sham group were also used for measuring calcitonin gene-related peptide (CGRP) levels in addition to CGRP mRNA. In the single CSD group, 10 rats were used with five for CSD and sham, respectively. (B) A representative trace showing CSD propagation and magnitude (indicated as area under the curve, AUC, grey lines).

ACSF and placement of ACSF-moistened cotton over the hole. For the sham group ($n = 12$), 1 μl ACSF was used. In both groups, five repeated CSD or sham episodes were elicited at 40-minute intervals. Both electroencephalogram (to monitor depth of anesthesia) and direct current potentials (to monitor CSD events) were recorded and analyzed using LabVIEW. The electrode was removed and wound sutured after the fifth CSD episode. Ibuprofen (5–10 mg) and mupirocin ointment (0.4–0.8 mg) were applied. At 24 hours after the fifth CSD episode, the rat was re-anesthetized for euthanasia and tissue removal.

For the single CSD group ($n = 5$), CSD induction, CSD recording, and post-surgery care were the same as that for the repeated CSD, except that only one CSD episode was elicited by 1 μl of 3 M KCl. For the sham group ($n = 5$), 1 μl ACSF was used. At 24 hours, the rat was re-anesthetized for euthanasia and tissue removal.

qPCR

All quantitative polymerase chain reaction (qPCR) assays on multiple CSD tissue samples were performed blinded at the University of Iowa using coded samples shipped from XJTLU. Some of those samples were also tested at XJTLU as an internal control for measurements on the single CSD samples, which were done at XJTLU. In both locations, the same protocols and reagents were used. Whole cortex or cortical regions (50–100 mg) were homogenized in 1 ml TRIzol (Sigma-Aldrich) and RNA concentration and purity measured by Nano-Drop (Thermo Scientific); 1 μg total RNA was reverse transcribed into cDNA using the GoScript™ RT system (Promega). qPCR was performed in duplicate using 1/20th of the cDNA reaction on a Bio-Rad CFX Connect using SYBR-Green Master Mix (Takara Clontech), except for 18S rRNA, which used 1/20,000th of the cDNA. Primers (forward, reverse) were: CGRP (NM_001033953.2) 5′AACCTTGGAAAGCAGCCCAGGCATG3′, 5′GTGGGCACAAAGTTGTCCTTCACCA3′; and three reference genes: peptidylprolyl isomerase A (PPIA) (NM_017101.1) 5′TTGCTGCAGACATGGTCAAC3′, 5′TGTCTGCAAACAGCTCGAAG3′; β-actin (ACTB) (NM_001101.3) 5′ACGGTCAGGTCATCACTATGG3′, 5′AGCCACCAATCCACACAG3′; and 18S rRNA (NR_046237.1) 5′ATGGCCGTTCTTAGTTGGTG3′, 5′AACGCCACTTGTCCCTCTAA3′. All qPCR data from multiple CSD samples were analyzed using both absolute quantification of CGRP mRNA (with standard curves) and relative fold change ($2^{-\Delta\Delta Cq}$ method) normalized to each contralateral hemisphere. The single CSD samples were analyzed only by the relative fold change ($2^{-\Delta\Delta Cq}$ method) normalized to the sham tissue. Standard curves were generated using plasmids containing PCR products in pCR2.1 (Invitrogen) (confirmed by sequence). CGRP mRNA levels were normalized to the product-based geometric mean of the three reference genes (28), calculated as the cube-root of the product of the reference genes $(\text{PPIA} \times \beta\text{-actin} \times 18\text{S})^{1/3}$ divided by 10,000. Similar results were observed when CGRP levels were normalized to each individual reference gene. CGRP levels are mean ± SEM.

ELISA

Protein extraction and detection from cortex homogenates followed the manufacturer's instructions using the

rat CGRP enzyme-linked immunosorbent assay (ELISA) kit (Bertin Pharma). To minimize the number of animals, cortical regions were snap frozen, pulverized, and split to allow both protein and RNA extractions. Due to the small amounts of tissue, it was necessary to combine motor, somatosensory, and visual cortices for protein, and set aside cingulate and frontal cortices for only RNA. All protein samples were rapidly homogenized within 15 seconds in 2 N acetic acid at 2 ml/100 mg tissue, then heated at 90°C for 10 minutes, centrifuged at 10,000 *g* for 30 minutes, dried for 1 hour, and stored at −80°C. Immediately before assay, samples were reconstituted with enzyme immunoassay (EIA) buffer, and analyzed using a microplate reader. CGRP levels are mean ± SEM.

Data analysis

For qPCR data, statistical analyses were performed using GraphPad Prism software as follows: comparisons across groups were done using an ordinary one-way analysis of variance (ANOVA) Kruskal–Wallis test; comparisons between ipsilateral *versus* contralateral hemispheres within the group were done using one-tailed Wilcoxon –*t*-test; comparisons between CSD and sham groups were done using one-tailed Mann–Whitney *t*-test. For ELISA data, normal distribution was confirmed by SPSS 16.0 software, and statistical analyses were performed using GraphPad Prism software with comparisons across groups using one-way ANOVA; comparisons between ipsilateral versus contralateral hemisphere within the group using one-tailed paired *t*-test; comparisons between CSD and sham groups using one-tailed unpaired *t*-test.

Results

Detection of experimentally induced CSD in rats

In the sham group, ACSF administration was insufficient to elicit CSD. In the CSD group, 1 µl of topical 3 M KCl onto the dura resulted in a CSD wave that began ~2–3 minutes after administration (Figures 1A and 1B). CSD propagation was identified by a transient, negative shift of the direct current–potential, which was observed in all CSD rats monitored by this means. For the rats that underwent multiple CSD events, the magnitude of each event was approximately 9 mV × minutes and there was no significant difference in the number or magnitude of CSD episodes over the 5 KCl applications ($p = 0.89$) (not shown). When summed up, the mean accumulative magnitude of CSD for each rat was 53.0 ± 10.2 mV × minutes in the multiple CSD group ($n = 14$) and 5.9 ± 1.8 mV × minutes ($n = 5$) in the single CSD group. Generally, only a single CSD wave was observed after each of the applications; although in four rats a second wave was observed after one of the applications in the multiple CSD group.

Increased cortical CGRP gene expression at 24 hours post-multiple CSD

In the sham group, the copy number of contralateral and ipsilateral CGRP mRNA was 13.5 ± 2.9 and 14.1 ± 2.2, respectively ($p = 0.69$), indicating that the surgical procedure did not significantly change CGRP gene expression (Figure 2A).

In the CSD group, the copy number of CGRP mRNA in the contralateral hemisphere was 18.6 ± 2.2, which is not significantly different from that of contralateral hemisphere in sham rats ($p = 0.14$; Figure 2A), demonstrating that repeated unilateral CSD does not affect CGRP gene expression in the contralateral hemisphere. In contrast, repeated CSD events in the ipsilateral hemisphere significantly increased the CGRP mRNA copy number to 79.1 ± 22.7 at 24 hours post-CSD ($p < 0.001$; Figure 2A). Comparison of relative ipsilateral CGRP levels normalized to the contralateral hemisphere of each rat agrees with the measured absolute levels. The sham group showed a 1.3 ± 0.4-fold increase between hemispheres, whereas the CSD group had a significantly greater 3.8 ± 0.8-fold increase ($p = 0.004$; Figure 2B).

No increased CGRP gene expression at 24 hours post-single CSD

In the single CSD group, CSD ipsilateral cortex did not show a significant change in CGRP mRNA levels. There was a 1.28 ± 0.06-fold change compared with that in sham ipsilateral group ($p = 0.11$; Figure 3). Contralateral samples were not included in this test, as it was shown that surgery did not significantly alter CGRP gene expression during the multiple CSD tests (Figure 2). Thus, it is very unlikely an elevation of CGRP gene expression in the contralateral cortex would be observed with single CSD.

Regional induction of CGRP in the cortex

We then examined CGRP mRNA levels in discrete regions of the cortex. In the sham group, CGRP mRNA levels in the contralateral and ipsilateral frontal, motor, somatosensory, and visual cortices were similar (Figure 4A). The cingulate had slightly higher CGRP mRNA levels in the sham contralateral (16.7 ± 4.0) and ipsilateral (32.9 ± 12.0) cortices (Figure 4A), which is consistent with a previous report that the rat cingulate has elevated CGRP relative to other cortical regions (29). There was no significant

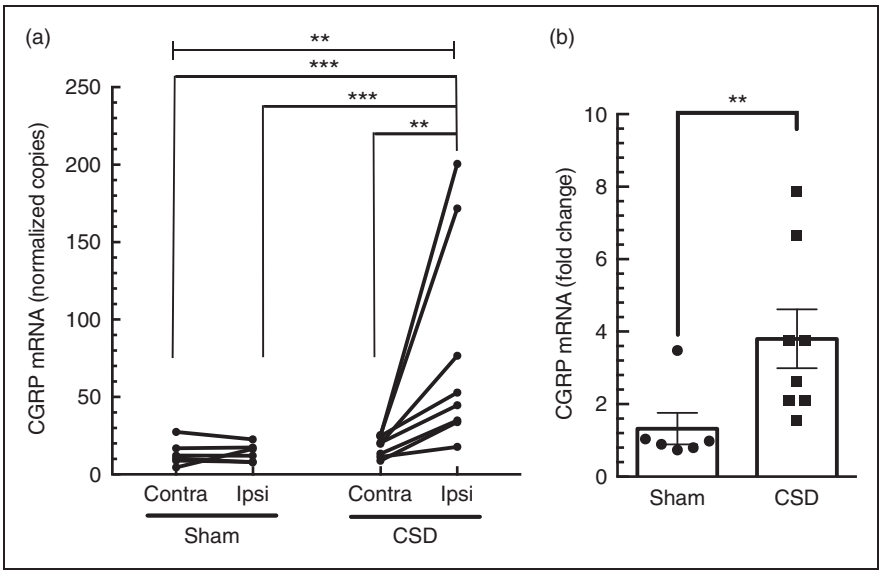

Figure 2. Ipsilateral calcitonin gene-related peptide (CGRP) mRNA is upregulated 24 hours post-multiple cortical spreading depression (CSD). (a) Absolute levels of CGRP mRNA were significantly elevated in the ipsilateral (ipsi), but not contralateral (contra), cortex post-CSD. There was no significant increase in the sham-treated rats. Data for individual rats are shown with lines connecting the paired cortices. (b) Comparison of CGRP mRNA levels between contralateral and ipsilateral cortices shown for individual rats (left panel) and as the fold change (right panel). Increased relative expression of CGRP mRNA in the ipsilateral normalized to contralateral cortex. In both (a) and (b), sham ($n = 6$), CSD ($n = 8$), $^{**}p < 0.01$; $^{***}p < 0.001$.

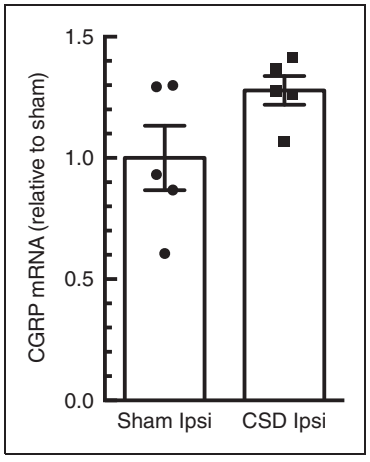

Figure 3. Ipsilateral calcitonin gene-related peptide (CGRP) mRNA is not altered 24 hours post-single cortical spreading depression (CSD). Comparison of CGRP levels between ipsilateral (ipsi) cortices of CSD rats ($n = 5$) normalized to sham rats ($n = 5$). There was no significant difference ($p = 0.11$).

change in CGRP mRNA content between contralateral and ipsilateral hemispheres of sham frontal, cingulate, or somatosensory cortices ($p = 0.16$, 0.11, and 0.22, in respective order), indicating that the surgery does not alter CGRP mRNA expression in these regions. However, a slight, but significant, increase in CGRP mRNA was observed in the motor and visual cortices of sham rats ($p = 0.016$ and 0.031, respectively; Figure 4A).

Following CSD, CGRP mRNA levels were significantly increased in the ipsilateral frontal, motor, somatosensory, and visual cortices when compared with sham ($p = 0.013$, 0.001, 0.001, and 0.001, respectively; Figure 4A). In contrast, CSD did not alter CGRP mRNA levels in the ipsilateral cingulate cortex compared with sham ($p = 0.45$; Figure 4A). As with the whole cortex, comparison between CSD and sham cohorts of the relative CGRP levels normalized to the contralateral hemisphere of each rat agreed with the absolute levels. In the CSD rats, there were significant increases in the ipsilateral compared with contralateral hemispheres of the frontal cortex (8.0 ± 1.8, $p = 0.013$), motor cortex (9.5 ± 3.1, $p = 0.013$), somatosensory cortex (15.3 ± 4.0, $p = 0.001$), and visual (14.5 ± 5.4, $p = 0.001$) compared with sham rats (Figure 4B). Also, as seen with absolute expression data, the normalized cingulate cortex did not exhibit a CSD-induced increase over sham (1.6 ± 0.3, $p = 0.45$; Figure 4B).

Increased CGRP peptide expression at 24 hours post-multiple CSD

Aliquots of somatosensory, motor, and visual cortices used for RNA analyses were combined and used for parallel peptide measurements (see Methods). In the sham group, CGRP peptide levels were 1.4 ± 0.5 ng/g tissue in the ipsilateral hemisphere and 1.8 ± 0.1 ng/g tissue in contralateral ($p = 0.27$), indicating that surgical procedures do not alter overall CGRP expression

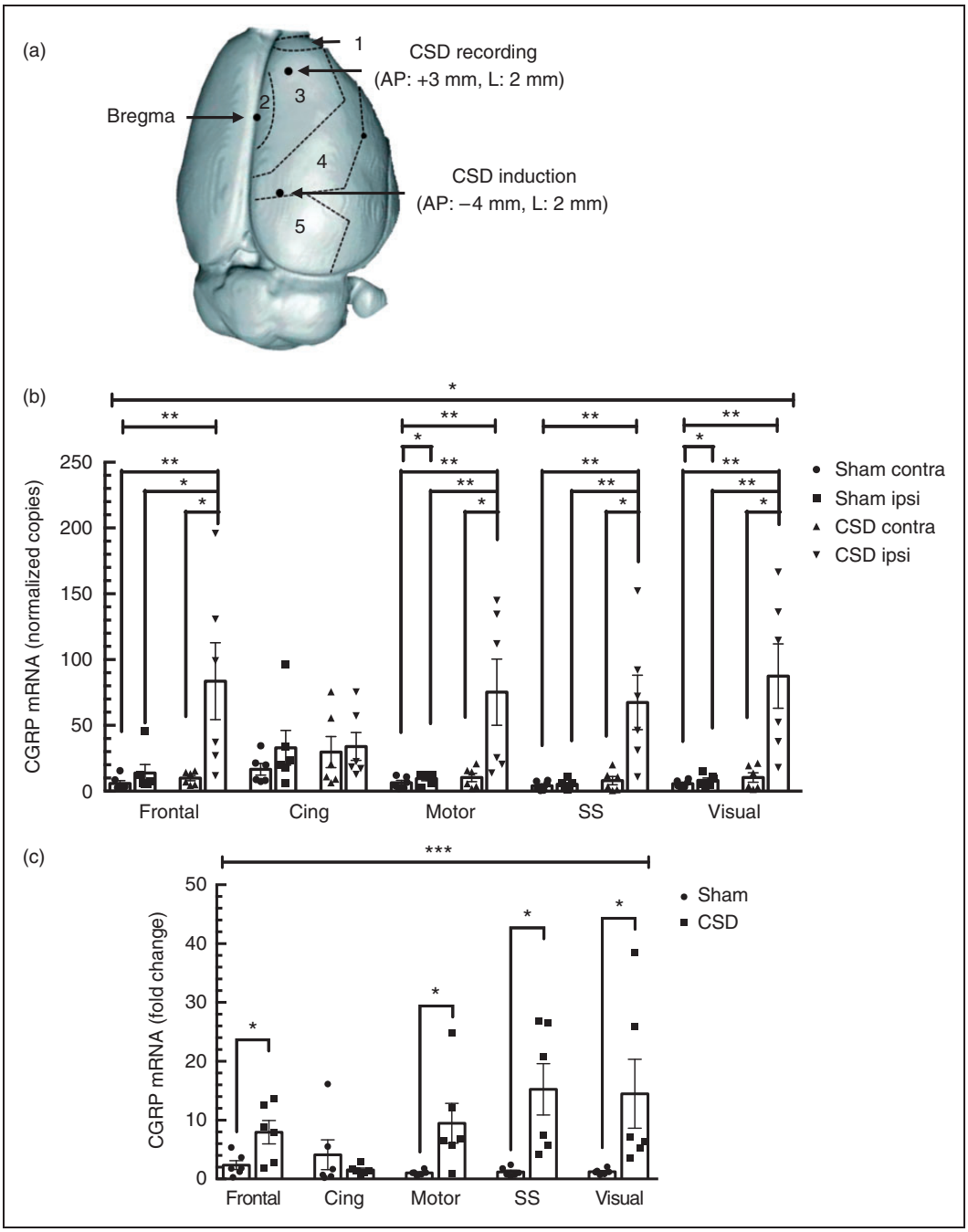

Figure 4. Multiple cortical spreading depression (CSD)-induced calcitonin gene-related peptide (CGRP) mRNA expression shows regional specificity. (a) Top view of rat brain cortical regions used for dissections. Cortical regions are designated as 1 = frontal, 2 = cingulate, 3 = motor, 4 = somatosensory, and 5 = visual. The CSD recording and induction sites are also indicated. (b) Absolute levels of CGRP mRNA were significantly elevated in ipsilateral (ipsi) frontal, motor, somatosensory (SS), and visual cortices, but not in the cingulate (Cing) cortex, or the contralateral (contra) hemispheres, 24 hours post-multiple CSD. (c) Significant increases in relative ipsilateral CGRP mRNA were observed in the frontal, motor, somatosensory, and visual cortices, but not in the cingulate cortex, at 24 hours post-multiple CSD. In both panels, sham ($n = 6$), CSD ($n = 6$), $^{*}p < 0.05$; $^{**}p < 0.01$; $^{***}p < 0.001$.

under these conditions (Figure 4). In the CSD ipsilateral cortex, the CGRP level was 4.0 ± 0.6 ng/g tissue, which was about 2.9-fold higher than sham ipsilateral cortex ($p = 0.014$; Figure 5).

Discussion

In this study, we have shown that unilateral multiple CSD is sufficient to upregulate CGRP mRNA and peptide levels in the ipsilateral cerebral cortex. The RNA

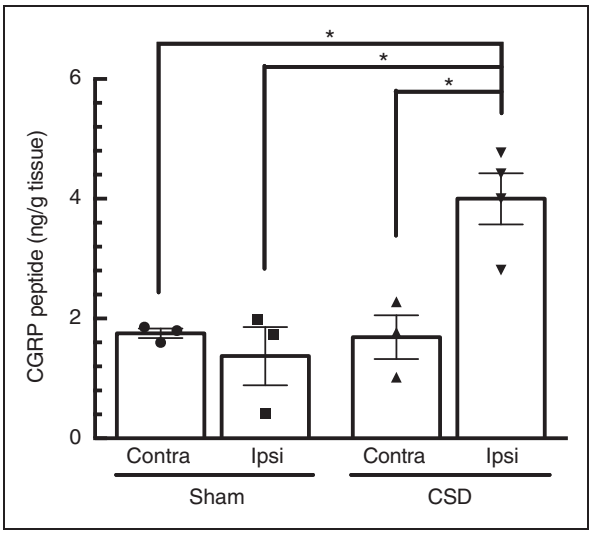

Figure 5. Ipsilateral calcitonin gene-related peptide (CGRP) peptide levels are upregulated post-multiple cortical spreading depression (CSD). CGRP peptide levels are significantly elevated in ipsilateral (ipsi) cortex 24 hours post-CSD ($n = 3$), but not the contralateral (contra) hemispheres, nor in sham rats ($n = 3$), $^*p < 0.05$.

induction was widespread across much of the cerebral cortex: in the frontal, motor, somatosensory, and visual cortices, but not in the cingulate cortex. The lack of induction in the cingulate is consistent with reports that CSD propagation is less efficient in this region (30). Importantly, the fact that CGRP mRNA levels were similarly increased in multiple cortical regions indicates that the elevated expression is attributed to CSD, rather than depolarization in the immediate area of KCl application. These data extend an earlier *in vitro* study showing that CSD induced CGRP release in rat neocortical slices (24). Thus, CSD might contribute to the elevated CGRP in the CSF of some migraine patients. However, it is very unlikely that cortical CGRP contributes to the elevation of CGRP in the external jugular vein during migraine. Indeed, Piper et al. (31) clearly documented that CGRP release into the external jugular vein was not increased by experimental CSD in the cat. Whether CSD increases synthesis in the trigeminal ganglia remains to be determined. A recent study reported that CSD increases the number of CGRP-positive cells in rat trigeminal ganglia (32), which may point to increased synthesis. Overall, these data provide evidence linking CSD and CGRP expression that may contribute to migraine pathogenesis.

A key finding of our study was that multiple CSD events were required for robust induction of the CGRP gene. The experimental protocol we used was designed to elicit multiple CSD events similar to that used in other laboratories (9,23,33–35), but which also likely differs from human migraine. Indeed migraine aura is believed to involve only a single CSD event. On the other hand, TBI is commonly associated with up to hundreds of CSD waves that can occur over days following the injury (10–12). To our knowledge, the possibility that individuals with a history of head trauma and spreading depression exhibit elevated CGRP levels has not been investigated. However, in a recent study, Elliott and colleagues observed a sustained elevation of CGRP in the brainstem (most likely from the trigeminal nerve) for at least 4 weeks in rodents exposed to controlled cortical impact injury (36). This injury can cause one to four CSD events over several hours (37). More limited studies have also reported elevated CGRP in other rodent TBI models (38,39). Whether from TBI or migraine, there is increasing evidence that CSD affects behavior and likely potentiates nociception that may in part involve CGRP. CSD activates meningeal nociceptors and central trigeminovascular neurons (7,8,40), and an immediate effect of CSD is reduced movement and freezing responses (41,42). Nonetheless, a limitation of animal CSD studies remains extrapolation to humans, especially as CSD propagation is limited by prominent sulci in the human brain that are absent in the lissencephalic rodent brain. Within this limitation, we predict that TBI may increase CGRP levels to alter brain plasticity and predispose patients to migraine-like post-traumatic headaches.

How might CSD increase cortical CGRP gene expression? While speculative, one mechanism may be generation of reactive oxygen species (ROS). Migraineurs have elevated plasma levels of a ROS-induced lipid peroxidation products (43). In rats, CSD produces ROS in the cortex and trigeminal nerve (44,45). Likewise, the ROS-responsive COX2 gene has been reported to be upregulated by CSD (16). Moreover, ROS-induced CGRP gene expression can be inhibited with antioxidant treatment in rat trigeminal ganglia (26). In light of these observations, we speculate that CSD-induced ROS production can lead to pro-inflammatory cascades that upregulate the CGRP gene. Interestingly, a recent analysis of the literature concluded that oxidative stress is a shared feature of most migraine triggers (43).

We have provided evidence showing that CSD upregulates CGRP gene expression in the cortex. Given the promising potential of CGRP-based therapeutics for treating and preventing migraine, a link between CSD and CGRP further emphasizes the importance of CSD as a target for migraine drug development (46,47). The significance of our finding is that CSD may be a mechanism by which CGRP levels become elevated for a prolonged period in some migraine patients. While there are multiple mechanisms that can potentially increase CGRP expression, including nitric oxide (48) and cytokines (33,48,49), this is the first report of a

physiological *in vivo* mechanism that may elevate cortical CGRP gene expression in migraine and post-traumatic headache. Given CGRP's role as a neuromodulator (17), this elevation may potentially contribute to cortical hyperexcitability and sensory abnormalities in migraine.

Article highlights

- Multiple CSD events can trigger CGRP gene expression in discrete regions of the rat cerebral cortex.
- This is the first *in vivo* evidence for a mechanism to initiate and maintain elevated CGRP levels in migraine and post-traumatic headache.

Acknowledgements

We are grateful for advice and training from Dan Kaufmann and KC Brennan (University of Utah) and advice from Sajedeh Eftekhari (UCLA) and Karin Warfvinge and Lars Edvinsson (Lund University). We also thank Liwen Jiang (XJTLU) for technical support on single CSD experiments.

Declaration of conflicting interests

The authors declared no potential conflicts of interest with respect to the research, authorship, and/or publication of this article.

Funding

The authors disclosed receipt of the following financial support for the research, authorship, and/or publication of this article: Wangwenli Charitable Foundation (RD0006), NIH (NS075599), Veterans Affairs Medical Center (1IO1RX002101), and Department of Defense USAMRAA (W81XWH-16-1-0071).

References

1. Lipton RB, Bigal ME, Diamond M, et al. Migraine prevalence, disease burden, and the need for preventive therapy. *Neurology* 2007; 68: 343–349.
2. Cutrer FM and Huerter K. Migraine aura. *Neurologist* 2007; 13: 118–125.
3. Ayata C and Lauritzen M. Spreading depression, spreading depolarizations, and the cerebral vasculature. *Physiol Rev* 2015; 95: 953–993.
4. Hadjikhani N, Sanchez Del Rio M, Wu O, et al. Mechanisms of migraine aura revealed by functional MRI in human visual cortex. *Proc Natl Acad Sci U S A* 2001; 98: 4687–4692.
5. Charles A and Brennan K. Cortical spreading depression-new insights and persistent questions. *Cephalalgia* 2009; 29: 1115–1124.
6. Pietrobon D and Moskowitz MA. Pathophysiology of migraine. *Annu Rev Physiol* 2013; 75: 365–391.
7. Zhang X, Levy D, Noseda R, et al. Activation of meningeal nociceptors by cortical spreading depression: Implications for migraine with aura. *J Neurosci* 2010; 30: 8807–8814.
8. Zhang X, Levy D, Kainz V, et al. Activation of central trigeminovascular neurons by cortical spreading depression. *Ann Neurol* 2011; 69: 855–865.
9. Karatas H, Erdener SE, Gursoy-Ozdemir Y, et al. Spreading depression triggers headache by activating neuronal Panx1 channels. *Science* 2013; 339: 1092–1095.
10. Dreier JP. The role of spreading depression, spreading depolarization and spreading ischemia in neurological disease. *Nat Med* 2011; 17: 439–447.
11. Lauritzen M, Dreier JP, Fabricius M, et al. Clinical relevance of cortical spreading depression in neurological disorders: Migraine, malignant stroke, subarachnoid and intracranial hemorrhage, and traumatic brain injury. *J Cereb Blood Flow Metab* 2011; 31: 17–35.
12. Hartings JA, Shuttleworth CW, Kirov SA, et al. The continuum of spreading depolarizations in acute cortical lesion development: Examining Leao's legacy. *J Cereb Blood Flow Metab*, Epub ahead of print 21 June 2016. DOI: 10.1177/0271678X16654495.
13. Dreier JP, Woitzik J, Fabricius M, et al. Delayed ischaemic neurological deficits after subarachnoid haemorrhage are associated with clusters of spreading depolarizations. *Brain* 2006; 129: 3224–3237.
14. Hartings JA, Bullock MR, Okonkwo DO, et al. Spreading depolarisations and outcome after traumatic brain injury: A prospective observational study. *Lancet Neurol* 2011; 10: 1058–1064.
15. Takizawa T, Shibata M, Kayama Y, et al. Temporal profiles of high-mobility group box 1 expression levels after cortical spreading depression in mice. *Cephalalgia* 2016; 36: 44–52.
16. Urbach A, Bruehl C and Witte OW. Microarray-based long-term detection of genes differentially expressed after cortical spreading depression. *Eur J Neurosci* 2006; 24: 841–856.
17. Russo AF. Calcitonin gene-related peptide (CGRP): A new target for migraine. *Annu Rev Pharmacol Toxicol* 2015; 55: 533–552.
18. Hansen JM, Hauge AW, Olesen J, et al. Calcitonin gene-related peptide triggers migraine-like attacks in patients with migraine with aura. *Cephalalgia* 2010; 30: 1179–1186.
19. Lassen LH, Haderslev PA, Jacobsen VB, et al. CGRP may play a causative role in migraine. *Cephalalgia* 2002; 22: 54–61.
20. van Dongen RM, Zielman R, Noga M, et al. Migraine biomarkers in cerebrospinal fluid: A systematic review and meta-analysis. *Cephalalgia*. Epub ahead of print 17 February 2016. DOI: 10.1177/0333102415625614.

21. Bigal ME, Walter S and Rapoport AM. Therapeutic antibodies against CGRP or its receptor. *Br J Clin Pharmacol* 2015; 79: 886–895.
22. Edvinsson L. CGRP receptor antagonists and antibodies against CGRP and its receptor in migraine treatment. *Br J Clin Pharmacol* 2015; 80: 193–199.
23. Wang M. Cortical spreading depression and calcitonin gene-related peptide: A brief review of current progress. *Neuropeptides* 2013; 47: 463–466.
24. Tozzi A, de Iure A, Di Filippo M, et al. Critical role of calcitonin gene-related peptide receptors in cortical spreading depression. *Proc Natl Acad Sci U S A* 2012; 109: 18985–18990.
25. Hansen JM and Ashina M. Calcitonin gene-related peptide and migraine with aura: A systematic review. *Cephalalgia* 2014; 34: 695–707.
26. Raddant AC and Russo AF. Reactive oxygen species induce procalcitonin expression in trigeminal ganglia glia. *Headache* 2014; 54: 472–484.
27. Park KY, Fletcher JR, Raddant AC, et al. Epigenetic regulation of the calcitonin gene-related peptide gene in trigeminal glia. *Cephalalgia* 2011; 31: 614–624.
28. Vandesompele J, De Preter K, Pattyn F, et al. Accurate normalization of real-time quantitative RT-PCR data by geometric averaging of multiple internal control genes. *Genome Biol* 2002; 3RESEARCH0034.
29. Bhatt DK, Gupta S, Ploug KB, et al. mRNA distribution of CGRP and its receptor components in the trigeminovascular system and other pain related structures in rat brain, and effect of intracerebroventricular administration of CGRP on Fos expression in the TNC. *Neurosci Lett* 2014; 559: 99–104.
30. Eiselt M, Giessler F, Platzek D, et al. Inhomogeneous propagation of cortical spreading depression-detection by electro- and magnetoencephalography in rats. *Brain Res* 2004; 1028: 83–91.
31. Piper RD, Edvinsson L, Ekman R, et al. Cortical spreading depression does not result in the release of calcitonin gene-related peptide into the external jugular vein of the cat: Relevance to human migraine. *Cephalalgia* 1993; 13: 180–183. discussion 49.
32. Yisarakun W, Chantong C, Supornsilpchai W, et al. Up-regulation of calcitonin gene-related peptide in trigeminal ganglion following chronic exposure to paracetamol in a CSD migraine animal model. *Neuropeptides* 2015; 51: 9–16.
33. Jander S, Schroeter M, Peters O, et al. Cortical spreading depression induces proinflammatory cytokine gene expression in the rat brain. *J Cereb Blood Flow Metab* 2001; 21: 218–225.
34. Ayata C. Pearls and pitfalls in experimental models of spreading depression. *Cephalalgia* 2013; 33: 604–613.
35. Rangel YM, Kariko K, Harris VA, et al. Dose-dependent induction of mRNAs encoding brain-derived neurotrophic factor and heat-shock protein-72 after cortical spreading depression in the rat. *Brain Res Mol Brain Res* 2001; 88: 103–112.
36. Elliott MB, Oshinsky ML, Amenta PS, et al. Nociceptive neuropeptide increases and periorbital allodynia in a model of traumatic brain injury. *Headache* 2012; 52: 966–984.
37. von Baumgarten L, Trabold R, Thal S, et al. Role of cortical spreading depressions for secondary brain damage after traumatic brain injury in mice. *J Cereb Blood Flow Metab* 2008; 28: 1353–1360.
38. Song Y, Bi L, Zhang Z, et al. Increased levels of calcitonin gene-related peptide in serum accelerate fracture healing following traumatic brain injury. *Mol Med Rep* 2012; 5: 432–438.
39. Hang CH, Shi JX, Li JS, et al. Levels of vasoactive intestinal peptide, cholecystokinin and calcitonin gene-related peptide in plasma and jejunum of rats following traumatic brain injury and underlying significance in gastrointestinal dysfunction. *World J Gastroenterol* 2004; 10: 875–880.
40. Bolay H, Reuter U, Dunn AK, et al. Intrinsic brain activity triggers trigeminal meningeal afferents in a migraine model. *Nat Med* 2002; 8: 136–142.
41. Fioravanti B, Kasasbeh A, Edelmayer R, et al. Evaluation of cutaneous allodynia following induction of cortical spreading depression in freely moving rats. *Cephalalgia* 2011; 31: 1090–1100.
42. Tepe N, Filiz A, Dilekoz E, et al. The thalamic reticular nucleus is activated by cortical spreading depression in freely moving rats: Prevention by acute valproate administration. *Eur J Neurosci* 2015; 41: 120–128.
43. Borkum JM. Migraine triggers and oxidative stress: A narrative review and synthesis. *Headache* 2016; 56: 12–35.
44. Shatillo A, Koroleva K, Giniatullina R, et al. Cortical spreading depression induces oxidative stress in the trigeminal nociceptive system. *Neuroscience* 2013; 253: 341–349.
45. Viggiano A, Viggiano E, Valentino I, et al. Cortical spreading depression affects reactive oxygen species production. *Brain Res* 2011; 1368: 11–18.
46. Costa C, Tozzi A, Rainero I, et al. Cortical spreading depression as a target for anti-migraine agents. *J Headache Pain* 2013; 14: 62.
47. Noseda R and Burstein R. Migraine pathophysiology: Anatomy of the trigeminovascular pathway and associated neurological symptoms, cortical spreading depression, sensitization, and modulation of pain. *Pain* 2013; 154(Suppl 1): S44–S53.
48. Bellamy J, Bowen EJ, Russo AF, et al. Nitric oxide regulation of calcitonin gene-related peptide gene expression in rat trigeminal ganglia neurons. *Eur J Neurosci* 2006; 23: 2057–2066.
49. Richter F, Lutz W, Eitner A, et al. Tumor necrosis factor reduces the amplitude of rat cortical spreading depression in vivo. *Ann Neurol* 2014; 76: 43–53.

Original Article

Cephalalgia
An International Journal of Headache

International Headache Society

Sarcoma family kinase activity is required for cortical spreading depression

Cephalalgia
0(0) 1–11

DOI: 10.1177/0333102417748572
journals.sagepub.com/home/cep

SAGE

Fan Bu[1,2], Yan Wang[2], Liwen Jiang[1,2], Dongqing Ma[1,2], John P Quinn[3] and Minyan Wang[1,2]

Abstract

Objectives: Sarcoma family kinase activity is associated with multiple diseases including ischemia and cancer; however, its role in the mechanism of migraine aura has been less well characterised. This study aims to investigate whether sarcoma family kinase is required for cortical spreading depression.

Methods: Cortical spreading depression was induced by topical application of K^+ to the cerebral cortex and was monitored using electrophysiology in rats, and intrinsic optical signal in mouse brain slices. Drugs were perfused into the contralateral cerebral ventricle for pharmacological manipulations in rats. Western blot analysis was used for detecting the level of phosphorylated, and total, sarcoma family kinase in the ipsilateral cortex of rats.

Key results: The data demonstrate that a single cortical spreading depression in rats induced ipsilateral cortical sarcoma family kinase phosphorylation at the Y416 site. Deactivation of sarcoma family kinase by its inhibitor (3-(4-chlorophenyl) 1-(1,1-dimethylethyl)-1*H*-pyrazolo[3,4-*d*pyrimidin-4-amine) suppressed the elevated enzyme activity and cortical susceptibility to cortical spreading depression. Interestingly, the inhibitory effect of the N-methyl-D-aspartate receptor antagonist NVP-AAM077 on cortical spreading depression was reversed by the sarcoma family kinase activator pYEEI (EPQY(PO_3H_2)EEEIPIYL), suggesting a link between this enzyme and N-methyl-D-aspartate receptors. Similarly, after deactivation of sarcoma family kinase, a reduction of sarcoma family kinase phosphorylation and cortical susceptibility to cortical spreading depression was observed with NVP-AAM077.

Conclusions: We conclude that activation of sarcoma family kinase is required for cortical spreading depression, and this process is regulated by recruiting N-methyl-D-aspartate receptors. This study provides novel insight for sarcoma family kinase function in the mechanism of migraine aura.

Keywords

Migraine, cortical spreading depression, sarcoma family kinases, N-methyl-D-aspartate receptors

Date received: 22 July 2017; revised: 11 October 2017; 2 November 2017; accepted: 4 November 2017

Introduction

Sarcoma family kinases (SFK) are a family of non-receptor protein tyrosine kinases. Five members of SFK are expressed in the mammalian central nervous system: Src, Fyn, Yes, Lck and Lyn (1). SFK phosphorylation acts as a regulatory hub converging multiple intracellular signaling cascades and membrane proteins including N-methyl-D-aspartate (NMDA) and neuronal purinergic P2X7 receptors (2–6). SFK is associated with multiple diseases including neuropathic pain (7), stroke (2) and cancer (8). A recent study shows that a SFK selective inhibitor, 3-(4-chlorophenyl) 1-(1,1-dimethylethyl)-1H-pyrazolo[3,4-d]pyrimidin-4-amine (PP2), reduces the frequency of multiple cortical spreading depression (CSD) in mice. However whether the SFK activity is involved in a single CSD, the putative underlying mechanism of migraine with aura (9) has not been elucidated.

The link between SFK and NMDA receptors is well documented. SFK can couple to the NMDA receptor,

[1]Department of Biological Sciences, Xi'an Jiaotong-Liverpool University (XJTLU), Suzhou, China
[2]Centre for Neuroscience, Xi'an Jiaotong-Liverpool University (XJTLU), Suzhou, China
[3]Department of Molecular and Clinical Pharmacology, Institute of Translational Medicine, University of Liverpool, Liverpool, UK

Corresponding author:
Minyan Wang, Department of Biological Sciences, Xi'an Jiaotong-Liverpool University, Suzhou, 215123, China.
Email: minyan.wang@xjtlu.edu.cn

forming a complex in a rat stroke model (4), and the activated SFK and NMDA receptor interaction is thought to be via the adapter protein, NADH dehydrogenase subunit 2 (ND2) (10). During anoxia/ischemia, SFK can be recruited by the activation of the NMDA receptor, leading to the opening of the neuronal hemichannel pannexin 1 (Panx1) (2); this correlates with the fact that Panx1 channels can be opened after CSD induction in mice (11). It was reported that NMDA receptor coupling with Src and the sustained neuronal depolarization during ischemia can be suppressed by the competitive NMDA receptor antagonist, (2R)-amino-5-phosphonopentanoate acting on the ligand-binding site for glutamate (4). Given that competitive antagonists targeting the NMDA receptor NR2 major subunit suppress CSD genesis and propagation (12–14), NR2A and NR2B may be key subunits of the receptor involved in any potential SFK activity in CSD.

In this report, we have investigated whether cortical SFK can be activated by a single CSD in rats. We subsequently examined whether deactivation of SFK phosphorylation reduces the likelihood of CSD occurrence and if it correlates with a reduction of SFK phosphorylation. To complement that model, we investigated a functional link between SFK activity and NMDA receptors during CSD. We reason that SFK phosphorylation, if it occurred, would likely be increased after CSD, which in turn is required for CSD propagation. SFK signaling during CSD is regulated, at least in part, by activation of NMDA receptors.

Materials and methods

Animals

A total of 34 adult male Sprague Dawley rats (328.1 ± 30.8 g, mean $\pm$ SD) and 20 adult male C57BL6 mice (21.4 ± 1.5 g, mean $\pm$ SD) were purchased from Shanghai SLAC Laboratory Animal Corporation Ltd. The sample size of animals was estimated based on previous studies on cortical spreading depression susceptibility. Animals were housed in the Experimental Animal Centre of Soochow University under agreement with Xi'an Jiaotong-Liverpool University (XJTLU) for at least 1 week with food and water available *ad libitum* before use. Animal procedures were approved by the Ethical Review Panels of Soochow University and performed during the light phase of the cycle in accordance with relevant national and provincial guidelines.

In vivo experiment

Animal surgery and CSD induction. Rats were anaesthetized with isoflurane (5% for induction, 2.5-3.5% during surgery, 1–1.5% for maintenance) in O_2:N_2O, with the animal breathing spontaneously as previously reported (14). The depth of anesthesia was monitored and adjusted through examination of the electroencephalogram (EEG) signal and by absence of whisker movements and lack of reaction to brief tail pinches. Rectal temperature of animals was maintained at 37°C.

Three burr holes were drilled in the parietal bone. One of these burr holes (1 mm, i.d, coordinates: 0.8 mm posterior and 1.8 mm lateral to bregma) was drilled in the left side, which was used for implanting a stainless steel cannula (0.38 mm i.d, RWD Life Science) into the intracerebral ventricle (*i.c.v.*, 3.5 mm deep from the cortical surface) which was used for drug perfusion (Figure 1(a)). The other two burr holes were drilled in the right side (Figure 1(a)): The posterior one (1 mm, i.d, coordinates: 5 mm posterior and 2 mm lateral to bregma) with dura intact for CSD induction; and the anterior one (0.8 mm, i.d, coordinates: 3 mm anterior and 2 mm lateral to bregma) was used for the implantation (0.9 mm deep from the cortical surface) of an Ag/AgCl electrode (0.1 mm, i.d, Applied Neuroscience). The EEG and direct current (DC) potential were derived between the Ag/AgCl electrode and a reference electrode placed under the scalp. The subsequent experimental procedure was carried out after at least one hour of stabilization.

As described previously (14), a single CSD was induced by topical application of 1 µl of 3 M KCl (Sigma-Aldrich) for 5 minutes, although occasionally two CSD waves were observed. After CSD induction, KCl was quickly replaced by artificial cerebrospinal fluid (ACSF) (composition in mM: 2.5 NaCl, 250 KCl, 1.18 $MgCl_2$, 1.26 $CaCl_2$; pH 7.3 adjusted with 1 M NaOH, not buffered) for 5 minutes to enable CSD propagating across the ipsilateral cortex (14).

Recording of EEG and extracellular DC potential. As reported previously (14), EEG and DC signals were amplified using an AC/DC pre-amplifier (NL834, Digitimer Ltd). The alternating current component in 1–30 Hz provided the EEG ($\times$5000 overall amplification) (15). The DC component in 0–30 Hz provided the DC potential ($\times$250 overall amplification). All the recorded variables were continuously displayed and recorded by Labview 11.0 (NI Instruments) during the experiment. The spreading depolarization wave of CSD was recognized as a transient negative shift (Figure 1(b)), demonstrating successful CSD induction.

In vivo experimental design. Series 1: Our previous study shows that the NR2A-preferring NMDA receptor antagonist, NVP-AAM077 (NVP), perfused through microdialysis probes suppresses CSD in rats (14). In this study, we investigated whether the drug perfused *i.c.v.* also suppresses CSD and cortical SFK phosphorylation

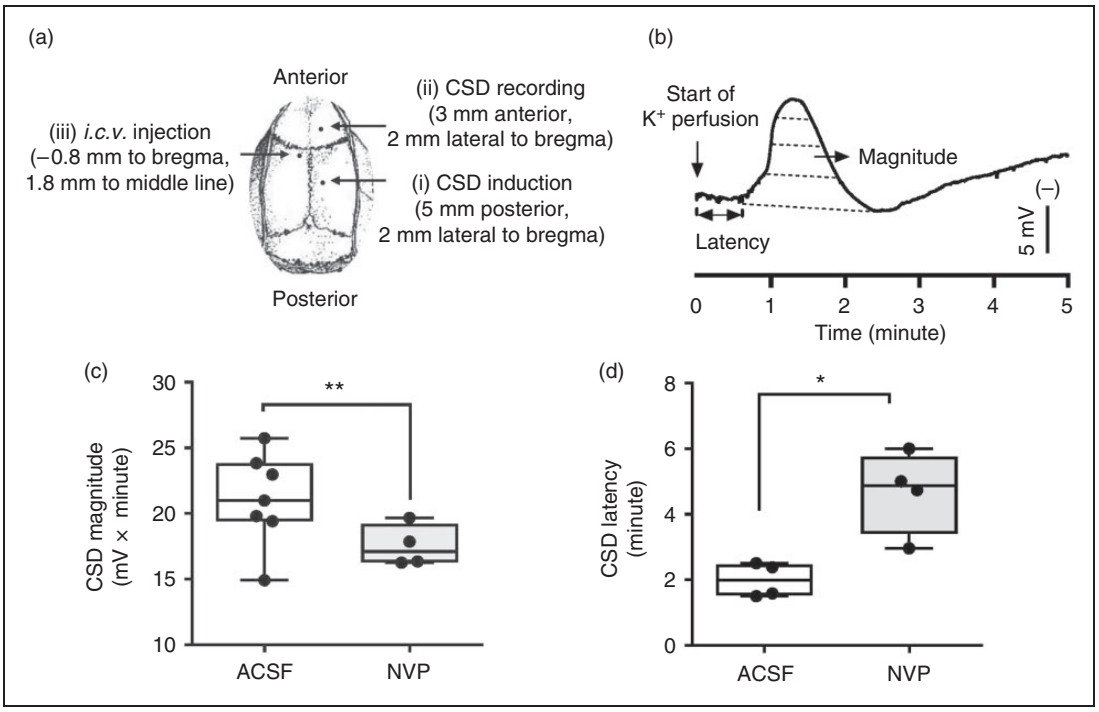

Figure 1. Effects of the NMDA receptor antagonist, NVP, perfused into contralateral ventricle on CSD in rats. (a). CSD was induced by topical application of 1 μl of 3 M KCl for 5 minutes onto cortex with dura intact via the posterior burr hole on the right parietal bone. The ipsilateral anterior hole was used for CSD recording. NVP (i) or ACSF (ii) was perfused through a cannula implanted in the contralateral ventricle (*i.c.v.*) at 120 minutes prior to CSD induction. In the sham group (iii), only ACSF was perfused in the absence of KCl application as the control. The whole ipsilateral cortical tissue was subsequently used for detecting SFK activity after the *in vivo* experiment. (b). A representative trace showing CSD propagation wave after *i.c.v.* perfusion of ACSF. CSD magnitude (mV × minute, dashed area) and latency (L, minute) were used for quantifying CSD. The effect of 0.3 nmol NVP on CSD magnitude are shown in panel (c) and latency in panel (d). All the values shown are median (range). $^{*}p < 0.05$, $^{**}p < 0.01$, Mann-Whitney test with one-tailed calculation was used for comparison of ACSF and NVP groups.

induced by CSD in rats. Three groups were designed: (i) the known anti-CSD drug, NVP (synthesized by Yi Li from XJTLU) (n = 5) with a total 0.3 nmol NVP applied. (ii) ACSF was used for both the CSD group ($n = 7$); and (iii) the sham group ($n = 5$).

Series 2: We examined whether CSD could induce SFK activation, and if so, whether the activation of SFK after CSD and the cortical susceptibility to CSD could be suppressed by SFK inhibition. Four groups were designed: (i) The SFK selective inhibitor, PP2 (#1407, Tocris) (16) with final 2.5 nmol used (n = 7); (ii) the negative control for PP2, PP3 (1-Phenyl-1*H*-pyrazolo[3,4-*d*]pyrimidin-4-amine, #2794, Tocris) with total 2.5 nmol used as the negative control (n = 7); (iii) ACSF was perfused for CSD group (n = 7) and (iv) sham group (n = 5) where no KCl was applied. In order to minimize animal use, both the CSD and sham groups from series 1 were also used in this series.

In the above two series, each drug or ACSF was perfused *i.c.v.* using a syringe pump (CMA100, CMA/Microdialysis) at 0.5 μl/minute for 10 minutes starting at 120 minutes before CSD induction. Rats in each group were immediately sacrificed as soon as CSD recordings were completed. Rat cortices were dissected for subsequent detection of levels of SKF phosphorylation in order to address whether CSD induced SFK phosphorylation, and if so, whether this elevation was altered with SFK or NMDA receptor inhibition.

Protein preparation

Ipsilateral cortices from rats were homogenized in the presence of protease inhibitor (04693116001, Roche) and phosphatase inhibitor (#5870, CST) for subsequent detection of SFK phosphorylation. Total protein was harvested from supernatant after tissue lysate was centrifuged at 13,000 rpm for 10 minutes at 4°C. Protein concentration was determined using Bicinchoninic Acid Protein Assay Kit (P0010, Beyotime).

Western blotting

Proteins were denatured with 4 × NuPAGE® LDS Sample Buffer (NP0007, Invitrogen) by boiling for

5 minutes, separated on a 10% sodium dodecyl sulfate–polyacrylamide gel and subsequently transferred onto nitrocellulose membranes. Non-specific binding of antibody was blocked with 5% milk in Tris-Buffered Saline with Tween-20 (TBST) for 1 hour at room temperature (RT).

The level of SFK (~60 kDa) phosphorylation at Y416 amino acid (PY416 SFK), a strong indicator of SFK activation (17), and β-actin (~45 kDa) as the reference under CSD condition (18) were detected using western blot analysis. Each membrane was cut into two parts horizontally, which were incubated with anti-PY416 monoclonal SFK antibody (anti-rabbit, #6943, CST, 1:500) and β-actin monoclonal antibody (anti-rabbit, #4970, CST, 1:1000) separately overnight at 4°C. Excess primary antibody was removed by TBST, membranes and the membranes incubated with horseradish peroxidase-labeled secondary antibody (AB10058, Sangon Biotech) at 1:5000 for 1 hour at RT. Proteins were detected by Western bright enhanced chemiluminescence working solution (K-12045-D50, Advansta). In order to further detect the level of total SFK (~ 60 kDa), the anti-PY416 SFK antibody on the nitrocellulose membrane was stripped away using 0.2 M NaOH for 15 minutes at 37°C. The membrane was then washed using TBST and the same process repeated, starting from non-specific binding blocking except that anti-SFK monoclonal antibody (anti-rabbit, #2109, CST) at 1:1000 but not anti-PY416 SFK antibody was used. Protein expression level was subsequently quantified using ImageJ software, and data was normalized to β-actin for comparison.

In vitro experiment

Mouse brain slice preparation. The mouse brain slice model of CSD was established by referencing those reported previously in the mouse brain slice (19,20), rat brain slice (21) and chick retina (22) with modifications as below. Briefly, the mouse brain was removed and the cerebrum was cut along the midline and coronal sections (400 μm) were prepared using a vibratome (7000 smz-2, Campden, UK) with coordinates between 1 to 3 mm posterior to bregma, each containing somatosensory and visual cortices that are highly associated with migraine aura (9,23). Brain slices were quickly transferred into ice-cold oxygenated NMDG-HEPES cutting solution (24) with minor modifications to maintain osmolality around 300 mOsm and improve tissue survival time. Of these, HEPES was added into the modified cutting solution (composition in mM: 93 NMDG, 2.5 KCl, 1.2 NaH_2PO4, 30 $NaHCO_3$, 20 HEPES, 25 glucose, 5 L-ascorbic acid, 2 thiourea, 3 sodium pyruvate, 10 $MgSO_4$, 0.5 $CaCl_2{\cdot}2H_2O$; bubbled with 95% O_2 and 5% CO_2; pH 7.4) in order to prevent tissue edema (25). After 15 min stabilization at room temperature, brain slices were transferred into Kreb's solution (composition in mM: 126 NaCl, 2.5 KCl, 2.4 $CaCl_2{\cdot}2H_2O$, 1.3 $MgCl_2{\cdot}6H_2O$, 18 $NaHCO_3$, 1.2 NaH_2PO_4, 10 Glucose; bubbled with 95% O_2 and 5% CO_2; pH 7.4) and maintained for 80 minutes prior to carrying out further procedures. In order to reduce the animal use, at least two brain slices from each mouse were used and they were assigned to different experimental groups.

CSD induction and imaging of mouse cortical slice. Each brain slice was placed in a chamber and submerged in Kreb's solution with a perfusion rate of 3 ml/minute using a peristaltic pump (Reglo ICC, Ismatec). Unless otherwise stated, CSD was induced in the somatosensory region by ejection of 33 μl of 260 mM KCl at 25 μl/minute using a syringe pump (CMA/400, CMA/Microdialysis). The coronal slice was illuminated for 50 ms, starting when CSD was elicited, using a high-power LED spotlight (625 nm peak wavelength, SLS-0307-A, Mightex) driven by a computer-controlled power supply (LED controller, SLC-SA04-US, Mightex). For each KCl application, changes in the reflected intrinsic optical signal in each cortical slice were recorded for 15 minutes at 2 Hz with a charge-coupled device monochrome camera (Rolera-XR, ROL-XR-F-M-12, Qimaging) using Image Pro Plus software (IPP7; Media Cybernetics) (22). Camera exposure and illumination were synchronized using an external trigger (TG1006, TTI).

Intrinsic optical imaging of CSD was captured from each 1800-frame sequence, in which an area of interest (AOI) parallel to the CSD wave front was delineated manually in layers 4 to 6 of the somatosensory cortex that were distant from the site of KCl application. For each picture within the sequence, gray levels of the pixel constituting the AOI were corrected by subtracting the respective dark background. Changes in this value were plotted against time (i.e. 1800 data points over 15 minutes), providing the dynamic changes within the AOI. This signal is synchronous with the sudden cellular depolarization that characterizes the excitation phase of CSD (26).

In vitro experimental design. Series 3: In order to explore a functional link between SFK and NMDA receptor during CSD, we investigated whether the inhibitory effect of NVP on CSD could be altered by co-application of an SFK activator in the mouse brain slice. Four groups were designed: (i) Kreb's control ($n = 6$); (ii) NVP, at 0.1 μM ($n = 7$); (iii) NVP and the SFK activator, pYEEI (27) (sequence: EPQY(PO_3H_2)

EEEIPIYL, APeptide Ltd, China) at 0.3 μM (n = 7); and (iv) NVP and the negative analog of SFK activator, YEEI (sequence: EPQYEEEIPIYL, APeptide Ltd, China) at 0.3 μM (n = 8). Two CSD episodes were elicited in each experiment with a 45-minute interval for tissue recovery. The drug or vehicle was perfused 45 minutes prior to the second CSD induction for 1 hour, that is, the first CSD was under Kreb's perfusion in both the control and drug groups; however, the drug replaced Kreb's solution in the drug group prior to the second CSD.

Data presentation and statistical analysis

For *in vivo* data analysis, electrophysiological data on CSD was quantified as described previously (14) using the Labview program. The following parameters were defined: (i) Area under the curve (AUC, mV × minute) of CSD waves was used to reflect CSD magnitude. Although very occasionally, in the case where more than one CSD wave was elicited, the AUC of the first CSD wave in each rat was used for comparison; and (ii) latency (minute), the time difference between the start of KCl application to the starting point of the rising phase of the first CSD wave. Both CSD magnitude and latency were used to reflect cortical susceptibility to CSD.

For the image analysis, intrinsic optical imaging of CSD was quantified as reported previously (22), for each CSD wave. Latency was calculated by the time interval between the starting point of KCl ejection and that of CSD elicitation. AUC was calculated by gray levels × minute. In each image sequence related to a given CSD, the distance of 1 mm between two images in the same CSD wave, divided by the difference in their exposure time, allowed the calculation of CSD propagation rate (mm/minute). In order to eliminate variations of AOI chosen in each individual experiment, CSD magnitude and latency within each different test were given in delta intensity between the second CSD and the first CSD episode relative to that of the first CSD wave (i.e. initial control) respectively.

The abnormal distribution test using Shapiro-Wilk was confirmed using Prism software. All values were given in median (range). The Mann-Whitney test was used for comparing two independent groups with two-tailed calculation, except for one-tailed calculation for investigating the effects of NVP on CSD in rats. Significant differences are shown as $*p < 0.05$ and $**p < 0.01$. Correlation analysis was carried out between CSD characteristics and levels of SFK phosphorylation of individual experiments with NMDA receptor inhibition or SFK deactivation.

Results

NMDA receptor inhibition suppressed CSD in rats

We investigated whether the NMDA receptor antagonist, NVP, perfused *i.c.v* suppresses CSD in rats. In the ACSF group, topical application of 3 M KCl for 5 minutes typically elicited one CSD wave that was identified by a transient negative shift of DC potential (Figure 1(b)); however, two CSD waves were observed in two out of seven rats. The CSD magnitude and latency was 20.99 (10.82) mV × minute (n = 6) and 1.98 (1.00) minutes (n = 4), respectively (Figure 1(c), (d)). Compared with the CSD group, 0.3 nmol NVP perfused into contralateral *i.c.v*. markedly reduced CSD magnitude to 17.10 (3.42) mV × minute (n = 4, $p = 0.009$, Figure 1(c)). In addition, CSD latency was significantly prolonged to 4.86 (3.04) minutes (n = 4, $p = 0.014$, Figure 1(d)). Overall, these data are consistent with that reported previously in the chick retina (22,28) and rat (14).

CSD-induced ipsilateral cortical SFK activation

Results regarding whether CSD could induce SFK phosphorylation demonstrate that both phosphorylated SFK at amino acid Y416 and total SFK were detected in the ipsilateral cortex of rats with a molecular weight of 60 KDa (Figure 2(a)). In the sham group, the relative intensity of PY416 SFK and total SFK was 0.27 (0.22) (n = 5) and 0.95 (0.18) (n = 4) respectively (Figure 2(b)). In the CSD group, the relative intensity of PY416 SFK was 0.97 (0.7) (n = 5), which was significantly increased compared with that of the sham group ($p = 0.008$), demonstrating that a single CSD is sufficient to induce SFK phosphorylation. In contrast, the level of total SFK was not different to that of the sham group CSD (n = 6).

SFK inhibition suppressed CSD-induced SFK activation

We examined whether SFK phosphorylation induced by CSD could be suppressed by the SFK selective inhibitor, PP2. When 2.5 nmol PP3, the negative control for PP2, was perfused into *i.c.v*, the level of phosphorylated SFK in the ipsilateral cortex was 0.98 (0.45), which is similar to that of the CSD-only group (n = 4, Figure 2(b)). Similarly, total SFK level with 1.09 (0.21) was not altered (n = 3). However, 2.5 nmol PP2 perfused into the *i.c.v* markedly reduced the level of phosphorylated SFK to 0.44 (0.28) (n = 5). This reduction was significantly different from that of either the PP3 group ($p = 0.016$) or CSD group ($p = 0.032$). In contrast, the level of total SFK was not altered by PP2 (n = 4).

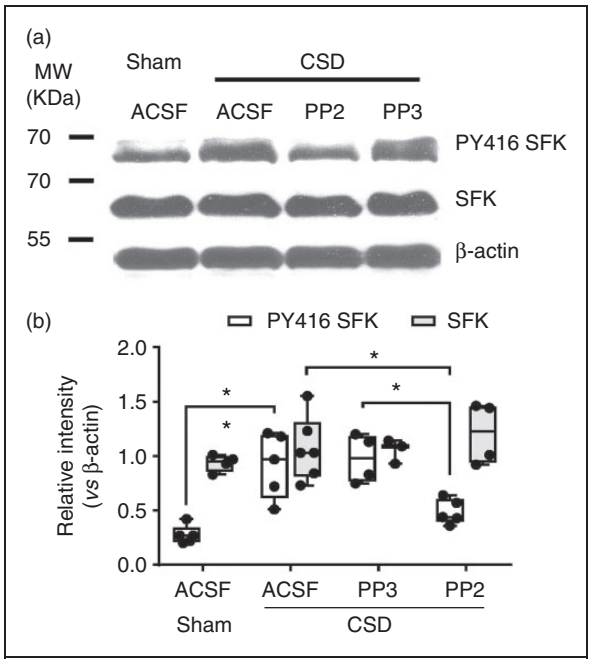

Figure 2. Detection of SFK activity after CSD and effects of PP2 on SFK activation induced by CSD in the ipsilateral cortex of rats. (a) Representative immunoblotting of PY416 SFK and total SFKs treated with *i.c.v.* perfusion of ACSF, PP3 or PP2 in response to CSD. Equal loading of samples was indicated by the β-actin intensity. Phosphorylation at Y416 amino acid (PY416) levels indicated activated SFK and total SFK levels indicated SFK expression. Samples without CSD induction from the sham group are used as control. (b) Quantitative analysis of relative intensity of PY416 SFK and total SFK normalized to β-actin. All the values shown are median (range). $*p < 0.05$, $**p < 0.01$, Mann-Whitney test, two-tailed calculation, was used for the comparison of PY416 SFK or total SFK levels between sham vs. CSD only group; ACSF vs. PP3 or PP2 group; as well as PP3 vs. PP2 group.

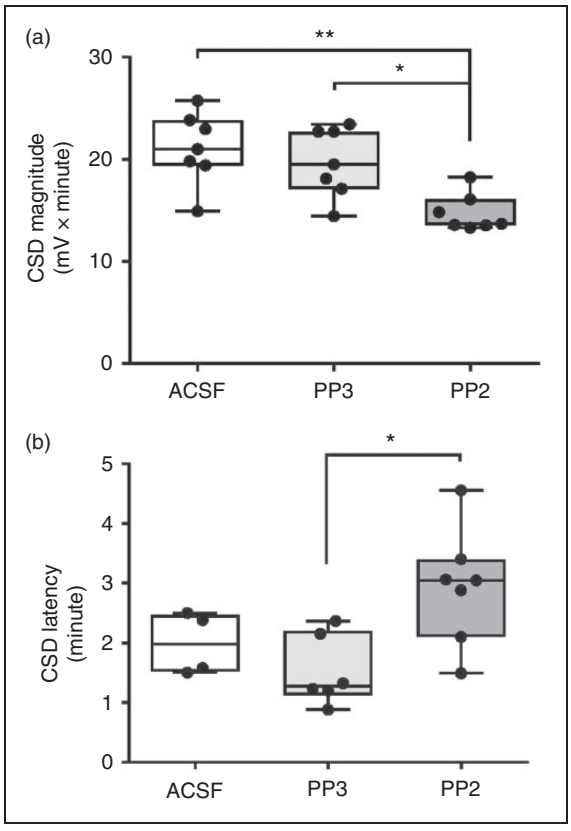

Figure 3. Effects of SFK inhibition on the magnitude (a) and latency (b) of CSD in rats. The SFK inhibitor PP2 at 2.5 nmol, its negative analog PP3 at 2.5 nmol or ACSF was perfused into the contralateral *i.c.v.* 2 hours prior to CSD induction. All the values shown are median (range). $*p < 0.05$, $**p < 0.01$, Mann-Whitney test, two-tailed calculation, was used for the comparison of CSD latency and magnitude between ACSF vs. PP3, ACSF vs PP2, and PP3 vs PP2 groups.

SFK inhibition suppressed CSD

To further our analysis, we addressed whether inhibition of SFK activity by PP2 could suppress cortical susceptibility to CSD in rats. In the ACSF group, the CSD magnitude and latency were 20.99 (10.82) mV × minute (n = 7), 1.98 (1) minutes (n = 4) respectively (Figure 3). PP3 at 2.5 nmol perfused into *i.c.v.* did not alter all these parameters (Figure 3). In contrast to PP3 but similar to NVP (Figure 1), PP2 at 2.5 nmol markedly suppressed the magnitude of CSD to 13.68 (4.93) mV × minute (n = 7) compared with either the PP3 group (n = 7, $p = 0.011$) or ACSF group (n = 7, $p = 0.002$, Figure 3(a)). In addition, PP2 also prolonged CSD latency to 3.05 (3.06) minutes (n = 7), which was significantly different to that of the PP3 group (n = 6, $p = 0.014$, Figure 3(b)).

The inhibitory effect of NMDA receptor antagonist on CSD was reversed by SFK activation

The mouse brain slice CSD model was validated using NVP. In the Kreb's group, changes in CSD magnitude and latency in the second episode over the first CSD were −5.30 (32.58) (n = 5) and 29.0 (90) (n = 6) respectively (Figure 4(c), (d)). The propagation rate was 6.29 (4.07) mm/minute (n = 5) (Figure 4(e)). Compared with the Kreb's group, perfusion of NVP at 0.3 μM significantly suppressed the magnitude of CSD and CSD propagation rate with the reduction to −35.89 (20.89) (n = 5, $p = 0.008$) and 4.55 (3.33) mm/minute (n = 7, $p = 0.018$) (Figure 4(c) and (e)). These results are consistent with the previous studies in chick retina (22) and rats (14), suggesting the mouse brain slice CSD model is valid for investigating NMDA receptor pharmacology.

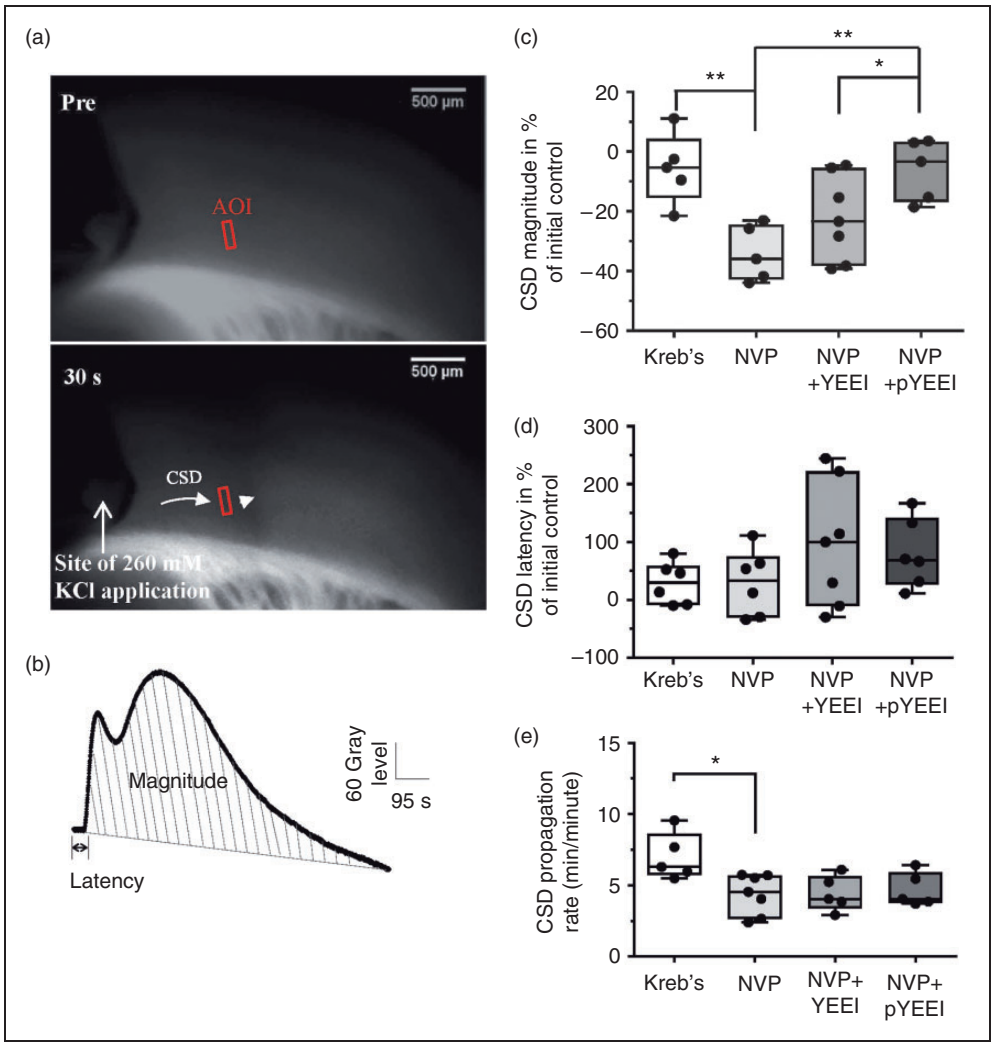

Figure 4. Effects of SFK activation on the suppression of CSD by NVP in the mouse brain slice. (a) Representative images of mouse cortical slice before ((a), upper) and after ((a), lower) K^+-induced CSD in the mouse coronal slice. CSD was plotted by the kinetic changes in gray level intensity within the selected area of interest (AOI, area within the red rectangle). The same AOI along CSD wave front (indicated by the short arrow) was selected and used for all images of the sequence under study. (b) Representative traces shows CSD wave treated with bath perfusion of Kreb's. All the averaged gray levels within the AOI were plotted against time to generate the CSD wave showing a biphasic pattern. CSD magnitude was indicated by the area under the curve of CSD wave. CSD latency is the time interval required for eliciting depolarization from the start point of KCl application. Propagation rate of CSD (mm/minute) reflects the velocity of CSD wave propagating across cortex. Panels (c)–(e) show effects of the SFK activator, pYEEI, at 0.1 μM on the CSD magnitude (c), latency (d) and propagation rate (e) in the presence and absence of NVP at 0.3 μM. YEEI at 0.1 μM was set as the scramble control of pYEEI. In order to minimize data variation, CSD magnitude (c) and latency (d) were presented as changes in reflected difference in light intensity between CSD2 and CSD1 (i.e. delta CSD magnitude and latency) relative to the initial control. All the values shown are median (range). *$p < 0.05$, **$p < 0.01$, Mann-Whitney test, two-tailed calculation, was used for the comparison between two independent groups.

In contrast to that reported previously in rats (14), the CSD latency was not altered by NVP compared with the Kreb's group (Figure 4(d)). The mechanism for this difference is not known, but may be associated with different tissues used in these studies, that is, the rat cortex *in vivo* versus the mouse brain slice in this experiment.

We utilized this model to address whether the inhibitory effect of NVP on CSD could be reversed by the SFK activator. The brain slice treated with the negative control, YEEI, at 0.1 μM in the presence of NVP, resulted in changes in the magnitude and latency of CSD, which were −23.25 (34.62) (n = 7, Figure 4(c)) and 100 (274.4) (n = 7, Figure 4(d)) respectively.

The propagation rate was 4.05 (3.18) mm/minute (n = 5, Figure 4(e)). These results were similar to the result of the NVP group. Interestingly, exposing a cortical slice to pYEEI at 0.1 μM (n = 5) reversed the suppressive effect of NVP on CSD magnitude, which was significant compared with the NVP + YEEI group ($p = 0.018$) or NVP alone group ($p = 0.008$, Figure 4(c)). However, neither the CSD latency (Figure 4(d)) nor CSD propagation rate (Figure 4(e)) was altered by pYEEI.

The NMDA receptor antagonist suppressed CSD-induced cortical SFK activation

Whether CSD-induced elevation of SFK phosphorylation was suppressed by NMDA receptor inhibition was further examined. In the sham group, the relative intensity of phosphorylated SFK and total SFK of the ipsilateral cortex were 0.31 (0.22) (n = 5) and 0.84 (0.25) respectively (n = 5, Figure 5(b)). As described above, CSD significantly increased the level of phosphorylated SFK to 0.59 (0.67) (n = 8, $p = 0.002$), but it did not alter the level of total SFK (n = 8, Figure 5(b)). Compared with that of the CSD group, 0.3 nmol NVP perfused into *i.c.v.* significantly reduced the level of phosphorylated SFK induced by CSD to 0.32 (0.27) (n = 5, $p = 0.006$, Figure 5(b)). However, the level of total SFK was not altered by application of NVP (n = 5, Figure 5(b)).

Reduced cortical susceptibility to CSD correlates with a lower level of SFK phosphorylation by PP2 and NVP

We further carried out correlation analysis of CSD latency and magnitude with levels of ipsilateral cortical SFK phosphorylation with and without NMDA receptor inhibition or SFK deactivation in rats. The results showed that after PP2 perfusion *i.c.v* at 120 minutes prior to CSD induction, lower levels of SFK phosphorylation showed a tendency for negative correlation with the increased CSD latency (Figure 6(a)) and a positive correlation with the reduced magnitude (Figure 6(c)). Similarly, after perfusion of NVP at 120 minutes prior to CSD induction, the lower levels of SFK phosphorylation also showed a strong negative correlation with the increased CSD latency (Figure 6(b)), whereas its correlation with the reduced CSD magnitude was not pronounced relative to the control (Figure 6(d)).

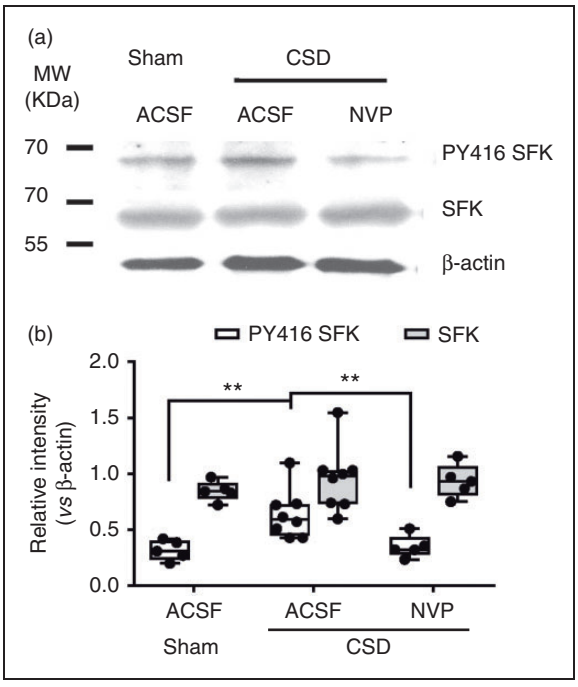

Figure 5. Effects of NMDA receptor inhibition on CSD-induced SFK activation in the ipsilateral cortex of rats. (a) Representative immunoblotting of PY416 SFK and total SFKs treated with *i.c.v.* perfusion of NVP at 0.3 nmol (i) or ACSF (ii) in response to CSD. Samples without CSD induction (iii) from the sham group were used as control. Equal loading of samples was indicated by the β-actin intensity. PY416 levels indicated activated SFK and total SFK levels indicated SFK expression. (b) Quantitative analysis of relative intensity of PY416 SFK and total SFKs normalized to β-actin. All the values shown are median (range). $^{**}p < 0.01$, Mann-Whitney test, two-tailed calculation, was used for the comparison of PY416 SFK or total SFK levels between ACSF groups with vs. without CSD; and ACSF vs. NVP groups with CSD.

Discussion

In this study, we used *in vivo* and *in vitro* approaches to show that a single CSD rapidly promotes SFK phosphorylation while deactivation of SFK reduces the likelihood of CSD occurrence, which coincides with the lower level of SFK phosphorylation. Further investigation shows that this can be regulated by NMDA receptors. This finding provides novel insight into SFK signaling in the mechanisms underpinning migraine aura, indicating that SFK may be a potential target for migraine prophylaxis.

A key finding of our study is that SFK activity is required for CSD propagation. A single CSD rapidly promoted the ipsilateral cortical SFK phosphorylation at its active Y416 site, and this elevation of SFK phosphorylation was prevented by the SFK inhibitor perfused into the contralateral *i.c.v.* of rats (Figure 2). Consistent with this, SFK inhibition also reduced cortical susceptibility to CSD as PP2 suppressed CSD magnitude and prolonged CSD latency in rats (Figure 3). We conclude that a single CSD induces rapid SFK activation, which in turn contributes to CSD propagation. Further correlation analysis demonstrated that the reduction of cortical susceptibility to

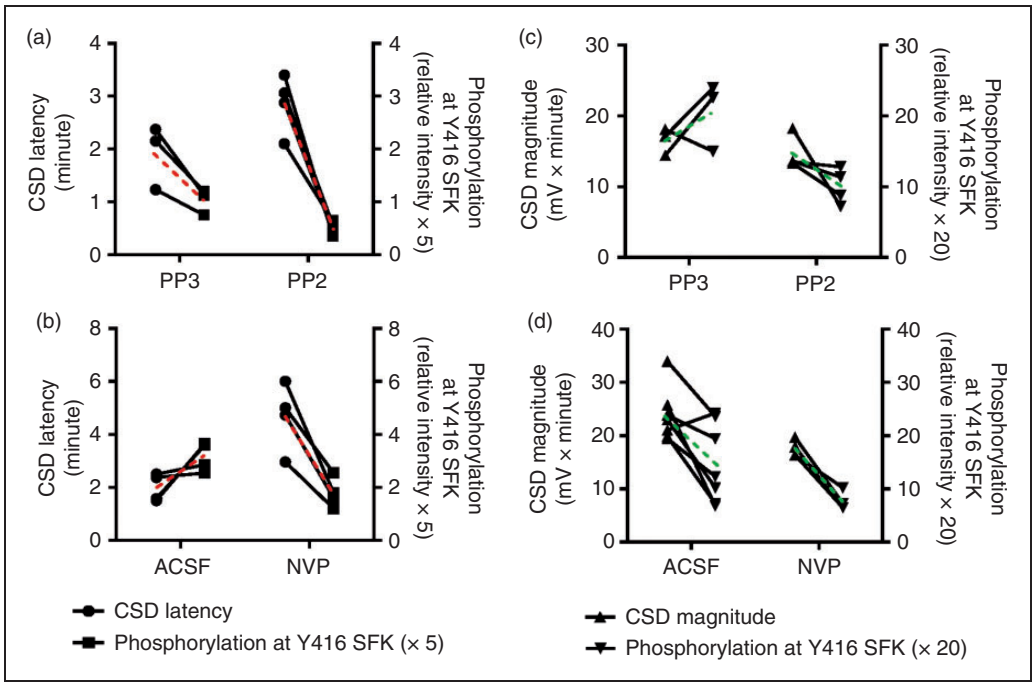

Figure 6. Correlation analysis of CSD characteristics with levels of ipsilateral cortical SFK phosphorylation at Y416 site with and without SFK deactivation or NMDA receptor inhibition in rats. ((a), (b)). The increased CSD latency strongly *negatively* correlated with the reduction of SFK phosphorylation after PP2 (a) or NVP (b) perfusion *i.c.v* at 120 minutes prior to CSD induction. ((c), (d)); the reduced CSD magnitude *positively* correlated with a lower SFK phosphorylation after perfusion of PP2 (c) or NVP (d) at 120 minutes prior to CSD induction. Black lines show correlation between each CSD parameter and respective level of SFK phosphorylation of individual experiments. Red dotted lines indicate the averaged correlation between CSD latency and SFK phosphorylation. Green dotted lines indicate the averaged correlation between CSD magnitude and SFK phosphorylation.

CSD showed stronger positive correlation with a lower level of SFK phosphorylation after PP2 was perfused 2 hours prior to CSD induction than after PP3 application (Figure 6(a) and (c)). These data suggest that deactivation of SFK was able to reduce the likelihood of CSD occurrence, which coincides with a lower level of SFK phosphorylation. Given that migraine aura is believed to involve only a single CSD event (29), the critical role of SFK activity in CSD suggests that SFK activation is involved in the pathophysiology of migraine aura. These data extend a recent study in mice showing that intraperitoneal injection of PP2 inhibited the frequency of multiple CSD (6). The finding is also consistent with SFK activation being induced by multiple cell stresses (30) and tissue damage (31).

SFK activity is a known regulatory hub at which multiple signaling pathways converge, for example, coupling intracellular and membrane proteins including P2X7 and NMDA receptors (2,3,32). One explanation to account for a key role of SFK activity in CSD is a link with the P2X7 receptors, as tyrosine kinase plays a pivotal role in P2X7 receptor-mediated cellular responses and is involved in the initial steps leading to Panx1 channel opening (33), which can be opened by CSD (11). Alternatively, SFK activity in CSD could be regulated by the activation of NMDA receptors. Firstly, SFK is known to couple with the NMDA receptor, forming an SFK-NMDA receptor complex (4). Secondly, in this study, we demonstrated a functional link between SFK and NMDA receptors during CSD. The reduced CSD magnitude in the mouse brain slice with NVP was no longer observed when the SFK activator was co-applied (Figure 4). Additionally, elevation of SFK phosphorylation at Y416 amino acid induced by a single CSD was prevented by NMDA receptor inhibition by NVP (Figure 5), which is consistent with that observed with the SKF inhibitor, PP2 (Figure 3). Interestingly, the increase in CSD latency showed a strong negative correlation with a lower level of SFK phosphorylation after NVP was perfused 2 hours prior to CSD induction (Figure 6(b)). This indicates that NMDA receptor inhibition reduces the likelihood of CSD occurrence, which subsequently further reduces SFK phosphorylation. Collectively, these data, together with the fact that NMDA receptor and its major subunits, NR2A and NR2B, contribute to CSD genesis and propagation *in vivo* (13,14,22), supports the model that we propose, that SFK activity contributing to CSD propagation is regulated by recruiting NMDA

receptors. This is consistent with the previous finding that SFK can be recruited by activation of NMDA receptors leading to Panx1 channel opening during anoxia/ischemia (2).

The mechanism by which SFK activity is regulated by NMDA receptors in CSD is not known, but one candidate might be a Ca^{2+} influx as the synaptic NMDA receptor contributes to K^{+}-triggered CSD via calcium entry (34); and accumulation of cytoplasmic calcium can activate SFK through multiple signaling, including the NMDA receptor (3,35). Alternatively, SFK may directly act on the NMDA receptor by phosphorylation of NR2A/B subunits (1), which are known key players in CSD genesis and propagation (12–14). Interestingly, the fact that uncoupling Src from the ND2-NMDA receptor by Src40-49 (10) did not alter CSD magnitude or the cortical susceptibility to CSD in the mouse brain slice (data not shown) does not support any involvement of Src (10). It is possible that Fyn might be involved in this process, as PP2 preferentially inhibits Fyn, but not Src, at nanomolar concentrations (36).

In summary, our data provides strong evidence that a single CSD is sufficient to induce SFK phosphorylation, which in turn regulates cortical susceptibility to CSD. This positive feedback loop associated with CSD can be regulated by NMDA receptors. It remains to be resolved if elevation of SFK activity by CSD would subsequently trigger Panx1 channel opening. Given that CSD is the accepted underlying cause of migraine with aura, our finding gives new clues about the molecular and cellular mechanism of migraine with aura and may constitute a new strategy for migraine prophylaxis.

Article highlights

- A single CSD is sufficient to rapidly increase SFK phosphorylation, which in turn facilitates CSD propagation.
- Deactivation of SFK reduces the likelihood of CSD occurrence, which coincides with lower level of SFK phosphorylation.
- SFK activity required for CSD propagation is regulated by activation of NMDA receptors.
- This is the first *in vivo* evidence showing SFK activity may play a pivotal role in the mechanism of migraine aura.

Acknowledgements

The authors thank Wangwenli Charitable Foundation and XJTLU research development fund for financial support. We are grateful for the provision of NVP from Yi Li at Department of Chemistry, XJTLU.

Declaration of conflicting interests

The authors declared no potential conflicts of interest with respect to the research, authorship, and/or publication of this article.

Funding

The authors received no financial support for the research, authorship, and/or publication of this article.

References

1. Salter MW and Kalia LV. Src kinases: A hub for NMDA receptor regulation. *Nat Rev Neurosci* 2004; 5: 317–328.
2. Weilinger NL, Tang PL and Thompson RJ. Anoxia-induced NMDA receptor activation opens pannexin channels via Src family kinases. *J Neurosci* 2012; 32: 12579–12588.
3. Thomas SM and Brugge JS. Cellular functions regulated by Src family kinases. *Annu Rev Cell Dev Biol* 1997; 13: 513–609.
4. Weilinger NL, Lohman AW, Rakai BD, et al. Metabotropic NMDA receptor signaling couples Src family kinases to pannexin-1 during excitotoxicity. *Nat Neurosci* 2016; 19: 432–442.
5. Yeatman TJ. A renaissance for SRC. *Nat Rev Cancer* 2004; 4: 470–480.
6. Chen SP, Qin T, Seidel JL, et al. Inhibition of the P2X7-PANX1 complex suppresses spreading depolarization and neuroinflammation. *Brain* 2017; 140: 1643–1656.
7. Tan YH, Li K, Chen XY, et al. Activation of Src family kinases in spinal microglia contributes to formalin-induced persistent pain state through p38 pathway. *J Pain* 2012; 13: 1008–1015.
8. Frame MC. Src in cancer: Deregulation and consequences for cell behaviour. *Biochim Biophys Acta* 2002; 1602: 114–130.
9. Hadjikhani N, Sanchez Del Rio M, Wu O, et al. Mechanisms of migraine aura revealed by functional MRI in human visual cortex. *PNAS* 2001; 98: 4687–4692.
10. Gingrich JR, Pelkey KA, Fam SR, et al. Unique domain anchoring of Src to synaptic NMDA receptors via the mitochondrial protein NADH dehydrogenase subunit 2. *PNAS* 2004; 101: 6237–6242.
11. Karatas H, Erdener SE, Gursoy-Ozdemir Y, et al. Spreading depression triggers headache by activating neuronal Panx1 channels. *Science* 2013; 339: 1092–1095.

12. Marrannes R, Willems R, De Prins E, et al. Evidence for a role of the N-methyl-D-aspartate (NMDA) receptor in cortical spreading depression in the rat. *Brain Res* 1988; 457: 226–240.
13. Peeters M, Gunthorpe MJ, Strijbos PJ, et al. Effects of pan- and subtype-selective N-methyl-D-aspartate receptor antagonists on cortical spreading depression in the rat: Therapeutic potential for migraine. *J Pharmacol Exp Ther* 2007; 321: 564–572.
14. Bu F, Du R, Li Y, et al. NR2A contributes to genesis and propagation of cortical spreading depression in rats. *Sci Rep* 2016; 6: 1–9.
15. Obrenovitch TP, Urenjak J and Wang M. Nitric oxide formation during cortical spreading depression is critical for rapid subsequent recovery of ionic homeostasis. *J Cereb Blood Flow Metab* 2002; 22: 680–688.
16. Bain J, McLauchlan H, Elliott M, et al. The specificities of protein kinase inhibitors: an update. *Biochem J* 2003; 371: 199–204.
17. Smart JE, Oppermann H, Czernilofsky AP, et al. Characterization of sites for tyrosine phosphorylation in the transforming protein of Rous sarcoma virus (pp60v-src) and its normal cellular homologue (pp60c-src). *PNAS* 1981; 78: 6013–6017.
18. Wang Y, Li Y and Wang M. Involvement of CGRP receptors in retinal spreading depression. *Pharmacol Rep* 2016; 68: 935–938.
19. Tottene A, Conti R, Fabbro A, et al. Enhanced excitatory transmission at cortical synapses as the basis for facilitated spreading depression in Ca(v)2.1 knockin migraine mice. *Neuron* 2009; 61: 762–773.
20. Tang YT, Mendez JM, Theriot JJ, et al. Minimum conditions for the induction of cortical spreading depression in brain slices. *J Neurophysiol* 2014; 112: 2572–2579.
21. Tozzi A, de Iure A, Di Filippo M, et al. Critical role of calcitonin gene-related peptide receptors in cortical spreading depression. *PNAS* 2012; 109: 18985–18990.
22. Wang M, Chazot PL, Ali S, et al. Effects of NMDA receptor antagonists with different subtype selectivities on retinal spreading depression. *Br J Pharmacol* 2012; 165: 235–244.
23. Lauritzen M. Pathophysiology of the migraine aura. The spreading depression theory. *Brain* 1994; 117: 199–210.
24. Chen Q, Cichon J, Wang W, et al. Imaging neural activity using Thy1-GCaMP transgenic mice. *Neuron* 2012; 76: 297–308.
25. MacGregor DG, Chesler M and Rice ME. HEPES prevents edema in rat brain slices. *Neurosci Lett* 2001; 303: 141–144.
26. Dahlem MA and Muller SC. Image processing techniques applied to excitation waves in the chicken retina. *Methods* 2000; 21: 317–323.
27. Park SH, Won J and Lee KH. Design and characterization of non-phosphopeptide inhibitors for Src family SH2 domains. *Bioorg Med Chem Lett* 2002; 12: 2711–2714.
28. Jia Y, Zhou J, Bu F, et al. Synergistic suppression of cortical spreading depression under NR2A and NR2B inhibition. *Pharmacol Pharm* 2015; 6: 573–579.
29. Hadjikhani N, Sanchez Del Rio M, Wu O, et al. Mechanisms of migraine aura revealed by functional MRI in human visual cortex. *PNAS* 2001; 98: 4687–4692.
30. Huang CC, Lim PH, Hall AC, et al. A key role for KCl cotransport in cell volume regulation in human erythroleukemia cells. *Life Sci* 2011; 88: 1001–1008.
31. Shahidullah M, Mandal A and Delamere NA. Damage to lens fiber cells causes TRPV4-dependent Src family kinase activation in the epithelium. *Exp Eye Res* 2015; 140: 85–93.
32. Iglesias R, Locovei S, Roque A, et al. P2X7 receptor-Pannexin1 complex: Pharmacology and signaling. *Am J Physiol Cell Physiol* 2008; 295: C752–C760.
33. Bravo D, Maturana CJ, Pelissier T, et al. Interactions of pannexin 1 with NMDA and P2X7 receptors in central nervous system pathologies: Possible role on chronic pain. *Pharmacol Res* 2015; 101: 86–93.
34. Zhou N, Rungta RL, Malik A, et al. Regenerative glutamate release by presynaptic NMDA receptors contributes to spreading depression. *J Cereb Blood Flow Metab* 2013; 33: 1582–1594.
35. Della Rocca GJ, van Biesen T, Daaka Y, et al. Ras-dependent mitogen-activated protein kinase activation by G protein-coupled receptors. Convergence of Gi- and Gq-mediated pathways on calcium/calmodulin, Pyk2, and Src kinase. *J Biol Chem* 1997; 272: 19125–19132.
36. Ferrari SM, La Motta C, Sartini S, et al. Pyrazolopyrimidine derivatives as antineoplastic agents: With a special focus on thyroid cancer. *Mini Rev Med Chem* 2016; 16: 86–93.

NEUROSCIENCE
RESEARCH ARTICLE
L. Jiang et al. / Neuroscience 382 (2018) 23–34

The Transient Receptor Potential Ankyrin Type 1 Plays a Critical Role in Cortical Spreading Depression

Liwen Jiang, [a,b] **Yan Wang,** [a] **Yuewei Xu,** [b] **Dongqing Ma** [a,b] **and Minyan Wang** [a,b]*

[a] *Centre for Neuroscience, Xi'an Jiaotong-Liverpool University, Suzhou 215123, China*

[b] *Department of Biological Sciences, Xi'an Jiaotong-Liverpool University, Suzhou 215123, China*

Abstract—The transient receptor potential ankyrin type-1 (TRPA1) channels have been proposed as a potential target for migraine therapy. Yet the role of cortical TRPA1 channels in migraine mechanism has not been fully understood. Cortical spreading depression (CSD) is known as an underlying cause of migraine aura. The aim of this study is to investigate if cortical TRPA1 activity is required for CSD genesis and propagation. A mouse brain slice CSD model with intrinsic optical imaging was applied for TRPA1 signaling pharmacology. The results showed that the TRPA1 agonist, umbellulone, facilitated the propagation of submaximal CSD. Correspondingly, an anti-TRPA1 antibody and two selective TRPA1 antagonists, A967079 and HC-030031, prolonged the CSD latency and reduced magnitude, indicating a reduced cortical susceptibility to CSD under TRPA1 deactivation. Furthermore, the TRPA1 agonist, allyl-isothiocyanate (AITC), reversed the suppression of CSD by HC-030031, but not by A967079. Interestingly, the inhibitory action of A967079 on CSD was reversed by exogenous calcitonin-gene-related peptide (CGRP). Consistent to TRPA1 deactivation, the prolonged CSD latency was observed by an anti-CGRP antibody in the mouse brain slice, which was reversed by exogenous CGRP. We conclude that cortical TRPA1 is critical in regulating cortical susceptibility to CSD, which involves CGRP. The data strongly suggest that deactivation of TRPA1 channels and blockade of CGRP would have therapeutic benefits in preventing migraine with aura.

Key words: cortical spreading depression, migraine, the transient receptor potential ankyrin type 1, calcitonin-gene-related peptide, mouse brain slice.

INTRODUCTION

Migraine is a complex neurological disorder characterized by recurrent unilateral throbbing head pain. Around 16 percent of world's population regularly suffer debilitating symptoms, which ranks top 6 causes of global years lived with disability worldwide. A common component of these headaches for many migraineurs is the aura, which precedes migraine symptoms in up to one third of patients (Cutrer and Huerter, 2007). Migraine aura may include visual, sensory, language, or brainstem symptoms. Meanwhile, 81% of these migraines with aura are also associated with migraine without aura (Queiroz et al., 1997). The pathologic mechanism by which migraine aura develops has not been fully elucidated. Cortical spreading depression (CSD), a transient propagating excitation of synaptic activity followed by depression, has been increasingly regarded as an underlying cause of migraine aura. CSD is directly linked with the aura phase of migraine (Lauritzen, 1994, Hadjikhani et al., 2001; Moskowitz, 2007) and triggers migraine-like behavior through generating neuro-inflammatory responses (Karatas et al., 2013). CSD also activates nociceptor (Zhang et al., 2010; Shatillo et al., 2013) and induces a delayed persistent activation of central trigeminal neurons (Zhang et al., 2011). Certain drugs such as topiramate and sumatriptan that can relieve migraine pain also suppress CSD (Unekawa et al., 2012; Wiedemann et al., 2012; Guedes et al., 2017). Anti-CSD drugs may be therefore related to aura suppression in migraine patients and CSD has therefore become a useful model for studying migraine mechanism (Pietrobon and Moskowitz, 2013; Wang, 2013; Russo, 2015).

The transient receptor potential ankyrin type 1 (TRPA1) is a type of nonselective transmembrane cation channel with 17 ankyrin repeats on its N-terminal. TRPA1 is a sensor of oxidative, nitrative and electrophilic stress (Vay et al., 2012). In peripheral

*Correspondence to: M. Wang, SA451, Department of Biological Sciences, Xi'an Jiaotong-Liverpool University, 111 Ren Ai Road, Suzhou Industrial Park, Suzhou 215123, China.
E-mail address: Minyan.wang@xjtlu.edu.cn (M. Wang).

Abbreviations: AITC, allyl-isothiocyanate; AOI, area of interest; AUC, area under the curve; CGRP, calcitonin-gene-related peptide; CNS, central nervous system; CSD, cortical spreading depression; IOS, intrinsic optical signal; PNS, peripheral nervous system; ROS, reactive oxidative species; SFK, sarcoma family kinase; TRPA1, transient receptor potential ankyrin type-1.

https://doi.org/10.1016/j.neuroscience.2018.04.025
0306-4522/

nervous system (PNS), the channel is expressed in mouse dural afferent neurons (Story et al., 2003; Huang et al., 2012) and axons with terminations in trigeminal nucleus caudalis (Kim et al., 2010). While in the central nervous system (CNS), TRPA1 expression has also recently been reported in cortex of rats and mice (Lee et al., 2016; Kheradpezhouh et al., 2017), as well as hippocampal pyramidal (Story et al., 2003) neurons of rats (Julius, 2013; Kheradpezhouh et al., 2017).

Majority studies have focused on peripheral TRPA1 channels, highlighting the involvement of TRPA1 in migraine pain in addition to thermal and chemical sensations (Julius, 2013; Trevisan et al., 2013). Gain-of-function mutation of TRPA1 channels contributes to a familial episodic pain syndrome (Kremeyer et al., 2010). Experimental studies show that activation of TRPA1 channels increases the activation threshold of rodent meningeal afferents (Denner et al., 2017) and triggers migraine-like behavior in rats (Nassini et al., 2012; Benemei et al., 2014). Supporting the role of peripheral TRPA1 in pain pathways, a recent study further shows an active role of TRPA1 in counteracting nitroglycerin-induced hyperalgesia at the trigeminal level (Demartini et al., 2017). Based on these data in the literature, TRPA1 has been proposed as an emerging target for developing drugs to relieve migraine pain (Benemei et al., 2014; Dussor et al., 2014). Yet, the role of central TRPA1 in mechanism of migraine aura remains unclear.

TRPA1 is associated with key signals that are known players in migraine pathology, of which a key signal is calcitonin gene-related peptide (CGRP), a known target of migraine prevention (Edvinsson, 2015; Russo, 2015; Wang et al., 2016b). In medulla-pons, cervical spinal cord and trigeminal ganglion, TRPA1 antagonism is associated with a significant inhibition of nitroglycerin-induced increase in mRNAs of c-fos and CGRP (Demartini et al., 2017). Consistently, inhibition of TRPA1 blocks CGRP release induced by reactive oxidative species (ROS) (Shatillo et al., 2013) and environmental irritant-induced TRPA1 activation stimulates CGRP release in the trigeminal ganglion (Nassini et al., 2012). Conversely, TRPA1 activation leads to trigeminal neuronal activation via CGRP (Benemei et al., 2014; Dussor et al., 2014; Kunkler et al., 2015) and releases CGRP in rodent meningeal afferents (Denner et al., 2017). However, the role of central TRPA1 signaling in pain pathways has comparably been unexplored. TRPA1 is also reported to be associated with neurotransmitter release including GABA in the hippocampus (Shigetomi et al., 2011) and glutamate in brain stem neurons (Sun et al., 2009). A recent study showed that activation of TRPA1 modulates activity of pyramidal neurons in rodent cortex (Kheradpezhouh et al., 2017), indicating a functional role of cortical TRPA1 in migraine pathology.

In this study, we hypothesized that cortical TRPA1 plays a crucial role in migraine aura pathophysiology. We examined how modulation of cortical TRPA1 channel alters cortical susceptibility to CSD using an *in vitro* CSD model. We further examined if cortical TRPA1 signaling during CSD involves CGRP. Our findings indicate the importance of cortical TRPA1 in mechanism of migraine aura and the channel as a potential target for migraine aura prevention.

EXPERIMENTAL PROCEDURES

Animal use

A total of 70 C57BL6 mice (male, 21.0 ± 2.9 g, mean ± SD) were purchased from Shanghai SLAC Laboratory Animal Corporation Ltd. The mice were housed in the Experimental Animal Centre of Soochow University under agreement with Xi'an Jiaotong-Liverpool University (XJTLU) for at least 1 week before use with food and water available *ad libitum*. Animal procedures were approved by the Ethical Review Panels of Soochow University and experiments were performed in accordance with relevant national and provincial guidelines.

Imaging of mouse brain slice CSD

In order to explore how modulation of TRPA1 alters CSD, a mouse brain slice CSD model was applied by referencing to the literature (Bu et al., 2017). Briefly, the mouse brain was dissected and cerebrum was cut along the midline. Coronal sections (400 μm) of the right brain were prepared using a vibratome (7000 smz-2, Campden, UK) at coordinates between 1 and 3 mm posterior to bregma, each showing somatosensory and visual cortices as they are highly associated with migraine pain (Lauritzen and Fabricius, 1995; Hadjikhani et al., 2001). Brain slices were quickly transferred into ice-cold oxygenated NMDG-HEPES cutting solution (93 mM NMDG, 2.5 mM KCl, 1.2 mM NaH_2PO_4, 30 mM $NaHCO_3$, 20 mM HEPES, 25 mM glucose, 5 mM L-ascorbic acid, 2 mM thiourea, 3 mM sodium pyruvate, 10 mM $MgSO_4$, 0.5 mM $CaCl_2{\cdot}2H_2O$; bubbled with 95% O_2 and 5% CO_2; pH 7.4). After 15-min stabilization at room temperature, brain slices were transferred into Kreb's solution (126 mM NaCl, 2.5 mM KCl, 2.4 mM $CaCl_2{\cdot}2H_2O$, 1.3 mM $MgCl_2{\cdot}6H_2O$, 18 mM $NaHCO_3$, 1.2 mM NaH_2PO_4, 10 mM Glucose; bubbled with 95% O_2 and 5% CO_2; pH 7.4) and maintained for at least 80 min prior to carrying out further procedures. In order to minimize animal use, at least two brain slices were used from each mouse and each slice randomly received a different drug treatment to ensure all data generated within each group were from independent biological samples.

CSD induction and intrinsic optical imaging

Intrinsic optical signal (IOS) has been used for studying CSD, which offers good spatial and temporal resolution simultaneously, making it reliable for studying pathophysiological events occurring at the cortical level (Tozzi et al., 2012; Tang et al., 2014; Bu et al., 2017). Each mouse brain slice was placed in a recording chamber and submerged in Kreb's solution with a perfusion rate of 3 ml/minute using a peristaltic pump (Reglo ICC, Ismatec; Wertheim, Germany). Unless otherwise stated, CSD was induced by ejection of 33 μl of 260 mM KCl at 25 μl/minute using a high-precision syringe pump

(CMA/400, CMA/Microdialysis; Solna, Sweden). The coronal slice was illuminated for 50 ms, starting at the same time when CSD was elicited, using a high-power LED spotlight (625-nm peak wavelength, SLS-0307-A, Mightex, Pleasanton, USA) driven by a computer controlled power supply (LED controller, SLC-SA04-US; Mightex, Pleasanton, USA). For each KCl application, changes in the reflected IOS in each cortical slice were recorded for 15 min at 2 Hz with a charge-coupled device monochrome camera (Rolera-XR, Qimaging, Surrey, Canada) at the maximum spatial resolution using Image Pro Plus software (IPP7; Media Cybernetics, UK). Camera exposure and illumination were synchronized using an external trigger (TG1006, TTI, Cambridgeshire, UK).

Experimental design

A total of five series of experiments were designed.

Series 1: The mouse brain slice CSD model in our laboratory was previously used for studying the functional link between NMDA receptor and sarcoma family kinase (SFK) in CSD (Bu et al., 2017). However, it has not been used for studying the function of TRPA1 signaling. Therefore, prior to exploring the role of TRPA1 in CSD, the mouse brain slice CSD model was validated using a potent CGRP receptor antagonist, BIBN4096, preferably selective for calcitonin-receptor-like receptor and receptor activity modifying protein 1 binding pocket of CGRP receptors (Doods et al., 2000). BIBN4096 was chosen because this drug was previously shown to suppress CSD in the rat brain slice (Tozzi et al., 2012) and CGRP, the ligand of CGRP-receptor can be released in response to TRPA1 activation induced by environmental irritants (Nassini et al., 2012). The three groups were: (i) Kreb's control (n = 6); (ii) DMSO at 0.003% as the vehicle control (n = 6); and (iii) BIBN4096 (Tocris, 4561, Bristol, UK) at 1 μM (n = 6). Two CSD episodes were elicited in each experiment with a 45-min interval for tissue recovery. The drug or vehicle was perfused 45 min prior to the 2nd CSD induction for 1 h, i.e., the first CSD was under Kreb's perfusion in both control and drug group. However, the drug replaced Kreb's solution in the drug group prior to the 2nd CSD. In order to minimize animal use, Kreb's control group was also used as the control for the following groups, i.e., series 2 group (viii) and series 4 group (xiii).

Series 2: In order to examine how modulation of TRPA1 alters CSD, we firstly tested if TRPA1 activation could promote the propagation of CSD induced by 260 mM KCl in the mouse brain slice using a TRPA1 agonist, umbellulone (083M4714V, Sigma) acting on the cysteine residues of N-terminus of TRPA1 (Zhong et al., 2011; Mihara and Shibamoto, 2015). This drug was chosen as it is capable of activating trigeminal system and inducing headache (Nassini et al., 2012). Submaximal CSD was also induced by KCl at lower concentrations (5 and 50 mM) in order to uncover a possible TRPA1-induced amplification in this phenomenon. The following six groups were designed: (iv, v) Kreb's control (n = 6) and 15 μM of umbellulone (n = 5) respectively with CSD induced by 5 mM KCl; (vi, vii) Kreb's control (n = 8) and 15 μM of umbellulone (n = 5) respectively with CSD induced by 50 mM KCl; (viii, ix) Kreb's control (n = 6) and 15 μM of umbellulone (n = 4) respectively with CSD induced by 260 mM KCl. The concentration of umbellulone was chosen at 15 mM, at which is selective for TRPA1 (Zhong et al., 2011; Nassini et al., 2012). Similar to series 1, two CSD episodes were elicited in each experiment at a 45-min interval for tissue recovery. The drug or vehicle was perfused 45 min prior to the 2nd CSD induction for 1 h.

Series 3: We then examined whether TRPA1 inhibition by an anti-TRPA1 antibody could prevent the occurrence of CSD. The three groups were: (x) Kreb's control (n = 6); (xi) 0.025 μM of the unconjugated rabbit IgG (H + L) (anti-IgG antibody, Sangon, D110502, n = 7) and (xii) 0.015 μM of the anti-TRPA1 antibody that conjugates to N-terminal of human TRPA1 (Merck Millipore, ABN1009, n = 6). In this series, two CSD episodes were elicited in each experiment with a 2-h interval for sufficient antibody–antigen binding. The antibody was incubated with the brain slice for 1 h starting as soon as the 1st CSD recording was completed. In order to minimize the animal use, the anti-IgG antibody group was also used for series 5 group (xxiii).

Series 4: In order to confirm the inhibitory effects of the anti-TRPA1 antibody on CSD, we further examined if deactivation of TRPA1 could prevent the occurrence of CSD by two TRPA1 antagonists: HC-030031 (SIGMA, H4415), which has unknown binding site of TRPA1 and A967079 (Tocris, Bristol, UK), a selective TRPA1 antagonist (Chen et al., 2011) that targets the pore-forming region between S5 and S6 and the first pore helix of the channel (Paulsen et al., 2015), in the absence or presence of a commonly used TRPA1 agonist, allyl-isothiocyanate (AITC, Sigma–Aldrich, 36682) that targets both the N-terminal domain (Cys-415/422/622 in mTRPA1) (Andrade et al., 2012) and the S6 region (Benedikt et al., 2009). The following groups were designed: (xiii) Kreb's control (n = 6); (xiv) DMSO at 0.03% (n = 6) as the vehicle control; (xv) HC-030031 at 6 μM (n = 6); (xvi) co-application of HC-030031 at 6 μM with AITC (Sigma–Aldrich, 36682) at 50 μM (n = 7); (xvii) A967079 at 1 μM (n = 7); (xviii) co-application of A967079 at 1 μM with AITC at 50 μM (n = 6). In the same series, we further explored a possible involvement of CGRP in TRPA1-mediated CSD by co-application of A967079 at 1 μM with exogenous CGRP peptide (sequence: SCNTATCVTH RLAGLLSRSG GVVKDNFVPT NVGSEAF-NH2, disulfide bridge between 2 and 7, A-peptide Ltd, Shanghai) at 0.5 μM (n = 7) in group (xiv). The protocol was the same as that in series 1 and 2, i.e., two CSD episodes were elicited in each experiment with a 45-min interval. Corresponding drugs or vehicles were perfused 45 min prior to the 2nd CSD induction for 1 h.

Series 5: We then extended the study to confirm the involvement of CGRP in CSD by testing whether an anti-CGRP antibody would alter CSD. The three groups were: (xxiii) 0.025 μM of the anti-IgG antibody (n = 7); (xxiv) an anti-CGRP antibody that recognizes endogenous levels of total CGRP proteins (CST,

14959S, $n = 6$) at 0.4 μM; (xxv) CGRP at 10.5 μM pre-incubated with the anti-CGRP antibody at 0.4 μM overnight at 4 °C before their co-application as the control ($n = 6$). The protocol was the same as that in series 3, i.e., two CSD episodes were elicited in each experiment with a 2-h interval for sufficient antibody–antigen binding. The antibody was incubated with the brain slice for 1 h starting as soon as the 1st CSD recording was completed.

IOS image and statistical analysis

For each 1800-frame sequence, an area of interest (AOI) parallel to the CSD wave front was delineated manually in layers 4 to 6 of somatosensory cortex that was distant from the site of KCl application (Fig. 1A). For each picture within the sequence, gray levels of the pixel constituting the AOI were corrected by the subtracting the respective dark background. Changes in this value were plotted against time (i.e., 1800 data points over 15-min recording), providing the dynamic changes in IOS within the AOI. This signal was synchronous of the sudden cellular depolarization that characterizes the excitation phase of CSD.

As reported earlier (Wang et al., 2012), for each CSD wave, latency (the time interval between the starting point of KCl ejection and that of CSD elicitation) was calculated to reflect cortical susceptibility to CSD. A prolonged CSD latency would indicate reduced cortical susceptibility to CSD. The area under the curve (AUC, gray levels × min ute) was used as an index of CSD magnitude. In the case where CSD was abolished by drug (s), CSD latency was counted as 15 min, i.e., the maximal recording period of each CSD wave, and the AUC was counted as zero. In order to eliminate the variations of AOI chosen in each individual experiment, CSD latency and magnitude within each different test were given as mean ± SEM in percentages relative to that of the 1st CSD wave (i.e., initial control) respectively. The difference in distance that CSD propagated before (1st CSD episode) and after drug application (2nd CSD episode) in each submaximal CSD experiment was calculated to observe if the TRPA1 activator could exacerbate CSD. Mann–Whitney's U test, one-tailed, was used for comparison of each parameter between each two independent groups. $^{*}p < 0.05$ was considered as significance.

RESULTS

Validation of mouse brain slice CSD model

Each KCl application at 260 mM ejected on the mouse brain slice led to changes in the optical signals as indicated as a dark gray wave front slowly propagating from the KCl application site across the cortex (Lower image, Fig. 1A). The resulting changes in optical signal indicate observable CSD wave and the pattern was biphasic (Fig. 1B), which is consistent with what was observed previously (Bu et al., 2017).

We validated this mouse brain slice CSD model using BIBN4096. In Kreb's control group, there was no difference in CSD latency (128.7% ± 27.5% relative to initial baseline) and magnitude (104.2% ± 11.9% relative to initial control) (Fig. 1C, D). DMSO at 0.003% did not alter CSD latency (150.6% ± 25.5%) and magnitude (95.1% ± 7.8%) (Fig. 1C, D, $n = 6$ for both groups). As expected, BIBN4096 at 1 μM markedly prolonged CSD latency to 16.4 folds, which was significant when compared to that of the DMSO group (Fig. 1C, $p = 0.0206$). The drug also slightly reduced the CSD magnitude, but the reduction did not reach significance (Fig. 1D). It was noted that at 1 μM, the drug completely abolished CSD wave in 2/6 brain slices. The inhibitory effect of BIBN4096 on cortical susceptibility to CSD under study is consistent with that reported previously in the rat cortical slice (Tozzi et al., 2012) and chick retina (Wang et al., 2016a), indicating the validity of the mouse brain slice migraine model under study.

Umbellulone facilitates CSD propagation

In order to explore if TRPA1 channel activation would promote CSD propagation, we firstly examined if umbellulone could exacerbate CSD induced by KCl at different concentrations to uncover a possible TRPA1 activation-induced amplification. In the control group, when KCl at 5 mM was applied, CSD was detected in all 6 mouse slices after the 1st KCl ejection and 4 out of 6 after the 2nd KCl ejection (data not shown), suggesting KCl at 5 mM did not induce reproducible CSD. During the 2nd CSD induction, umbellulone at 15 μM was unable to sufficiently amplify either the sub-threshold CSD induced by 5 mM KCl or alter CSD that was successfully induced in 3 out of 5 slices in the presence of the drug (data not shown).

When the concentration of KCl was applied at 50 mM, CSD was successfully elicited in all cortical slices in the 1st episode of Kreb's control group; and CSD were observed in 7 out of 8 slices in the 2nd CSD episode. These data suggest that 50 mM was an optimal concentration for eliciting submaximal CSD. The CSD latency and magnitude in the 2nd CSD episode were 232.9% ± 30.4% and 81.7% ± 21.8% relative to respective values of the 1st CSD episode (Fig. 2A, B). In the presence of umbellulone at 15 μM, CSD depolarization waves were found in 4 out of 5 slices with CSD latency and magnitude with ratio of 387.2% ± 157.0% and 79.5% ± 41.2% in respective order, which was not significant when compared to Kreb's group (Fig. 2A, B). The distance difference that CSD propagated between the 1st and 2nd CSD episode in the umbellulone group increased 9.6-fold relative to Kreb's control group (Fig. 2C, $p = 0.0079$), suggesting TRPA1 activation facilitates CSD to propagate a longer distance than control.

When KCl was applied at 260 mM, CSD was elicited in all brain slices throughout the experiment in both groups. In Kreb's control group, the CSD latency and magnitude in the 2nd CSD episode were 128.7% ± 27.5% and 104.2% ± 11.9% respectively (Fig. 2A, B). In the umbellulone group, the CSD latency and magnitude were 149.6% ± 24.3% and 107.2% ± 8.0% respectively in the 2nd CSD episode (Fig. 2A, B),

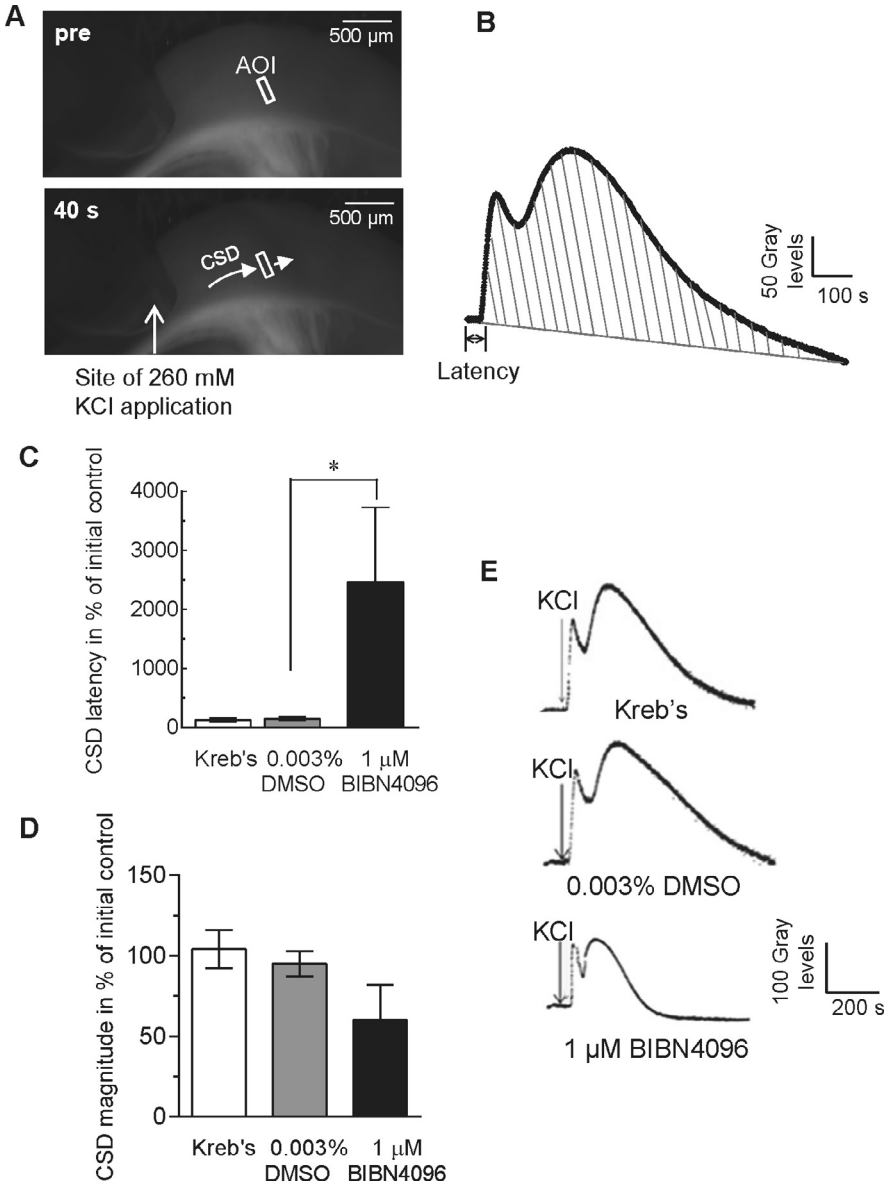

Fig. 1. This figure shows representative images and traces of CSD as well as validation of the mouse brain slice CSD model. Representative images of the mouse cortical slice before (A, upper) and after (A, lower) CSD induced by 260 mM KCl ejection in the mouse coronal slice and plot of CSD wave, i.e., kinetic changes in gray level intensity within the selected area of interest (AOI, right). The same AOI (A, rectangle within left picture) along CSD wave front (pointed by the short arrow) was selected and used for all images of the sequence under study. All the averaged gray levels within the AOI were plotted against time to generate the CSD wave showing a biphasic pattern (B). From these plots, CSD latency (second), i.e., time interval required for eliciting depolarization from the starting point of KCl application, was used for reflecting cortical susceptibility to CSD. The area under the curve (AUC, gray level × minute) of CSD wave was determined by image analysis for reflecting CSD magnitude. Validation of the mouse brain slice migraine model is shown in the lower and right panel. The bar charts show effects of BIBN4096 on CSD latency (C) and magnitude (D) during the 2nd CSD episode (relative to respective value in the 1st CSD). The corresponding representative traces of CSD in control, vehicle control and the drug groups are shown in (E). Data were presented as percentage of their initial levels. All data were indicated as mean ± SEM. Data were analyzed by Mann–Whitney's *U* test, one-tailed, for comparison between 1 μM of BIBN4096 ($n = 6$) and 0.003% DMSO control ($n = 6$), $^{*}p < 0.05$.

which was not different from that of control. The reason the drug at 15 μM did not alter these parameters is unknown but it may result from that TRPA1 channels being fully opened during CSD induced by 260 mM KCl. The difference in CSD propagating distance could not be measured in this condition as CSD waves across the whole cortex of mouse.

Anti-TRPA1 antibody suppresses CSD

We examined whether TRPA1 inhibition by the anti-TRPA1 antibody would suppress CSD. The results showed that in Kreb's control group, CSD latency for the 2nd CSD episode was 170.1% ± 38.9% of initial baseline, and CSD magnitude was 72.4% ± 7.1% (Fig. 3A, B). These parameters were not significantly different in the anti-IgG antibody group (Fig. 3A, B). Differently, when the brain slice was pre-incubated with the anti-TRPA1 antibody at 0.015 μM, CSD latency was prolonged 3.6-fold relative to that of the 1st CSD wave, which was significant different ($p = 0.0087$, Fig. 3A) compared to that in the anti-IgG antibody group. Conversely, the anti-TRPA1 antibody reduced the CSD magnitude in the 2nd CSD episode to 40.7% ± 10.1%, and this was significant when compared to that of the anti-IgG antibody control ($p = 0.0325$, Fig. 3B).

Both HC-030031 and A967079 suppress CSD

We further confirmed that TRPA1 deactivation suppresses CSD under the application of the TRPA1 inhibitors, HC-030031 and A967079. In the DMSO vehicle group, CSD latency and magnitude in the 2nd CSD episode were similar to that of the 1st CSD episode (Fig. 4A, B). Similar to the anti-TRPA1 antibody, HC-030031 markedly prolonged CSD latency with 5.6-fold increase relative to that of the 1st CSD wave, which was significant when compared with 0.03% DMSO group ($p = 0.002$, Fig. 4A). Corresponding to this, the reduction in CSD magnitude by 6 μM of HC-030031 was also observed when compared with DMSO group (Fig. 4B, $p = 0.02$). Consistently, A967079 at 1 μM also markedly prolonged CSD latency with 28.3-fold increase (Fig. 4A, $p = 0.01$) when compared with 0.03% DMSO group. Correspondingly, A967079 at 1 μM reduced the CSD magnitude to 44.8 % ± 17.0% (Fig. 4B, $p = 0.01$). The suppression of A967079 at 1 μM was pronounced

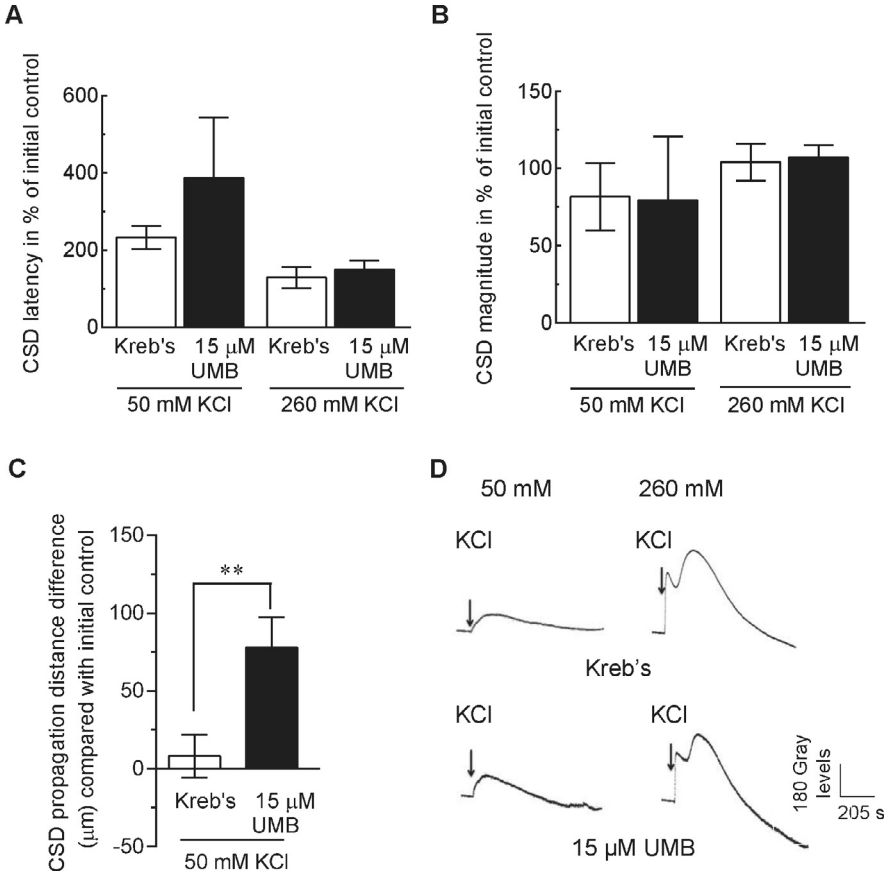

Fig. 2. Effects of umbellulone on the latency (A), magnitude (B) and propagation distance (C) of CSD induced by KCl at 50 mM or 260 mM respectively. There were two groups under 50 mM KCl ejection for submaximal CSD induction: Kreb's (n = 6) as control and 15 μM of umbellulone (n = 4), and another two groups for CSD induction under 260 mM KCl application: Kreb's (n = 6) as control and 15 μM of umbellulone (n = 4). The data show that umbellulone facilitated submaximal CSD to propagate in the mouse brain slice. Mann–Whitney's U test, one-tailed, for significance between respective control and umbellulone group ($^{**}p < 0.01$). Representative traces showing CSD induction elicited by KCl at 50 mM or 260 mM respectively in the absence and presence of umbellulone (D).

and this drug completely abolished CSD wave in 3/7 brain slices.

AITC abrogates CSD inhibition by HC-030031

We further examined if TRPA1 deactivation suppresses CSD could be reversed by co-application with the TRPA1 agonist, AITC. In the presence of AITC at 50 μM, the prolongation of CSD latency and reduction in CSD magnitude by HC-030031 at 6 μM was no longer observed (Fig. 4A) and significance between HC-030031 at 6 μM in the absence and presence of AITC group was seen in both CSD latency (p = 0.001) and CSD magnitude (p = 0.007). While the inhibitory effects of A967079 on CSD was slightly restored by AITC, insignificant differences were observed between A967079 at 1 μM in the absence and presence of AITC in both CSD latency (p = 0.27, Fig. 4A) and CSD magnitude (p = 0.22, Fig. 4B). The insignificance may be related to the large variation of the data resulting in complete blockade of CSD in 3 out 7 brain slices. When compared with DMSO group, co-application of A967079 and AITC maintains the significant differences in both CSD latency (p = 0.03, Fig. 4A) and CSD magnitude (p = 0.046, Fig. 4B).

CGRP abrogates CSD inhibition by A967079

Given that there is a link between TRPA1 and CGRP (Shatillo et al., 2013; Demartini et al., 2017) and deactivation of cortical TRPA1 suppresses CSD (Fig. 4), we further examined if cortical TRPA1 signaling in regulating CSD involves CGRP in the mouse brain slice. In the presence of CGRP at 0.5 μM, the prolonged CSD latency by A967079 at 1 μM was no longer observed in the mouse brain slice. However, insignificance between A967079 at 1 μM in the absence and presence of CGRP group was seen (Fig. 4A). This may be due to that 3/7 CSD waves being completely abolished by A967079 at 1 μM in the absence of CGRP; while no CSD was abolished in the presence of CGRP, leading to large variations in the data generated (p = 0.159, Fig. 4A). Correspondingly, CGRP also reversed the reduced CSD magnitude by A967079 at 1 μM to 101.1% ± 8.9% (Fig. 4B), and this was significant when compared to that in 1 μM A967079 alone group only (p = 0.01, Fig. 4B). Collectively, our results show that exogenous CGRP abrogated the suppressive effect of A967079 on CSD (Fig. 4A–C), indicating the involvement of CGRP in TRPA1 signaling in CSD.

Suppression of CSD by anti-CGRP antibody

In order to confirm the involvement of CGRP in CSD, we examined if the anti-CGRP antibody would also prevents the occurrence of CSD and if these effects could be reversed by exogenous CGRP. As expected, pre-incubation of the anti-CGRP antibody at 0.4 μM markedly increased the latency to 7.1-fold relative to that of the 1st CSD (Fig. 5A), which is consistent to the results under TRPA1 deactivation. This increase in CSD latency was significant when compared with the anti-IgG antibody group (p = 0.0022, Fig. 5A). Unlike TRPA1 inhibition under both anti-TRPA1 antibody and A967079 application, this antibody did not exhibit any significant effect on CSD magnitude (Fig. 5B). When exogenous CGRP at 10.5 μM was co-incubated with the anti-CGRP antibody, the prolonged CSD latency by the anti-CGRP antibody was completely reversed (Fig. 5A, p = 0.0011). These data support a key role of CGRP in regulating CSD. Unlike CSD latency, there was no

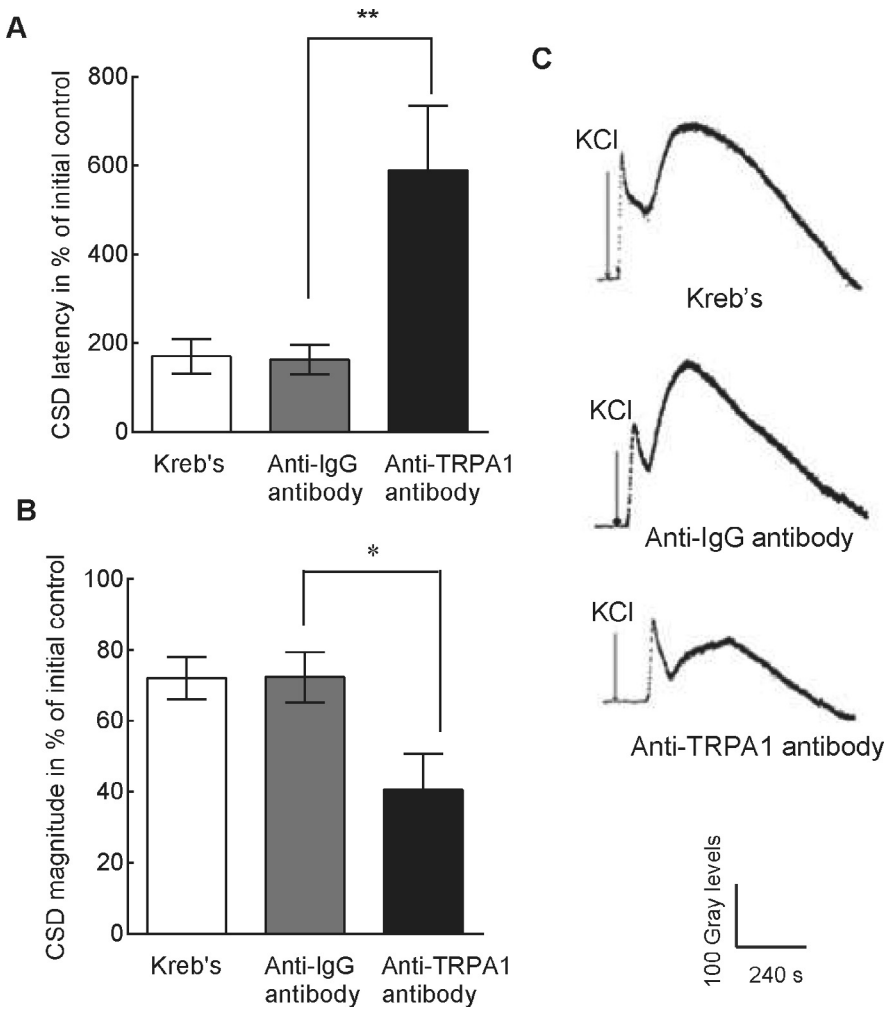

Fig. 3. Deactivation of TRPA1 channels by the anti-TRPA1 antibody suppresses CSD. Panels A and B show that the anti-TRPA1 antibody reduced cortical susceptibility to CSD as indicated by the prolonged CSD latency (A) and reduced magnitude (B). Three groups were designed: Kreb's (n = 6) as control, 0.025 μM of the anti-IgG antibody (n = 6) negative control and 0.015 μM of the anti-TRPA1 antibody (n = 6). (C) Representative traces of CSD in each group. All values given are means ± SEM. Mann–Whitney's U test, one-tailed, for significance between anti-IgG and anti-TRPA1 antibodies (A, B, $^{*}p < 0.05$, $^{**}p < 0.01$).

difference in CSD magnitude in the presence and absence of the peptide under CGRP blockade (Fig. 5B).

DISCUSSION

In this study, we applied a mouse brain slice CSD model to study the role of cortical TRPA1 channels in the mechanism of migraine aura. Our results show that cortical TRPA1 is critical in regulating cortical susceptibility to CSD and the channel signaling during CSD involves CGRP. The data strongly suggest cortical TRPA1 channels as a potential target for preventing migraine aura.

One of key findings of this study is that cortical TRPA1 activation plays a pivotal role in CSD propagation. First, TRPA1 activation by umbellulone facilitated submaximal CSD to propagate longer distance in the mouse brain slice (Fig. 2). These data are consistent with that TRPA1 activation triggers nociceptive-like behavior in mice (Nassini et al., 2012) and are in line with the clinical evidence that TRPA1 channel agonists cause migraine or non-migraine headaches (Kelman, 2007; Benemei et al., 2014) as well as gain of function with a point mutation of TRPA1 channels causes a familial episodic pain syndrome (Kremeyer et al., 2010). Second, Deactivation of TRPA1 channel by both the anti-TRPA1 antibody and two TRPA1 antagonists prevented the occurrence of CSD as indicated by the prolonged CSD latency and reduced CSD magnitude (Figs. 3 and 4), suggesting desensitization of TRPA1 could form a therapeutic strategy for preventing migraine aura. Third, the ability of the TRPA1 activator, AITC, in reversing the HC-030031-suppressed CSD further supports the role of cortical TRPA1 in CSD. These data complement those findings in the peripheral that functional desensitization of the channel by parthenolide attenuates headache-like responses to dural application of AITC (Materazzi et al., 2013). These findings also extend the known action of cortical TRPA1 in CNS that the channel activation modulates pyramidal neuron activity in the cortex of rodents (Kheradpezhouh et al., 2017), and is associated with hippocampal cannabinoid receptors (Storozhuk and Zholos, 2017) as well as promotes release of glutamate in brain stem (Sun et al., 2009). Collectively, the data support TRPA1 channel as a potential target for preventing migraine aura.

In this study, a complete blockade of CSD by A967079 was observed in 3 out 7 mouse brain slice, while this was not observed with the anti-TRPA1 antibody and HC-030031 (Fig. 4). The reason to account for this difference is not known. One possibility is that these drugs have different binding properties to TRPA1 channels. While HC-030031 has uncertain binding site (Gupta et al., 2016), the antagonist A967079 targets the pocket between S5 and S6 that are involved in ion conduction and pore forming of the channel (Klement et al., 2013; Paulsen et al., 2015), while the antibody conjugates to the N-terminal domain of the channel (Millipore) that is associated with sensing stimulators such as ROS and oxygen (Kadkova et al., 2017). These data suggest that both the pore forming region and N-terminal regions of the channel are involved in CSD. It was also noted that AITC reversed CSD suppressed by A967079 to a smaller extent (insignificant, Fig. 4) than that by HC-030031, which may be due to that

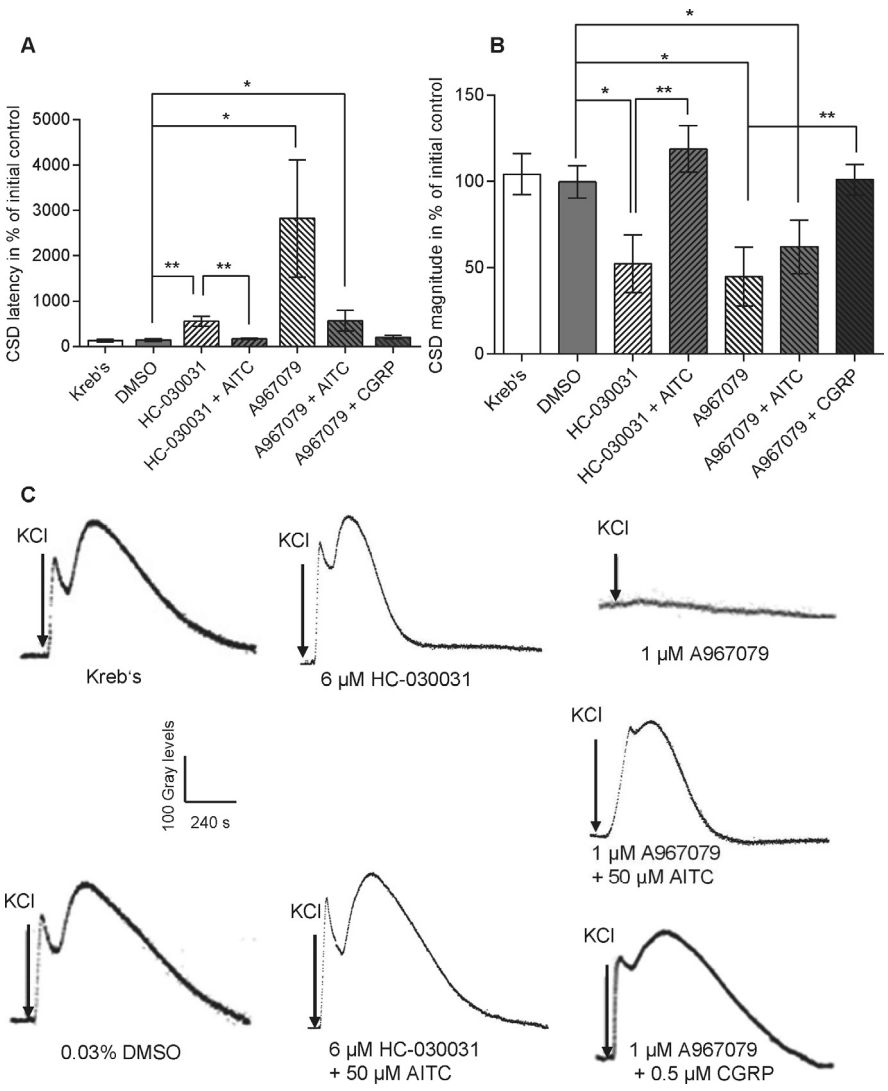

Fig. 4. The role of TRPA1 in CSD in the mouse brain slice involving CGRP. Effects of the TRPA1 antagonists A967079 and HC-030031 with or without AITC and exogenous CGRP on CSD latency (A) and magnitude (B) in the mouse brain slice. Seven groups were designed: Kreb's (n = 6) as control, 0.03% DMSO (n = 6) vehicle control, 6 μM of HC-030031 (n = 6), 6 μM of HC-030031 with 50 μM of AITC (n = 7), 1 μM of A967079 (n = 7), 1 μM of A967079 with 50 μM of AITC (n = 6) and 1 μM of A967079 with 0.5 μM of CGRP (n = 7). The data showed reduction in cortical susceptibility to CSD by both A967079 and HC-030031, and the inhibitory effect of HC-030031 was reversed by AITC, and to a lesser extent those of A967079. The suppression of A967079 was reversed by exogenous CGRP, suggesting the involvement of CGRP in TRPA1 regulated CSD. Representative traces of CSD wave in each group are shown in C. Of which, CSD was completed blocked by A967079 in 3 out 7 slices. All values given are means ± SEM. Mann–Whitney's U test, one-tailed, for significance between each group (A, B, $^{*}p < 0.05$, $^{**}p < 0.01$).

they act on different binding regions of TRPA1, i.e., N-terminal domain (Andrade et al., 2012) and S6 region of TRPA1 for AITC (Benedikt et al., 2009), while pore-forming region between S5 and S6 of TRPA1 for A967079 (Klement et al., 2013). The fact that the inhibitory effects of HC-030031 were reversed by AITC further suggests a possible involvement of N-terminal and/or pore-forming regions of TRPA1 in CSD.

We propose that the action of TRPA1 on CSD observed under study occurs through those channels located in the cortex rather than indirectly through peripheral TRPA1. The cortical action of these channels on CSD can be supported by that TRPA1 is expressed in mouse cortex (Kheradpezhouh et al., 2017) and TRPA1 expression in rat cortical neurons are [Sun et al., 2009 #902] [Yazgan and Naziroglu, 2016 #685] increased under pathologies conditions associated with Alzheimer's disease (Lee et al., 2016). However, it remains to be further investigated whether the action of cortical TRPA1 during CSD is neuronal or glial.

The molecular mechanism by which cortical TRPA1 channel regulates cortical susceptibility to CSD has not been reported previously, but TRPA1 signal pathways are divergent involving multiple signals such as Ca^{2+} (Yazgan and Naziroglu, 2016), glutamate (Sun et al., 2009), SFK (Katsura et al., 2006), GABA (Shigetomi et al., 2011) and CGRP (Kunkler et al., 2011). One plausible explanation is that the function of TRPA1 on CSD may attribute to its highly permeable property to Ca^{2+} (Shigetomi et al., 2011). Increased cytosolic Ca^{2+} concentration is often used as an indicator of TRPA1 channel activation in neurons of the rat hippocampus and dorsal root ganglion (Yazgan and Naziroglu, 2016); Importantly, elevation of Ca^{2+} influx accelerates CSD propagation velocity in rats (Torrente et al., 2014).

Secondly, the function of TRPA1 channels regulating CSD may also be associated with ROS as TRPA1 is a sensor of different external stimuli, such as oxidative stress or noxious impacts (Vay et al., 2012; Shatillo et al., 2013; Benemei et al., 2014; Yamamoto and Shimizu, 2016). This is possible because umbellulone, AITC and the anti-TRPA1 antibody, all of which have putative binding domain at the N-terminal of TRPA1 that is sensitive to external stimuli, were capable of regulating CSD in this study (Figs. 2–4). Additionally, these channels can be activated by ovariectomy-induced mitochondrial oxidative stress as indicated by increased cytosolic Ca^{2+} concentration in neurons of the rat hippocampus and dorsal root ganglion (Yazgan and Naziroglu, 2016). Supporting this notion is that ROS release is elevated after CSD induction not only in the ipsilateral cerebral cortex but also in meninges and trigeminal ganglia of rats (Shatillo et al., 2013). The antioxidant, ascorbate, in turn, can reduce

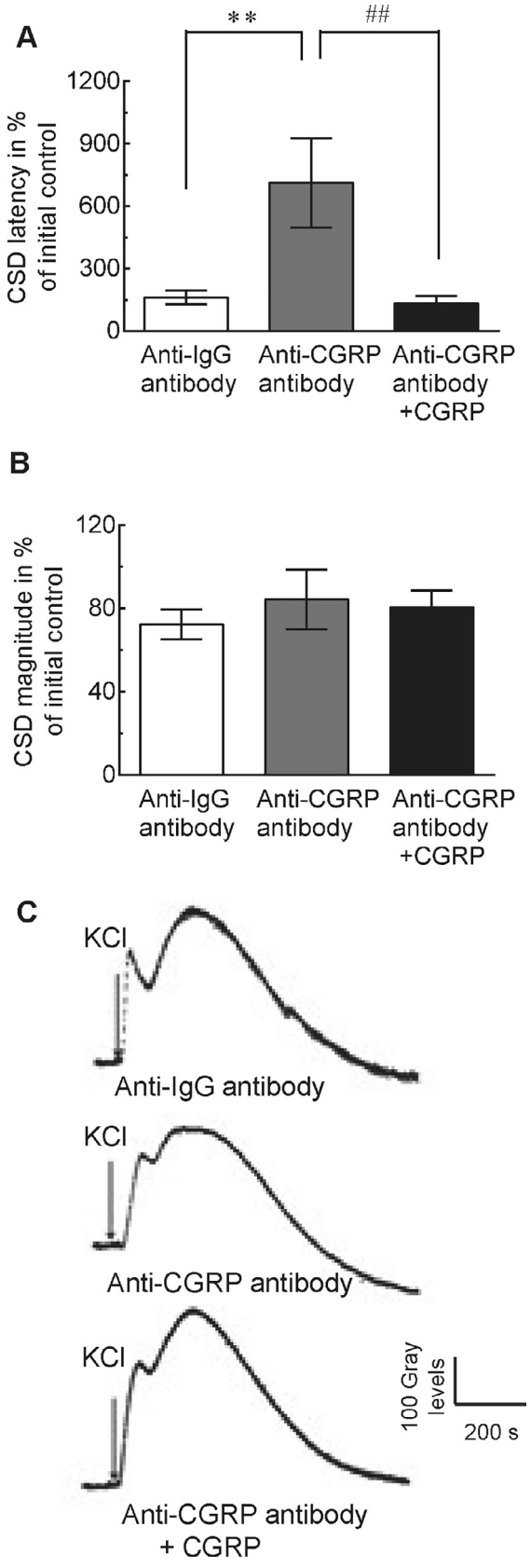

cortical susceptibility to CSD in the rat hippocampal slice (Grinberg et al., 2013).

Another promising explanation on cortical TRPA1 in regulating CSD can be linked to CGRP. This notion can be well supported by that peripheral evidence. In the trigeminal nociceptive system, TRPA1 inhibition can block ROS-triggered CGRP release (Kunkler et al., 2011; Shatillo et al., 2013). In rat trigeminal ganglia neurons, TRPA1 activation by environmental irritants stimulates CGRP release (Kunkler et al., 2011) and in the dural blood flow, both TRPA1 and CGRP receptor antagonists can block TRPA1 activation-triggered increase (Kunkler et al., 2011). Further, in CNS, CSD induction promotes CGRP release in brain slices (Shi et al., 2010; Tozzi et al., 2012) and cerebral cortex of rats (Wang et al., 2016b). Moreover, the ability of exogenous CGRP in abrogating the suppressive effect of A967079 on CSD in the mouse brain slice (Fig. 4), suggests the involvement of CGRP in cortical TRPA1 signaling in CSD. This was supported by that reduction in cortical susceptibility to CSD was observed by the anti-CGRP antibody, which action was also reversed by exogenous CGRP (Fig. 3). Consistently, prolongation of CSD latency was seen by the CGRP receptor antagonist (Fig. 1). Collectively, we propose that there may be a positive loop during CSD that Ca^{2+} influx resulting from the opening of TRPA1 channels leads to CGRP release, acting on CGRP receptors, which in turn regulates cortical susceptibility to CSD.

It was noted that reduction in CSD magnitude was only observed by application of the anti-CGRP receptor antibody but not the receptor antagonist. The reason to account for this difference is not known, but it may be related to that there are more than one CGRP responsive receptors (Walker and Hay, 2013). CGRP and CGRP receptor monoclonal antibodies are capable of preventing migraine (Dodick et al., 2014; Bigal et al., 2015; Walter and Bigal, 2015; Giamberardino et al., 2017). So far, there is no clinical data available demonstrating the effect of monoclonal anti-CGRP antibodies on aura. Interestingly, a recent paper showed that Fremanezumab, a monoclonal anti-CGRP antibodies (CGRP-mAb), can prevent the activation and sensitization of high-threshold trigeminovascular neurons induced by CSD (Melo-Carrillo et al., 2017), suggesting a potential explanation for selectivity to migraine headache. While anti-CGRP antibodies are thought to be of predominantly peripheral site of action, our data on the anti-CGRP antibody in preventing CSD support the important role of

Fig. 5. Effects of the anti-CGRP antibody on CSD latency (A) and magnitude (B) in the mouse brain slice. Three groups were designed: the anti-IgG antibody at 0.025 μM (n = 6) as the control, the anti-CGRP antibody at 0.4 μM in the absence (n = 6) or presence of 10.5 μM of CGRP peptide (n = 6). The data showed marked reduction in cortical susceptibility to CSD by the anti-CGRP antibody. Data were plotted as percentage of their initial levels and indicated as mean ± SEM. Mann–Whitney's U test, one-tailed, for significance between control and antibody groups. $^{**}p < 0.01$ was considered significant. Representative traces of CSD wave in each group are shown in C. (Unekawa et al., 2012; Guedes et al., 2017).

CGRP in migraine with aura, which may have a central site of action.

One limitation of this study is the large variation of the image data within each group, which may be partly due to each coronal section being prepared from slightly different coordinates (between 1 and 3 mm posterior to bregma). Another limitation of this study is that the conclusion drawn largely replies the use of a group of agonists and antagonists that are selectively binding to TRPA1, further *in vivo* studies are necessary using TRPA1 knockout mice to clarify the role specific regions of TRPA1 in CSD. Further, as TRPA1 is a sensor of oxidative stress (Benemei et al., 2014; Yazgan and Naziroglu, 2016) and the cysteine residues of TRPA1 channels are target of nitric oxide (NO) and NO nitrosylation (Yoshida et al., 2006), it remains to be further investigated how cortical TRPA1 channels interact with ROS and NO during CSD.

In summary, we conclude that TRPA1 plays a critical role in regulating cortical susceptibility to CSD involving CGRP. These data suggest cortical functions of TRPA1 are involved in the mechanism of migraine aura. Desensitization of TRPA1 channels and blockade of CGRP would have therapeutic benefits in preventing migraine with aura.

ACKNOWLEDGMENTS

The authors thank Wangwenli Charitable Foundation, China and XJTLU research development fund for financial support, Wenjie Zhang from XJTLU for technical help; Fan Bu from XJTLU for his helpful comments and Blair Grubb at University of Liverpool for helpful communications.

AUTHOR CONTRIBUTION

Liwen Jiang did experiments, data analysis and manuscript preparation; Yan Wang performed experiments, data analysis and manuscript preparation; Yuewei Xu carried out the *in vitro* experiment and data analysis.

Dongqing Ma undertook the experiments and manuscript editing.

Minyan Wang provided overall project supervision, manuscript preparation and financial support.

CONFLICT OF INTEREST

The authors declare no conflict of interests.

REFERENCES

Andrade EL, Meotti FC, Calixto JB (2012) TRPA1 antagonists as potential analgesic drugs. Pharmacol Ther 133:189–204.

Benedikt J, Samad A, Ettrich R, Teisinger J, Vlachova V (2009) Essential role for the putative S6 inner pore region in the activation gating of the human TRPA1 channel. BBA 1793:1279–1288.

Benemei S, Fusi C, Trevisan G, Geppetti P (2014) The TRPA1 channel in migraine mechanism and treatment. Br J Pharmacol 171:2552–2567.

Bigal ME, Dodick DW, Rapoport AM, Silberstein SD, Ma Y, Yang R, Loupe PS, Burstein R, Newman LC, Lipton RB (2015) Safety, tolerability, and efficacy of TEV-48125 for preventive treatment of high-frequency episodic migraine: a multicentre, randomised, double-blind, placebo-controlled, phase 2b study. Lancet Neurol 14:1081–1090.

Bu F, Wang Y, Jiang L, Ma D, Quinn JP, Wang M (2017) Sarcoma family kinase activity is required for cortical spreading depression. Cephalalgia. 333102417748572.

Chen J, Joshi SK, DiDomenico S, Perner RJ, Mikusa JP, Gauvin DM, Segreti JA, Han P, Zhang XF, Niforatos W, Bianchi BR, Baker SJ, Zhong C, Simler GH, McDonald HA, Schmidt RG, McGaraughty SP, Chu KL, Faltynek CR, Kort ME, Reilly RM, Kym PR (2011) Selective blockade of TRPA1 channel attenuates pathological pain without altering noxious cold sensation or body temperature regulation. Pain 152:1165–1172.

Cutrer FM, Huerter K (2007) Migraine aura. Neurologist 13:118–125.

Demartini C, Tassorelli C, Zanaboni AM, Tonsi G, Francesconi O, Nativi C, Greco R (2017) The role of the transient receptor potential ankyrin type-1 (TRPA1) channel in migraine pain: evaluation in an animal model. J Headache Pain 18:94.

Denner AC, Vogler B, Messlinger K, De Col R (2017) Role of transient receptor potential ankyrin 1 receptors in rodent models of meningeal nociception – experiments in vitro. Eur J Pain 21:843–854.

Dodick DW, Goadsby PJ, Silberstein SD, Lipton RB, Olesen J, Ashina M, Wilks K, Kudrow D, Kroll R, Kohrman B, Bargar R, Hirman J, Smith J (2014) Safety and efficacy of ALD403, an antibody to calcitonin gene-related peptide, for the prevention of frequent episodic migraine: a randomised, double-blind, placebo-controlled, exploratory phase 2 trial. Lancet Neurol 13:1100–1107.

Doods H, Hallermayer G, Wu D, Entzeroth M, Rudolf K, Engel W, Eberlein W (2000) Pharmacological profile of BIBN4096BS, the first selective small molecule CGRP antagonist. Br J Pharmacol 129:420–423.

Dussor G, Yan J, Xie JY, Ossipov MH, Dodick DW, Porreca F (2014) Targeting TRP channels for novel migraine therapeutics. ACS Chem Neurosci 5:1085–1096.

Edvinsson L (2015) CGRP receptor antagonists and antibodies against CGRP and its receptor in migraine treatment. Br J Clin Pharmacol 80:193–199.

Giamberardino MA, Affaitati G, Costantini R, Cipollone F, Martelletti P (2017) Calcitonin gene-related peptide receptor as a novel target for the management of people with episodic migraine: current evidence and safety profile of erenumab. J Pain Res 10:2751–2760.

Grinberg YY, Dibbern ME, Levasseur VA, Kraig RP (2013) Insulin-like growth factor-1 abrogates microglial oxidative stress and TNF-alpha responses to spreading depression. J Neurochem 126:662–672.

Guedes RCA, Araujo M, Vercosa TC, Bion FM, de Sa AL, Pereira Jr A, Abadie-Guedes R (2017) Evidence of an inverse correlation between serotonergic activity and spreading depression propagation in the rat cortex. Brain Res 1672:29–34.

Gupta R, Saito S, Mori Y, Itoh SG, Okumura H, Tominaga M (2016) Structural basis of TRPA1 inhibition by HC-030031 utilizing species-specific differences. Sci Rep 6:37460.

Hadjikhani N, Sanchez Del Rio M, Wu O, Schwartz D, Bakker D, Fischl B, Kwong KK, Cutrer FM, Rosen BR, Tootell RB, Sorensen AG, Moskowitz MA (2001) Mechanisms of migraine aura revealed by functional MRI in human visual cortex. PNAS 98:4687–4692.

Huang D, Li S, Dhaka A, Story GM, Cao YQ (2012) Expression of the transient receptor potential channels TRPV1, TRPA1 and TRPM8 in mouse trigeminal primary afferent neurons innervating the dura. Mol Pain 8:66.

Julius D (2013) TRP channels and pain. Annu Rev Cell Dev Biol 29:355–384.

Kadkova A, Synytsya V, Krusek J, Zimova L, Vlachova V (2017) Molecular basis of TRPA1 regulation in nociceptive neurons. A review. Physiol Res 66:425–439.

Karatas H, Erdener SE, Gursoy-Ozdemir Y, Lule S, Eren-Kocak E, Sen ZD, Dalkara T (2013) Spreading depression triggers

headache by activating neuronal Panx1 channels. Science (New York, NY) 339:1092–1095.
Katsura H, Obata K, Mizushima T, Sakurai J, Kobayashi K, Yamanaka H, Dai Y, Fukuoka T, Sakagami M, Noguchi K (2006) Activation of Src-family kinases in spinal microglia contributes to mechanical hypersensitivity after nerve injury. J Neurosci 26:8680–8690.
Kelman L (2007) The triggers or precipitants of the acute migraine attack. Cephalalgia 27:394–402.
Kheradpezhouh E, Choy JMC, Daria VR, Arabzadeh E (2017) TRPA1 expression and its functional activation in rodent cortex. Open Biol 7.
Kim YS, Son JY, Kim TH, Paik SK, Dai Y, Noguchi K, Ahn DK, Bae YC (2010) Expression of transient receptor potential ankyrin 1 (TRPA1) in the rat trigeminal sensory afferents and spinal dorsal horn. J Comp Neurol 518:687–698.
Klement G, Eisele L, Malinowsky D, Nolting A, Svensson M, Terp G, Weigelt D, Dabrowski M (2013) Characterization of a ligand binding site in the human transient receptor potential ankyrin 1 pore. Biophys J 104:798–806.
Kremeyer B, Lopera F, Cox JJ, Momin A, Rugiero F, Marsh S, Woods CG, Jones NG, Paterson KJ, Fricker FR, Villegas A, Acosta N, Pineda-Trujillo NG, Ramirez JD, Zea J, Burley MW, Bedoya G, Bennett DL, Wood JN, Ruiz-Linares A (2010) A gain-of-function mutation in TRPA1 causes familial episodic pain syndrome. Neuron 66:671–680.
Kunkler PE, Ballard CJ, Oxford GS, Hurley JH (2011) TRPA1 receptors mediate environmental irritant-induced meningeal vasodilatation. Pain 152:38–44.
Kunkler PE, Zhang L, Pellman JJ, Oxford GS, Hurley JH (2015) Sensitization of the trigeminovascular system following environmental irritant exposure. Cephalalgia 35:1192–1201.
Lauritzen M (1994) Pathophysiology of the migraine aura. The spreading depression theory. Brain 117(Pt 1):199–210.
Lauritzen M, Fabricius M (1995) Real time laser-Doppler perfusion imaging of cortical spreading depression in rat neocortex. NeuroReport 6:1271–1273.
Lee KI, Lee HT, Lin HC, Tsay HJ, Tsai FC, Shyue SK, Lee TS (2016) Role of transient receptor potential ankyrin 1 channels in Alzheimer's disease. J Neuroinflamm 13:92.
Materazzi S, Benemei S, Fusi C, Gualdani R, De Siena G, Vastani N, Andersson DA, Trevisan G, Moncelli MR, Wei X, Dussor G, Pollastro F, Patacchini R, Appendino G, Geppetti P, Nassini R (2013) Parthenolide inhibits nociception and neurogenic vasodilatation in the trigeminovascular system by targeting the TRPA1 channel. Pain 154:2750–2758.
Melo-Carrillo A, Noseda R, Nir RR, Schain AJ, Stratton J, Strassman AM, Burstein R (2017) Selective inhibition of trigeminovascular neurons by fremanezumab: a humanized monoclonal anti-CGRP antibody. J Neurosci 37:7149–7163.
Mihara S, Shibamoto T (2015) The role of flavor and fragrance chemicals in TRPA1 (transient receptor potential cation channel, member A1) activity associated with allergies. Allergy Asthma Clin Immunol 11:11.
Moskowitz MA (2007) Genes, proteases, cortical spreading depression and migraine: impact on pathophysiology and treatment. Funct Neurol 22:133–136.
Nassini R, Materazzi S, Vriens J, Prenen J, Benemei S, De Siena G, la Marca G, Andre E, Preti D, Avonto C, Sadofsky L, Di Marzo V, De Petrocellis L, Dussor G, Porreca F, Taglialatela-Scafati O, Appendino G, Nilius B, Geppetti P (2012) The 'headache tree' via umbellulone and TRPA1 activates the trigeminovascular system. Brain 135:376–390.
Paulsen CE, Armache JP, Gao Y, Cheng Y, Julius D (2015) Structure of the TRPA1 ion channel suggests regulatory mechanisms. Nature 520:511–517.
Pietrobon D, Moskowitz MA (2013) Pathophysiology of migraine. Annu Rev Physiol 75:365–391.
Queiroz LP, Rapoport AM, Weeks RE, Sheftell FD, Siegel SE, Baskin SM (1997) Characteristics of migraine visual aura. Headache 37:137–141.
Russo AF (2015) Calcitonin gene-related peptide (CGRP): a new target for migraine. Annu Rev Pharmacol Toxicol 55:533–552.
Shatillo A, Koroleva K, Giniatullina R, Naumenko N, Slastnikova AA, Aliev RR, Bart G, Atalay M, Gu C, Khazipov R, Davletov B, Grohn O, Giniatullin R (2013) Cortical spreading depression induces oxidative stress in the trigeminal nociceptive system. Neuroscience 253:341–349.
Shi H, Li JH, Ji CF, Shang HY, Qiu EC, Wang JJ, Jing XH (2010). [Effect of electroacupuncture on cortical spreading depression and plasma CGRP and substance P contents in migraine rats]. Zhen ci yan jiu = Acupuncture research / [Zhongguo yi xue ke xue yuan Yi xue qing bao yan jiu suo bian ji] 35:17–21.
Shigetomi E, Tong X, Kwan KY, Corey DP, Khakh BS (2011) TRPA1 channels regulate astrocyte resting calcium and inhibitory synapse efficacy through GAT-3. Nat Neurosci 15:70–80.
Storozhuk MV, Zholos AV (2017) TRP channels as novel targets for endogenous ligands: focus on endocannabinoids and nociceptive signalling. Curr Neuropharmacol.
Story GM, Peier AM, Reeve AJ, Eid SR, Mosbacher J, Hricik TR, Earley TJ, Hergarden AC, Andersson DA, Hwang SW, McIntyre P, Jegla T, Bevan S, Patapoutian A (2003) ANKTM1, a TRP-like channel expressed in nociceptive neurons, is activated by cold temperatures. Cell 112:819–829.
Sun B, Bang SI, Jin YH (2009) Transient receptor potential A1 increase glutamate release on brain stem neurons. NeuroReport 20:1002–1006.
Tang YT, Mendez JM, Theriot JJ, Sawant PM, Lopez-Valdes HE, Ju YS, Brennan KC (2014) Minimum conditions for the induction of cortical spreading depression in brain slices. J Neurophysiol 112:2572–2579.
Torrente D, Mendes-da-Silva RF, Lopes AA, Gonzalez J, Barreto GE, Guedes RC (2014) Increased calcium influx triggers and accelerates cortical spreading depression in vivo in male adult rats. Neurosci Lett 558:87–90.
Tozzi A, de Iure A, Di Filippo M, Costa C, Caproni S, Pisani A, Bonsi P, Picconi B, Cupini LM, Materazzi S, Geppetti P, Sarchielli P, Calabresi P (2012) Critical role of calcitonin gene-related peptide receptors in cortical spreading depression. PNAS 109:18985–18990.
Trevisan G, Hoffmeister C, Rossato MF, Oliveira SM, Silva MA, Ineu RP, Guerra GP, Materazzi S, Fusi C, Nassini R, Geppetti P, Ferreira J (2013) Transient receptor potential ankyrin 1 receptor stimulation by hydrogen peroxide is critical to trigger pain during monosodium urate-induced inflammation in rodents. Arthritis Rheum 65:2984–2995.
Unekawa M, Tomita Y, Toriumi H, Suzuki N (2012) Suppressive effect of chronic peroral topiramate on potassium-induced cortical spreading depression in rats. Cephalalgia 32:518–527.
Vay L, Gu C, McNaughton PA (2012) The thermo-TRP ion channel family: properties and therapeutic implications. Br J Pharmacol 165:787–801.
Walker CS, Hay DL (2013) CGRP in the trigeminovascular system: a role for CGRP, adrenomedullin and amylin receptors? Br J Pharmacol 170:1293–1307.
Walter S, Bigal ME (2015) TEV-48125: a review of a monoclonal CGRP antibody in development for the preventive treatment of migraine. Curr Pain Headache Rep 19:6.
Wang M, Chazot P, Ali S, Duckett S, Stevens RS, Obrenovitch TP (2012) Effects of NMDA receptor antagonists with different subtype-selectivities on retinal spreading depression. Br J Pharmacol 165:235–244.
Wang M (2013) Cortical spreading depression and calcitonin gene-related peptide: a brief review of current progress. Neuropeptides 47:463–466.
Wang Y, Li Y, Wang M (2016a) Involvement of CGRP receptors in retinal spreading depression. Pharmacol Rep 68:935–938.
Wang Y, Tye AE, Zhao J, Ma D, Raddant AC, Bu F, Spector BL, Winslow NK, Wang M, Russo AF (2016b) Induction of calcitonin gene-related peptide expression in rats by cortical spreading depression. Cephalalgia.

Wiedemann M, Lyhs B, Bartels JP, Sieber M (2012) The pharmacological control of neuronal excitability in the retinal spreading depression model of migraine. Curr Med Chem 19:298–302.

Yamamoto S, Shimizu S (2016) Significance of TRP channels in oxidative stress. Eur J Pharmacol 793:109–111.

Yazgan Y, Naziroglu M (2016) Ovariectomy-induced mitochondrial oxidative stress, apoptosis, and calcium ion influx through TRPA1, TRPM2, and TRPV1 are prevented by 17beta-estradiol, tamoxifen, and raloxifene in the hippocampus and dorsal root ganglion of rats. Mol Neurobiol.

Yoshida T, Inoue R, Morii T, Takahashi N, Yamamoto S, Hara Y, Tominaga M, Shimizu S, Sato Y, Mori Y (2006) Nitric oxide activates TRP channels by cysteine S-nitrosylation. Nat Chem Biol 2:596–607.

Zhang X, Levy D, Kainz V, Noseda R, Jakubowski M, Burstein R (2011) Activation of central trigeminovascular neurons by cortical spreading depression. Ann Neurol 69:855–865.

Zhang X, Levy D, Noseda R, Kainz V, Jakubowski M, Burstein R (2010) Activation of meningeal nociceptors by cortical spreading depression: implications for migraine with aura. J Neurosci 30:8807–8814.

Zhong J, Minassi A, Prenen J, Taglialatela-Scafati O, Appendino G, Nilius B (2011) Umbellulone modulates TRP channels. Pflugers Arch 462:861–870.

(Received 4 October 2017, Accepted 18 April 2018)
(Available online 30 April 2018)